

FORMULATION OF NOVEL POLYMER COATED IRON OXIDE NANOPARTICLES

Ahmed Abushrida, BPharm

**Thesis submitted to the University of Nottingham for the degree of
Doctor of Philosophy**

December 2011

CONTENTS

CONTENTS	i
ABSTRACT	xv
ACKNOWLEDGEMENTS	xvii
ABBREVIATIONS	xviii
LIST OF FIGURES	xx
LIST OF TABLES	xxv
CHAPTER 1.....	1
1. INTRODUCTION.....	1
1.1 A Brief Overview of Iron Oxide Nanoparticles	1
1.2 Review of Iron Oxide Nanoparticles	1
1.3 Properties of Iron Oxide Nanoparticles	3
1.4 Synthesis of Iron Oxide Nanoparticles	5
1.4.1 Co-precipitation Method.....	5
1.4.2 Gas phase Methods	8
1.4.3 Aerosol / vapour Methods.....	9
1.4.4 Thermal Decomposition Method.....	9

1.4.5	Polyols Method.....	10
1.4.6	Microemulsion Method.....	10
1.4.7	Flow Injection Method.....	11
1.4.8	Electrochemical Method	12
1.5	Surface Coating	13
1.5.1	Dextran.....	13
1.5.2	Polyethylene Glycol (PEG).....	14
1.5.3	Poly(D, L-lactic-co-glycolic acid) (PLGA)	15
1.5.4	Polyvinyl alcohol.....	16
1.5.5	Alginate.....	17
1.5.6	Chitosan	17
1.5.7	Silica	19
1.5.8	Gold	20
1.5.9	Other Polymer coated iron oxide nanoparticles	21
1.6	Applications of Iron Oxide Nanoparticles	23
1.6.1	Magnetic Resonance Imaging (MRI)	23
1.6.2	Drug Delivery.....	29
1.6.3	Hyperthermia.....	32

1.6.4	Tissue Repair	33
1.7	Colloidal Stabilisation.....	34
1.7.1	Fundamental Methods to Stabilise Colloidal Particles	35
1.8	Uptake of Nanoparticles by Cells	36
1.8.1	Mononuclear Phagocyte System (MPS)	36
1.8.2	Mechanism of Intracellular Uptake	37
1.9	Effect of Particles and Surface Coating	39
1.10	Poly(Glycerol Adipate) Polymer	41
1.11	Aims of this Project	42
CHAPTER 2.....		44
2. MATERIALS AND METHODS		44
2.1	Materials.....	44
2.1.1	Reagents and Buffers	44
2.2	Methods.....	45
2.2.1	Synthesis of Iron Oxide Nanoparticles	45
2.2.1.1	The effect of pH on the size.....	45
2.2.1.2	Preparation of iron oxide nanoparticles (IONPs).....	45
2.2.2	Stability of Uncoated Iron Oxide Nanoparticles	46

2.2.3	Synthesis of Carboxymethyl Dextran	46
2.2.3.1	Determination of degree substitution of carboxy methyl dextran. ...	47
2.2.4	Preparation of Iron Oxide Nanoparticles Coated with Carboxymethyl dextran in the absence or presence of CMD	47
2.2.4.1	In the absence of CMD	47
2.2.4.2	In the presence of CMD	48
2.2.5	Dextran Coated Iron Oxide Nanoparticles	48
2.2.6	Poly (glycerol adipate) PGA Coated Iron Oxide Nanoparticles	48
2.2.7	Optimisation of Nanoparticle Coating Produced with PGA	49
2.2.8	Purification of PGA-Coated Iron Oxide Nanoparticles	50
2.2.9	Modification of PGA Polymers	50
2.2.9.1	Synthesis of PGA 40% C_{18} by acylation of backbone PGA	50
2.2.10	Poly(glycerol adipate) 40% C_{18} Coated IONPs	51
2.2.11	0.1% Tween80-coated PGA-coated IONPs and PGA 40% C_{18} coated IONPs	52
2.2.12	0.1% Albumin-coated PGA-coated IONPs and PGA 40% C_{18} -coated IONPs	52
2.2.13	PEGylated PGA 40% C_{18}	52
2.2.14	PEGylated PGA 40% C_{18} Coated IONPs	53
2.2.15	Stability of Iron Oxide Nanoparticles Coated with polymer	53

2.2.16	RBITC Labelled PGA-Coated Iron Oxide Nanoparticles	53
2.2.17	Determination of Fluorescent Dye Loading.....	54
2.2.18	Cell Culture Studies.....	54
2.2.18.1	Preparation of the nanoparticles for cell work	54
2.2.18.2	C6 cell	55
2.2.18.3	Preparation of media for C6 cell line.....	55
2.2.18.4	Routine cell culture.....	55
2.2.18.5	Washing coverslips	55
2.2.18.6	Coating coverslips with poly-D-Lysine (PDL)	56
2.2.18.7	Cell staining for fluorescence microscopy.....	56
2.2.18.8	Cell staining for confocal microscopy	56
2.2.18.9	Qualitative nanoparticle uptake by cells study.....	56
2.2.18.10	Qualitative uptake of nanoparticles in C6 cells.....	57
2.2.18.11	Qualitative uptake and metabolism of nanoparticles in C6 cell	57
2.2.18.12	Evaluation of time-dependent uptake of NPs by cells growing in monolayer culture using TEM	57
2.2.18.13	Dehydration and embedding of cells	57
2.2.18.14	Quantitative NP uptake study dependent on dose and time	58
2.2.18.15	Quantitative determination of loss of nanoparticles from cells	58
2.2.18.16	Aggregate cultures.....	59

2.2.18.17	Cell aggregate uptake of RBITC NPs.....	59
2.2.19	Instrumental Methods	59
2.2.19.1	Measurement of particle size	59
2.2.19.2	Surface charge measurement.....	60
2.2.19.3	Transmission electron microscopy	60
2.2.19.4	Nuclear magnetic resonance spectroscopy (NMR)	60
2.2.19.5	Fourier transformed infrared spectroscopy (FTIR)	61
2.2.19.6	Flow cytometry.....	61
2.2.19.7	Method of measuring cell uptake NPs by flow cytometry	62
2.2.19.8	Fluorescence microscopy.....	62
2.2.19.9	Confocal laser scanning microscopy	63
2.2.19.10	Method of fluorescence studies	64
CHAPTER 3.....	65
3. SYNTHESIS OF IRON OXIDE NANOPARTICLES AND NANOPARTICLES COATED WITH CARBOXYMETHYL DEXTRAN AND DEXTRAN	65
3.1	INTRODUCTION	65
3.2	Aim of the chapter	67
3.3	Methods.....	67
3.4	RESULTS	68

3.4.1	Iron Oxide Nanoparticle Preparation and Characterisation	68
3.4.2	Particle Size	68
3.4.3	Zeta Potential	69
3.4.4	TEM Images	70
3.4.5	The Effect of pH on the Stability of IONPs	72
3.4.6	Stability of IONPs	72
3.4.7	Carboxylated Dextran	75
3.4.8	IONP Coated with CMD and Dextran	75
3.4.8.1	CMD-IONPs	76
3.4.8.2	Dextran-coated iron oxide nanoparticles	79
3.5	Discussion	81
3.5.1	IONP Preparation and Characterisation	81
3.5.1.1	Particle size	82
3.5.1.2	Zeta potential	83
3.5.1.3	Stability of uncoated iron oxide nanoparticles	83
3.5.1.4	The effect of pH on the size of IONPs	84
3.5.2	Carboxylated Dextran	85
3.5.3	Coated Iron Oxide with CMD and Dextra	85
3.5.3.1	Particle size	86

3.5.3.2 Zeta potential	88
3.6 CONCLUSIONS	88
CHAPTER 4.....	90
4. POLY (GLYCEROL ADIPATE) AND PGA 40%C_{18} COATED IRON OXIDE NANOPARTICLES	90
4.1 INTRODUCTION	90
4.2 Aims of the Chapter	93
4.3 Methods.....	93
4.4 Results.....	94
4.4.1 Coated IONPs Using Different PGAs and two Different Methods.....	94
4.4.1.1 Zeta potential	98
4.4.2 Optimisation of IONPs Coating Produced with PGA 0% Modified	99
4.4.3 Morphology.....	108
4.4.3.1 Zeta potential	111
4.4.4 Modification of PGA polymers	111
4.4.4.1 Synthesis of PGA 40% C_{18} by acylation of backbone PGA	111
4.4.5 PGA 40% C_{18} coated IONPs.....	117
4.4.5.1 Particle size and morphology.....	117
4.4.5.2 Zeta potential	122

4.4.6	Particle Stability	122
4.4.6.1	0.1% Tween 80-coated PGA 0%-IONPs and PGA 40% C_{18} -IONPs.....	123
4.4.6.2	0.1% Albumin-coated PGA coated IONPs and PGA 40% C_{18} coated IONPs.....	123
4.4.7	Colloidal Stabilisation of IONP	123
4.4.8	Purification of PGA-IONPs.....	126
4.5	Discussion	128
4.5.1	Different PGAs-coated Iron oxide particles using two different methods.....	128
4.5.2	Particle Size and Zeta Potential.....	132
4.5.3	Optimisation of Nanoparticle Coating Produced with PGA 0%	133
4.5.4	Zeta Potential.....	136
4.5.5	Modification of PGA Polymers.....	136
4.5.5.1	Synthesis of PGA 40% C_{18} by Acylation of Backbone PGA.....	136
4.5.6	PGA 40% C_{18} Coated IONPs	137
4.5.7	0.1% Tween 80% Coated PGA 0%-IONPs and PGA 40% C_{18} -IONPs.....	139
4.5.8	0.1% Albumin Coated PGA 0% Coated-IONPs and PGA 40% C_{18} Coated IONPs.	140
4.5.9	Stability of IONPs Coated with Polymers	141

4.5.10 Purification of PGA 0% Coated IONPs.....	142
4.6 CONCLUSIONS	142
CHAPTER 5.....	144
5. PEGYLATED POLY (GLYCEROL ADIPATE) 40%C_{18} COATED IRON OXIDE NANOPARTICLES	144
5.1 INTRODUCTION	144
5.2 Aims of the Chapter	145
5.3 Methods.....	146
5.4 Results.....	146
5.4.1 PEGYLATED PGA 40% C_{18}	146
5.4.2 NMR Analysis	149
5.4.3 PEGylated PGA 40% C_{18} -IONPs	152
5.4.3.1 TEM photomicrographs and DLS analysis	152
5.4.3.2 Zeta potential	158
5.4.4 Stability of PEG-PGA 40% C_{18} Coated IONPs.....	159
5.5 Discussion	160
5.5.1 PEGYLATED PGA 40% C_{18}	160
5.5.2 PEGylated PGA 40% C_{18} -IONPs	161

5.5.2.1	Zeta potential	163
5.5.3	Stability of PEG–PGA 40 % C ₁₈ –IONPs.....	163
5.6	CONCLUSION	164
CHAPTER 6.....		166
6. INTERACTION OF COATED NANOPARTICLES WITH CELLS IN CULTURE		166
6.1	INTRODUCTION	166
6.2	Methods.....	168
6.3	Results.....	169
6.3.1	Qualitative Nanoparticle Uptake Study: Dose-dependent uptake of RBITC labelled NPs by cells.....	169
6.3.1.1	0.1 % Tween–PGA 40% C ₁₈ coated IONPs	169
6.3.1.2	PEG–PGA 40% C ₁₈ coated IONPs	172
6.3.2	Time-dependent Uptake of RBITC Labelled NPs by Cells.....	174
6.3.2.1	0.1% Tween–PGA 40% C ₁₈ –IONPs.....	174
6.3.2.2	PEG–PGA 40% C ₁₈ –IONPs	175
6.3.3	Time-dependent Metabolism of RBITC Labelled NPs by Cells.....	176
6.3.3.1	0.1 % Tween–PGA 40% C ₁₈ coated IONPs.....	176
6.3.3.2	PEG–PGA 40% C ₁₈ –IONPs	178

6.3.4	Dose-dependent uptake of RBITC Labelled NPs by Monolayer using Confocal Fluorescence Microscope	181
6.3.4.1	0.1% Tween-PGA 40% C_{18} -IONPs	181
6.3.4.2	PEG-PGA 40% C_{18} -IONPs	182
6.3.5	Metabolism and Redistribution of RBITC Labelled NPs by C6 Cell Monolayers using Confocal Fluorescence microscopy	183
6.3.5.1	0.1% Tween-PGA 40% C_{18} -IONPs	184
6.3.5.2	PEG-PGA 40% C_{18} -IONPs	185
6.3.6	Uptake of RBITC Labelled NPs by C6 Cells Cultured as a Spherical Aggregate using Confocal microscopy	186
6.3.7	Time-dependent Uptake of RBITC Labelled NPs by C6 cell Aggregates Using Confocal Fluorescence microscope	187
6.3.7.1	0.1% Tween-PGA 40% C_{18} -IONPs	187
6.3.7.2	PEG-PGA 40% C_{18} -IONPs	192
6.3.8	cytometry Investigation of Uptake of RBITC Labelled NPs by C6 Monolayer cell cultures	197
6.3.8.1	Dose-dependent uptake of RBITC labelled PGA 40% C_{18} -IONPs and PEG-PGA 40% C_{18} -IONPs by cells	197
6.3.8.2	Time-dependent uptake of RBITC labelled PGA 40% C_{18} -IONPs and PEG-PGA 40% C_{18} -IONPs by cells	198
6.3.8.3	Time-dependent uptake of RBITC labelled PGA 40% C_{18} -IONPs and PEG-PGA 40% C_{18} -IONPs by C6 cells using flow cytometry studies to investigate retention of RBITC labelled nanoparticles within C6 cells	199
6.3.9	Localisation NPs in C6 cells using TEM	200

6.3.9.1	Time-dependence uptake of PGA 40% C_{18} -IONPs by C6 cells and localisation in cells using TEM.....	200
6.3.9.2	PEG-PGA 40% C_{18} -IONPs	205
6.4	DISCUSSION.....	210
6.4.1	Uptake into Monolayers.....	211
6.4.2	Effects of Time and Dose.....	218
6.4.3	Metabolism and Retention of Nanoparticles Uptake with time	219
6.4.4	Uptake into Aggregates.....	220
6.4.5	Overview	221
	CHAPTER 7.....	223
7.	SUMMARY AND CONCLUSIONS.....	223
7.1	Aims and objectives.....	223
7.2	Overall Summary	224
7.2.1	Iron Oxide Nanoparticle Manufacture	224
7.2.2	Dextran-Coated Iron Oxide Nanoparticles	225
7.2.2.1	Synthesis of Carboxymethyl dextran	225
7.2.3	Different Substitutions of PGA-coated IONPs using two different Methods	225
7.2.4	PEGylated PGA 40% C_{18}	227

7.2.4.1	PEGylated PGA 40% C_{18} coated iron oxide nanoparticles	227
7.2.5	Stability of Coated Iron Oxide Nanoparticles.	228
7.2.6	Coated IONPs Uptake by Cells	228
7.3	FUTURE WORK	230
	REFERENCES	232

ABSTRACT

The aim of this study was to investigate how to produce iron oxide nanoparticles, with the potential for long circulation times or the ability to preferentially reach particular tissues.

The preparation of iron oxide nanoparticles was achieved using inorganic solution methods to prepare particles of small size using a narrow size distribution. The nanoparticles were coated with dextran and carboxymethyl dextran as reference materials using the same method as in the preparation of the iron oxide nanoparticles.

This project investigated the use of the biodegradable polymer poly(glycerol adipate) (PGA) as a coating for iron oxide nanoparticles. PGA is already used in drug delivery systems and showed an ability to control the rate of release of the drug. PGA can be readily modified with pendant functional groups leading to modifications of the physicochemical properties of the polymer. It can also be readily modified to form copolymers with the hydrophilic polymer poly(ethylene glycol) (PEG). PGA 40% acylated with stearic acid (PGA 40% C_{18}) and the PEGylated copolymer PEG–PGA 40% C_{18} were synthesised for this work.

The formulation of coated iron oxide nanoparticles was investigated using PGA and modified PGA polymers. The coating process was optimised producing small coated nanoparticles were measured by TEM and the best sizes are (16 ± 5 nm with PGA while with, modified PGA is 23 ± 7 nm and with PEG–PGA 40% C_{18} is 16 ± 4 in diameter). The PGA–IONPs were over-coated by incubation with albumin and Tween. The coated particles were characterised by DLS, zeta potential, and transmission electron microscopy. The colloidal stability of the various particle formulations was investigated using increasing salt concentrations. These demonstrated that PGA–coated nanoparticles were more stable than the existing dextran formulations, and that increased stability was obtained by overcoating with

albumin or Tween. A further increase in stability was seen with PEG-PGA coated nanoparticles.

The cellular uptake of the RBITC labelled nanoparticle formulations was studied on the C6 medulloblastoma cell line using monolayer and 3-D aggregate cultures using fluorescence microscopy, confocal microscopy, transmission electron microscopy (TEM) and flow cytometry. The results indicated that these particles were readily internalised in C₆ cells, but with an unusual subcellular distribution. Uptake was dependent on both nanoparticle concentration and incubation time. The incubation of cells with internalised particles demonstrated that particles were metabolised and fluorescence was lost from cells over a period of 4–12 hours. TEM studies showed that, after 1 hour, nanoparticles were found in all subcellular compartments, but that the route of entry into cells could not be readily determined. Experiments using 3-D cell cultures demonstrated that nanoparticles were readily taken up into aggregates, with nanoparticles penetrating deep into the aggregates.

Overall, these studies demonstrated novel formulations of iron oxide nanoparticles coated with well-defined biodegradable PGA polymer layers, which were stable against aggregation under physiological conditions. These formulations show promise for use in a variety of medical applications.

ACKNOWLEDGEMENTS

I would like to express my sincere gratitude to my supervisor Dr Martin Garnett for his invaluable advice and support throughout my project. He was very helpful and supportive, was always make me up through the whole period of my studies.

I would particularly like to thank Dr Terry Parker for his help and guidance in the cell work.

Thank you to Dr Paraskevi Kallinteri for her help and support in the initial setting up of the project and for guiding me throughout. Thanks to Christy and all the technicians who have given their time, their knowledge and their resources in the drug delivery.

A special thanks to Mahmoud, Samer, Bader, Abdulghani, Abed Alnaser, Abde nour and all my friends in drug delivery. Thanks also to all the people working in our school for their help.

I extend my gratitude to Hammed Massod for what he did for me. I will never forget that.

I would also like to acknowledge all my friends in Libya.

Finally, my deepest gratitude goes to the best woman ever in my life, my mother, who is always with me and prays for me.

A special thanks to Maerim, Alsida, Amna, my nephews Mourad, Magdi and my best friend, brother and twin Soliman, for their love and support. Without their encouragement, I could not have finished this project. To my late brother, I wish you were here now.

Thank you Allah, my creator and sustainer, for giving me the power and hope to finish my Ph.D. Without you nothing can ever happen.

ABBREVIATIONS

2-D	Two Dimensional
3-D	Three Dimensional
CDI	Carbonyldiimidazole
CLSM	Confocal Laser Scanning Microscopy
CMD	Carboxy Methyal Dextran
DAPI	4', 6- Diamidino-2-Phenylindole, Dilactate
DCM	Dichloromethane
DLS	Dynamic Light Scattering
EDTA	Ethylene Diamine Tetraacetic
FBS	Fetal Bovine Serum
FTIR	Fourier Transform Infrared Spectroscopy
GPC	Gel Permeation Chromatography
HEPES	N-(2-hydroxyethyl) piperazine-N- (2-ethanesulphonic acid)
IDP	Interfacial Deposition Method
IONP	Iron Oxide Nanoparticles
MEM	Minimum Essential Medium
MFI	Mean Fluorescence Intensity
MION	Monocrystalline Iron Oxide Nanoparticles
M-PEG	Methoxypoly(ethylene glycol)
MPS	Mononuclear Phagocyte System

MRI	Magnetic Resonance Imaging
NCS	Newborn Celf Serum
NPs	Nanoparticles
PAA	Poly(acrylic acid)
PBS	Phosphate –Buffer Saline
PDL	Poly-D-Lysine
PEG	Poly(Ethylene Glycol)
PFA	Paraformaldehyde
PGA	Poly(Glycerol Adipate)
PGA 40% C_{18}	Acylation of PGA by 80%
PLGA	Poly(lactic acid-co-glycolic acid)
PVA	Poly(vinyl Alcohol)
R	Proton Relaxation Rate
RBITC	Rhodamine B Isothiocyanate
SPION	Suprparamagnetic Iron Oxide Nanoparticle
SUPW	Super Ultra-Pure Water
T	Relaxation Time
T1	Longitudinal Relaxation Times
T2	Transverse Relaxation Time
TEM	Transmission Electron Microscope
USPION	Ultrasmlal Paramagnetic Iron Oxide

LIST OF FIGURES

Figure 1-1: Intracellular pathways of nanoparticles and sorting.	39
Figure 2-1: Synthesis of Carboxymethyl Dextran.	47
Figure 2-2: Structure of poly (glycerol adipate) backbone.	48
Figure 2-3: Synthesis of poly(glycerol adipate) PGA.	49
Figure 2-4: Structure of poly(glycerol adipate) 40% C ₁₈	51
Figure 2-5: Synthesis of poly(glycerol adipate) 40%.	51
Figure 2-6: Structure of PEGylated poly(glycerol adipate) backbone substituted with acyl group 40% C ₁₈	53
Figure 2-7: Principle of Flow Cytometry.	62
Figure 2-8: Principle of confocal laser scanning microscop.	64
Figure 3-1: The particle size distribution of IONPs by DLS.	69
Figure 3-2: TEM images for uncoated IONPs.	71
Figure 3-3: The effect of pH on the stability of IONPs.	72
Figure 3-4 : Preparation pH 0.5 (Peak 1): IONP stability over 7 days.	73
Figure 3-5 : Preparation pH 1 (peak 1): IONP stability over 7 days..	74
Figure 3-6: Preparation pH 1 (peak 2): IONP stability over 7 days..	74
Figure 3-7: The particle size distribution of CMD –IONP by DLS.	77
Figure 3-8: The particle size distribution of CMD–IONP by DLS.	77
Figure 3-9 : TEM image for CMD–IONP.	78
Figure 3-10: TEM image for CMD–IONP.	78
Figure 3-11: The particle size distribution of dextran coated IONPs by DLS.	79
Figure 3-12: TEM image of dextran coated IONPs.	80
Figure 4-1: IONPs coated with different polymers using the IDP method.	95
Figure 4-2: IONPs coated with different PGA by sonication method.	95

Figure 4-3: TEM image of PGA 60% C_8 -IONPs by using IDP method.....	97
Figure 4-4: TEM image of PGA 100% C_8 -IONPs by using sonication method.....	97
Figure 4-5: Different amounts of polymer with constant volume of acetone.....	101
Figure 4-6: Different volumes of acetone with constant amount of the polymer...	103
Figure 4-7: Range of amounts of polymer with constant volume of acetone (2 ml)...	106
Figure 4-8: TEM image of PGA 0% (1 mg) with (2 ml) of acetone-IONPs.....	108
Figure 4-9: TEM image of PGA 0% (0.5 mg) with (2 ml) of acetone-IONPs.....	109
Figure 4-10: TEM images of PGA 0% (0.2 mg) with (2 ml) of acetone-IONPs.....	109
Figure 4-11: TEM image of PGA 0% (0.1 mg) with (2 ml) of acetone-IONPs.....	110
Figure 4-12: Structure of PGA backbone.....	112
Figure 4-13: NMR spectrum for poly(glycerol adipate) backbone.....	112
Figure 4-14: Structure of PGA 40% C_{18}	113
Figure 4-15: NMR spectrum for poly (glycerol adipate) 40% C_{18}	113
Figure 4-16: GPC elution profile for poly(glycerol adipate) backbone.....	114
Figure 4-17: GPC elution profile for poly (glycerol adipate) 40% C_{18}	115
Figure 4-18: FTIR of poly(glycerol adipate) backbone.....	116
Figure 4-19: FTIR of poly(glycerol adipate) 40% C_{18}	116
Figure 4-20: The particle size distribution of 0.5 mg PGA 40% C_{18} -IONPs by DLS.....	118
Figure 4-21: The particle size distribution of 0.2 mg PGA 40% C_{18} -IONPs by DLS.....	118
Figure 4-22: The particle size distribution of 0.1 mg PGA 40% C_{18} -IONPs by DLS.....	119

Figure 4-23: TEM images of 0.5 mg PGA 40% C_{18} -IONPs.....	120
Figure 4-24: TEM images of 0.2 mg PGA 40% C_{18} -IONPs.....	121
Figure 4-25: TEM images of 0.1 mg PGA 40% C_{18} -IONPs.....	121
Figure 4-26: Stabilities of IONPs and IONPs coated with PGA 0% or dextran...	124
Figure 4-27: Stabilities of PGA 0% -IONPS and PGA 40% C_{18} -IONPs with different concentrations of electrolytes.....	125
Figure 4-28: TEM image of purification PGA 0%-IONPs.....	127
Figure 5-1: Synthetic scheme for poly(gthylene glycol) coupled to 40% C_{18} substituted poly(glycerol adipate).....	147
Figure 5-2: GPC elution profile for poly(glycerol adipate) substituted with 40% C_{18}	148
Figure 5-3: GPC elution profile for poly(ethylene glycol) coupled to poly(glycerol adipate) substituted with 40% C_{18}	148
Figure 5-4: Structure of poly (ethylene glycol) (PEG).	149
Figure 5-5: NMR spectrum for poly (ethylene glycol) (PEG).....	149
Figure 5-6: Structure of poly (ethylene glycol)-PGA 40% C_{18}	150
Figure 5-7: NMR spectrum for PEG-PGA 40% C_{18}	150
Figure 5-8 : FTIR for PGA 40% C_{18}	151
Figure 5-9: FTIR of PEG-PGA 40% C_{18}	151
Figure 5-10: TEM image of 0.2 mg PEG-PGA 40% C_{18} -IONPs.....	153
Figure 5-11 : TEM image of 0.1 mg PEG-PGA 40% C_{18} -IONPs.....	154
Figure 5-12: TEM Image of 0.05 mg PEG-PGA 40% C_{18} -IONPs.....	155
Figure 5-13: The particle size distribution of 0.2 mg PEG-PGA 40% C_{18} -IONPs by DLS.....	156

Figure 5-14: The particle size distribution of 0.1mg PEG-PGA 40% C ₁₈ -IONPs by DLS.....	156
Figure 5-15: The particle size distribution of 0.05 mg PEG-PGA 40% C ₁₈ -IONPs by DLS.....	157
Figure 5-16: Stabilities of different formulations of PEG-PGA 40% C ₁₈ -IONPs...	159
Figure 6-1: Fluorescence microscopy images of PGA 40% C ₁₈ -IONPs without Tween incubated with C6 cell for 2 h in the presence of serum	170
Figure 6-2: Fluorescence microscopy images of PGA 40% C ₁₈ -IONPs with Tween 0.1% incubated with C6 cell for 2 h in the presence of serum.....	171
Figure 6-3: Fluorescence microscopy images of PGA 40% C ₁₈ -IONPs without Tween incubated with C6 cells for 2 h in the absence of serum.....	172
Figure 6-4: Fluorescence microscopy images of PEG-PGA 40% C ₁₈ -IONPs in different concentration incubated with C6 Cell for 2 h in the presence of serum...	173
Figure 6-5: Fluorescence microscopy images of 0.1% Tween PGA 40% C ₁₈ -IONPs incubated with C6 cells for different time periods without washing.....	175
Figure 6-6: Fluorescence microscopy images of PEG-PGA 40% C ₁₈ -IONPs incubated with C6 cells for different times periods without washing.....	176
Figure 6-7: Fluorescence microscopy images of 0.1% Tween-PGA 40% C ₁₈ -IONPs incubated with C6 cells for different time periods in presence of serum.....	177
Figure 6-8: Fluorescence microscopy images of untreated C6 cells as control for both 0.1% Tween-PGA 40% C ₁₈ and PEG-PGA 40% C ₁₈ coated IONPs time-dependent metabolism studies.....	179
Figure 6-9: Fluorescence microscopy images of PEG-PGA 40% C ₁₈ -IONPs incubated with C6 cells for different time periods.....	180
Figure 6-10: Confocal laser micrograph of C6 cell monolayer incubated with 0.1 % Tween- PGA 40% C ₁₈ -IONP for 2 h.....	181
Figure 6-11: Confocal laser micrograph of C6 cell monolayer incubated with PEG-PGA 40% C ₁₈ -IONPs for 2 h.....	183

Figure 6-12: Confocal laser micrograph of C6 cell monolayer incubated with 0.1% Tween– PGA 40% C_{18} –IONPs for different time periods.....	184
Figure 6-13: Confocal laser micrograph of C6 cell monolayer incubated with PEG– PGA 40% C_{18} –IONPs different time periods.....	185
Figure 6-14: Phase-contrast micrographs illustrating the aggregates formed by the rotation method and C6 monolayer cells.....	186
Figure 6-15: Confocal fluorescence microscopy images of 0.1 % Tween–PGA 40% C_{18} –IONPs incubated with C6 cells aggregates for different time periods.....	188
Figure 6-16: Confocal fluorescence microscopy images gallery of 0.1 % Tween–PGA 40% C_{18} – IONPs incubated with C6 cells aggregates for different time periods.....	191
Figure 6-17: Confocal fluorescence microscopy images of PEG–PGA 40% C_{18} –IONPs incubated with C6 cells aggregates for different time periods.....	193
Figure 6-18: Confocal fluorescence microscopy images gallery of PEG–PGA 40% C_{18} –IONPs incubated with C6 cells aggregates for different time periods.....	196
Figure 6-19: RBITC labelled PGA 40% C_{18} –IONPs and PEG–PGA 40% C_{18} –IONPs taken up by C6 cells monolayer depended on dose using flow cytometry.....	198
Figure 6-20: Time-dependent uptake of RBITC labelled PGA 40% C_{18} –IONPs and PEG–PGA 40% C_{18} –IONPs by cells in monolayer culture using flow cytometry.....	199
Figure 6-21: Retention study of RBITC labelled PGA 40% C_{18} –IONPs and PEG–PGA 40% C_{18} –IONPs within C6 cells using flow cytometry.....	200
Figure 6-22: Electron micrographs for PGA 40% C_{18} –IONPs incubated with C6 for different time periods.....	205
Figure 6-23: Electron micrographs for PEG–PGA 40% C_{18} –IONPs incubated with C6 cells for different time periods.....	209

LIST OF TABLES

Table 1-1: Diagnostic imaging modalities and contrast media.	27
Table 1-2: Examples of polymers that have been used as imaging agents	28
Table 3-1: IONP Coated Degree of substitution of COOH on dextran.....	75
Table 3-2: The zeta potential and sizes of uncoated nanoparticles and CMD and dextran coated iron oxide nanoparticles.....	80
Table 4-1: Shows examples of ξ potential of PGAs–IONPs	99
Table 4-2: Surface charge and sizes of the best formulations with different amounts of PGA 0%–IONPs.....	111
Table 4-3: The surface charge and sizes of PGA 40% C_{18} –IONPs.....	122
Table 5-1: Sizes of PEG–PGA 40% C_{18} –IONPs measured by DLS and TEM.....	157
Table 5-2: Zeta potential of different formulations of PEG–PGA 40% C_{18} –IONPs.....	158

CHAPTER 1

1. INTRODUCTION

1.1 A Brief Overview of Iron Oxide Nanoparticles

Iron oxide nanoparticles (IONP) have been studied extensively over the past few decades to fabricate various novel contrast agents. Considerable research has been directed towards developing particles with an appropriate size and stability and modifying their properties by coating them with biodegradable polymers, to enhance their application in providing high resolution in magnetic resonance imaging (MRI) and as a good diagnostic agent.

Over 50 years ago the application of small IONPs was investigated for *in vitro* diagnostic tests (Gilchrist et al., 1957). Since then, studies on different types of iron oxides have been carried out in the field of magnetic particles with a small size of about 5–20 nm in diameter. Studies reported to date have dealt with maghemite, γ - Fe_2O_3 , or magnetite, Fe_3O_4 . Of these two, magnetite is a very promising candidate and subsequently its biocompatibility has already been tested (Schwertmann and Cornell, 1991)

1.2 Review of Iron Oxide Nanoparticles

A basic requirement for the use of nanoparticles in different areas in medical applications is a controlled particle size distribution. Superparamagnetic iron oxide nanoparticles (SPIONs) with suitable surface modification can be used for applications such as MRI contrast agents, drug delivery, tissue repair, hyperthermia, detoxification of biological fluids and immunoassay. For all these applications, the particle size must be smaller than 100 nm with a narrow distribution and have high magnetisation values (Gupta and Gupta, 2005).

The control of particle size is most important because the properties of the nanocrystals rely greatly on the dimension of the nanoparticles. Many studies have investigated the behaviour of the nanoparticles, and others have focussed on improving their applications, the stability of the particles and the control of surfactants (Laurent et al., 2008).

The type of method used for producing nanoparticles is very important. Additionally, the stability of the uncoated nanoparticles should be addressed as the aggregation process due to Van der Waals forces is the principal disadvantage of IONPs.

To prevent aggregation the nanoparticle must be coated by degradable nontoxic and biocompatible polymer. There are many polymers which have been used to coat iron oxide particles, such as dextran, poly(ethylene glycol) (PEG), poly(lactide-co-glycolide) (PLGA), and poly(vinylalcohol) (PVA). The nature of surface coatings and their subsequent geometric arrangement on nanoparticles determines not only the overall size of the colloid but also plays a significant role in the biokinetics and biodistribution of nanoparticles in the body. Some authors have reviewed the different factors related to the clearance of the IONPs from blood: particle size, dose, surface charge, coating material, and stability in physiological environment. The IONPs could also bind enzymes, nucleotides and drugs. Moreover, it has been proposed that, by using an external magnetic field, nanoparticles can be directed to a tumour, organ or tissue. (Gupta and Gupta, 2005).

Various methods have been developed for the preparation of IONPs (Mornet et al., 2006). The co-precipitation technique is a very cheap and simple method (Qu et al., 1999). Hydrothermal synthesis techniques are an alternative method for the preparation of highly crystalline IONPs (Wang et al., 2005). But there is no direct way to control the size and the shape of the final particles (Figuerola et al., 2010). Over the last ten years, significant advances have been made on the colloidal synthesis of nanocrystals in high-boiling point organic solvents (Park et al., 2004). There are others, such as sol-gel reactions, thermal decomposition method, etc.

Characterisation of the nanoparticles, including their physicochemical properties and structure, can be done using techniques such as direct light scattering (DLS), Transmission electron microscopy (TEM), X-ray diffraction and photon correlation spectroscopy. There are many factors affecting the properties of nanoparticles such as the chemical and physical size, surface coating and the thickness of surface coating. The nanoparticles have a large surface area. Furthermore, the attractive forces between the particles make them aggregate. To overcome all these problems, nanoparticles can be coated by polymers. There are two kinds of polymer: natural, like dextran, and synthetic like PVA. The coating must be hydrophilic and biocompatible so that the particles can disperse in biological fluids. Also the surface coating has an effect on the magnetic behaviour of nanoparticles. Agglomeration will occur when the particles have a strong magnetic attraction or the polymers have a short length. On the other hand particles with sufficiently low ferromagnetic effects and polymers with long length can produce sufficient repulsive forces to prevent the agglomeration (Huber, 2005).

The copolymers typically have a hydrophobic part that acts as an anchor and a hydrophilic part which forms tails to prevent bridge flocculation between one particle and another particle. Polymers must cover the entire surface of particles in order to overcome this aggregation problem (Storm et al., 1995). The iron oxide core can be coated with polymers during the synthesis process and it must be a long chain. However, the pH and temperature have an effect on the surface bound polymers (Enochs et al., 1993). Covering particles by a dense brush of polymers, e.g. dextran, prevents the particles reacting with blood proteins and receptors (Weissleder et al., 1995a).

1.3 Properties of Iron Oxide Nanoparticles

The size of particles usually refers to the total diameter of the particles including the iron oxide and coating. Because the smallest capillaries are 4 μm in diameter, particles or aggregates larger than this size will be captured and precipitated and this could cause emboli within the capillary bed of the lungs (Kreuter, 1983).

Particles tend to aggregate based on their magnetic energy, thus reducing their surface charge. As a result, this could lead to precipitation that may cause a very high risk if the particles are injected. The surface charge and aggregation behaviour of the particles in the blood must be known (Storm et al., 1995). Nanoparticles were eliminated immediately via macrophages of the mononuclear phagocytic system (MPS) because the defence system in the body recognised them as being alien to the body (Muller et al., 1997).

Particle sizes smaller than 4 μm are taken up by the cells of the reticuloendothelial system, mainly in the liver (60–90%) and spleen (3–10%) (Neuberger et al., 2005). While it is more likely that small particles up to 100 nm will be phagocytosed through liver cells, there is a tendency for particles larger than 200 nm to be filtered by the venous sinuses of the spleen (Moghimi et al., 2001). When particles with sizes in the range between 30 and 100 nm are injected intravenously, the larger particles will be eliminated by the liver from the blood faster than the small particles. Therefore, the larger particles are, the shorter is their plasma half-life-period (Chouly et al., 1996b). The uptake can be classified according the particle size, as phagocytosis of all size, or pinocytosis (particles <150 nm) (Muller et al., 1997). Phagocytes recognise and remove the larger particles, while smaller particles can be removed by all types of cell through pinocytosis. An increase in particles size leads to an increase in the phagocytotic activity (Maaßen et al., 1993).

For particles smaller than about 15 nm the cooperative phenomenon of ferromagnetism cannot be seen for longer periods and temporary magnetisation does not remain after the particles have been subject to a temporary external magnetic field (Sorensen, 2002).

Ferromagnetic particles occur when unpaired electron spins align themselves spontaneously. Then the material is able to exhibit magnetisation without being in a magnetic field. Single atoms cannot exhibit ferromagnetism, but when a number of atoms unite in solid form, ferromagnetic properties arise and particles exhibit permanent magnetisation once the ferromagnetic particles are removed from the field. The ferromagnetic material will initially oppose the field change soon after

field reversal, but finally the majority of domains will have turned their magnetisation vectors and the same inverse magnetisation is achieved. However, when the dimensions of ferromagnetic materials is reduced to particle dimensions smaller than a particular domain, the particles are no longer ferromagnetic but exhibit superparamagnetism (Elliott, 1998).

In the case of paramagnetic particles, a magnetic field is altered by the magnetic materials present in it. If a particle contains magnetic moments that can be aligned in an external magnetic field, this will amplify the field. Such substances exhibit the property of paramagnetism. In contrast to ferromagnetic materials (ferromagnetism), no permanent magnetization remains in paramagnetic materials when they are removed from the magnetic field. Paramagnetism can be understood by postulating permanent atomic magnetic moments, which can be reoriented in an external field. These moments can be either due to orbiting electrons or due to atomic nuclei. The torque applied by an external magnetic field on these moments will tend to orientate them parallel to the field (Chen, 1986).

1.4 Synthesis of Iron Oxide Nanoparticles

Numerous methods can be used to synthesise IONPs for medical applications and especially for medical imaging applications. These methods include thermal hydrolysis, sol-gel syntheses, hydrothermal reactions, microemulsions, sonochemical reactions, flow injection synthesis, electrospray syntheses, hydrolysis and thermolysis of precursors, and the common method co-precipitation, which is widely used for preparation of IONPs.

1.4.1 Co-precipitation Method

The wet chemical method has many advantages for producing IONPs. It is simple and efficient and has the capability of control over the size, composition and even the shape of the nanoparticles (Gupta and Curtis, 2004a, Gupta and Wells, 2004 and Reimers and Khalafalla, 1972). Iron oxide, either Fe_3O_4 or $\gamma\text{-Fe}_2\text{O}_3$, can be produced

using the co-precipitation of Fe^{2+} and Fe^{3+} aqueous salt solutions by addition of a base (Reimers and Khalafalla, 1972). The size, shape and composition of nanoparticles can be controlled according on the type of salts used (sulphates, nitrates, chlorides, etc.), ionic strength of the media, Fe^{2+} and Fe^{3+} ratio, and pH (Hadjipanayis and Siegel, 1993 and Sjoegren et al., 1994).

In the traditional way, magnetite is prepared by adding a base to an aqueous mixture of Fe^{2+} and Fe^{3+} chloride at a 1:2 molar ratio. The precipitated magnetite is black in colour. (Schwertmann and Cornell, 1991 and Cotton, 1988)

Aqueous co-precipitation of Fe^{3+} and Fe^{2+} at a ratio of 2:1 to prepare the magnetite nanoparticle is usually carried out in the presence of a base at pH 8–14 under anaerobic conditions. Magnetite is sensitive to oxidation and not stable in the air. This could critically affect the physical and chemical properties of the IONPs. Often the particles are coated with organic or inorganic molecules during the precipitation process to prevent the oxidation caused by air and also the formation of aggregates. To overcome the oxidation of Fe_3O_4 nanoparticles as which depends on oxidation speed and species, the reaction must be under a N_2 atmosphere to protect the particles and to reduce the size, when compared with methods without removing the oxygen (Gupta and Curtis, 2004a and Kim et al., 2001). The influence of different wet-chemical synthesis parameters such as iron (II) iron (III) ratio or varying pH and ionic strength on the resulting iron oxide structure have been described by (Jolivet et al., 1992 and Tronc et al., 1992).

Electronic or ion transfers are dependent upon the pH of the suspension. In basic medium, the oxidation of magnetite involves the oxidation–reduction of the surface of magnetite. Under anaerobic and acidic conditions, surface Fe^{2+} ions are desorbed as hexa-aquo complexes in solution (electron and ion transfer) according to:



Where A and B stand for tetrahedral and octahedral sites, respectively, and L represents a vacancy. Maghemite nanoparticles, bearing a high positive charge

density ($\sigma \approx 0.3 \text{ C m}^{-2}$ at pH 2, and low ionic strength, $10^{-2}/5.10^{-2} \text{ mol l}^{-1}$), carry high positive charge density and can easily be dispersed in acidic water, forming cationic sols practically free from aggregation. Maghemite particles could easily be concentrated aqueous dispersions when resulting from oxidation of magnetite (Jolivet and Massart, 1983, Jolivet et al., 1997 and Prene et al., 1993).

There is no migration of iron ions towards the interior of particles. Electrons and presumably protons are injected into the particle from the ferrous hydroxide adsorbed layer. This layer crystallises as spinel and the reaction stops when equal populations of Fe^{3+} and Fe^{2+} in the octahedral sub-lattice are reached. Similar electron transfers occur during adsorption of ferric ions on magnetite (Belleville et al., 1992).

Several parameters can influence the properties of the particles produced. These parameters include:

- Nature of salt
- Concentration of salts
- Volume ratio of the salt phase
- Temperature
- Ionic strength

This method has many advantages. It can easily produce a large number of nanoparticles (Laurent et al., 2008).

(Babes et al., 1999) have investigated the basics of the co-precipitation process, the influence of different parameters (media composition, iron II / iron III ratio, injection fluxes, iron, temperature, and oxygen) on magnetic properties, size and morphology.

Results by (Gnanaprakash et al., 2007) showed that the initial pH and temperature of the ferrous and ferric salt solution before initiation of the precipitation reaction and

the final pH are critical parameters controlling the formation of magnetite and nanoparticles.

1.4.2 Gas phase Methods

Gas phase methods for preparing nanomaterials is based on thermal decomposition (pyrolysis), reduction and disproportionation, oxidation, or other reactions to precipitate solid products from the gas phase (Pierson, 1999). In the chemical vapour deposition (CVD) process, a carrier gas stream with precursors is delivered continuously by a gas delivery system to a reaction chamber maintained under vacuum at high temperature ($> 900\text{ }^{\circ}\text{C}$) (Tavakoli et al. and 2007, Chang et al., 1994a). The products stick together and form aggregates or nanoparticles after the CVD reactions take place in the heated reaction chamber. Growth and agglomeration of the particles are minimised via rapid expansion of the two-phase gas stream at the outlet of the reaction chamber. Then heat treatment of the nano powders in various high-purity gas streams allows all the properties, such as compositional and structural modifications, particle purification and crystallisation, as well as transformation to a desirable size, composition, and morphology, to take place (Tavakoli et al., 2007 and Pierson, 1999). Important factors influencing the production of the nanoparticles are low concentrations of precursor in the carrier gas, as well as rapid expansion and quenching of the nucleated clusters or nanoparticles as they exit from the reactor (Tavakoli et al., 2007 and Chang et al., 1994b).

Laser pyrolysis of organometallic precursors is dependent on the resonant interaction between laser photons and one or more gaseous species, reactants or sensitiser. A sensitiser is an energy transfer agent that is excited by absorption of CO_2 laser radiation and transfers the absorbed energy to the reactants by collision (Dumitrache et al., 2005). The technique includes heating a flowing mixture of gases with an uninterrupted wave CO_2 laser to initiate and sustain chemical reaction until a critical concentration of nuclei is reached in the reaction zone, and homogeneous nucleation of particles occurs (Tartaj et al., 2005). The nucleated particles formed during the

reaction are entrained by the gas stream and are collected at the exit (Tartaj et al., 2003a).

1.4.3 Aerosol / vapour Methods

Spray and laser pyrolysis are good direct techniques for producing small particles based on chemical processes to provide a high level of production; by spraying a solution into a series of reactors where the aerosol droplets undergo evaporation of the solvent and solute condensation within the droplet, followed by drying and thermolysis of the precipitated particle at higher temperature (Pecharromán et al., 1995). Very small IONPs with a size about 5 nm are obtained by this method (Veintemillas-Verdaguer et al., 1998).

1.4.4 Thermal Decomposition Method

This method depends on two main routes to form the ferrites through hydrothermal conditions by oxidation or neutralisation of mixed metal hydroxides through the reaction of different ferrous salts as in the first method (Willard et al., 2004). Small particle sizes between 4–20 nm have been obtained using this method in the presence of alcohol, oleylamine and oleic acid. Particles can be transformed into a hydrophilic form by adding a bipolar solvent (Sun et al., 2004a). A modification of this method was done by Maity et al., (2009) who used solvent-free thermal decomposition just in the presence of the stabilising surfactant and produced small nanoparticles around 5 nm in diameter. Different parameters of the thermal decomposition procedure can be used to obtain high crystallinity and narrow size distribution and particle sizes between 4.9 to 14.1 nm in diameter.

Further modification of this method by Ahniyaz et al., (2008) using thermal decomposition of an iron 2-methoxy-ethoxide with surfactant-free conditions together with oleic acid yielded relatively monodisperse iron oxide nanocrystals and resulted in an average size of about 5.6 nm.

1.4.5 Polyols Method

The polyol process is a chemical method which refers to the use of polyols such as ethylene glycol and diethylene glycol to reduce metal salts to metal particles. Preparation of a variety of inorganic compound with non-aggregated particles has been successful. The polyols in this method often work as high boiling solvents and reducing agents, and also as stabilisers to control the growth of particles and prevent the aggregation of the particles. One of the important advantages of this method is that it can control experimental conditions. Moreover, it is easy to scale up (Fievet et al., 1989b and Claus and Hans-Otto, 2001).

In a similar reaction procedure with a variety of liquid polyols, including ethylene glycol, diethylene glycol, triethylene glycol and tetraethylene glycol $\text{Fe}(\text{acac})_3$ (acac acetyl cetonate) have been reduced to magnetite. The size obtained by this method was 20 nm in diameter and required only a single iron rich precursor and further reducing agent and surfactants (Cai and Wan, 2007).

By using hybrid (organo-inorganic) aerosols and the temperature of pyrolysis, the method depended on utilising ethanol/water solutions containing iron inorganic salts and mono- or polysaccharides and produced nanoparticles with sizes from 50 to 400 nm in diameter (Tartaj et al., 2007).

1.4.6 Microemulsion Method

The aqueous phase, containing Fe^{3+} (1M) and Fe^{2+} (0.5 M) in 0.1 M HCL, prevents oxidation with different ratios of microemulsion containing a volume ratio of cyclohexane. The method is based on stirring the mixture under a N_2 atmosphere at room temperature for 10 min then stirring again at 50°C. Base microemulsion was injected to precipitate the particles and the change of colour to black was evidence of the formation of magnetite particles and their aggregation. Particles were subjected to washing with 0.5% tetramethylammonium hydroxide and a large amount of

acetone to remove the surfactants and flocculate the particles. Particles were dried at 65°C for at least 24h (Vidal-Vidal et al., 2006).

Chin and Yaacob, (2007) have adopted this method to prepare IONPs at room temperature via water in oil microemulsion, resulting in IONPs which were spherical in shape and less than 10 nm.

In the opposite way, Capek, (2004) used one microemulsion. IONPs were obtained in bis(2-ethylhexyl) sulfosuccinate AOT microemulsions with a stopped-flow technique. The processes of nucleation and growth can be observed in the production of nanoparticles that after precipitation and drying showed no aggregates in TEM images with a size less than 4 nm.

1.4.7 Flow Injection Method

This method is a modified version of manufacturing zinc oxide nanoparticles (Wang and Muhammed, 1999). The idea of this technique is that it consists of continuous injection of reagents into a carrier stream. One reagent injected might be sufficient. The reaction mixture transfers into the capillary reactor at the same time as the reaction takes place.

By the ratio between the length of the manifold and the pumping rate, the residence time of the particles in the reaction mixture can easily be controlled. Mechanically, a propulsion unit, injection manifold, capillary reactor, and product collector are connected to the flow injection system. The most important part of the system is the injection manifold, which could be T- or X-shaped, where the reagents mix head-on with high accuracy in time and amount. The manifold function can be provided by an injection valve with segmentation capabilities. The function of the propulsion unit is the transportation of solutions through the system.

The time of the reacting mixture residence can be defined by the pumping rate and dimensions of the capillary reactor. The additional features, such as inert atmosphere and temperature control, that could be provided by the injection system have led to

the development of this method and nanoparticles have been obtained with a narrow size distribution in the range 2–7 nm in diameter (Salazar-Alvarez et al., 2006).

1.4.8 Electrochemical Method

This method consists of an electrolytic cell with anode and cathode, using an iron plate and stainless steel thin sheet as anode and cathode respectively where the space between them was 5 mm. The pH was maintained at 10 with concentrated sodium hydroxide solution and the electrolyte was $\text{Na}_2\text{S}_2\text{O}_3$ with a concentration of 0.02 mol/L. The applied current density was defined at the start by adjusting the voltage, until the change of the colour of the mixture to black occurred during the first 20 min. The electrolysis reaction was directly controlled by imposing the temperature, current density and intense agitation for a specific time. The final product was centrifuged and the residue was removed by deionised water at constant temperature in a hydrogen stream into the reactor for reduction at constant flow rate (2 L/h) for 3 h. The particles were then cooled to room temperature under a hydrogen atmosphere. To modulate the magnetic properties of the composites the reduction temperature was varied between 300 and 400°C.

IONPs have been synthesised within the pores of mesoporous silica (MS) microspheres by an electrochemical method to produce IONPs with a diameter of 20 nm inside the pore of MS spheres (Wang et al., 2007). Sizes varying from 20 to 30 nm of IONPs have been obtained using electrochemical method (Cabrera et al., 2008).

IONPs having an average size of 6.2 nm with a quite narrow distribution were synthesised with new parameters based on electro-precipitation in ethanol medium. The reaction precipitated the $\text{Fe}(\text{OH})_3$. The next step was reduction of iron hydroxide to magnetite in presence of hydroxyl ions which are generated at the cathode (Ibrahim et al., 2009).

1.5 Surface Coating

A variety of biodegradable polymers have been used to coat the IONPs. Polymers can be manipulated by modifying with different functional groups to increase the stability of the nanoparticles. These coatings can also protect the nanoparticles *in vitro* and *in vivo*. This review will cover both natural organic polymers and synthetic polymers.

1.5.1 Dextran

Dextran is a polysaccharide $(C_6H_{10}O_5)_n$, composed exclusively of alpha-D(1-6) linkages with some unusual 1,3 glucosidic linkages at branching points. Dextran is used to coat IONPs in aqueous solution, resulting in particles with overall sizes between 20–50 nm (Tueng et al., 1993).

The first report of the formation of magnetite in the presence of dextran was by Molday and MacKenzie, (1982). Co-precipitation is the most common method to obtain polysaccharide-coated iron oxide particles (Goetze et al., 2002). An average magnetite core size of 7.1 nm was found by X-ray diffraction and that of 8 nm was found by transmission electron microscopy. An average diameter of 25 nm was observed for dextran coated IONPs by scanning electron microscopy and a hydrodynamic diameter of 25–300 nm was obtained by photon correlation spectroscopy. The coated particles showed a weak negative charge in the buffer solutions at pH between 5.5 and 9.5 (Xu et al., 2005).

By using the Molday co-precipitation method, ferumoxtran-10 and ferumoxides have been produced (Lee et al., 2002). The effects of the molecular weight of dextran upon the formation and the stability, on size, morphology, coating efficiency and magnetic property have all been investigated. Dextran with molecular weights of 3000, 10,000, 20,000 and 40,000 have been used. The low molecular weight dextran gave the smaller desired particle size of 77.80 nm, while increasing the molecular weight resulted in a particle size increase to 121.4 nm, 156.2 nm and 192.1 nm respectively (Hong et al., 2009).

A comparison has been made between the laser pyrolysis technique and co-precipitation method for preparation of dextran coated IONPs to explore the mechanism of adsorption of the dextran on the surface of IONPs. At 25–500 °C, the mechanism of adsorption is probably hydrogen bonding between dextran hydroxyl groups and the iron oxide particle surface (Carmen Bautista et al., 2005).

Dextran provides hydroxyl functional groups that can be substituted, carboxymethyl dextran (CMD) being very common. IONPs coated by CMD using a co-precipitation method with diameters of about 90 nm and 120 nm were produced. The stability of particles against aggregation was investigated over a period of more than one week. A strong agglomeration and increase of particle size was observed after one day (Dutz et al., 2007).

1.5.2 Polyethylene Glycol (PEG)

Poly(ethylene glycol) (PEG) is non-toxic and non-immunogenic, and provides high steric stabilisation. Its uncharged hydrophilic residues and high surface mobility keep the particles apart and stable in aqueous solution and prevent protein adsorption to the particles and adhesion to cells (Yasugi et al., 1999 and Zhou et al., 2003). Therefore, the presence of covalently immobilised PEG on the surface of IONPs is most likely to enhance the biocompatibility and stabilisation of the nanoparticles. PEG has chains with some terminal functionality and can be coupled with biopolymers to create biodegradable copolymers such as poly(ϵ -caprolactone)-poly(ethylene glycol)-poly(ϵ -caprolactone) (PCL-PEG-PCL, PCEC) copolymers (Gou et al., 2008).

PEG polymers with molecular weights below 100,000 Da are amphiphilic and soluble in water. They are also soluble in many organic solvents, such as methylene chloride, toluene, acetone, chloroform, and ethanol. This allows PEG to be reacted with IONP surfaces using different chemistries that require the use of either aqueous or organic solvents (Veisoh et al., 2010). Various methods of coating were developed to prepare small (60–100 nm) and ultrasmall (20–35 nm) particles without size separation processes (Acar et al., 2005).

Iron nanoparticles were coated with PEG diacid via the grafting of aminopropylsilane groups and the coupling of oxidised PEG through the formation of a covalent bond. PEG diacid is covalently coated on the surface of the nanoparticles via at least one of their carboxylic groups, leaving the other COOH group available for further chemical reaction. PEG diacid coated IONPs were investigated by TEM and found to have an approximately spherical shape and an average diameter of 20 nm (Feng et al., 2008).

Kumagai et al., (2009) have reported a method to synthesise block copolymer-coated IONPs by chelation between the carboxylic acid groups in poly(ethylene glycol)–poly(aspartic acid) block copolymer (PEG–PAsp) and Fe on the surface of the IONPs. The TEM image showed PEG–PAsp-coated nanoparticles forming clusters with a size range of 100 nm, the hydrodynamic diameter with DLS and shown to be in the range of 100 to 120 nm with a unimodal distribution, for Asp/Fe ratios ranging from 0.02–0.5.

In a one-step procedure, IONPs were coated with silanated monomethoxy poly(ethylene glycol) (m-PEG) in aqueous medium. The mean particle sizes of the nanoparticles determined by X-ray diffraction and TEM gave an average size of 20 nm in diameter (Hu et al., 2008).

1.5.3 Poly(D, L-lactic-co-glycolic acid) (PLGA)

Poly(dl-lactic-co-glycolic acid) is a biocompatible, biodegradable and non-toxic material used for preparing nanoparticles and microparticles. PLGA is a copolymer of lactic and glycolic acid (Zimmer and Kreuter, 1995 and Bala et al., 2004).

Lee et al., (2004) have prepared magnetic nanoparticles of Fe₃O₄ encapsulated within PLGA for MRI contrast agents by using an emulsification diffusion method. The size was reduced to 120 nm by increasing the homogeniser speed up to 22,000 rpm.

Zhao et al., (2009) have produced poly(lactic acid) (PLA)-coated magnetic nanoparticles using uncapped PLA with free carboxylate groups. Magnetic microspheres (MMS) with the matrix material PLGA or PLA were then formed by the emulsion solvent evaporation method. The physical properties of these particles were compared to those of oleate-coated or oleate/sulphonate bilayer coated magnetic particles. PLA coated IONPs using w/o emulsion resulted in particle sizes of 180 ± 50 nm diameter. The polymer shell showed high protection of particles in pH 5.5 to 10.8 sensitivity with respect to the stability of magnetite particles (Gómez-Lopera et al., 2006).

1.5.4 Polyvinyl alcohol

PVA is a water-soluble polymer and has isolated hydroxyl functional groups, which can adsorb and complex with metal ions (Jiu et al., 2002).

Xu and Teja, (2008) have modified the surface of IONPs with PVA by continuous hydrothermal synthesis. The final polymer coated particles produced at different concentrations of PVA showed different sizes from 7 to 27 nm. The average particle size was shown to increase with temperature and residence time, and is accompanied by morphology changes in some cases. (Mahmoudi et al., 2010) have reported synthesis of IONPs with PVA by precipitation of iron oxide salts in PVA aqueous solution at various temperatures and at different concentrations. The results suggest that the PVA binds to the surface of the nanoparticles due to the presence of OH groups on the polymer chains and the nanoparticles. Also, using the same method, PVA coated super-paramagnetic iron oxide nanoparticles (SPION) of 6-10 nm core and 30 nm hydrodynamic sizes were obtained. The IONPs were first obtained by classical co-precipitation in water. A thermochemical treatment and centrifugation was then applied to obtain well-dispersed primary nanoparticles. PVA of molecular weight 12,000 was used to coat the particles (Schöpf et al., 2005).

Lee et al., (1996) found that crystallinity of the core decreased with increasing concentration of PVA present during the synthesis of iron oxide particles in the range of 4–10 nm through a precipitation reaction to form a stable dispersion. Binding

between the surface of nanoparticles and the polymer was found using FTIR absorbance shifts.

1.5.5 Alginate

Alginate is a linear polymer composed of α -D-mannuronate (M) and α -L-guluronate (G) units linked by α -1,4 and α -1,3 glycosidic bonds. M and G units are organised in MM, GG and MG blocks (Rocher et al., 2010).

Alginate-coated IONPs showed good biocompatibility and some magnetic targeting under a magnetic field. The high stability provided by alginate coated IONPs may be attributed to the binding of the carboxyl group of alginate to iron oxide (Ma et al., 2007).

Morales et al., (2008) and Finotelli et al., (2004) have prepared alginate-coated particles by dropping commercial sodium alginate solution (3%) into aqueous ferric chloride solution.

Two samples were prepared, sample A with 0.01 M and sample B with 0.5 M ferric chloride solution, which produced preformed IONPs encapsulated in Ca-alginate beads. IONPs coated with alginate were Fe_3O_4 with a core diameter of 5–10 nm and had a hydrodynamic diameter of 193.8 nm. ζ -potential was -65.0 mV with good stability (Ma et al., 2008).

1.5.6 Chitosan

Chitosan is a hydrophilic, biocompatible, biodegradable, alkaline, non-toxic natural polymer (Chung et al., 2005). Chitosan-coated IONPs varied from 10 to 80 nm with the different molecular weight of the chitosan (Zhi et al., 2006).

Tsai et al., (2010) have reported a simple method to coat IONPs *in situ* precipitation of ferrous hydroxide by the alkaline treatment of chitosan. Ammonium hydroxide

solution was rapidly added to the brown solution under sonication at 50 °C. The results revealed that the IONPs coated with chitosan had a hydrodynamic diameter of 87.2 nm.

Zhang et al., (2010b) have prepared chitosan coated IONPs via a novel photochemical method in an emulsifier-free aqueous system at room temperature. The results, using scanning electron microscopy (SEM) and TEM showed that the chitosan-coated nanoparticles were a regular shape with a mean diameter of 41 nm. However, the average size was 64 nm when measured by photon correlation spectroscopy.

Microspheres composed of SPION with spherical particle size about 15nm were synthesised and embedded in the presence of polyglucosamine (chitosan) by a sonochemical method. The ferrofluid, a solution of SPION-embedded chitosan, was sprayed on the surface of an alkali solution with a nozzle to produce IONPs in chitosan microspheres of 100–150 μm . The SPION-chitosan microspheres showed a strong enhancement of MR image contrast similar to the ferrofluid *in vitro* (Kim et al., 2007)

In another study, IONPs were synthesised by a classic method, co-precipitation resulting in a mean particle size of 14.1 nm. These particles were then dispersed well in two polymers, chitosan or *o*-carboxymethylchitosan OCMCS. The results revealed the mean particle radius as measured by DLS of 42 nm for chitosan/ Fe_3O_4 nanoparticles, and 38 nm with OCMCS/ Fe_3O_4 . Fe_3O_4 nanoparticles have net positive charge and OCMCS stabilised magnetic Fe_3O_4 nanoparticles have functional carboxyl groups (Zhu et al., 2008).

Chitosan coated IONPs have also been prepared by a crosslinking method. Oleic acid modified IONPs were firstly prepared by co-precipitation, chitosan was then added to coat the surface of the nanoparticles by physical absorption. The average size of such chitosan coated IONPs was approximately 10.5 nm. The chitosan coated IONPs had a remarkable heating effect which has great potential in hyperthermia therapy (Qu et al., 2010).

1.5.7 Silica

Coating of IONPs with a silica layer provides a chemically inert surface in biological systems for the core of IONPs (Deng et al., 2005).

The two main methods for coating IONP with silica, the Stöber method and the reverse micelle method, have both been used for the preparation of different inorganic nanoparticles. The Stöber method is an easy method for coating nanoparticles with a layer of silica simply by mixing the nanoparticles, aqueous solution and alkoxysilane in alcohol. With the sol–gel method, the reaction ends in a short time or at a maximum will take several hours. The parameters which are very important to control the coating thickness are the optimisation of solvent components and volume of alkoxysilane (Narita et al., 2009).

The uncoated IONPs with a particle size of 30 nm were prepared by a coprecipitation method which was followed by coating with silica using the Stöber method. The size of the coated nanoparticles was 50 nm using TEM (Khosroshahi and Ghazanfari, 2010).

Using another method by Lien and Wu, (2008) to coat IONPs, thermosensitive polymers were grafted onto the surfaces of 6 nm monodisperse IONPs coated with silica. The nanoparticles were synthesised using reverse microemulsions and free radical polymerisation. The nanoparticles produced contained a layer of silica coated onto the surface of nanoparticles in the range from 20 to 30 nm. The poly(*N*-isopropylacrylamide) (PNIPAM) grafted silica-coated IONPs were produced with different ratios of PNIPAM. The particle sizes of three samples increased by around 3–5 nm compared to that of pure silica coated IONPs as determined by TEM. PNIPAM grafted onto SiO₂/Fe₃O₄ nanoparticles were confirmed by FT-IR spectra.

Amine modified silica coated IONPs were prepared using a water-in-oil microemulsion technique, which employed amine-modified silica as the shell and iron oxide as the core of the magnetic nanoparticles. The particle size of the core was

8 nm while the coating increased the particle size up to 40 ± 5 nm (Ashtari et al., 2005).

Deng et al., (2005) used the sol–gel method for the preparation of silica-coated IONPs. The particle size of coated nanoparticles was 40 nm using TEM.

Silica coated IONPs with about 10 nm diameter IONP cores and about 2 nm thick silica shells were prepared using a co-precipitation method, and then the nanoparticles were covalently bonded with amine and carboxyl groups. The presence of the functional groups was proved by FTIR spectra (Jang and Lim, 2010).

1.5.8 Gold

Gold is another inorganic coating that has been used to coat nanoparticles and act like a coating polymer to enhance the stability. These properties give gold a particularly attractive surface chemistry for IONPs. However, one limitation is that gold-coating can weaken the magnetic properties of IONPs (Dale 2005).

The formation of a gold shell on the IONPs was achieved by an iterative reduction method using hydroxylamine as a reductant. The surface of the gold coated IONPs was further functionalised with mercapto-hexadecanoic acid (MHA) to bind the positively charged Arg6-esterase effectively. The gold-coated IONPs had a size distribution of 50–100 nm in diameter with an average size of about 70 nm, while the core IONPs had a size of 8–10 nm (Jeong et al., 2006).

Gold was coated onto IONPs using a facile reverse micelle procedure and the effect of water to surfactant molar ratio on the size was investigated. The particles were coated by polyglycerol through capping with thiol followed by polymerisation of glycidol. It was shown that ultrafine nanoparticles 9–16 nm could be synthesised with a thin gold layer of about 2 nm thicknesses (Jafari et al., 2010).

Lu et al., (2006) have prepared well dispersed nanoparticles comprised of a citrate stabilized gold shell and Fe oxide core. Results from (TEM) and energy dispersive

spectroscopy (EDS) indicated that the particle coated was with gold and had a size larger than 10 nm in diameter.

Monosized core/shell, IONPs/gold with magnetic–optic multifunctional properties were synthesised using a modified nanoemulsion method in the presence of poly(vinylpyrrolidone) (PVP) as the surfactant. The iron oxide /gold core–shell were prepared by seeding the iron nanoparticles core and then coating with a gold shell. The particle size of coated IONPs using TEM, was 8.7 nm, while the uncoated IONPs had a size of 3–6 nm diameter, FTIR confirmed that the PVP was bound to the surface of the nanoparticles (Liu et al., 2010).

1.5.9 Other Polymer coated iron oxide nanoparticles

IONPs have been coated with many other polymers to improve their stability and protect them in the biological environment. For example, superparamagnetic IONPs were coated with polyethylenimine and then conjugated with DNA. IONPs were prepared by the co-precipitation method. PEI coating of IONPs followed this procedure: the iron oxide suspension was mixed at various ratios with 25 kDa polyethylenimine PEI. An average size was 27 ± 12 nm as obtained by TEM. The complexes were added to cells and exposed to permanent and pulsating magnetic fields. The presence of these magnetic fields significantly increased the transfection efficiency (Steitz et al., 2007).

IONPs could be stabilised during the synthesis by oleic acid using the co precipitation method, and then further stabilised by coating them with PEI and co-polymer using direct ligand-exchange reactions. The first layer coating the IONPs was PEI. The second was formed by poly(ethylene oxide) PEI. The hydrodynamic diameter of IONPs was 10 nm and 30 nm with a core size of 10 nm. The nanoparticles coated with PEG-g-PEI showed an average hydrodynamic diameter of 25 nm, however, the nanoparticles coated with PEI had smaller hydrodynamic sizes of 14–15 nm (Duan et al., 2008).

Magnetic polymer nanospheres were also prepared using new procedures based on miniemulsion polymerisation. A stable water-based dispersion of sodium dodecyl sulfate and oleic acid coated magnetite aggregates was first synthesised as a bilayer and mixed with monomer styrene miniemulsion. The second step was another encapsulation of magnetite into monomer droplets using miniemulsification. The particle size of the latex-3 particles showed a diameter of 8 nm of superparamagnetic magnetite particles and after encapsulating within the polymer nanosphere the size increased to an average diameter of 80 nm (Zheng et al., 2005).

Another study showed that superparamagnetic particles could be stabilised with polyaniline. The polyaniline and IONPs composite was formed by polymerisation in the presence of the ferrofluid. IR spectra confirmed the composition on the surface of the oxide particles (Kryszewski and Jeszka, 1998).

Hu et al., (2006) have prepared a magnetite/poly(L-lactic acid) composite using a solvent evaporation/extraction technique in an oil/water emulsion. The average size of the composite was about 200 nm. However, the size of the core was 6.2 ± 0.7 nm in diameter. The composite was then loaded with an anti-cancer drug.

A method based on the so-called anionic polymerisation procedure to coat IONPs resulted in a shell of poly(ethyl-2-cyanoacrylate). The particle size of coated IONPs was determined by TEM to be 144 ± 15 nm. The images showed the layer coating the nanoparticles, and the thickness of the polymer shell was about 30 nm (Arias et al., 2007).

Ma et al., (2009) have also described the coating of IONPs with polyacrylic acid (PAA) to prevent the aggregation of the IONPs using chemical co-precipitation. PAA oligomer of low molecular weight was used as a dispersing agent and coating. The TEM result revealed that the average diameter of uncoated particles was 9.2 ± 2.6 nm while coated nanoparticles size using dynamic light scattering measurement indicated a hydrodynamic diameter of 246 ± 11 nm.

In drug delivery using ethylcellulose, coated IONPs were synthesised by an emulsion solvent evaporation process. The particles were then used as a drug carrier loaded

with diclofenac sodium for arthritis treatment. The particle size was measured using TEM showing an average diameter of 430 ± 40 nm and a spherical shape. The nanoparticles showed good loading, and a slow drug release profile (Arias et al., 2009).

1.6 Applications of Iron Oxide Nanoparticles

IONPs have been used a research tool for a variety of applications over the last decade. IONPs have been applied in various medical fields, and numerous reports have emerged using IONPs as a powerful tool to perform different functions. Currently, IONPs are commercially available and approved. In addition to being a research tool, IONPs hold great promise in MRI, drug delivery, cellular labelling/cell separation, tissue repair, hyperthermia treatment, etc.

1.6.1 Magnetic Resonance Imaging (MRI)

Diagnostic medical imaging has been the subject of enormous improvements over the last 35 years with the development of techniques such as MRI. This is one of the most useful non-invasive methods in the application of diagnostic imaging and is characterised by its high resolution of soft-tissues and by its absence of exposure to radiation. MRI, both in preclinical and clinical settings, has many advantages: high speed, clear image and high resolution with relative accessibility and low cost better than other techniques such as positron emission tomography (Wang et al., 2006).

To recognise the difference between healthy and pathological tissues, MR imaging uses contrast agents that can be localised to a particular tissue or cellular epitope which will permit the visualisation and characterisation of different disease states (Morawski et al., 2005). Today the main contrast agents are, firstly, paramagnetic gadolinium based contrast agents which shorten the longitudinal relaxation time (T1) and increase the contrast of the image (positive enhancement) (Hanns-Joachim et al., 2003). Secondly, IONPs, which shorten the transverse relaxation time (T2) and

provide many advantages as contrast agents, such as improved contrast, carrying high payloads and long circulation times (Cormode et al., 2010).

Magnetic resonance imaging relies on the nuclear magnetic resonance of protons in a molecule, and for medical imaging, specifically follows water. It can act in different tissues to give a picture of anatomical structure. The characteristic measure in MRI is the proton relaxation rate (R) or its inverse, the relaxation time (T).

There are two types of proton relaxation times, the longitudinal relaxation time, T_1 , (spin–lattice relaxation) and the transverse relaxation time, T_2 (spin–spin relaxation). Moreover, there are two types of contrast agents, positive and negative; positive acts on T_1 to give a positive enhancement of the signal appearing bright on the MRI scan. The negative agents provide negative enhancement, appearing as dark spots in the scan (Kubaska et al., 2001). Comparing gadolinium-based contrast agents and superparamagnetic iron oxide nanoparticles in terms of rates, SPION can produce enhanced relaxation in certain organs at lower doses than paramagnetic ions (Corot et al., 2006, Wang et al., 2001). Gadolinium contrast agents are commonly used in MRI but are non-specific with rapid accumulation in the liver, so they only permit a short time-imaging window (Fahlvik et al., 1990).

Overall, the transverse relaxation (T_1 and T_2) effect of SPION is mainly used in detection of liver lesions by MR imaging. The shortening of T_2 relaxation times in the transverse relaxation occurs when SPION are distributed in reticuloendothelial cells, such as Kupffer cells (KCs), according to phagocytic activity, and because of local field inhomogeneities that produce rapid dephasing of neighbouring proton spins. However, because of the lack of reticuloendothelial cells, liver tumours such as metastatic liver cancer cannot absorb these agents. Therefore, the contrast between tumour tissue and surrounding normal liver tissue is improved because of signal loss in the liver tissue (Saini et al., 1987).

Currently, only two SPION preparations have been approved for clinical use especially for liver MR imaging, such as Ferumoxides (i.e. Endorem® in Europe, Feridex® in the USA and Japan, Advanced Magnetix, USA) coated with dextran (Weissleder et al., 1989).

Ma et al., (2008) have used MRI to provide information on liver tumour by using IONPs coated with alginate. The nanoparticles were rapidly cleared from serum and accumulated mainly in the liver and spleen with a total percentage of more than 90% after intravenous injection and could have the capability to enhance detection of a liver tumour as contrast agents in MRI. IONPs prepared by laser-induced pyrolysis have been coated with dextran to give a hydrodynamic diameter of 50 nm, their ^1H NMR relaxation times and the magnetic properties of these particles showed they are suitable for use as contrast agents for MRI. Two important factors affect the relaxation properties, in particular particle and crystal size for the transverse relaxation rate, R2 (Morales et al., 2003).

Patel et al., (2008) have developed contrast agents comprising of PLGA encapsulated SPION, which were applied as a MRI contrast agent in the liver of a rabbit. The change in spin relaxation time occurred because the nanoparticles in the liver interact with the hydrogen nuclei around the nanoparticles. Comparing the images before and after the injection showed the image with high resolution. For this reason, PLGA encapsulated SPIONs (II) might be used as an MRI contrast agent.

Tanaka et al., (2008) modified SPIOs with biotin, hemin, and 5-phosphorylated DNA via the ligand exchange method. From the DLS measurements the particle size was 51.2 ± 22.4 nm and these nanoparticles could be expected to be potential applications both as a contrast agent and for cell cycle monitoring.

Microbubbles with a polyvinyl alcohol (PVA) outer layer and a poly(DL-lactide) (PLA) inner layer were prepared using a double emulsion solvent evaporation interfacial deposition (water-in-oil-in-water emulsion) process. The PLA and PVA double-layered polymer shell of 50–70 nm thicknesses can let the 12 nm SIONPs be loaded heterogeneously in their shell to significantly enhance magnetic susceptibility (Yang et al., 2009).

IONPs coated with non-magnetic precursor microgel, which is made up of polymerised methacrylic acid (MAA) and ethyl acrylate (EA) crosslinked with di-allyl phthalate (DAP), have been used for *in vivo* tracking of stem cells after

transplantation by labelling primary endothelial progenitor stem cells with magnetic particles. They can be tracked by magnetic resonance. The nanoparticles showed hydrodynamic diameters of 87–766 nm. Micro-gel iron oxide particles might be a useful tool for the study of relaxation induced by magnetic particles and cellular tracking by MRI (Lee et al., 2010).

C2-coated superparamagnetic IONPs can induce a significant increase in image contrast where the regions have a large number of apoptotic cells. The C2 is a domain of synaptotagmin I which binds to anionic phospholipids in cell membranes. The protein bound with the SPION can be detected by using MRI. The detection of apoptotic cells using this candidate diagnostic agent was illustrated *in vitro* with isolated apoptotic tumour cells and *in vivo* in a tumour treated with chemotherapeutic drugs (Blankenberg et al., 1997).

IONPs give diagnostic opportunities to detect diseases and understand their mechanisms. Nanoparticles are used widely to give more information on diseases, such as location. Medical imaging has been traditionally based on the use of X-rays and radioactive substances. The newer diagnostic imaging modalities, such as ultrasound and magnetic resonance, are now well-established techniques in patient management. Details of four major diagnostic imaging modalities in routine clinical settings with the physical basis of the techniques are illustrated in (Table 1.1).

Table 1-1: Diagnostic imaging modalities and contrast media.

Modality	Physical basis	Equipment	Image contrast media
X-ray imaging	Attenuation X-rays	X-ray generator, Radiographic film	Absorption of X-rays by high atomic weight
X-ray CT	Attenuation X-rays	Scanning X-ray generator, Detector array and Computer	Compounds mainly containing Iodine
Ultrasound Doppler ultrasound	Reflection of sound	Piezoelectric, Scan converter frequency	Encapsulated gas bubbles
MRI	Magnetic moment of moment of ^1H	Magnetic RF transmitter	Reduced T^1 and T^2
Nuclear imaging	Gamma emitting radiopharmaceutical	Scintillation camera, Image workstation	tissue concentration of radiopharmaceutical suitable ligand and radiolabel e.g. $^{99\text{m}}\text{Tc}$, ^{123}I and ^{111}In

Diagnostics such as MRI and ultrasound are starting to develop clearer imaging and more accuracy (Perkins, 1998). Organic and inorganic polymers are used as nanoparticles or contrast agents, evenly coating the metal nanoparticles to reduce systemic toxicity and increase drug bioavailability. Here, in Table 1.2, are examples of the polymers used as imaging and contrast agents (Perkins, 2002).

Table 1-2: Examples of polymers that have been used as imaging agents.

Polymer	Reference
Radiopharmaceuticals	
99m Tc-DTPA-BCP	Pimm <i>et al</i> (1995)
99m Tc-DTPA-MPEG	Bogdanov <i>et al</i> (1994)
X-ray contrast	
Polymer based on iodine complex	Bogdanov <i>et al</i> (1995)
Ultrasound contrast	
Polymeric micro balloons	Schneider <i>et al</i> (1992 and 1994)
MRI contrast	
Gd-DTPA-cascade polymer	Schwickert <i>et al</i> (1995)
CMDGd-DTPA	Siauve <i>et al</i> (1996)
Carboxymethyl dextran	Wiener <i>et al</i> (1994) and Schmitt and Willich (1997)
Dendrimer Gd chelates	Berthezene <i>et al</i> (1992)
Polylysine Gd-DTPA Gd-DTPA-PG.polyglucose macrocomplex	Harika <i>et al</i> (1995)

However, there are other methods of diagnostic imaging, such as X-ray where contrast agents are non-specific materials dependent on the use of dense materials to attenuate the X-ray photons, for example barium orally or iodine by the intravenous route. Polymer based contrast agents are attractive for use as vascular contrast agents in X-ray because they are polymers having a long clearance time in circulation, such as methoxy-polyethylene glycol (MPEG) and incorporate iodine for CT imaging (Perkins, 2002). Contrast agents for X-ray photons such as barium and iodine for the site specific targeting of X-ray contrast agents has not proven to be of any clinical value, mainly because the reporter moieties (barium and iodine) have to be delivered in such large amounts that it is not considered to be a viable possibility (Perkins, 2002).

Another important diagnostic imaging modality is nuclear medicine imaging, which relies on physiological processes and on the administration of radiolabelled tracers. This technique is for tissue imaging. There are many materials used for specific organs such as TC-99 m-bone scanning, lipophilic materials for cardiac and brain and biological materials such as pooled human serum albumin and monoclonal antibodies. Viral contamination is the main problem caused by human blood products. As a result, some radiopharmaceuticals cannot be supplied, e.g. serum albumin used for the measurement of plasma volume and macro-aggregates of serum albumin and for lung perfusion imaging (Hindle and Perkins, 1995). Ultrasound contrast agents work based on the production of a backscattered echo within the frequency range between 1 and 20 MHz. Contrast agents for ultrasound rely on an injectable formulation of constant gas-filled microbubbles which produce a strong reflection of the incident sound beam (Schneider et al., 1992). Polymers like polybutyl-2 cyanoacrylate with a wall thickness of 100 nm are enough to protect the enclosed gas bubble from dissolution in the blood stream and sufficiently elastic to oscillate in the ultra-sound field (Perkins, 2002).

1.6.2 Drug Delivery

Classic pharmaceuticals have many problems with systemic drug administration, including biodistribution throughout the body. There is also the lack of drug specificity for the pathological site and the need for a large dose to give a high concentration in the site, which could lead to side effects. Drug targeting could overcome some of these problems (Torchilin, 2000b). For example, through the targeting of the drug immobilised on magnetic materials under the action of an external magnetic field (Berry and Curtis, 2003), or to improve the target of drug binding with another molecule which recognises the target site, such as protein, hormones, antibodies, lectins, charged molecules and some low molecular weight ligands such as folate (Sudimack and Lee, 2000).

In drug delivery, the charge and surface chemistry of magnetic particles and the size have strong effects on blood circulation and the bioavailability of the particles within

the body (Chouly et al., 1996a). The first clinical trial in humans with magnetic targeting were reported by Lubbe et al., (1996). These trials used IONPs coated with starch and anionic phosphate, then the cationic binding to the positively charged amino sugars of epirubicin was possible. Successful preliminary animal trials led to human trials, the treatment consisting of intravenous infusion of the chemically bound drug and a course of conventional chemotherapy. During the infusion and for 45 min after, a magnetic field was built up as close to the unsuccessfully pre-treated tumour as possible (Bonadonna et al., 1993).

The physiological parameters of the patient, such as body weight, blood volume, cardiac output, peripheral resistance of the circulation system and organ function, all affect the external magnetic field in addition to the problem of placing the magnetic field close to the target location (Lubbe et al., 2001). The size of the nanoparticles plays a very important role in drug delivery which affects the adsorption of the drug and reaching the defective tissue with maximum dose and minimum side effect. This as a result changes the response of the organ to the drug.

After injection, large particles with diameters larger than 200 nm are easily removed by the spleen and ultimately eliminated by the cells of the phagocytic system, causing decreased blood circulation times. However, particles with diameters of less than 10 nm are rapidly removed through extravasation and renal clearance. Particles with sizes from 10 to 100 nm in diameter are optimal for intravenous injection and demonstrate the most prolonged blood circulation times. These particles are small enough both to evade RES of the body as well as to penetrate the small capillaries of the body tissues and so could offer the most effective distribution in certain tissues (Pratsinis and Vemury, 1996).

After offering all these advantages with the clear route of the nanoparticles in the body, the nanoparticles provide encouragement to use as tools for studies in this field. (Kayal and Ramanujan, 2010) have shown that, after administration of iron oxide nanoparticles coated with PVA containing doxorubicin, up to 45% of the adsorbed drug was released in 80 h, indicating the success of drug delivery via magnetic particles. IONPs were covered by glycerol mono-oleate and used as a drug

carrier. The anticancer chemotherapy agents paclitaxel and rapamycin anticancer showed high entrapment efficiency of about 95% and sustained release of encapsulated drug for more weeks under *in vitro* conditions. These results offer the possibility of improved therapeutic treatments of cancer cells (Dilnawaz et al., 2010).

Aminodextran-coated IONPs were synthesised as drug carriers detectable by MRI. Agents were based on a macromolecular backbone with a high density of sites for MRI reporters. This radiopharmaceutical is the first specifically designed anticancer drug carrier. The aim of these nanoparticles is to increase the pharmaceutical potential of the MRI technique (Saboktakin et al., 2010).

Gaihre et al., (2009) have reported the coating of IONPs with gelatine containing doxorubicin DXR and evaluated their potential as a carrier system for magnetic drug targeting. To understand their role, doxorubicin in coated iron oxide particles was prepared using adsorption and desolvation/cross-linking methods. Drug loading was carried out in various conditions of pH. The particles showed pH responsive drug release leading to progressive release of the drug at pH 4 compared to pH 7.4. The increase in the surface charge of coated particles after loading led to adsorption of positive doxorubicin to negative coated iron oxide particles, which indicated the loading had occurred. The increase or decrease in encapsulation efficiency was dependent on the surface charge of the coated particles and also confirmed the involvement of drug-to-particle interaction in the drug-loading.

Sun et al., (2008) have reported the development of a chlorotoxin (CTX) loaded IONP drug carrier that may potentially be used as an MRI contrast enhancement agent. The CTX immobilised on the surface of nanoparticles via PEG functional groups offers a platform to allow for conjugation of other diagnostic and therapeutic agents to develop further platforms for both improved visualisation and targeting. Drug delivery was demonstrated *in vitro* in 9L cells and *in vivo* in mouse tumour models and compared to studies with control nanoprobles. Cellular uptake experiments showed that the uptake of IONPs coated with PEG and CTX conjugates by glioma cells was considerably higher than that of control nanoparticles. MRI contrast in 9L cells cultured with IONPs coated with PEG–CTX at 100 µg Fe/mL for

1 h at 37 °C were visualised with TEM, which shows that PEG–CTX nanoparticles were internalised into the 9L cells cytoplasm. Then they examined the efficacy of CTX-conjugated nanoprobe in targeting glioma cells and providing contrast enhancement for MRI also under the same conditions.

Oleic acid coated IONPs in the presence of pluronic F-127 as stabiliser were used in both drug delivery and magnetic resonance imaging MRI *in vivo*. The drugs, doxorubicin and paclitaxel were incorporated into nanoparticles, either individually or together. This incorporation of drugs affected the physical size and zeta potential and magnetisation properties of the nanoparticles. Both of these drug nanoparticles showed high efficiency, either alone or in combination, for real time monitoring of drug distribution (Jain et al., 2008b).

1.6.3 Hyperthermia

Hyperthermia is being introduced as a new modality for cancer therapy. This is based on the principle that under an alternating magnetic field (AMF), a magnetic particle can create heat via hysteresis losses (Baker et al., 2006 and Hergt et al., 2004). The applications of IONPs for hyperthermia treatment were envisaged in the similar work of (Jordan et al., 1993). This experiment provided evidence of the capability of superparamagnetic particles to absorb the energy of an oscillating magnetic field and convert it into heat. This can be used *in vivo* to increase the temperature of the tumour and to damage the cell by hyperthermia (Jordan et al., 1999 and Moroz et al., 2002).

IONPs, prepared using the microemulsion method and then coated with a thin hexamethyldisilazane layer used to protect the iron core, replaced the cetyl trimethyl ammonium bromide (CTAB) coating on the particles. In the next step, phosphatidylcholine was coated on the nanoparticles' surface. These particles showed high magnetisation and increased hysteresis losses, improving its use for hyperthermia when compared with uncoated IONPs (Zhang et al., 2010a).

The effect of the particle size on this application was studied by Gonzales-Weimuller et al., (2009) who showed for the first time that, at a given frequency, the heating rates of superparamagnetic particles are dependent on particle size. The results showed that higher heating rates are possible by increasing the size of the particles from 4.6nm to about 12.5 nm. IONPs were coated with oleic acid by a co-precipitation method then coated with chitosan by crosslinking. The saturation magnetisation of the nanoparticles was 30.7 emu/g measured by magnetic measurement, and showed superparamagnetic properties at room temperature. The results indicated that the heating effect was significant and the heating could be adjusted by changing the concentration of nanoparticles (Qu et al., 2010).

IONPs were embedded in silica microparticles for treatment of cancer lesions by magnetically induced local hyperthermia. The injectable formulations form gels entrapping magnetic particles into a tumour. The nanoparticles provided the possibility of administration by syringe with a high proportion of IONPs to permit large heating capacities. Hydrogel (poloxamer, chitosan and organogel) were incorporated with nanoparticles and injected into human cancers in mice. Organogel 8% poly(ethylene-vinyl alcohol) in Dimethyl sulfoxide DMSO containing 40% w/v of magnetic nanoparticles showed magnetically induced local hyperthermia of the tumour where hydrogel alone did not show adequate magnetic response to induce hyperthermia (Le Renard et al., 2010).

1.6.4 Tissue Repair

Tissue repair using IONPs is accomplished either through separating two apposing tissue surfaces then heating the tissues sufficiently to join them, or through welding, where protein or synthetic polymer-coated nanoparticles are acting as a bridge between two tissue surfaces to improve joining of the tissues. Temperature at 55.5°C is the best to induce tissue union (Lobel et al., 2000).

Stem cells are the body's master cells and have a unique ability to renew themselves and give rise to other specialised cell types. These cells, therefore, have the potential to be used for transplantation purposes, for example, to replace

degenerated cells or in the repair of destroyed tissue, providing signals so that the stem cells can yield suitable cell types for the development of a tissue (Kiessling-Cooper and Anderson, 2003).

Using thrombin, which has been used for topical haemostasis and wound management for more than six decades, IONPs were bound to thrombin to show the efficiency of treatment for wounds and were compared with unbound thrombin using wounded rat skin. The investigation revealed that thrombin bound to IONPs increased the healing of the wound better than the free thrombin with reduced side effects compared to normal surgery (Ziv-Polat et al., 2010).

IONPs have also been used in transplant monitoring. For example, IONPs modified with the near-infrared fluorescent CY5.5 dye (MN-NIRF) and covered with dextran. Preliminary MRI on an islet phantom showed the possibility of detecting a signal drop in the analysis. After implantation under kidney capsules, many MRI examinations were implemented over half a year, with no significant change in the T_2 relaxation time in the labelled graft. Both implantation under kidney capsules and administration by intraportal infusion into diabetic mice models resulted in restoration of normoglycemia. The ability of the transplanted islets to secrete insulin was confirmed by *ex vivo* microscopy studies (Evgenov et al., 2006).

In comparison between IONPs coated with poly(vinyl pyrrolidone) (PVP) and commercial IONPs (Feridex formulation) for monitoring of pancreatic islets, the PVP coated nanoparticle labelled cells showed no changes in morphology and viability and showed higher iron accumulation because of the small nanoparticle size, which was 5–8 nm in diameter, and because of the biocompatibility of the PVP coating (Huang et al., 2009).

1.7 Colloidal Stabilisation

IONPs dispersed in a medium show Brownian motion and a natural tendency to adhere with each other and form aggregates due to the magnetic attractive forces between the particles. One of the main interactions is the Van der Waals long range

attractive forces between the particles. These interactions can be counteracted by electrical repulsive force between the particles created by the electric double layer at the particle surface, or by coating the particles with long chain polymers, performing a steric hindrance between the particles (Vennapusa et al., 2008 and Van Oss, 1994).

1.7.1 Fundamental Methods to Stabilise Colloidal Particles

There are two important methods to maintain the stability of nanoparticles which prevent the aggregation of the particles and provide long range repulsive force between the particles. This repulsive force should be as strong as the attractive force or equal to the range of the attractive interaction. To maintain stability a comparable number of counterions with opposite charge need to cover the particles. As a result, the charge becomes a neutral double layer of ions (Napper, 1989).

Steric stabilisation is achieved by the stabilising moiety chains extending into the continuous phase beyond the particle surface and isolating the ions and counterions of the ionic surfactant (Sung and Piirma, 1994). Steric stabilisation has been used widely because it has many advantages over electrostatic stabilisation, which are (1) independence of the presence of electrolytes, (2) effective also at high particle concentrations, (3) commonly, redispersion of flocculated particles can be readily achieved, (4) good freeze-thaw and dry-rehydrate stability, and (5) equal effectiveness in polar and nonpolar media (Storm et al., 1995).

Steric stabilisation is achieved by a layer of polymer chains attached to the surface of the particles and protects the particle from flocculation. The polymer chains in the thick steric layer repulse one another and are stretched from their free coil conformation, thus providing repulsion between particles. If the thickness of the coating is sufficient, this will prevent flocculation due to London-van der Waals attractions. Once sterically-stabilised particles are suspended in a polymer solution, the interactions are complicated by the repulsion between anchored and free chains (Gast and Leibler, 1986).

If the distance between two particles with adsorbed polymer layers become less than twice the thickness of the adsorbed layer then interaction between the two particles will occur. The steric repulsion has been evaluated in terms of difference in free energy ΔG over the interaction of the adsorbed layers. The Gibbs free energy change of the overlap interaction of the adsorbed layers can be calculated using the Gibbs equation $\Delta G = \Delta H - T\Delta S$ flocculation or coagulation occurs when ΔG is negative. However, stabilisation will take place when ΔG is positive. Many of the theoretical aspects of steric repulsion have been developed (Robert et al., 1972).

The other possibility of stabilisation is the generally accepted entropic stabilisation theory. The entropy term opposes flocculation whereas the enthalpy term favours it. The main role of the entropic contribution to the free energy of close approach could be titled entropic stabilisation (Napper, 1977).

The idea of this theory supposes that the second approaching adsorbed layer is not penetrable. Hence, the adsorbed layer is compressed and the polymer segments present in the interaction zone lose configurational energy in the compressed form but not in the uncompressed state. This causes a decrease in entropy and increase in ΔG . As a result, the net effect of repulsion between the particles results in avoiding the flocculation of the particles (Napper, 1989).

1.8 Uptake of Nanoparticles by Cells

1.8.1 Mononuclear Phagocyte System (MPS)

The efficient removal of foreign particulate material introduced into the bloodstream by the MPS has been known for a long time. About 3 decades ago it was shown that interfacial physicochemical events mediate the uptake of circulating foreign particles by MPS macrophages. The mononuclear phagocyte system is a group of cells comprising bone marrow progenitors, blood monocytes and tissue macrophages (Hume, 2006). These cells are widely distributed and occur strategically in several tissues of the body to recognise and clear altered and senescent cells, invading

particulates, as well as macromolecular ligands via a multitude of specialised plasma membrane receptors (Moghimi et al., 2001).

The rapid uptake of uncoated nanoparticles from the bloodstream by the macrophages of the MPS within seconds after intravenous administration make such particles ineffective as site-specific drug delivery devices. The cells involved, typically Kupffer cells or macrophages of the liver, cannot directly identify the nanoparticles themselves, but rather recognise specific opsonin proteins bound to the surface of the particles (Gref et al., 1994b and Frank and Fries, 1991).

1.8.2 Mechanism of Intracellular Uptake

Endocytosis is a complex mechanism which generally includes the processes of pinocytosis, nonspecific endocytosis, receptor-mediated endocytosis and phagocytosis, which is typically defined as endocytosis of large particles. Among the various types of receptors involved in endocytosis, the family of macrophage scavenger receptors are able to endocytose a wide array of polyanionic ligands and nanoparticles. *In vitro*, ferumoxide endocytosis by mouse peritoneal macrophages was dose-dependently inhibited by polyinosinic acid and fucoidan, suggesting that a scavenger receptor A (SR-A) mediated endocytosis is involved for this contrast agent (Raynal et al., 2004).

In general, phagocytosis is typically restricted to specialised mammalian cells, including macrophages, monocytes and neutrophils. Pinocytosis, which occurs in all cells, most commonly refers to the constitutive formation of smaller vesicles carrying extracellular fluid and macromolecules non-specifically bound to the plasma membrane. Receptor-mediated endocytosis includes clathrin-mediated endocytosis and caveolin-mediated endocytosis (Conner and Schmid, 2003).

Biologically, the main requirement for MRI is that the cells efficiently capture the IONPs they are exposed to by endocytosis pathways (Berry and Curtis, 2003). Particles taken and stored in coronary artery cells were described by (Panyam and Labhasetwar, 2003). The nanoparticles internalisation is in part through fluid phase

pinocytosis and in part through clathrin-coated pits. Caveoli and phagocytosis were not involved in nanoparticle uptake in this cell line. Following their uptake, nanoparticles were transported to primary endosomes and then probably to sorting endosomes. From sorting endosomes, a fraction of nanoparticles is sorted back to the cell exterior through recycling endosomes, while the remaining fraction is transported to secondary endosomes, which then fuse with lysosomes. Then the nanoparticles can escape the endo-lysosomes and enter the cytosolic compartment. The acidic pH of endo-lysosomes is schemed as the mechanism responsible for the endo-lysosomal escape of the nanoparticles. The early endosomes have an acidic pH (pH 5.5), while the later lysosomes have a lower pH (pH 4.5) and return to pH 7.4 in cytoplasm. The change of surface charge is from negative in early endosomes to positive in later endosomes and then back to positive in cytoplasm, therefore involving the transfer of protons / hydronium ions from the bulk solution to the nanoparticle surface under acidic conditions.

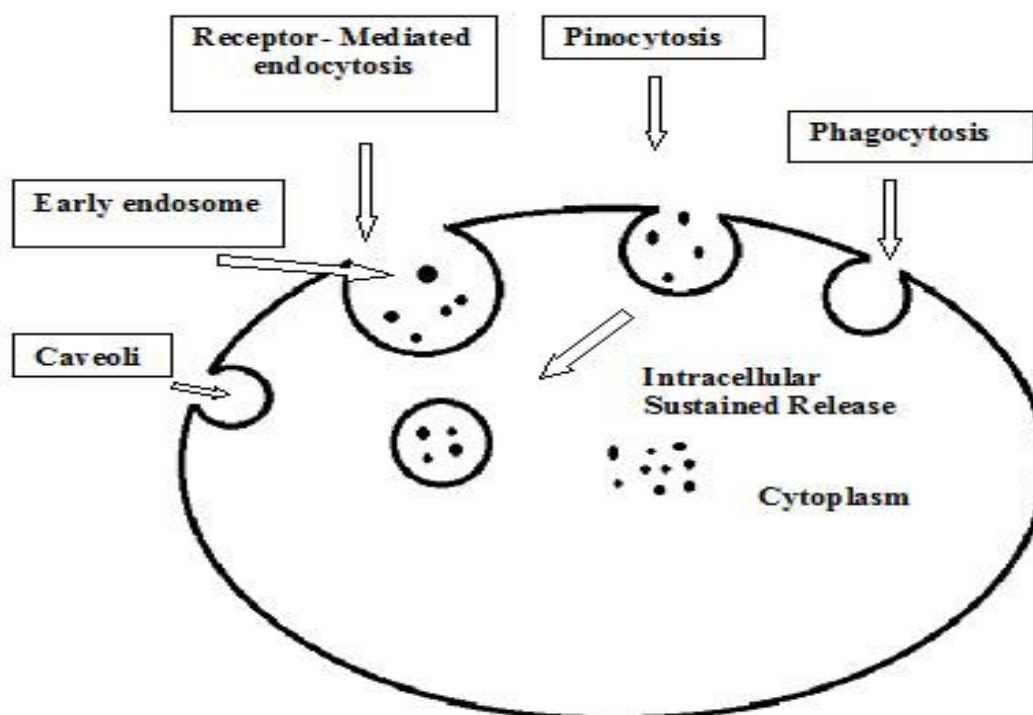


Figure 1-1: Intracellular pathways of nanoparticles and sorting.

After entering into the cell, nanoparticles taken up by phagocytosis or receptor-mediated endocytosis transfer to early endosomes and are then transported to the late endo-lysosome where they are degraded by high and low acidic compartments. A fraction of nanoparticles recycles back to the cell exterior while another fraction is transported to secondary endosomes/lysosomes from where nanoparticles may escape into the cytoplasm. Nanoparticles that escape into the cytoplasm could act as intracellular reservoirs for sustained release of an encapsulated therapeutic agent.

1.9 Effect of Particles and Surface Coating

The factors affecting biodistribution are particle size, surface charge, and surface coating and the type of coating and concentration, i.e. these are used to enhance the function of nanoparticles in all biomedical applications. Large particles with a diameter more than 200 nm are adsorbed by spleen phagocytic cells. However, small particles with a diameter less than 10 nm are quickly removed through extravasation and renal clearance. Particles which have sizes from 10–100 nm are suitable for injection and illustrate the most prolonged blood circulation times, their size being

very suitable to evade the RES of the body, and can enter the very small capillaries within the body tissues (Stolnik et al., 1995).

They are distributed in tissues according to their size and have two types of targeting. PASSIVE TARGETING, where SPIONs have a size more than 40 nm and thus accumulate in mononuclear phagocyte organs and are quickly cleared in less than 10 min by the reticuloendothelial system (Mornet et al., 2004). Ultrasmall paramagnetic iron oxide (USPIO) nanoparticles, on the other hand, are called monocrystalline iron oxide nanoparticles (MION)s and will have a size less than 40 nm with a polymer coating and a half-life of more than two hours. The second type of targeting is ACTIVE TARGETING, which is the surface coating by different biocompatible materials such as antibodies, proteins and DNA fragments and polysaccharides. These agents are specific for certain tissues because of specific biological interactions (Mikhaylova et al., 2004, Perez et al., 2003 and Illum et al., 2001). In ferrofluid, distribution parameters were found to depend on the sizes and coating materials of iron oxide particles in the fluid. The biodistribution of iron oxide with large size > 30 nm lead to accumulation in the lung and spleen. However, small size particles < 30 nm lead to accumulation in the liver, lymph nodes and bone marrow (Weissleder et al., 1995b). IONPs coated with $N(CH_3)_4OH$ showed a good distribution and superparamagnetic behaviour on MRI (Cheng et al., 2005).

IONPs were made with different hydrodynamic diameter of 10, 20, 33, 46 and 65 nm and then coated with carboxydextran. When injected intravenously they gave a good distribution with prolonged signal enhancement up to 25 minutes when compared to gadopentate dimeglumine (Allkemper et al., 2002). Superparamagnetic particles of 14 nm coated with poly(ethylene glycol) and phosphate micelle coating have good delivery into primary human dermal fibroblast cells. Particles showed good advantage for MRI intracellular molecular imaging (Nitin et al., 2004).

In another case, when iron oxide particles were coated with starch (starch-coated SPION) with size of 42 nm, which was smaller than commercially available magnetic nanoparticles, and injected into brain parenchyma they exhibited a

biocompatibility and a possibility of being transported in the extracellular space and being internalised in nerve cells to give good imaging (Kim et al., 2003a).

Many authors found that when iron oxide particles were coated with a thick layer of dextran, the particles accumulated in the lymph nodes (Papisov et al., 1993). The mechanism of particle uptake is that they infiltrate all the cells then into the bone marrow and reticulo-endothelial structures (liver, spleen and lymph). Iron oxide particles with diameter 30–150 nm coated with polymers such as albumin, silicones and starch can also be used as MRI contrast agents (Babes et al., 1999).

Bulte et al., (1999) have prepared magnetoliposomes with poly(ethylene glycol) coating as contrast agent and tried to increase the rapid uptake of the magnetoliposomes by the reticulo-endothelial cells. It can be seen from all these studies that the size, surface charge, kind of coating, the organ of the body and the concentration of iron all affect the biodistribution.

1.10 Poly(Glycerol Adipate) Polymer

Substituted poly(glycerol adipate) (PGA) was designed as a novel biodegradable polymer by Dr Martin Garnett and Dr Christopher St Pourçain and prepared by Dr Gillian Hutcheon. It has been synthesised from glycerol and divinyladipate using the enzyme Novozyme 435 as a catalyst.

PGA has been developed in response to the need for relatively higher drug loading and sustained release of encapsulated therapeutic agent. Moreover, PGA with hydrolysable ester bonds and side chains with hydroxyl groups offer flexibility to substitution by an aliphatic group such as C₈ and C₁₈ with a variety of proportions: 40%, 80% and 100%. Recently, PGA has been used in nanoparticles production for drug delivery by loading with anticancer drugs such as cytosine arabinoside and dexamethasone phosphate. It showed high loading and sustained release after side chain modifications. The best methods to prepare these nanoparticles and the use of overcoatings like Tween 80 have been investigated. In the cell work, PGA has been

used in investigating the cell uptake and metabolism and penetration in different cell types and models (Meng et al., 2006 and Puri et al., 2008).

PGA has also been used in microparticles to incorporate model protein with surface bound ligand to encourage cellular aggregation. In this study, PGA was coupled with different polymers through the hydroxyl groups. Coupling PGA to PEG has also been described by James Rimmer in his thesis (2009). Polymer PGA backbone and backbone acylated by aliphatic groups of aliphatic groups of hydroxyl group with proportions of 20%, 40%, 60%, 80% and 100% will be used as coatings through the thesis.

1.11 Aims of this Project

This project's aim was to establish a system for manufacturing polymer coated IONPs with small size suitable for use as contrast agents in MRI. The project emphasis will be on the polymer coatings and drug delivery aspects of the system

The project will go through the stages, which are necessary to build a strong basic system that could be used in a number of applications

The first aim is to develop a method with right parameters to produce model IONPs which are a suitable size to be candidate diagnostic agents in MRI. I will investigate the factors governing the particle size and produce particles with a suitable size for this work.

The second goal is using dextran and carboxymethyl dextran to coat these particles as reference. Dextran coated particles have been extensively investigated and are used clinically. This will give a starting point and help to identify and overcome some problems of coating iron oxide with those and other polymers.

The third objective is preparation of novel small size coated nanoparticles with novel polymer PGA and show in detail the influence of factors affecting the polymer coating of nanoparticles by using different methods adjusting the parameters effect

on the particles size, like the amount of polymer and solvent. The objective is to produce IONPs coated with biodegradable polymers in a simple process resulting in nanoparticles comparable in size with the best currently available formulations (i.e. a size range of 20–60 nm diameter)

The fourth aim is to improve the stability of nanoparticles and the chance for more modifications, by modifying PGA polymer and to assess the efficacy of the system. Also synthesis of PEGylated PGA 40% C_{18} will be carried out and this material used in coating nanoparticles.

The fifth aim is to assess the stability of the nanoparticles for use in physiological conditions.

The final project objective is investigation of uptake, metabolism and penetration of polymer coated nanoparticles by incorporating fluorescent dyes and using cell monolayers and aggregates in tissue culture model system.

CHAPTER 2

2. MATERIALS AND METHODS

2.1 Materials

All chemicals used in this project were purchased from Sigma-Aldrich (Poole, UK) unless specifically stated. The water was obtained from an ELGA purification system (resistivity 12-15M Ω cm⁻³, Maxima USF ELGA, Wycombe, UK). Water used in cell culture was of tissue culture grade.

The reagents used for cell work were obtained from Invitrogen Life Technologies Ltd. (Paisley, UK). Fluorescent dyes were purchased from Molecular Probes (Invitrogen, UK). All reagents used in TEM were from Agar Scientific Ltd. (Essex, UK).

2.1.1 Reagents and Buffers

HEPES (0.01M buffer N-(2-hydroxyethyl) piperazine-N'-(2-ethanesulphonic acid) was adjusted to pH 7.4 with sodium hydroxide.

Phosphate buffered saline (PBS, 0.01M, pH 7.4) was prepared by dissolving the tablets in 200ml in purified water.

Paraformaldehyde (8 g) was dissolved in 100 ml water including 3–4 drops of 5M Sodium hydroxide, heated to 60°C in a fume hood, then the solution became clear and was allowed to cool and was filtered.

Fixative 4% was prepared by mixing 80 ml of 10% paraformaldehyde and 100 ml 0.2M phosphate buffer pH 7.4. Water (20 ml) was added to the mixture and the pH was adjusted to between 7.2–7.5 and finally stored at $\leq 20^{\circ}\text{C}$.

4',6-diamidino-2-phenylindol dilactate (DAPI) was dissolved in water to prepare a 5mg/ml solution which was aliquoted to the final required concentration then stored at $\leq 20^{\circ}\text{C}$. Poly(D-Lysine) (PDL) for biological study was prepared to the required strength with water.

Newborn calf serum (NCS) was heated inactivated for 30 min in a water bath at 37°C . Minimum essential medium (MEM) was purchased from Gibco (Paisley, UK).

Trypsin/ethylene diamine tetra-acetic acid (EDTA) was composed of 0.25 % (w/v) trypsin and 0.01 % (w/v) EDTA in sterile PBS. All materials were stored at $\leq 20^{\circ}\text{C}$ for long term and $2-6^{\circ}\text{C}$ for short time storage.

2.2 Methods

2.2.1 Synthesis of Iron Oxide Nanoparticles

2.2.1.1 The effect of pH on the size

To establish a method to produce the right size of IONPs, four preparations were prepared using the co-precipitation method at different pH (7, 4, 2 and 0.5)

2.2.1.2 Preparation of iron oxide nanoparticles (IONPs)

IONPs were prepared by alkaline co-precipitation. Ferrous chloride tetrahydrate (0.49 g) was suspended in ferric chloride hexahydrate (1M, 5.06 ml). Pure water (6 ml) was added under nitrogen with rapid stirring then heated to 80°C for 1hr. The mixture was cooled to room temperature then precipitated by adding NaOH (6 M, 6.5 ml) rapidly. After adding 4 M HCL to the mixture to neutralise to pH 0.5, it was refluxed for 1 hr under nitrogen gas. In this step, the black colour turned brown. The reaction was allowed to cool to room temperature; the mixture was dialyzed using a MWCO 1000 dialysis tubing overnight against deoxygenated water to remove any salts. This modified method was based on that by (Kresse M, 1998).

2.2.2 Stability of Uncoated Iron Oxide Nanoparticles

To compare two samples of uncoated IONPs to identify the stability of the nanoparticles over a seven day period.

IONPs were prepared as above, except that at the neutralisation step, particles were adjusted to pH 0.5 and pH 1.0 before reflux and dialysis. Each nanoparticle sample was stored in a glass beaker covered with parafilm in the refrigerator at 4°C. The particles size of each sample was assessed daily for seven days using DLS.

2.2.3 Synthesis of Carboxymethyl Dextran

Different functionalised dextrans using chemical groups like carboxymethyl, benzylamide and sulphonate have been widely studied for more than fifteen years, particularly for biological heparin-like activities. The reaction to produce carboxymethyl dextrans (CMD) involves the carboxymethylation of hydroxyl group on D-glucose unit of carboxylic group (Mauzac. M., 1984 and Chaubet.F., 1995).

2.0 g of dextran (Mw 40,000) was dissolved in 42.5 ml distilled water and 20 ml of chloroacetate acid added. The carboxymethylation reaction was initiated by the addition slowly of 7.5 ml of 3.8 M NaOH. The system is subjected to contentious stirring during 1 h at room temperature. The reaction mixture was then diluted to 50 ml total volume with water. Carboxymethylation was allowed to proceed for 90 min at 60 °C with stirring. The reaction was then terminated by lowering the solution pH to 7 with 6 M HCl. The product was precipitated with 50 ml absolute methanol and allowed to stand overnight. The precipitate was dissolved in water, then was dialyzed by using a M WCO 100 dialysis tubing over night. The dialysed solution was rapidly frozen using liquid nitrogen and dried in freeze dried two days, giving a white powder. The method was based on (Rémi.H., 1998).

(CMD) with a degree of substitution (DS) of Carboxymethyl groups $DS > 0.9$ are precursors for the synthesis of derivatised dextrans termed CMD which present heparin-like biological properties (Rémi.H., 1998).

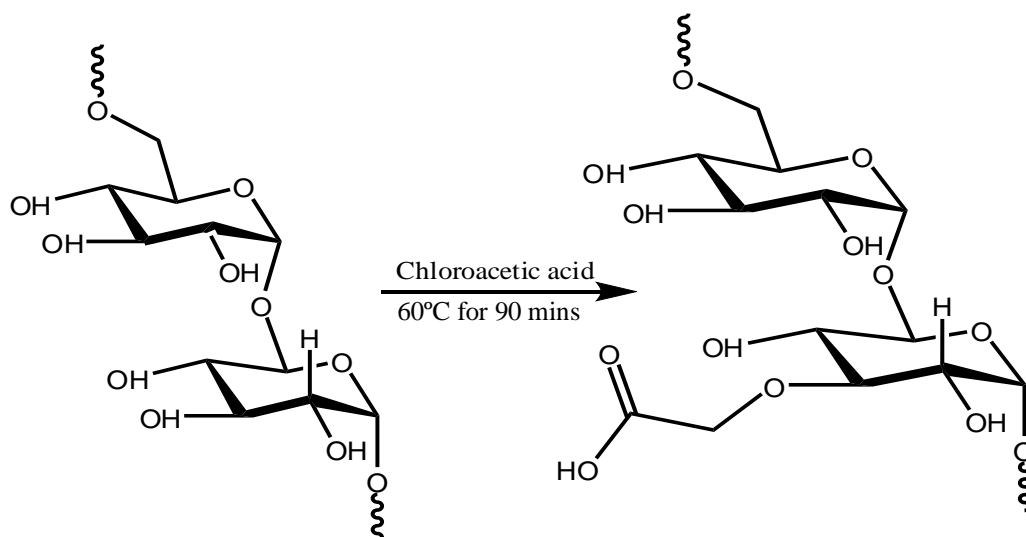


Figure 2-1: Synthesis of Carboxymethyl Dextran.

2.2.3.1 Determination of degree substitution of carboxy methyl dextran.

The substitution of carboxylic group on modified dextran was determined by dissolving 2 mg of the product in 3 ml of acetic acid and titrating with NaOH 0.1 M.

2.2.4 Preparation of Iron Oxide Nanoparticles Coated with Carboxymethyl dextran in the absence or presence of CMD

2.2.4.1 In the absence of CMD

An aqueous solution containing ferrous chloride tetrahydrate (0.49 g) and ferric chloride hexahydrate (6 M, 5.06 ml) was heated to 80°C with stirring under a nitrogen stream for 30 min. The product was then precipitated by rapid addition of NaOH (4 M, 3.4 ml) within 30 sec. After neutralisation with 6 M HCL, the mixture was refluxed for 1h. The mixture was dialysed using a MWCO 1000 dialysis tubing overnight. The CMD-coated nanoparticles were prepared by dissolving the CMD (1.9 g) into a minimum amount (2 ml) of pure water. The CMD solution was added slowly dropwise to the nanoparticles at 70°C under a nitrogen stream.

2.2.4.2 In the presence of CMD

In a typical procedure, CMD (1.9 g) was dissolved in pure water (6.3 ml) and then added dropwise to an aqueous solution containing ferrous chloride (0.49 g) in ferric chloride (6 M, 5.06 ml). The mixture was heated to 80°C with stirring under N₂ atmosphere for 1 h. After cooling to room temperature, the mixture was dialyzed with a membrane MWCO 1000 against water overnight to remove unincorporated inorganic material. These modified methods were based on (Kresse et al., 1998).

2.2.5 Dextran Coated Iron Oxide Nanoparticles.

The preparation of dextran (MW 1000 Da) coated IONPs was prepared as above in the presence of unmodified dextran.

2.2.6 Poly (glycerol adipate) PGA Coated Iron Oxide Nanoparticles

Poly (glycerol-adipate) (PGA) was provided by Dr G.A. Hutcheon and Dr S. Higgins of Liverpool John Moores University, U.K. The method of synthesis and structure of PGA are shown in Figs. 2.2 and 2.3 and were described by (Kallinteri. P., 2005).

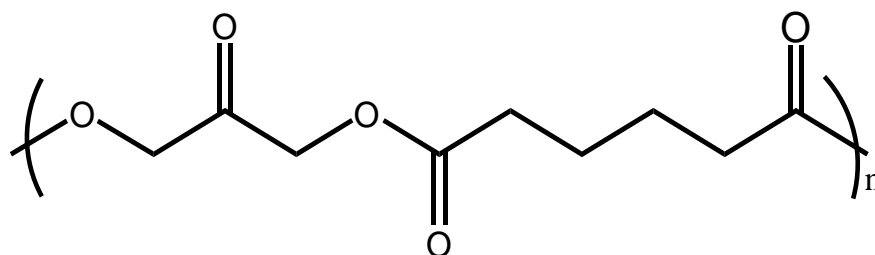


Figure 2-2: Structure of poly (glycerol adipate) backbone.

IONPs were coated with PGA by using the modified interfacial deposition method. Briefly, PGA (20 mg) was dissolved in acetone (2 ml) then the solution was added dropwise to an aqueous solution containing IONPs (2 ml) suspended in pure water (3 ml) under gentle stirring. The product was stirred overnight in a fume hood to

allow evaporation of the organic solvent. This modified method was based on that of Fessi et al. (1989) for polymer nanoparticle production.

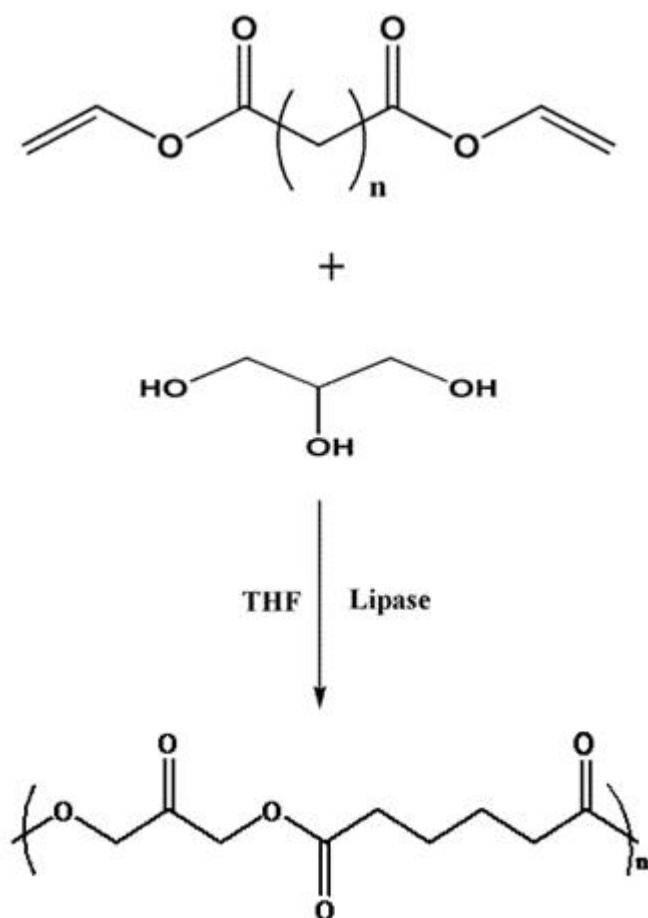


Figure 2-3: Synthesis of poly(glycerol adipate) PGA.

2.2.7 Optimisation of Nanoparticle Coating Produced with PGA

The important goal of this experiment was synthesise PGA coated nanoparticles with small size and thin coatings. Briefly, the amount of PGA was reduced (1 mg, 0.5 mg, 2 mg and 0.1 mg) and the amount of solvent (acetone) was increased using the interfacial deposition method. PGA samples (2 ml) were added to IONPs (5 ml) under stirring. The nanoparticles were then left stirring overnight in a fume hood to allow evaporation of the acetone.

2.2.8 Purification of PGA-Coated Iron Oxide Nanoparticles

A very low concentration of NaCl (200 μ L, 3 mM) was added to 1 ml of PGA coated IONPs. The mixture was left for 5 min then centrifuged for 2 min (MSE microcentaur microcentrifuge, 13,500 rpm) to remove large and uncoated aggregates. The supernatant was then used as purified polymer coated IONP.

2.2.9 Modification of PGA Polymers

2.2.9.1 Synthesis of PGA 40% C_{18} by acylation of backbone PGA

Dry THF (20 ml) was added to PGA (2 g, 0.16 mmol) in a round bottomed flask and refluxed under a nitrogen atmosphere at 80 °C to dissolve the polymer. Stearoyl chloride (656 mg, 43 mmol) was warmed to 25 °C in a small flask and dried THF (0.5 ml) added. The stearoyl chloride was then added to a flask containing the PGA. The flask containing stearoyl chloride was washed three times with dried THF and washings added to the mixture. Pyridine (0.5 ml) was also added to the mixture. The system was refluxed for two hours. The reaction was cooled to room temperature and (30 ml) of DCM added and then poured into a mixture of pure water (20 ml) and of 1 M HCl (0.5 ml) and washed twice in a separating funnel. The polymer was then washed using a further aliquot of acidified water as above. The initial reaction vessel was rinsed with DCM (10 ml), and the organic fraction then combined with the collected fraction. The organic fraction was washed twice with pure water (40 ml) following which the polymer was dried using $MgSO_4$. The product was filtered through a filter paper with DCM to remove flocculated $MgSO_4$. Product was obtained by removal of DCM using a rotary evaporator.

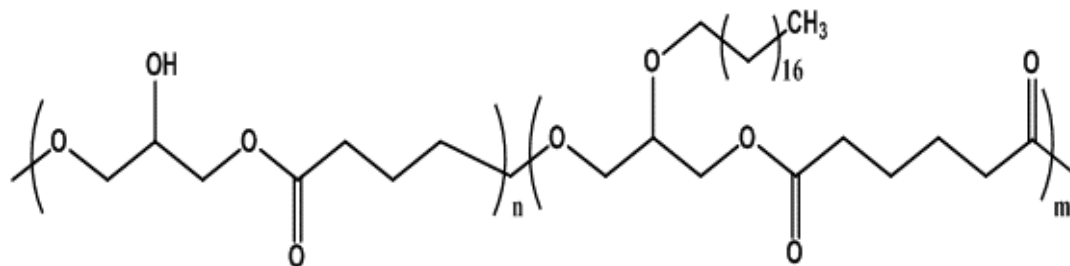


Figure 2-4: Structure of poly(glycerol adipate) 40% C_{18} .

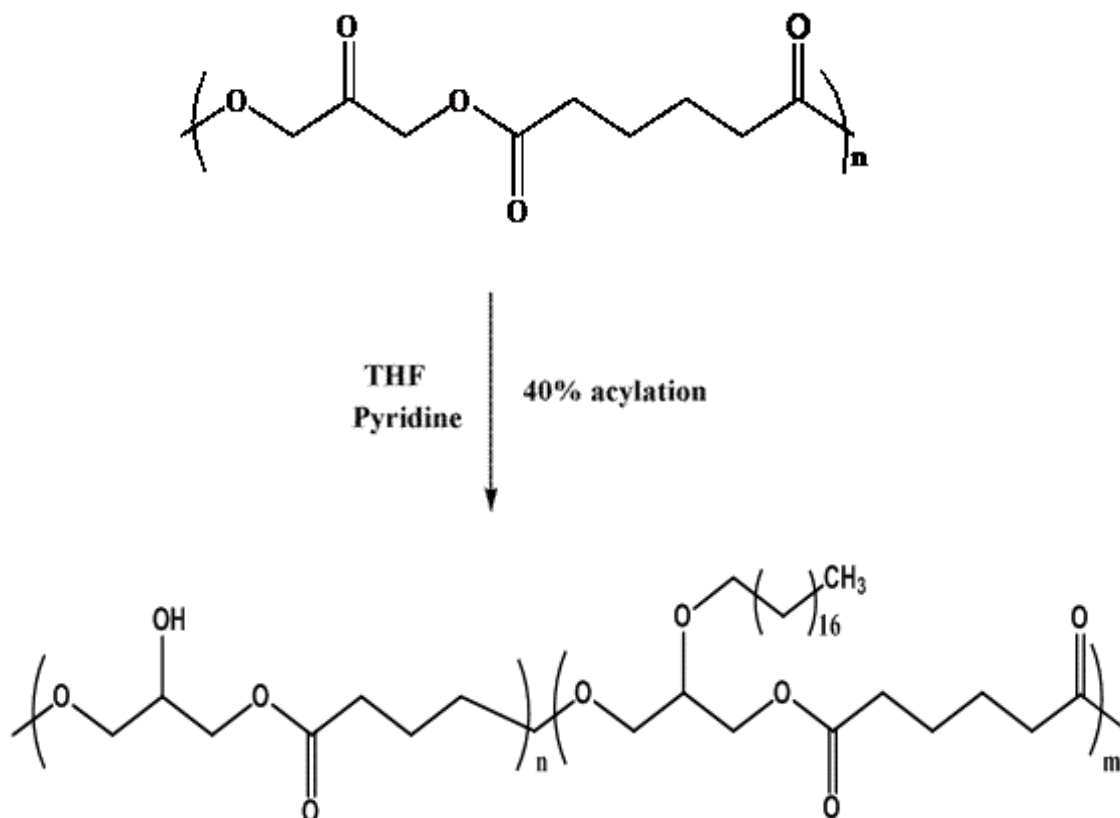


Figure 2-5: Synthesis of poly(glycerol adipate) 40%.

2.2.10 Poly(glycerol adipate) 40% C_{18} Coated IONPs

IONPs were coated with PGA 40% C_{18} using the interfacial deposition method with changes in the amount of polymer and solvent.

2.2.11 0.1% Tween80-coated PGA-coated IONPs and PGA 40% C_{18} coated IONPs

After coating the IONPs with the polymer, 0.1% Tween 80 (2 ml) was added to the 0.2 mg of polymers (PGA and PGA 40% C_{18}) coated IONPs and the stirred for 5 min.

2.2.12 0.1% Albumin-coated PGA-coated IONPs and PGA 40% C_{18} -coated IONPs

NPs were coated with 1% albumin in a method similar to that used for the 0.1% Tween 80 as above.

2.2.13 PEGylated PGA 40% C_{18}

PEGylated PGA substituted with 40% C_{18} acyl groups. Briefly, PEG-NH₂ with M_n of 2000 was dried by MgSO₄ in DCM and precipitated with cold ether, then filtered and dried under vacuum. Carbonyl di-imidazole (CDI) was prepared by dissolving CDI (40 mg, 0.25 mmol) in DCM (5 ml). The PEGylation reaction was carried out by dissolving PEG-NH₂ (110 mg, 0.05 mmol) in chloroform (3 ml) in a double-necked round-bottomed flask and then CDI (1 ml) solution was transferred to the CH₃-O-PEG-NH₂. The polymer PGA 40% C_{18} (600 mg, 0.05 mmol) was then dissolved in DCM (10 ml) under stirring. The CH₃-O-PEG-NH₂ solution was added to the PGA40% C_{18} solution. The resulting product was stirred for 7 days under a nitrogen atmosphere. After this time, the product was obtained by removal of the solvent by vacuum. Excess unreacted polymers PEG or PGA were also removed by washing the product by diethyl ether (1.5 ml) three times. The product was then allowed to dry for 30 min.

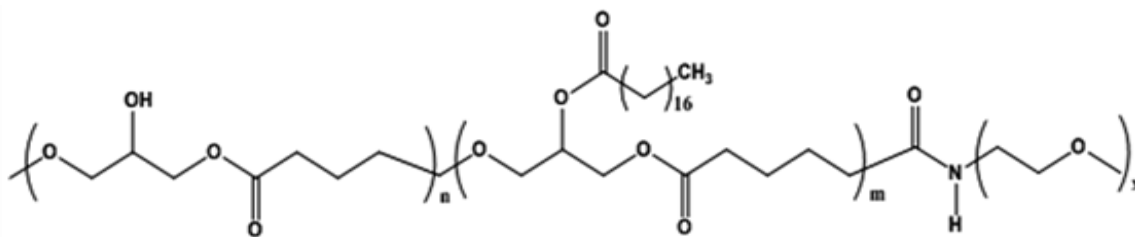


Figure 2-6: Structure of PEGylated poly(glycerol adipate) backbone substituted with acyl group 40% C_{18} .

2.2.14 PEGylated PGA 40% C_{18} Coated IONPs

Different amounts of PEG-PGA 40% C_{18} (0.2 mg, 0.1 mg and 0.05 mg copolymer in 2 ml acetone) were added dropwise to an aqueous solution containing IONPs (2 ml) suspended in pure water (3 ml) under gentle stirring. The product was stirred overnight in a fume hood to allow evaporation of the organic solvent. (This modified method was based on that of Fessi et al. 1994 for polymer nanoparticle production.)

2.2.15 Stability of Iron Oxide Nanoparticles Coated with polymer

The IONPs uncoated and coated were investigated by turbidity measurements following salting out with a range of NaCl concentrations (1 mM to 600 mM). After rapid homogenisation the samples were left for 5 min and then the turbidity was measured by light absorption at a wavelength of 500 nm.

2.2.16 RBITC Labelled PGA-Coated Iron Oxide Nanoparticles

RBITC labelled nanoparticles were prepared as follows. RBITC in acetone (125 μ l, 2 mg/ml) was added to PGA-coated IONPs (7 ml) under stirring for 5 min as the organic phase. The mixture was diluted into HEPES (0.01M, pH 7.4, and 7 ml) under magnetic stirring. The mixture was left stirring with an aluminium foil cover

overnight in fume hood to allow the acetone to evaporate. The product was dialyzed against pure water using a MWCO 1000 dialysis tubing to remove excess rhodamine.

2.2.17 Determination of Fluorescent Dye Loading

The amount of fluorescent dye encapsulated was determined by a direct method. Freeze-dried Rhodamine B Isothiocyanate (RBITC) labelled PGA-coated IONPs were dissolved in an acetone/methanol (2:1 ratio) organic solvent mixture. The fluorescent solution was measured at $\lambda_{Ex}=554$ nm, $\lambda_{Em}=575$ nm, slit width=5.0 (Hitachi F-4500 fluorescence spectrophotometer, Hitachi Scientific Instruments, Finchampstead, UK). The amount of fluorescent dye was calculated by using a standard curve of RBITC fluorescence in HEPES buffer (0.01 M, pH 7.4). The experiment was repeated with RBITC at concentrations ranging from 1.25 $\mu\text{g/ml}$ to 5 $\mu\text{g/ml}$.

2.2.18 Cell Culture Studies

2.2.18.1 Preparation of the nanoparticles for cell work

To avoid hypotonicity, nanoparticles in water (5 ml) were added to a 2x concentrated medium to give a stock particle solution. Particles were then used undiluted (1.0ml nanoparticles) or diluted 1:2, 1:5 and 1:10 in a normal cell culture medium to give various concentrations of the nanoparticles added to the cells, described as 0.5, 0.2 or 0.1 ml of nanoparticles. .

IONPs were calculated to be at a concentration of 0.34 M (19 mg/ml) with respect to iron. The concentration of coated IONPs was 0.07 M (3.92 mg/ml) diluted into medium to give amounts of 1.96, 0.98, 0.39 or 0.2 mg of nanoparticles added to cells.

2.2.18.2 C6 cell

The C6 cell line was obtained from the American tissue culture collection and is a brain derived rat glioma line which has fibroblast morphology and adherent growth properties.

2.2.18.3 Preparation of media for C6 cell line

These require full culture media supplemented with 10% foetal calf serum, sodium bicarbonate and 2 mM L-glutamine. 100 ml, 10x Minimum Essential Medium (MEM) (10 ml) was added to new-born calf serum (10 ml) and then sodium bicarbonate (5 ml) was added to the mixture followed by the addition of glutamine (one aliquot of 1 ml 200 mM glutamine). The medium was then made up to 100 ml with super ultra-pure water (SUPW) and filtered through a 0.2 µm sterile filter.

2.2.18.4 Routine cell culture

The C6 glioma tumour cells were cultured as monolayer in 75-cm² culture flask in medium composed of 10% foetal calf serum, 7.5% sodium bicarbonate, L-glutamine, MEM and SUPW. Cells were incubated at 37°C with 5% CO₂ and 100% humidity and passaged every 5–7 days at about 80%–90% subconfluency.

2.2.18.5 Washing coverslips

Coverslips were handled by wearing gloves to avoid deposition of fingerprints etc. SUPW (100 ml) was added to the coverslips in a 250 ml glass beaker then sonicated for 20–30 minutes and rinsed with running SUPW from the water tank for a 30 minute slow rinse. HCl (1M, 50 ml) was added after removing the water and sonicated for 20–30 minutes. The HCl was removed and the coverslips rinsed 6 times with water. The covers were then placed on a filter paper in a large petri dish using forceps, sealed, dried and heat-sterilised in an autoclave overnight.

2.2.18.6 Coating coverslips with poly-D-Lysine (PDL)

PDL was stored in aliquots (10 ml) in the freezer at 1 mg/ml. PDL (100 µg/ml) was prepared to coat coverslips. The coverslips were placed in 24 well plates and then enough PDL was pipetted until the surface was covered (approximately 1 ml) and then the coverslips were allowed to stand in a laminar flow hood overnight. The coverslips were washed three times with SUPW and after the last rinse were left to stand in a laminar flow hood overnight. The water was then removed and the coverslips left to dry in a laminar flow hood.

2.2.18.7 Cell staining for fluorescence microscopy

Medium was removed and then cells were washed and fixed then mounted with a drop of DAPI.

2.2.18.8 Cell staining for confocal microscopy

A stock solution of DAPI (20 µl) was diluted into PBS (10 ml). The stain (0.5 ml) was added to the cells and then left for 10 min, before the solution was removed.

2.2.18.9 Qualitative nanoparticle uptake by cells study

Cellular uptake studies were carried out with 0.1% Tween-PGA 40% C_{18} -coated IONPs and PEG-PGA 40% C_{18} coated IONPs. The subcellular localisation of nanoparticles following uptake was investigated using fluorescence microscopy and confocal fluorescence microscopy. C6 cells growing in monolayers on PDL-coated coverslips in 24 well plates were incubated with a quantity of RBITC labelled polymer coated IONPs for 2 h and then washed twice with PBS and fixed with 4% paraformaldehyde. The cells were washed again with PBS and left in PBS for microscopy. The uptake was evaluated either with or without serum present with different doses of particles (1 ml, 0.5 ml, 0.2 ml and 0.1 ml).

2.2.18.10 Qualitative uptake of nanoparticles in C6 cells

Uptake was determined in the continuous presence of particles. C6 cells growing in monolayers on PDL-coated coverslips in 24 well plates were incubated with polymer-coated IONPs for varying periods of time (1 h, 2 h, 4 h, 6 h, 8 h, 12 h, 18 h and 24 h) then washed. Cells were then mounted with a drop of DAPI, and visualised under fluorescence or confocal microscopy.

2.2.18.11 Qualitative uptake and metabolism of nanoparticles in C6 cell

C6 cells growing in monolayers on PDL coated coverslips in 24 well plates were incubated with polymer coated IONPs for 1 h then washed off and incubated for varying periods of time (1 h, 2 h, 4 h, 6 h, 8 h, 12 h, 18 h and 24 h). The cells were then mounted with a drop of DAPI, and visualised under fluorescence or confocal microscopy.

2.2.18.12 Evaluation of time-dependent uptake of NPs by cells growing in monolayer culture using TEM

To demonstrate subcellular localisation of NPs in the cells for different time periods, cells were seeded on an insert membrane in a 12 well plate and incubated overnight. NP suspension (1 ml) was added to the cells and incubated with media and serum at 37 °C for increasing time intervals from 1 h, 4 h, 12 h and 24 h before dehydration and embedding.

2.2.18.13 Dehydration and embedding of cells

C6 cells were incubated with NPs for (1 h, 4 h, 12 h, and 24 h and rinsed with PBS three times. The cells were fixed in 4 % PFA and 3% glutaraldehyde in cacodylate (0.1 M) buffer for 1 hr and then postfixed in 1% osmium tetroxide for 1h. The cells were dehydrated in a graded series of ethanol solutions (60 %, 80 % and 100 %) then they were soaked in a mixture of 100 % 1, 2-epoxypropane and agar embedding resin

at 1:1 ratio overnight at 4°C. After that they were soaked three times in fresh neat agar resin for 2 h and then placed in a vacuum oven at 60°C for 2 days for polymerisation of resin. The polymerised blocks were then cut into sections (80–100 nm thick). Then sections were placed on formvar-coated copper grids, stained with an aqueous solution of 2% uranyl acetate for 10 min and washed by soaking them in water about 10 times, then stained with Reynolds lead citrate for 5 min and washed again with water before visualisation. Samples were imaged under TEM with magnifications from 10,000 to 20,000x.

2.2.18.14 Quantitative NP uptake study dependent on dose and time

To demonstrate the amount of uptake of the NPs by the C6 cancer cells, C6 cells (1 ml, 1×10^6 cells) were put into Flow cytometry (FACS) tubes and NP suspensions were added in different doses 1 ml, 0.5 ml, 0.2 ml and 0.1 ml. The suspension was incubated for 2 h, and then centrifuged at 800 rpm for 5 min in an MSE centaur centrifuge (FISONS UK). The supernatant was removed, cells were washed once with PBS and centrifuged again. The supernatant was removed, cells were fixed with 4% PFA and kept until uptake was quantitated using FACS over time periods up to 24 h.

2.2.18.15 Quantitative determination of loss of nanoparticles from cells

C6 cells suspension at (1 ml, 1×10^6 cells) was put into flow cytometry tubes and NPs were added. The suspension was incubated for 1 h and the cells then centrifuged at 800 for 5 min. The supernatant was removed, and cells were washed once with PBS and were centrifuged again. The supernatant was removed and a medium with serum was added to the cells and the cells were incubated again for different time periods (1 h, 4 h, and 24 h), then cells were washed with PBS and fixed with 4% PFA and kept until flow cytometry measurement.

2.2.18.16 Aggregate cultures

C6 cells were grown in monolayers and detached from the substratum by using trypsin-EDTA. The C6 cell aggregates were formed using the rotation method. C6 cells (2 ml, 1×10^6 cells/ml) were cultured in C6 culture media in 10 ml screw top culture flasks (Scientific Laboratory Supplies, UK) and maintained at a constant rotation of 70 rev/min on an orbital shaker (Cole-Palmer, USA) at 37 °C overnight. Cultures were then observed and the medium was changed and the rotation decreased to 50 rev/min.

2.2.18.17 Cell aggregate uptake of RBITC NPs

After C6 cell aggregates were prepared (see 2.2.18.16) the growth medium was replaced with a new culture medium, then the aggregate suspension (50 µl) and fresh media (0.5 ml) were transferred to a well plate with a PDL-coated coverslip in 24-well plates. NPs were then added to the cells and incubated for a range of times (1 h, 4 h and 24 h) and at different doses (1 ml, 5 ml, 0.2 ml and 0.1 ml). At the end of the incubation period, aggregates were washed three times with PBS and fixed with 40% PFA paraformaldehyde for microscopic study.

2.2.19 Instrumental Methods

2.2.19.1 Measurement of particle size

Measurement of particle size was carried out using dynamic light scattering on a Viscotek 802 instrument. All measurements were performed at a temperature of 22 °C at a measuring angle of 90 °C to the incident beam. The analysis mode was CONTIN and 10 readings were taken for each sample. Data output is produced for a number of different parameters. Rh is the hydrated radius of the particles. The standard deviation (Std Dev) is the absolute value of the coefficient of variation. Percentage relative standard deviation (% RSD) is a normalized measure of dispersion obtained from the ratio of size and standard deviation.

2.2.19.2 Surface charge measurement

The ζ -potential of the nanoparticles was determined by laser Doppler anemometry (LDA). The principle of measurement of zeta potential is that an electric field is applied across the dispersion. Particles within the dispersion with a zeta potential will migrate toward the electrode of opposite charge with a velocity proportional to the magnitude of the zeta potential. This velocity was measured using the technique of laser Doppler anemometry. The frequency shift or phase shift of an incident laser beam caused by these moving particles is measured as the particle mobility, and this mobility is converted to the zeta potential by inputting the dispersant viscosity, then the velocity is analysed by a computer.

2.2.19.3 Transmission electron microscopy

The morphology of the particles was examined using TEM (Jeol Jem 1010 electron microscope, Japan). One uncoated IONP sample was examined using TEM without staining. One drop of the sample was placed for 1 minute on the copper grid with a formvar carbon film. The excess of the sample was whisked away with the aid of filter paper. The sample was then ready for analysis by TEM

A staining procedure was used for all other TEM analyses. A sample of particle suspension was diluted with 3% w/v phosphotungstic acid and adjusted to pH 7.5 with potassium hydroxide corresponding to a 1:1 ratio before examination. One drop of the sample was placed for 1 minute on a copper grid coated with a formvar carbon film. The excess of the sample was whisked away with the aid of filter paper. The sample was then ready for analysis by TEM.

2.2.19.4 Nuclear magnetic resonance spectroscopy (NMR)

Polymer samples (2 mg) were dissolved in 0.86 ml deuterated acetone, while pure amino acids (2 mg) were dissolved in deuterated methanol (1 ml) and subjected to NMR analysis. The NMR spectra were recorded on a Bruker 400 MHz spectrometer. The data was processed using the Omnispin software.

2.2.19.5 Fourier transformed infrared spectroscopy (FTIR)

Fourier transformed infrared (FT-IR) spectra were obtained on a Nicolet AVATAR 360 FT-IR spectrometer. Samples of polymers were prepared in KBr discs (2 mg sample in 200 mg KBr). The scanning range was 450–4000 cm^{-1} and the resolution was 1 cm^{-1} . Sample analyses were carried out using the E2 OMNIC software.

2.2.19.6 Flow cytometry

Flow cytometry (Fig 2.7) uses the principle of hydrodynamic focusing for presenting cells to a laser. The sample is injected into the centre of a sheath flow. The combined flow is reduced in diameter, forcing the cells into the centre of the stream and the sensing area of the flow chamber. One unusual feature of flow cytometry is that it measures fluorescence per cell or particle. This contrasts with spectrophotometry in which the percentage of absorption and transmission of specific wavelengths of light is measured for a bulk volume of sample. Cells or particles of interest intercept the light source. They scatter light and fluorochromes are excited to a higher energy state. This energy is released as a photon of light with specific spectral properties unique to different fluorochromes. Finally, scattered and emitted light from cells and particles is converted to electrical pulses by optical detectors. Collimated (parallel light waveforms) light is picked up by confocal lenses focused at the intersection point of cells and the light source. Light is sent to different detectors by using optical filters. The most common type of detector used in flow cytometry is the photomultiplier tube.

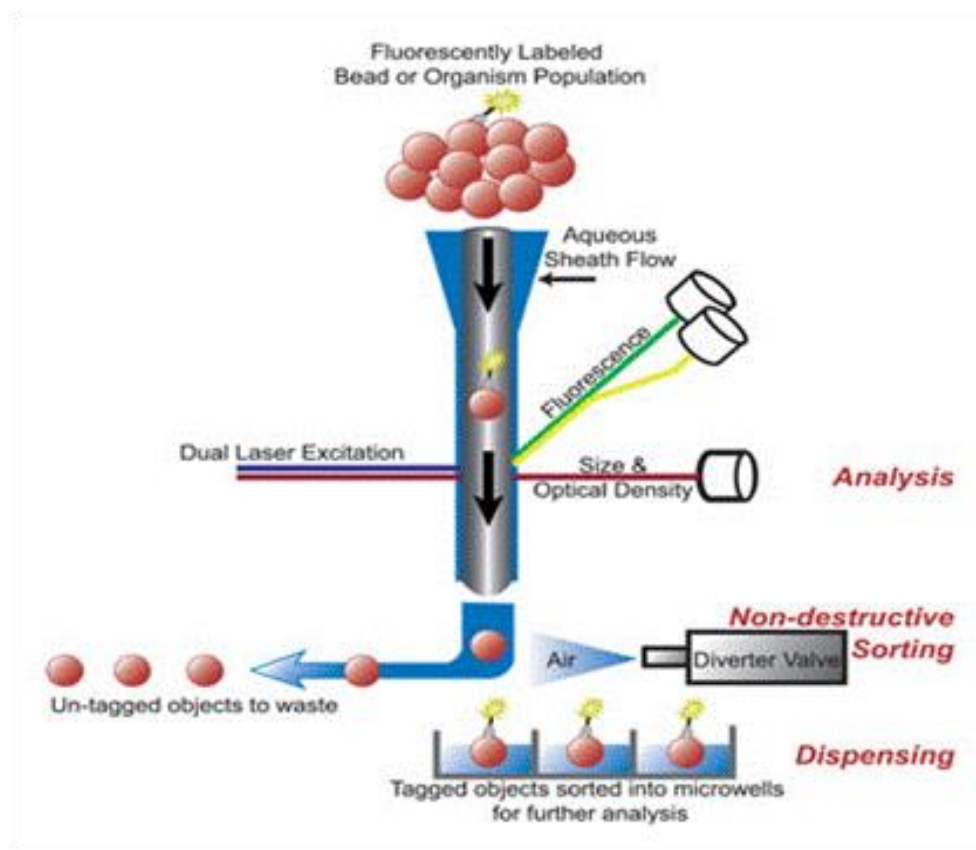


Figure 2-7: Principle of Flow Cytometry (website image).
(http://biology.berkeley.edu/crl/flow_cytometry_basic.html)

2.2.19.7 Method of measuring cell uptake NPs by flow cytometry

Cells were kept in 4% PFA tubes until quantitation by flow cytometry. The intracellular fluorescence intensity was determined on a Beckman coulter EPICS XL-MCL flow cytometer (BECKMAN Coulter, Buckinghamshire, UK) using XLSYSTEM IITM. The numbers of cells were measured by forward scatter while side scatter determined the amount of NP labelled with dye taken by cells.

2.2.19.8 Fluorescence microscopy

The principle of the fluorescence microscope is to let excitation light radiate the specimen and then sort out the much weaker emitted light to make up the image. The microscope has a filter that only permits passage of radiation with the desired

wavelength that matches your fluorescing material. The radiation collides with the atoms in the specimen and electrons are excited to a higher energy level. When they relax to a lower level, they emit light. To become visible, the emitted light is separated from the much brighter excitation light in a second filter. Here, the fact that the emitted light is of lower energy and has a longer wavelength is used. The fluorescing areas can be observed in the microscope and shine out against a dark background with high contrast.

2.2.19.9 Confocal laser scanning microscopy

The key working principle of the confocal laser scanning microscope (CLSM) is to restrict the illumination area by using an illumination point source. Hence, at a given time, merely local information from a very small sample area can be obtained. An image of the entire specimen surface is produced by a scanning mechanism. In addition to the small aperture used for illumination, a second small aperture is used in front of the detector. The intermediate image of the specimen in the back-focal plane of the objective lens is simultaneously placed in the focal plane of the collector lens (Fig. 2.8) which gives rise to the name "**confocal**". This leads automatically to a further important characteristic of the CLSM. Light rays with an origin off the optical axis and off the focal plane are focused in a different plane, and thus are excluded from image formation by the pinhole aperture. Because the CLSM is able to focus in the third dimension by moving step by step through the specimen, a laser, which has a small beam diameter and small beam divergence with high intensity, is generally used as a light source for CLSMs.

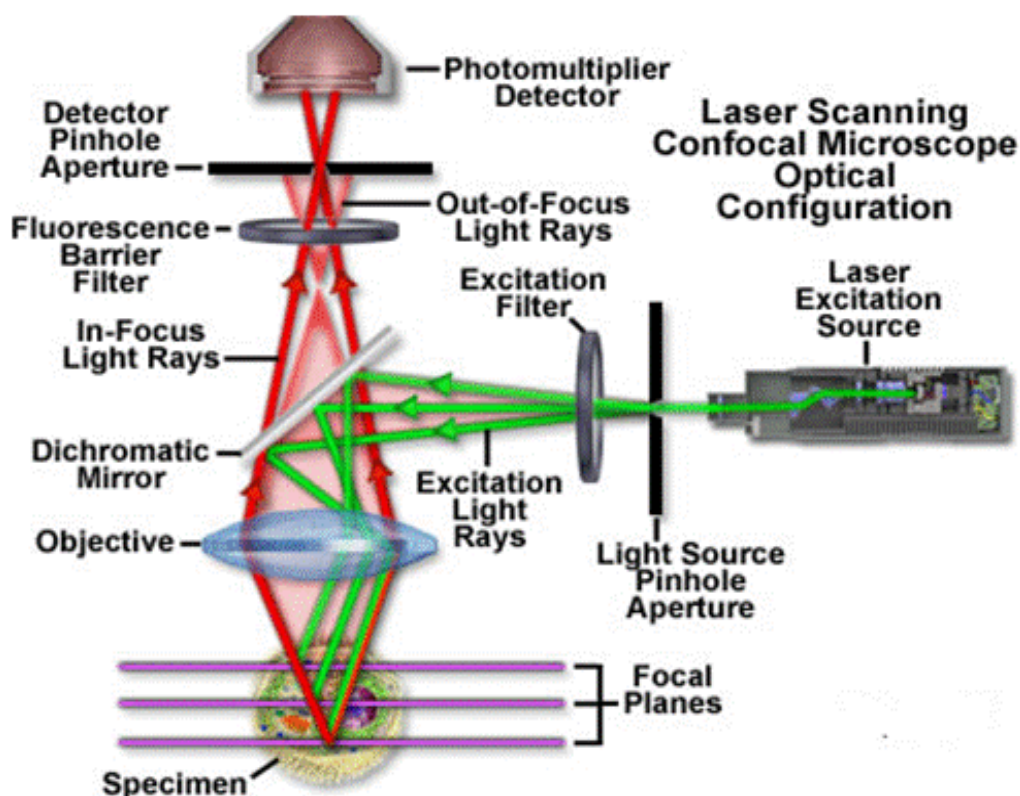


Figure 2-8: Principle of confocal laser scanning microscopy (website image). (http://www.fz-juelich.de/ibn/Light_microscopy/conf).

2.2.19.10 Method of fluorescence studies

The cells were carefully washed three times with PBS then fixed with 4% PFA, again washed three times with PBS, stained with DAPI and viewed using fluorescence microscopy (Leica DMRB, Leica Microsystem Wetzlar GmbH). Cell monolayers were imaged and visualised by adjusting the filters, which were DAPI for the nuclei and red plate for the rhodamine, using a high resolution camera and Openlab software. For confocal laser scanning fluorescence microscopy (Leica SP2 MP, Microsystem Ltd., UK) cells were pictured and viewed using UV laser (DAPI), 543 nm filter (RBITC), 488 nm filter (fluorescein) and 476 nm filter (Lyso Tracker).

CHAPTER 3

3. SYNTHESIS OF IRON OXIDE NANOPARTICLES AND NANOPARTICLES COATED WITH CARBOXYMETHYL DEXTRAN AND DEXTRAN

3.1 INTRODUCTION

Biodegradable polymers, synthetic and natural such as polysaccharides and proteins have been widely used and investigated for biomedical applications (Jeong et al., 1997 and Yamamoto et al., 1996). Dextran is a polysaccharide mainly composed of 1,6-linked D-glucopyranose residues. According to its biocompatibility and biodegradability, dextran and its derivatives have been used as blood substitutes and drug carriers (Hoste et al., 1994). Much work has been carried out to impart useful properties to dextran by different chemical modifications for various applications as drug carriers. (van Dijk-Wolthuis et al., 1997) developed non-degradable and degradable hydrogels using methacrylated dextrans and studied the degradation and drug release behaviour of the hydrogels. The degradation rate of the hydrogels was dependent on the amount of the encapsulated dextranase and the degree of substitution or crosslinking (Franssen et al., 1997). Carboxylated dextran is negatively charged because of the carboxyl group. Their function is to bind to cationic IONPs. The approach used in this work was to introduce carboxylic acid functionality in the form of a high acid value by acetic acid. The result showed a degree of substitution of carboxymethylated polysaccharide with dextran molecular weight of 10,000. Carboxylated polysaccharides with value of degree of substitution between 0.4 and 0.9 and a range of polymer molecular weights from 20,000 to 100,000 g/mol have been reported (Wotschadlo et al.,

2009a). Commercially available dextran-coated IONPs are currently in clinical use or in clinical trials as MRI contrast agents (Harisinghani et al., 1997).

IONPs have great potential as magnetic resonance (MRI) contrast agents due to their strong magnetic susceptibility and superparamagnetic properties (Koenig and Kellar, 1995 and Bulte and Kraitchman, 2004). The main problem with IONPs is the aggregation at biological pH, therefore the nanoparticles must be coated with biocompatible materials for medical applications. IONPs have been coated with many materials, including polyethylene glycol (PEG), starch and dextran, resulting in a size range from 200 to 1000 nm. Today the most common are dextran coated IONPs and these are the only clinically approved iron nanoparticle MRI contrast agents (Thorek et al., 2006). Various physical and chemical synthesis methods can produce small nanoparticles with an average size under 10 nm (Schutt et al., 1997 and Olsvik et al., 1994). Many studies have demonstrated different parameters to control size and shape. By changing the oxidising agents, spherical particles with mean diameter from 30 to 100 nm can be produced (Sugimoto and Matijevic, 1980). Ferrous and ferric hydroxides in aqueous media were mixed stoichiometrically producing spherical particles homogeneous in size (Massart and Cabuil, 1987).

Use of water-in-oil microemulsions resulted in a small size of IONP in the range 4–12 nm (Lopezquintela and Rivas, 1993). There are many methods producing different sizes of IONP, such as sonochemical, electrochemical, spray pyrolysis and laser pyrolysis. All these have advantages in obtaining a small size but are not suitable for lab work and are expensive to produce. The method and the synthetic parameters used have a great effect on the size. The IONPs in this study were prepared using the common method, which is coprecipitation where nanoparticles of small size can be obtained reproducibly, easily and at low cost. This will provide a suitable model nanoparticle of the correct size. Particles prepared by precipitation have saturation magnetisation higher than the particles prepared by the pyrolysis method (Tartaj et al., 2003b).

In this study, I present the preparation of IONPs and their characterisation by size, zeta potential and coating the particle with CMD and dextran using a co-precipitation method. The presence of free pendant hydroxyl groups on dextran allows the ready functionalisation of dextran to convert the nanoparticles to have a negative charge. Dextran and CMD were chosen as a coating for initial studies in order to compare results with established IONPs used as contrast agents. In this project, small IONPs were prepared to establish the method to obtain them and for coating with polymers based on reported methodology.

3.2 Aim of the chapter

- Synthesis of iron oxide nanoparticles.
- Production of IONPs with particle size less than 20 nm.
- Narrow particle size distribution of iron oxide nanoparticles.
- Synthesis of carboxymethyl dextran.
- Coating of IONPs with dextran and carboxymethyl dextran.

3.3 Methods

Preparation of iron oxide nanoparticles (see 2.2.1.2).

The effect of pH on the size of iron oxide nanoparticles (see 2.2.1.1).

Stability of iron oxide nanoparticles; nanoparticles were prepared using method described in (see 2.2.2).

Synthesis of carboxymethyl dextran (see 2.2.3).

Determination of degree substitution of carboxymethyl dextran (see 2.2.3.1).

Preparation of iron oxide nanoparticles coated with carboxymethyl dextran either during or after synthesis (see 2.2.4.1 and 2.2.4.2).

Preparation of dextran-coated iron oxide nanoparticles (see 2.2.5).

Measurement of particle size and zeta potential (see 2.2.19.1 and 2.2.19.2).

Transmission electron microscopy (TEM) (see 2.2.19.3).

3.4 RESULTS

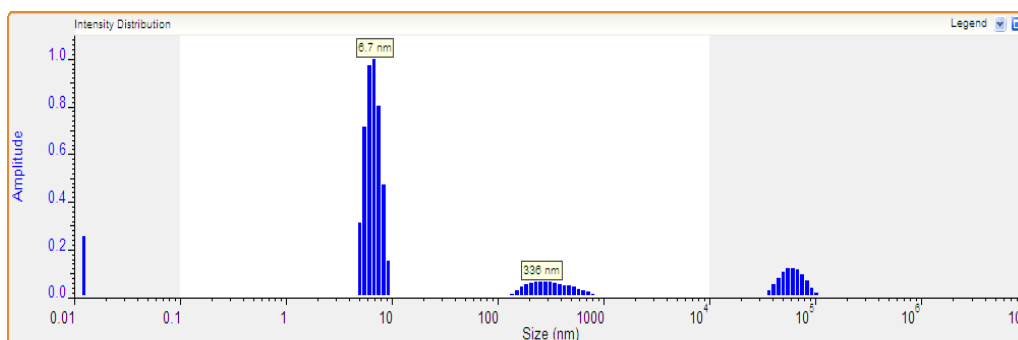
3.4.1 Iron Oxide Nanoparticle Preparation and Characterisation

The synthesis of IONPs using the co-precipitation method has been described in chapter 2. The co-precipitation method is more favoured for medical applications because it is possible to obtain uniform particles which are not soluble in water, only in certain solvents (Bumb et al., 2008). The first goal of this work was the synthesis of iron oxide nanoparticles with small size. The reaction pathway chosen for the preparation of iron oxide nanoparticles used a mixture of ferrous and ferric salts in alkaline medium, under a nitrogen atmosphere to prevent oxidation. The particles are protected from oxidation and this results in a reduced size in the absence of oxygen when compared with methods preparing them in the presence of oxygen (Kim et al., 2001). Deoxygenated water was also used in the mixture to prevent oxidation. Adjusting the pH by HCl in the synthetic process may reduce the size while maintaining the ratio of $\text{Fe}^{3+} : \text{Fe}^{2+}$ at 1: 1.

3.4.2 Particle Size

IONP prepared using the co-precipitation method were measured using DLS, and the results are shown in Table 3.2 and Figure (3.1). It is immediately

obvious that these uncoated nanoparticles are mainly of a very small size with very little aggregation. The particle sizes ranged between 6–13 nm when measured both by light scattering and electron microscopy. This indicates that, under the simple conditions of the preparative procedure, the resulting dispersions exhibited high homogeneity.



	Area %	Rh (nm)	Std Dev	% RSD
1	87.4	6.74	1.07	15.9
2	12.6	336.48	142.76	42.4

Figure 3-1: The particle size distribution of IONPs by DLS. Shows sample prepared by the co-precipitation method at pH 0.5.

3.4.3 Zeta Potential

The surface charge of the iron oxide nanoparticles is an important parameter for medical applications *in vivo* and *in vitro*. Uncoated nanoparticles have been measured in pure water; IONP showed a positive charge of 21.2 ± 7.3 mV, (Table 3.2).

3.4.4 TEM Images

A transmission electronic microscopy (TEM) study was carried out to analyse the morphology of iron oxide nanoparticles. Different batches showed the same mean particle size calculated by TEM when synthesised under the same conditions. Thus, samples were estimated to be 13.9 ± 3 nm in diameter when stained and 13.1 ± 9 nm unstained (Fig. 3.2). Samples showed that the particles are a spherical shape and smooth with a narrow size distribution. The image shows a few large particles or aggregates, but indicates that the majority of nanoparticles are single as also shown in the DLS results in figure 3.1. The particles measured by DLS are a very similar size to those viewed by TEM. In the absence of a coating, the IONP hydrodynamic value would be expected to be a similar size to the dehydrated value seen under vacuum.

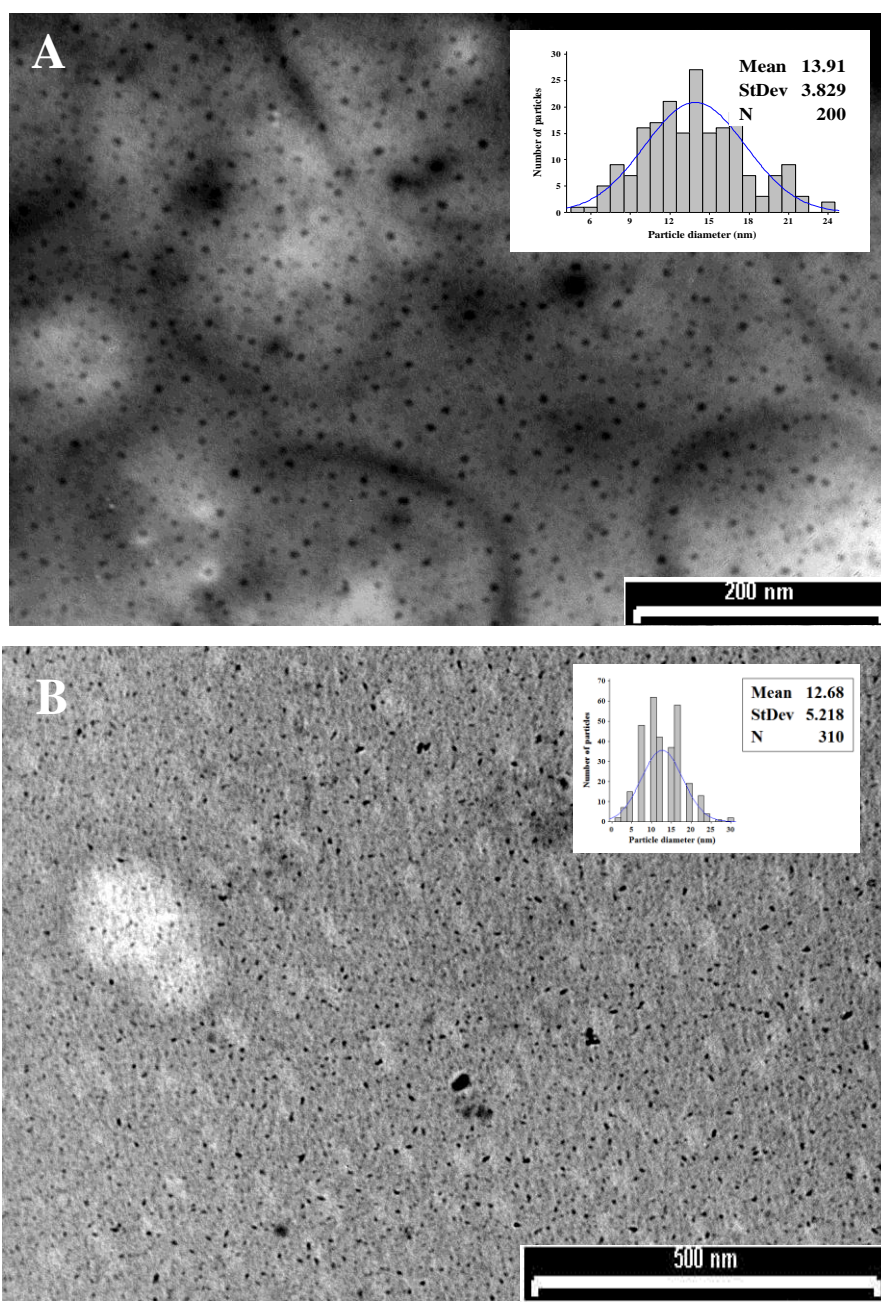


Figure 3-2: TEM images for uncoated IONPs. NPs were prepared under the same conditions (A Scale bar 200 nm and B 500 nm). Nanoparticles were prepared by co-precipitation and placed on copper grids, sample (A) was stained with 3% phosphotungstic acid for 2 minutes, and dried (Average size 13.9 ± 3 nm), while sample (B) was unstained (Average size 13.1 ± 9 nm). Images were taken at 100 k and 200 k magnification.

3.4.5 The Effect of pH on the Stability of IONPs

The pH of the IONP during synthesis and storage was studied. Three different preparations were made under the same conditions using the co-precipitation method to produce suspensions with a final pH of 0.5, 2.0, 4.0 and 7.0. were measured by DLS (Fig. 3.3). It was clearly shown that decreasing the pH was accompanied by a decrease in IONP size. At pH 0.5, the nanoparticles ended up with a small size below 20 nm. At pH 7.0, the IONPs showed a size above 70 nm, which was almost 3 times that at pH 2.0 or at pH 4.0.

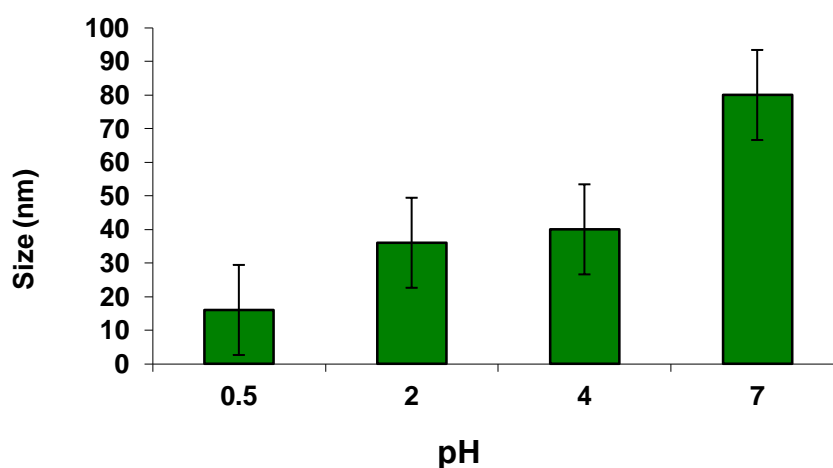


Figure 3-3: The effect of pH on the stability of IONPs.

3.4.6 Stability of IONPs

The colloidal stability of IONP suspension prepared in the experiment of Fig. 3.2 was checked by DLS analysis and compared with another preparation using the same method but acidified to pH 1.0. Where peaks reflect the population of the particles size. (Figs. 3.4, 3.5 and 3.6) and show the size distribution of IONP during storage. For particles at pH 0.5, no significant change was observed after this period with size constant at below 20 nm in diameter and

also the area showed one main, small nanoparticle population. (Fig. 3.4). Particles prepared at pH 1 are shown in figures 3.5 and 3.6. Two main nanoparticle peaks were observed in the pH 1 preparation. The first peak showed a small population of IONP with smaller size (20 nm in diameter) than the large peak (120 nm in diameter) but which was larger than IONP produced by acidification to pH 0.5. During the first day of incubation there was a small increase in particle size for both peaks, with no significant change in particle size on longer storage. The results show only the particles synthesised at pH 0.5 are stable enough to be used in further work.

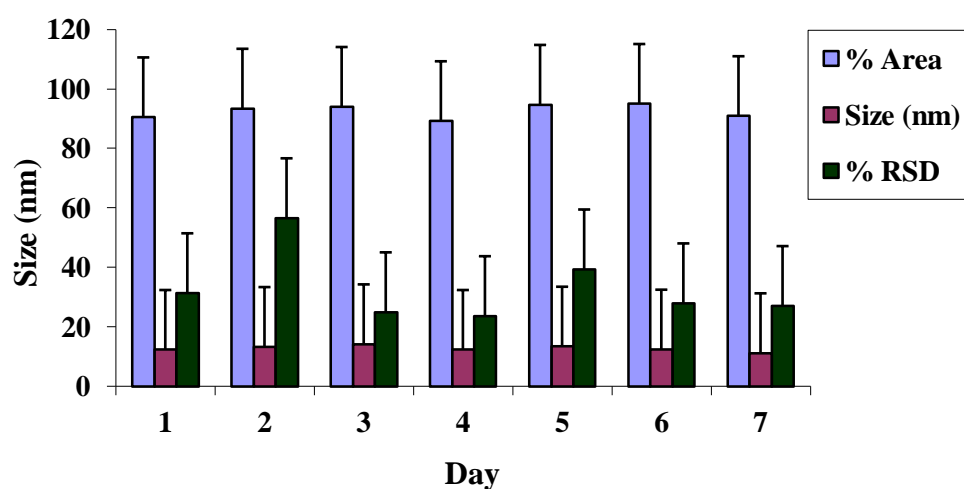


Figure 3-4 : Preparation pH 0.5 (Peak 1): IONP stability over 7 days. Peak 1 was the principle particle size in this preparation. IONP were prepared using the co-precipitation method on Day 1, acidified to pH 0.5, stored at 4°C and measured daily by DLS up to days 7.

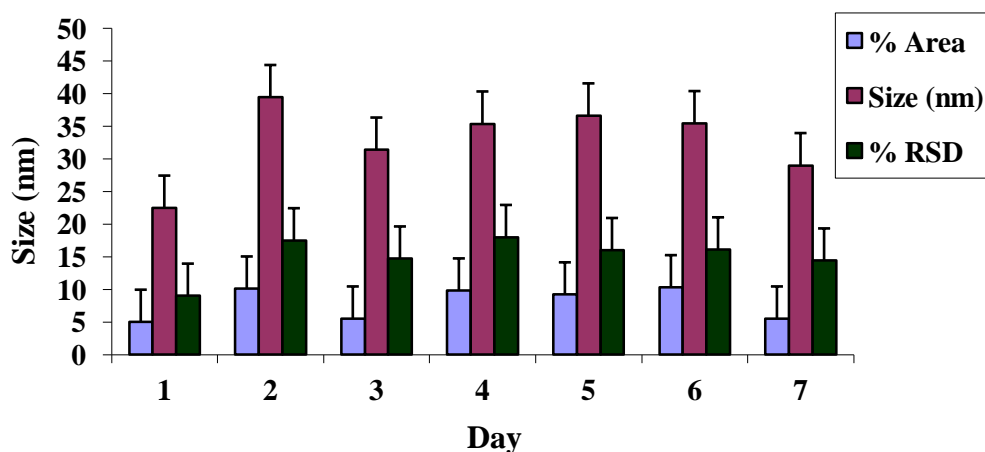


Figure 3-5 : Preparation pH 1 (peak 1): IONP stability over 7 days. IONP were prepared using the co-precipitation method on day 1, acidified to pH 1.0, stored at 4°C and measured daily by DLS up to day 7. This peak was a small proportion of the particles formed and showed particles smaller than pH1 preparation peak 2 but still bigger than the preparation at 0.5 pH.

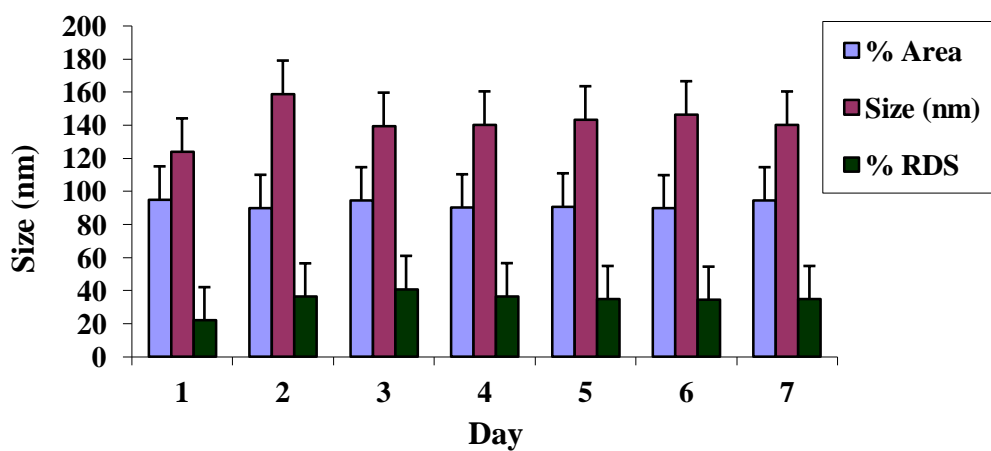


Figure 3-6 : Preparation pH 1 (peak 2): IONP stability over 7 days. IONP were prepared using the co-precipitation method on day 1, acidified to pH 1, stored at 4°C and measured daily by DLS for 7 days. The peak contained most of the particles formed at this pH, and were large particles.

3.4.7 Carboxylated Dextran

The synthesis of CMD involved the methylation of dextran. The carboxyl group of the monomer can readily react with the hydroxyl group on the dextran to form ester linkages as shown in Figure 2.1. The successful incorporation of the COOH into dextran was demonstrated by calculation of the degree of substitution. The CMD had degree of substitution values in the range 0.32 to 0.49 (Table 3.1). The number of COOH group in the CMDs preparations were calculated from acid-base titration.

Table 3-1: IONP Coated Degree of substitution of COOH on dextran.

Preparation	DSs
1	0.34
2	0.32
3	0.35
4	0.47
5	0.49
6	0.49

3.4.8 IONP Coated with CMD and Dextran

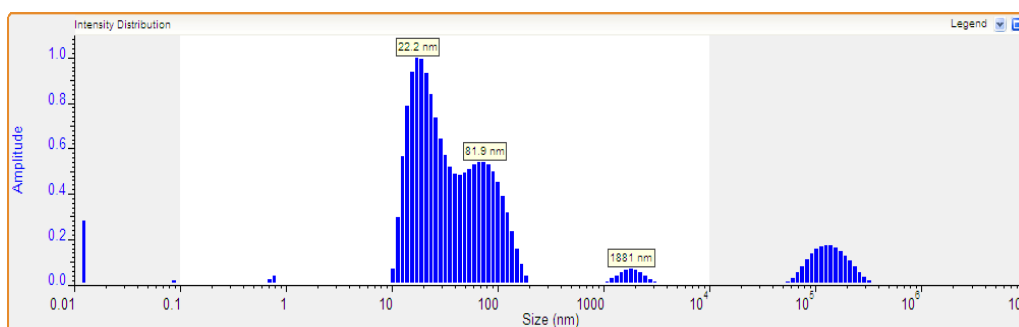
IONPs tend to aggregate and to be recognised by the reticuloendothelial system following surface adsorption of plasma protein. Coating the IONP is necessary to prevent both to prevent aggregation and in future work to reduce protein adsorption.

3.4.8.1 CMD-IONPs

Uncoated particles were prepared by the co-precipitation method and the reaction was carried out under standard conditions both in the absence of CMD and the presence of CMD. The resulting particle size distribution is shown in Table. 3.1. The uncoated IONP had a particle size 13 nm in diameter. Their zeta potential of 21.2 ± 7.3 mV was positive as expected from the literature.

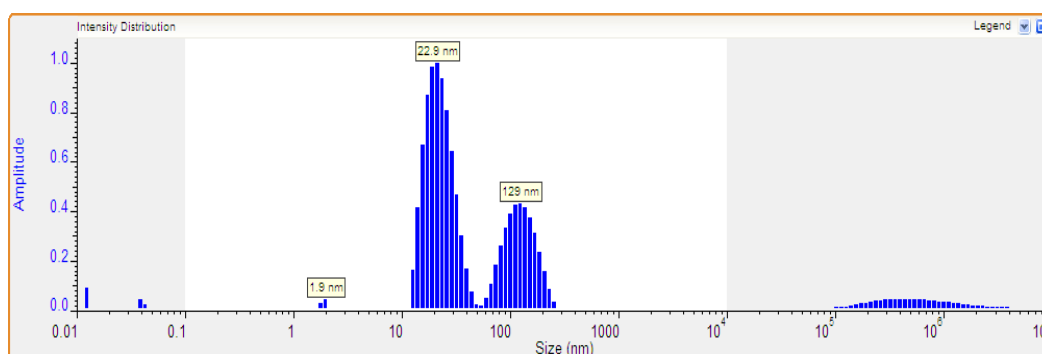
When CMD was added to IONP the diameter of CMD coated IONP (CMD-IONP) was increased to 41 ± 9 nm as measured by TEM (Fig. 3.9) and 44 and 163 nm when measured by DLS, the majority being the small size (Fig.3.7). These CMD-IONP had a zeta potential of -91.9 ± 53 mV (Table 3.2)

CMD-IONP prepared in the presence of carboxymethyl dextran showed an increase in size to 46 ± 10 nm measured by TEM (Table 3.2 and Fig. 3.10) similar to the CMD-IONP prepared by adding CMD to IONP. The final nanoparticles then displayed a negative zeta potential of -39.8 ± 0.5 mV, somewhat less than the nanoparticles coated with CMD after IONP preparation. We interpret the increase in the size and the high negative zeta potential to be a result of coating the iron oxide with negatively charged polymer. IONP coated in these two ways have a hydrodynamic diameter measured by DLS of 44 nm with IONP coated with polymer (Fig 3.7) and 46 nm when prepared in the presence of polymer (Fig 3.8) which is well in agreement with TEM measurements.



	% Area	Rh (nm)	Std Dev	% RSD
1	60.6	22.19	7.78	35.1
2	37.1	81.91	31.12	38
3	2.3	1881.23	426.41	22.7

Figure 3-7 : The particle size distribution of CMD –IONP by DLS. IONP were synthesised using the co-precipitation method and then coated with CMD.



	% Area	Rh (nm)	Std Dev	% RSD
1	0.5	1.90	0.09	4.9
2	66.6	22.94	6.71	29.2
3	33.0	128.53	41.30	32.1

Figure 3-8 : The particle size distribution of CMD–IONP by DLS. IONP synthesised in the presence of CMD in the suspension using co-precipitation method.

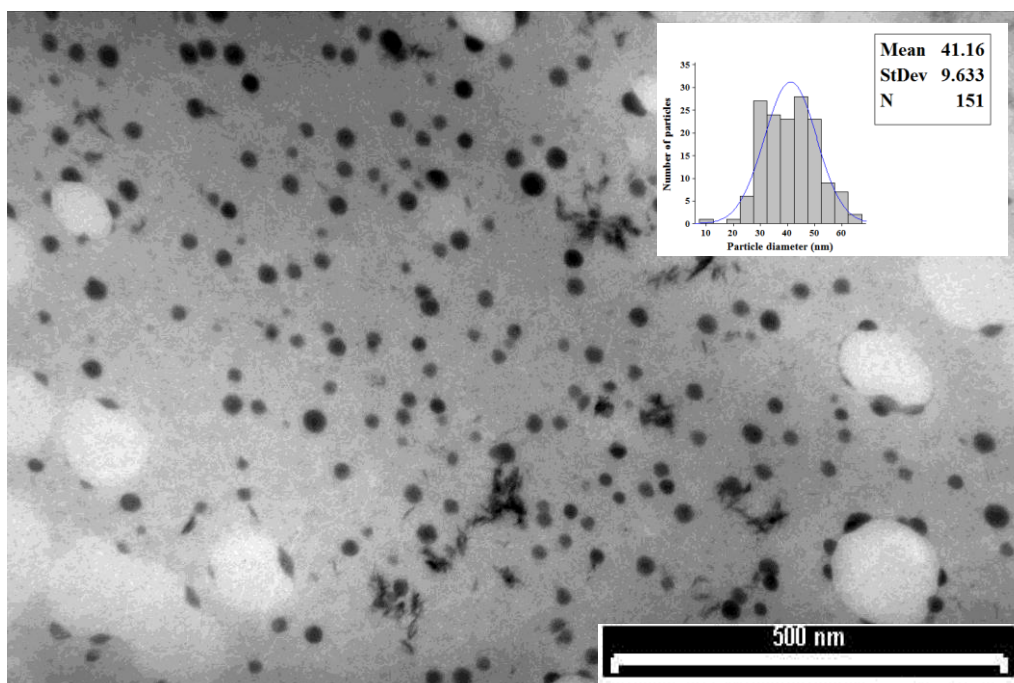


Figure 3-9: TEM image for CMD-IONP. The IONP were synthesised using the co-precipitation method and then coated with CMD (Average size 41 ± 9 nm). (Scale bar 500 nm).

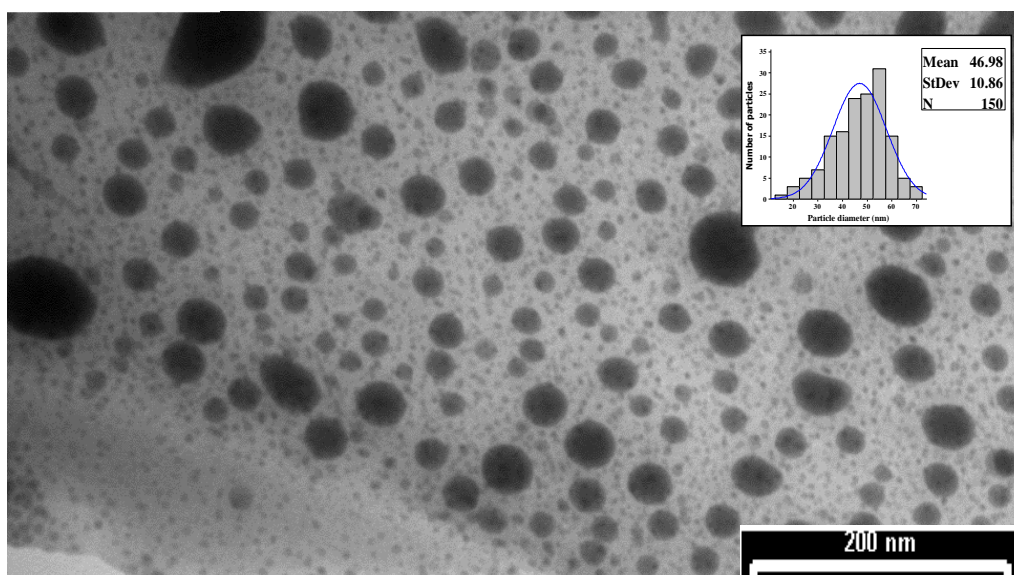
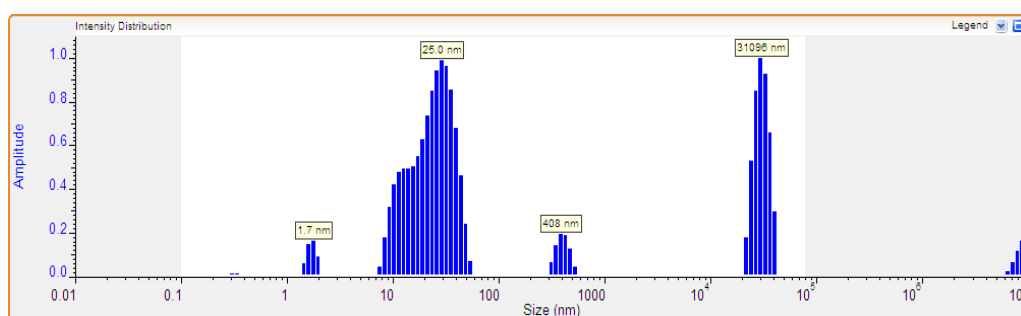


Figure 3-10: TEM image for CMD-IONP. Synthesised in the presence of CMD in the suspension (Average size 46 ± 10 nm). (Scale bar 200 nm).

3.4.8.2 Dextran-coated iron oxide nanoparticles

IONPs were coated with dextran using co-precipitation in the presence of the polymer. Comparison of the hydrodynamic diameter of CMD-IONPs and dextran-coated-IONPs (Fig 3.8 and 3.11 respectively) revealed a similar hydrodynamic diameter and size distribution for the dextran-IONPs, 46 nm compared to 50 nm. The average diameter for dextran coated IONP was 40 ± 12 nm measured by TEM (Fig 3.12). There was a significant effect of coating increasing the nanoparticle size from 13 ± 9 nm to 40 nm or 50 nm. The zeta potential values of dextran and CMD coated IONP were more negative than the IONPs (Table3.2), decreasing from $+21.2 \pm 7.3$ mV to -35.8 ± 0.5 mV with dextran. The dextran coated IONP was less negative than the CMD-IONP.



	% Area	Rh (nm)	Std Dev	% RSD
1	2.6	1.72	0.16	9.6
2	66	24.96	10.61	42.5
3	4.3	408.37	55.12	13.5

Figure 3-11: The particle size distribution of dextran coated IONPs by DLS. IONP were made using the co-precipitation method in the presence of dextran.

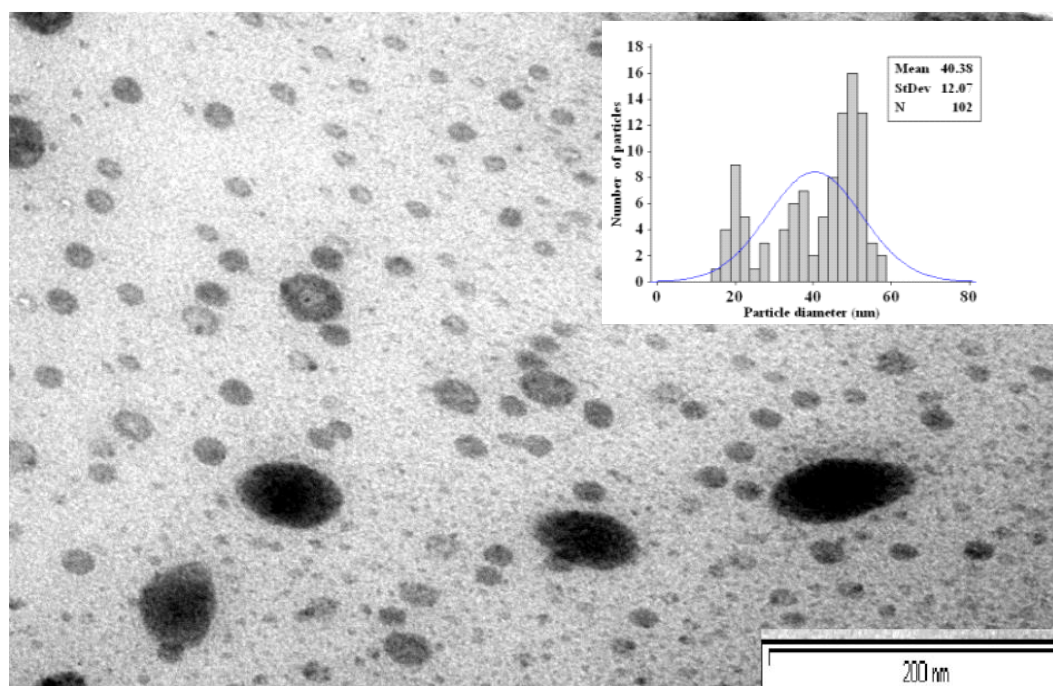


Figure 3-12: TEM image of dextran coated IONPs. IONP were made using the co-precipitation method in the presence of dextran (Average size 40 ± 12 nm) (Scale bar 200 nm).

The specifications for the CMD and Dextran coated IONP are summarised below in (Table 3.2) showing size determined by both DLS and TEM and also the zeta potential.

Table 3-2: The zeta potential and sizes of uncoated nanoparticles and CMD and dextran-coated iron oxide nanoparticles. The negative ζ -potential of the particles arose from the free terminal carboxyl groups of the polymer.

Nanoparticles	DLS NP diameter (nm)	TEM NP diameter (nm)	ζ -potential mV \pm S.D
IONP	13.48	13	21.2 ± 7.3
CMD–IONPcoated after IONP preparation	44 and 163	41 ± 9	-91.9 ± 53.1
CMD–IONP made in the presence of polymer	46 and 257	46 ± 10	-39.8 ± 0.7
Dextran–IONP made in the presence of polymer	50	40 ± 12	-30.8 ± 0.5

3.5 Discussion

3.5.1 IONP Preparation and Characterisation

The initial work concentrated on producing NPs in a range consistent with SPION reported in the literature and with a narrow particle size distribution. It was clear that this could be achieved by understanding the mechanism of NP formation and choosing the right procedure. The iron oxide nanoparticles produced in this project were produced by a co-precipitation method and determined to be in the size range 13 nm in a diameter by both DLS and TEM. This is a size range comprising most of the reported IONP and well within the required specification. Co-precipitation is the simplest, cheapest method which involves the simultaneous precipitation of Fe^{2+} and Fe^{3+} ions in basic aqueous media (Kang et al., 1996) was used.

IONP are very suitable for medical applications. IONP can be prepared with control of the size by a number of methods. By homogeneous precipitation reaction, including the separation of the nucleation and growth of nuclei, uniform particles can be obtained (Sugimoto, 2000). SPION of magnetite with a mean diameter of 10 nm and narrow size distribution were synthesized by the co-precipitation method using a homogenizer at a stirring velocity of 10,000 rpm (Valenzuela et al., 2009).

Small size particles have also been obtained using the precipitation method by reaction of iron (III) acetylacetonate in phenyl ether in the presence of oleylamine, alcohol and oleic acid under a high temperature (Sun and Zeng, 2002). Aqueous FeCl_3 and FeCl_2 solutions are mixed at a concentration ratio of $\text{Fe (III)/Fe (II)} = 2/1$ in an aqueous ammonia solution, yielding Fe_3O_4 NPs with diameters from 3 to 15 nm using the co-precipitation method. In order to prepare SPION with a narrow size distribution, several parameters should be

controlled including pH, temperature, and mixing method, as well as the nature and concentration of anions (Oh and Park, 2011).

3.5.1.1 Particle size

Nanoparticles with iron oxide core sizes of 13 nm can be used in a variety of medical applications and biological fields, SPION of 10 nm size used as MRI contrast agents are also used for many other purposes, such as non-viral gene delivery (Berry et al., 2003). Many investigations have reported a size of uncoated IONP of a similar size to the uncoated IONP produced in the present work. LaConte et al., (2005) reported that particles with diameters of 10–40 nm, including ultra-small SPIOs (USPIOs), are ideal for prolonged blood circulation, can pass through capillary walls, and are often phagocytosed by macrophages which carry them to bone marrow and lymph nodes. The method selected and modified resulted in smooth nanoparticles with no aggregation (Fig. 3.2). Types of uncoated IONP have been produced with different sizes. This was done by varying the methods used to prepare the NP core. Uncoated NPs with spherical shape and narrow size distribution with a mean diameter from 30 to 100 nm can be prepared from Fe (II) salt, a base and mild oxidant, nitrate ions (Sugimoto and Matijevic, 1980). IONP of 20–100 nm were obtained by controlling the temperature of reaction velocity at 5–10°C and the concentration of iron salts (Bergemann et al., 1999). IONP in a range of 4 nm to 12 nm were prepared using microemulsion method (Feltin and Pileni, 1997). Also IONP with size around 100 nm can be prepared by a disproportionation of ferrous ions in the organic media method (Fievet et al., 1989a). In the most common commercial method, spray pyrolysis, IONP were obtained with a mean diameter ranging from 5–60 nm according to the nature of the iron salt (González-Carreño et al., 1993).

Gupta and Curtis, (2004b) have prepared IONP by using the chemical precipitation method and these were found to be small in size, around 13.6 nm measured by TEM.

IONPs which are very uniform in size and shape have been prepared by the co-precipitation method in the present work. Particle diameters average size 13 nm were determined from TEM measurement (Fig.3.2). The particles were very smooth and with a good shape and there were no aggregates. The size of the IONPs measured by DLS was 13 nm in hydrodynamic diameter, while in TEM size was measured in a dried state.

3.5.1.2 Zeta potential

The IONPs suspension in water produced in the present work were characterised by a high positive zeta potential of 21.2 ± 7.3 mV (Table 3.2) at pH 0.5. It is generally agreed that iron oxide nanoparticles have a strong positive charge. A high value of zeta potential was found of 14 mV at pH 1 which may be explained due to the formation of Fe-OH_2^+ in acid medium (Yu and Chow, 2004).

3.5.1.3 Stability of uncoated iron oxide nanoparticles

During the synthesis of IONPs, the mixture was acidified to pH 0.5 to produce a small size. The particle was stored after synthesis in the fridge at 4°C (Figs.3.4, 3.5 and 3.6). To further investigate the stability during storage we synthesised the uncoated NP acidified to pH 1.0 for comparison. The IONPs which we routinely prepared at pH 0.5 showed high stability and had nearly the same size over the 7 day period while the IONP with higher pH 1, 4 and 7 had an average size of 80–200 nm.

Different hydrodynamic sizes of IONP about, 250 and 320 nm, indicating as aggregates after storage in water for 5 days (Chen et al., 2008).

Indeed, for this work, it was important that the IONPs produced could be maintained at their original size without aggregation, making them suitable for our work on coating particles for possible use as a contrast agent. Not much work has been done with IONP in order to investigate how long they can

maintained in an unaggregated form in storage. Although the IONPs in this study were uncoated, no obvious change of the size was detectable during the 7 days of the experiment. In addition, the IONPs were stored for more than a year and we found that particle sizes did not change over this longer period.

3.5.1.4 The effect of pH on the size of IONPs

The chemical stability and properties of nanoparticles is dependent on many parameters. One of the most important factors is pH during the process of synthesis of IONPs (Fig. 3.3). Variation of the co-precipitation method has been used to prepare nanoparticles. Generally, a basic aqueous solution of ferric and ferrous are precipitated as magnetite. At the same time some parameters can be changed, such as the ratio and nature of ferric and ferrous or reaction conditions, e.g. pH, temperature to control the size (Thunemann et al., 2006 and Schulze et al., 2006). The IONPs produced in this project were optimised by varying the pH during the synthesis, and the smallest size was observed at pH 0.5. It has been found that in the aqueous dispersion of nanoparticles pH has a major effect on the particle size. The pH and the ionic strength of the co-precipitation can be adjusted to control the size of nanoparticles over an order of magnitude 2–15 nm (Jolivet et al., 2000).

IONPs are often stabilised using fatty acyl moieties. In terms of particle size, the concentration of sodium oleate in reaction has an effect on the size of IONP together with an increase of solution pH. A pH lower than 11 resulted in a reduction in the size while at pH higher than 11 the particle size was increased (Sun et al., 2007). In IONPs that were prepared at different pH and then treated with trypsin, the size was between 8.5 to 25 nm (Kim et al., 2005a). IONP obtained at pH 9 gave a size of 30 nm while the mean diameter of the IONP was estimated to be 10 nm at pH 10 when measured by TEM (Lin et al., 2005).

The change of pH has a strong effect on the size, and it is useful to take this into account during synthesis. The ratio and type of salt, ionic strength of the

media and pH have an important role in controlling the size and shape of nanoparticles (Siegel, 1993 and Carl et al., 1994).

In conclusion, the results from this study show that it is possible to store uncoated nanoparticles that can be used subsequently at any time for up to a year without any change in the size.

3.5.2 Carboxylated Dextran

Dextran with Mw 40,000 was carboxylated by monochloroacetic acid. The effect of parameters such as reaction time, temperature, catalyst and the amount of reactants of DS of carboxylated dextran were examined and showed different values from 0.36 to 1.53 (Kim et al., 1999). The degree of substitution of carboxyl groups was found to be 4.6 mmol (Hildebrandt et al., 2007). It would be expected that COOH groups on CMD would be very attractive to Fe²⁺ ions, which is an advantage. The successful incorporation of the COOH group into dextran was demonstrated by titration and calculation of the carboxylic groups (Table 3.1).

3.5.3 Coated Iron Oxide with CMD and Dextra

In this project CMD and dextran have been both coated onto IONPs using a common method which is a co-precipitation. This led to a highly homogenous suspension with little aggregation of particles. The particles have a large surface area and have been coated and conjugated with biomolecules (enzymes, antibodies, DNA, etc.) and sugars (dextran, starch, albumin, poly(ethylene glycol) for a variety of uses (Luckarift et al., 2004, Kneuer et al., 2000, Santarelli et al., 1988 and Lesot et al., 1998).

Jarrett et al., (2007) have reported that dextran has been used for coating IONP because many investigators reported that it is non-toxic and is approved for clinical use. The most common method for coating IONP is co-precipitation

(Weissleder et al., 1990 and Kawaguchi et al., 2001). Polysaccharides are common as coatings for IONP (Weissleder et al., 1995c).

Coated IONPs made either in the presence of CMD or by subsequent addition of polymer and with dextran by subsequent addition of polymer showed no significant difference in size between these two methods, as shown in (Figs.3.9, 3.10 and 3.12) and (Table 3.1) DLS measurements showed similar sizes between the three formulations (Figs. 3.7,3.8 and 3.11). It has been reported that IONP have been coated with dextran by using two methods, laser pyrolysis and co precipitation (Carmen Bautista et al., 2005).

Different forms of dextran polymers, including carboxydextran and carboxymethyl dextran, have been used to produce SPIONs, Ferumoxtran-10 and ferumoxytol, using the co precipitation method (Laurent et al., 2008).

In a majority of studies on nanoparticle formulations, particle sizes have been correlated to the amount of polymer or the methods, including the parameters such as temperature and ratio of the iron salts, but not their combined effect. The co-precipitation method can be used for the preparation of CMD and dextran-coated IONP, and it is an easy, low cost and reproducible method.

3.5.3.1 Particle size

All the coated particles formed with polymers were larger in size than the uncoated particles (Fig. 3.2) and this proves the presence of the polymer on the IONP surface (Figs. 3.9, 3.10 and 3.12) and also the effect of hydration due to the coating layer on the size. Jarrett et al., (2007) have reported the effect of reaction time, pH, iron ratio and polysaccharide content on coating iron oxide with dextran sulphate produced in a range of sizes. Nanoparticles produced in the present work were shown to be spherical, well-dispersed and, in the larger particles, the denser IONP were seen within a the lighter matrix of the dextran coating. The nanoparticles are slightly larger in DLS because TEM

measurement corresponds to particles in a dried state, whereas the DLS measurement is of hydrated polymer coating (Figs. 3.7, 3.8 and 3.11).

Comparing other work where iron oxide nanoparticles were prepared with dextran and CMD coatings using the co precipitation method. CMD-IONP sizes of 75 nm mean particle diameter and 88 nm with dextran were reported by (Horák et al., 2007). CMD-IONP made in the presence of the polymer using the co-precipitation method were produced with a size around 20 nm as measured by TEM (Hildebrandt et al. 2007). SPION in commercial products Resovist and SHU555C, used as magnetic resonance imaging contrast agents, are polydisperse and covered with a thick layer of CMD producing average particle sizes between 3 and 62 nm (Chen et al., 2009). On the other hand, CMD-IONP measured using photon correlation spectroscopy and atomic force microscopy, the particle size core was from 6–40 nm and hydrodynamic particles size of coated nanoparticles was between 13–80 nm (Büscher et al., 2004).

Iron oxide nanoparticles coated in the presence of dextran under alkaline conditions were produced with a diameter from 40 nm to 60 nm (Duan et al., 2005). Commercial nanoparticles called ferumoxides are dextran-coated magnetite nanoparticles with a mean hydrodynamic size of approximately 141 nm (Jain et al., 2008a). By using the co-precipitation method to coat IONP with dextran mean aggregate sizes are 57 ± 17 nm were measured by TEM and hydrodynamic size around 214 ± 8 nm (Carmen Bautista et al., 2005).

CM-polysaccharide-coated IONPs were measured in dry state with sizes found from 140 nm to 200 nm in diameter (Wotschadlo et al., 2009b). IONPs coated with dextran prepared by laser pyrolysis were shown to produce sizes about 50 nm in diameter (Veintemillas-Verdaguer et al., 2004). The NP preparation procedure studied in this work investigated coating methods both in the presence and in the absence of the polymer, showing both can be used to prepare coated iron oxide nanoparticles.

The sizes of dextran and CMD coated IONPs prepared in the present work were very similar to those reported in the literature and for the commercially available IONP contrast agents.

3.5.3.2 Zeta potential

IONPs show a positive charge, but when they were coated with CMD there was a negative charge, most likely due to the presence of an ionised carboxyl group of the polymer present on the nanoparticle's surface. Dextran was carboxymethylated to introduce COOH to produce a negatively charged polymer. SPION was coated with carboxymethyl dextran by a co-precipitation method, providing COOH on iron oxide surface (Lee et al., 2009). To improve the interaction IONPs coated with CMD showed good interactions with tumour cells (Schwalbe et al., 2006). The results in Table 3.2 showed that the CMD-IONPs and dextran prepared in this work were highly negative. This means the particles were well coated with dextran and CMD.

The CMD-IONP prepared in the presence of polymer had a very similar zeta potential to the dextran-IONP prepared in the presence of polymer, whereas CMD-IONP prepared in the absence of polymer had a much more negative zeta potential. This suggests that when the polymer is present during IONP production, the carboxyl groups on CMD interact much more with the IONP but that when added afterwards, many more carboxyl groups are present on the CMD-IONP surface.

3.6 CONCLUSIONS

We have presented a controlled co-precipitation method which produced iron oxide nanoparticles. The pH was a crucial factor to control the IONP size. IONP with a 13 nm narrow size distribution was determined by TEM and DLS. The optimized conditions for producing small particle size can be achieved by changing the pH to 0.5 during synthesis. The IONPs showed high stability during a 7 day experiment but even longer operationally; from our records up

to 1 year without any change of the particle size. Carboxymethyl dextran was prepared starting from dextran ($\alpha\rightarrow6$ linked backbone) with a degree of substitution value in the range between 0.32–0.49. We have prepared CMD and dextran coated IONPs about 41 ± 9 nm, 46 ± 10 nm and 40 ± 12 nm in size respectively using the co-precipitation method, and these appear to be of a similar size specification to dextran and CMD–IONP described in the literature.

CHAPTER 4

4. POLY (GLYCEROL ADIPATE) AND PGA 40%C₁₈ COATED IRON OXIDE NANOPARTICLES

4.1 INTRODUCTION

Major phagocytic cells macrophages and neutrophils typically take up large particles >200nm but will also take up small hydrophobic particles. Small particles can also be taken by a variety of cell types including endothelial cells. Most coated contrast agents are mainly taken up by macrophages (Moghimi et al., 2005)

If the particles could be coated to both avoid macrophages and remain in circulation or be taken up by different cell types this could result in many different applications for these contrast agents. If we could use these PGA polymers as a delivery system by coating IONPs instead of incorporating drugs, we could perhaps develop better delivery for contrast agents. PGA nanoparticles coated with Tween have a good stability and selective uptake into tumour cells (Meng et al., 2006).

In fact, all biological compartments act as barriers to the passage of nanosized materials, with many other barriers to consider such as epithelium, which plays a role as a general barrier to prevent the materials entering into the body. The particles will therefore be injected into the blood and circulation where the body has a number of defences against pathogenic organisms such as protozoa, bacteria and viruses. Serum proteins act as opsonins and when the particles are hydrophobic they be easily coated by the proteins. The opsonins are mainly antibodies and complement factors which promote the binding of nanoparticles

to the phagocytic cells, especially macrophages and neutrophils in the mononuclear phagocyte system, which rapidly remove the particles from the bloodstream (Stolnik et al., 1995). The mechanism of protein adsorption leading to the elimination of the nanoparticles is based on different interactions, but specifically those between the hydrophobic part of the proteins with the hydrophobic surface on the nanoparticles (Rieger et al., 2007). Organs with high concentrations of mononuclear phagocytic cells are the liver, spleen and lymph nodes. Opsonised particles can be cleared from the circulation to the liver and spleen in less than 5 min (Illum et al., 1982). The ideal IONPs for biomedical applications should have a narrow size distribution and their surface should be coated with biocompatible hydrophilic materials to form a stable aqueous dispersion at the physiological pH of 7.4. Commonly, stabilisation of a ferrofluid is achieved by optimising the electrostatic repulsion of similarly charged surfaces, but stable IONPs coated with biocompatible polymer is necessary for biological applications. Recently, biocompatible and biodegradable polymers such as poly(D,L,lactide-co-glycolide) (PLGA), poly(D,L-lactide) (PLA), and poly(glycolide) (PGA) have been used (Kim et al., 2003b, Herrmann and Bodmeier, 1998 and Lin et al., 1985).

In order to prevent particle aggregation, because of attractive van der Waals or magnetic dipole-dipole interactions, a steric or electrostatic repulsion can be produced by coating the particles with polymers. Stability can be achieved by one or two fundamental mechanisms: either the presence of an electrical double layer on the particles or the presence of a polymer providing steric stabilisation (Majewski and Thierry, 2007).

IONPs have been coated using different methods and with different polymers. Different coatings have effects on both the nanoparticle size and also on their stability. Several methods have been used for coating, such as emulsion polymerisation, double emulsion, water-in-oil-in-water, evaporation, inverse microemulsion polymerisation, miniemulsion polymerisation and the emulsification–diffusion method or two-step emulsion polymerisation (Arias et

al., 2001, Gomez-Lopera et al., 2001, Deng et al., 2003, Zheng et al., 2005 and Lee et al., 2005).

Poly(ethylene imine) and poly(ethylene oxide)–block-poly(glutamic acid) coated IONP that were stored in sodium chloride 0.15 M for 30 days and 6 months showed no change of the particle size (Thunemann et al., 2006). Lyophilized solid lipid nanoparticles were stored for 6 and 9 months at 30°C/65% relative humidity and the size increased to 400 nm with just a few small sized particles about 40 nm (del Pozo-Rodriguez et al., 2009).

Recently, a novel polymer poly(glycerol-adipate) has also been used to create nanoparticles. It met with success in encapsulating a variety of different drugs and is a biodegradable polymer made from non-toxic monomers. These characteristics suggest that PGA polymers are useful for preparing nanoparticles for drug delivery. They have the capability to self-assemble into small particles and have showed the ability to entrap an anticancer drug with a high efficiency (Kallinteri et al., 2005). The presence of free pendant hydroxyl groups on the backbone introduces synthetic flexibility in the backbone as they are available for substitution with different functional groups and different chemistries and showed excellent drug incorporation. They also showed a good uptake into different cells, a long sustained drug release in physiological conditions and rapid drug release when taken up into cells.

In this study, a co-precipitation method was used to synthesise iron oxide nanoparticles for potential use as MRI contrast enhancement agents in the diagnosis of cancer and other diseases. The synthetic method described in chapter 3 was based on a solution of Fe^{2+} and Fe^{3+} salts in an alkaline medium.

In this chapter, iron oxide nanoparticle will be coated with PGA backbone and PGA 40% C_{18} polymers using a modified interfacial deposition (IDP) method. Either unmodified PGA (PGA 0%) or PGA with different acyl substitutions (different acyl chain lengths and different degrees of substitution) will be used to coat IONPs by using the interfacial deposition method (Fessi et al., 1989).

This method was previously used by our team and showed a good result in producing nanoparticles for drug delivery systems. The effect of the method and different PGAs on the particle size has been studied extensively (Meng et al., 2007b and Puri et al., 2008).

In this chapter various characterisation techniques have been applied to obtain information about the size, structure and coating of the nanoparticles. The nanoparticles were manufactured using various amounts of solvent and polymers under various conditions and were characterised using transmission electron microscopy (TEM) for morphological properties, DLS and zeta-potential for particle size surface charge. In this chapter, work establishing a new method based on the above technique to produce small polymer coated nanoparticles will be described. Also the further coating of the nanoparticles with Tween or albumin and their stability to aggregation will be determined. The nanoparticle properties of these systems will be assessed in terms of their colloidal stability in physiological media and their ability to interact with cells.

4.2 Aims of the Chapter

- To evaluate the methods of preparation of PGAs–IONPs and select the best method for coating nanoparticles.
- To determine the optimum method of PGA–IONPs to obtain small nanoparticles.
- To study the influence of polymer functionalisation and degree of acylation on coating IONPs.

4.3 Methods

Poly(glycerol adipate) PGA and different PGA–IONPs (see 2.2.6).

Optimisation of IONPs coating produced with PGA (see 2.2.7).

Modification of PGA polymers (see 2.2.9).

Synthesis of PGA 40% C_{18} by acylation of backbone PGA (see 2.2.9.1).

PGA 40% C_{18} coated IONPs (see 2.2.10).

0.1% Tween 80 coated–PGA 40% C_{18} –IONPs and PGA 40% C_{18} –IONPs (see 2.2.11).

0.1% Albumin–coated PGA 40% C_{18} –IONPs and PGA 40% C_{18} –IONPs (see 2.2.12).

Stability of IONPs coated with polymers (see 2.2.15).

Purification of PGA–IONPs (see 2.2.8).

4.4 Results

4.4.1 Coated IONPs Using Different PGAs and two Different Methods.

The effects of the method of coating and different polymer PGAs on nanoparticle size were investigated. PGA substituted with different acyl chain lengths at 20%, 60%, 80% and 100% substitution were studied to produce coated IONPs. There were two aims in these experiments: to determine whether the polymer specification influenced polymer coating of IONPs with the PGA polymer and to determine the best method to coat the IONPs with PGA. The two different methods were (1) a modified interfacial deposition method and (2) a sonication method were polymers added dropwise to 5 ml of IONPs. The product was sonicated at 30 W for 30 min. These were used to prepare PGA-coated IONPs by using a number of PGAs with different substitutions, The same amount of IONPs (5 ml) and polymers was used in both methods and all the polymers were used at 20 mg/ml dissolved in 1 ml of acetone, then all particles size of samples were measured using DLS

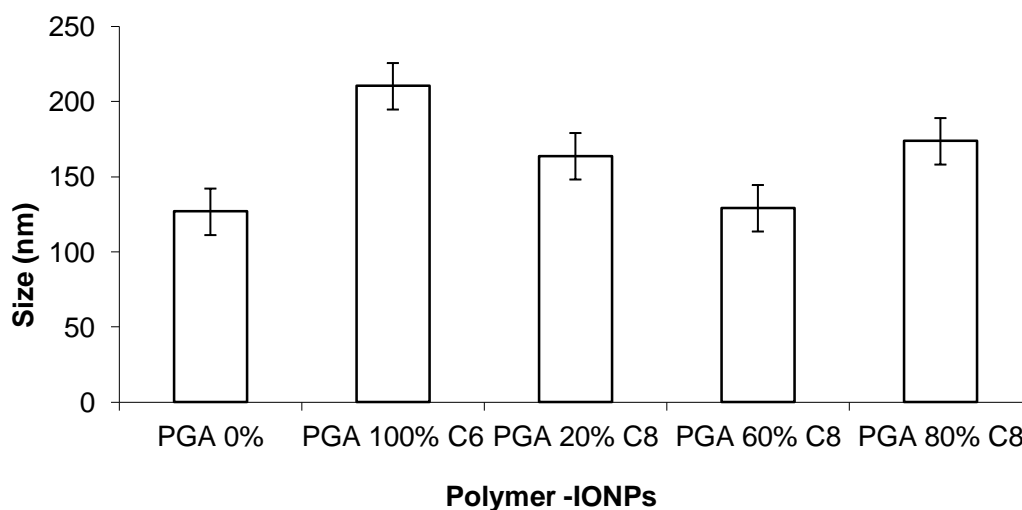


Figure 4-1: IONPs coated with different polymers using the IDP method.

Fig. 4.1 shows that the particle sizes produced by IDP method measured using DLS where PGA 0%–IONPs 126 nm in diameter and PGA 60% C_8 –IONPs 129 nm in diameter, were the smallest size, compared with other polymers where PGA 20% C_8 –IONPs, PGA 80% C_8 –IONPs and PGA 100% C_6 –IONPs were 163 nm in diameter, 173 nm in diameter and 210 nm in diameter, respectively.

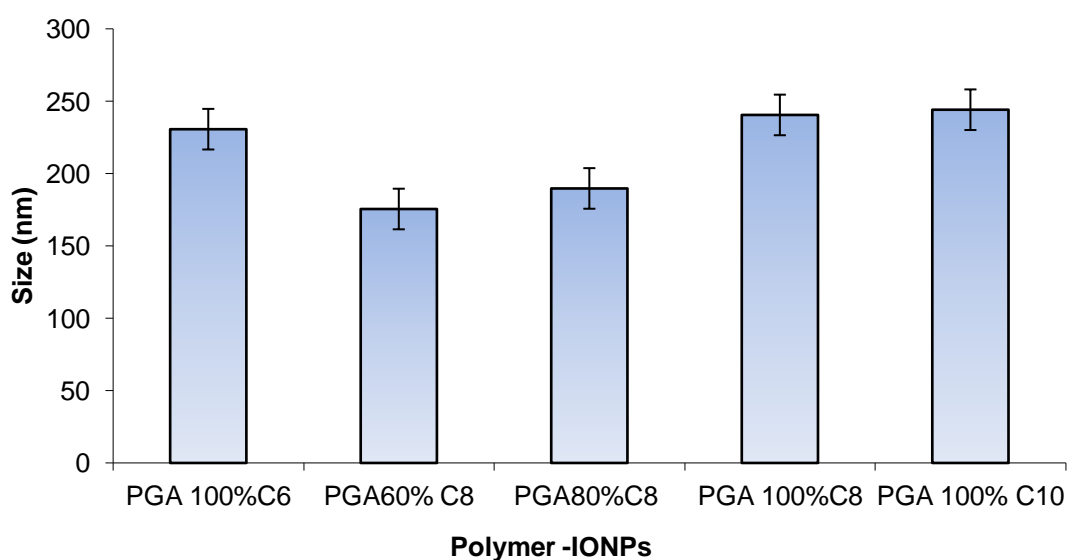


Figure 4-2: IONPs coated with different PGA by sonication method.

Fig. 4.2 shows the different PGAs–IONPs prepared using sonication. Sizes given are of diameter. Significant differences in trends could be observed between two methods. Comparing the particles obtained by IDP and particles prepared by sonication, mean hydrodynamic diameters between 120 nm to 160 nm were found for PGAs–IONPs prepared by IDP, while particles obtained by sonication method resulted in a range from 176 nm to 240 nm in diameter. Looking at some specific examples, PGA 60%C₈–IONPS were coated using two different methods. The hydrodynamic diameter of those prepared by sonication were measured with DLS and shown to be 176 nm in diameter, while the same polymer used for coating IONPs using the IDP method was smaller at 137 nm in diameter. Also the difference between the PGA 80%C₈ – IONPs gave 173 nm in diameter by IDP and 186 nm in diameter by sonication. With the sonication method the smallest IONPs was 176 nm in diameter, while with the IDP method the smallest size observed was 126 nm.

The polymer specification did affect the size of the coated particle, but there was no obvious correlation between the substitution and the size of coated nanoparticles. It was interesting to observe that the PGA 0% prepared using IDP were smaller than all the other preparations; however, it may be that the conditions used were still not optimal for our nanoparticles. Figs. 4.1 and 4.2 show the influence of the method of preparation on PGA–IONPs.

Fig. 4.3 shows the. PGA 60%C₈–IONP prepared by IDP which appeared to be spherical with a rounded surface where many small PGA 60%C₈–IONPs with different sizes can be seen. This result indicates the feasibility of coating of PGA 60%C₈–IONPs. The TEM image (Fig. 4.3) showed high populations of small particles in the background. In general, there are lots of small particles with around 84 ± 27.15 nm.

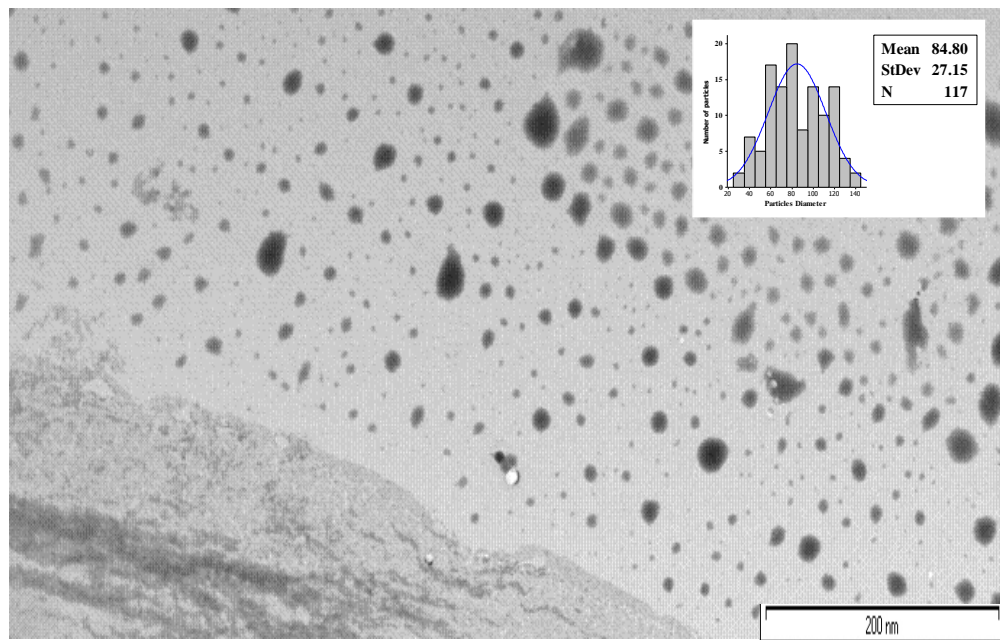


Figure 4-3: TEM image of PGA 60%C₈-IONPs by using IDP method. Showing mostly small particles with different sizes of large particles (Average size 84 ± 27 nm) (Scale bar 500 nm).

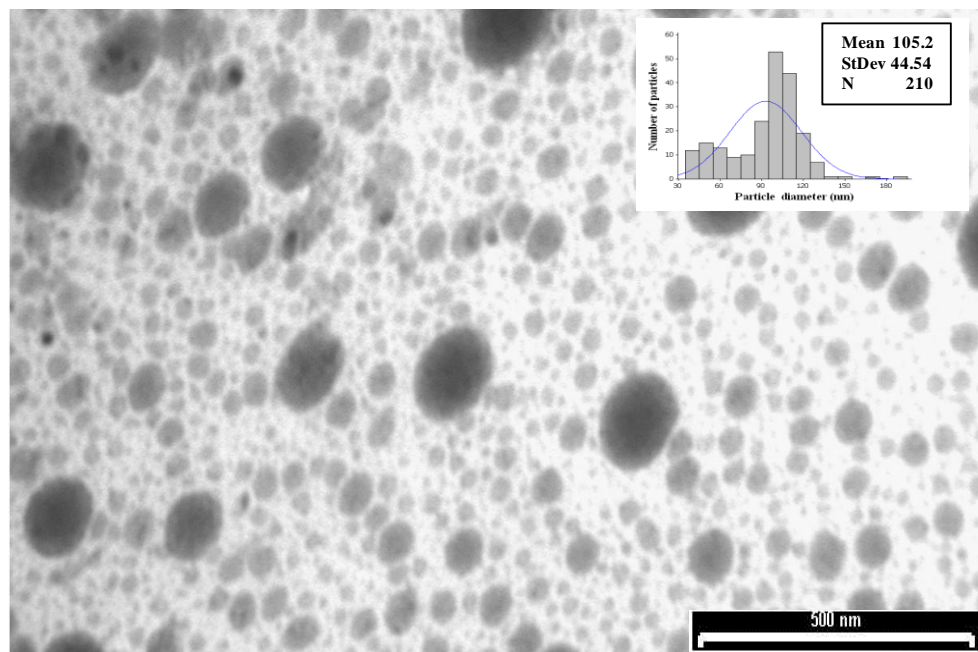


Figure 4-4: TEM image of PGA 100%C₈-IONPs by using sonication method. Showing mostly small particles with different sizes of large particles (Average size 105 ± 44 nm) (Scale bar 500).

Fig. 4.4 shows coated particles using the sonication method. The image showed that the NPs are almost spherical in shape. PGA 100%C₈ coated IONPs appeared similar in size and also had a low polydispersity. There are a lot of small coated particles and also large particles, the average size was around 105 ± 44 nm. Although the IDP method produced particles with a slightly smaller and narrower particle distribution, we would like to obtain still smaller and more monodisperse particles.

4.4.1.1 Zeta potential

Table 4.1 shows the zeta potential for IONPs coated with a number of PGAs with different substitutions either using the IDP method or by the sonication method. It shows that the zeta potential of all the particles is positive.

The zeta potential for the particles prepared by the sonication was around 25 ± 2.2 mV with 100% C₆, C₁₀ 25 ± 2.2 mV and C₈ 27 ± 5.1 mV which was very near to the uncoated and very near to the neutral. For the PGA0%–IONPs particles zeta potential became less positive: 5.3 ± 2.2 mV. Acylation of 60%C₈ and 20%C₈ increased positive zeta potential values to 31 ± 2.5 mV and 28.2 ± 3.9 mV. In the case of PGA 0%–IONPs and PGA 100%C₈–IONPs, using a different method for nanoparticles synthesis resulted in similar value. The zeta potential probably arose from the type of the acyl group attached on the polymers coated IONPs. The PGAs–IONPs were prepared using two methods leading to no significant difference between the preparations with regard to zeta potential. In the following experiments, we investigated a range of conditions for coating particles using PGA backbone.

Table 4-1: Shows examples of ξ potential of PGAs–IONPs.

Nanoparticles	Zeta potential mV \pm S.D	Method
IONPs	21.2 \pm 7.3	Co-precipitation
PGA 0%–IONPs	5.3 \pm 2.2	IDP
PGA 20% C ₈ –IONPs	28.2 \pm 3.9	IDP
PGA 60% C ₈ –IONPs	31.2 \pm 2.5	IDP
PGA 100% C ₆ –IONPs	22.8 \pm 4.1	Sonication
PGA 100% C ₈ –IONPs	27 \pm 5.1	Sonication
PGA 100% C ₁₀ –IONPs	25 \pm 2.2	Sonication

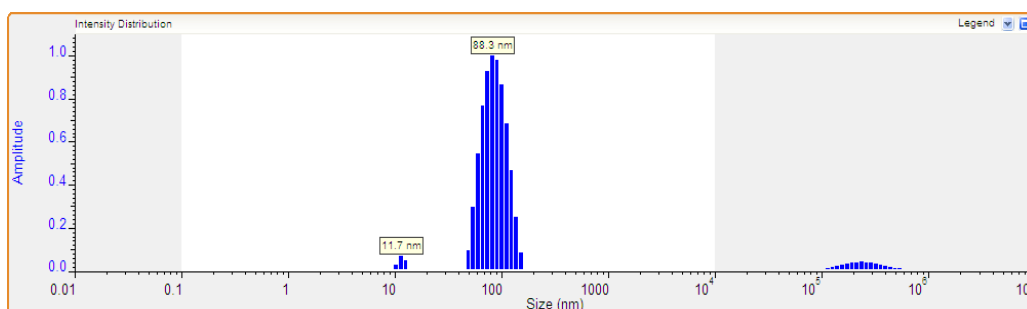
4.4.2 Optimisation of IONPs Coating Produced with PGA 0% Modified

The aim of this work was to determine how various formulation parameters affect the particle size. The amounts of polymers and acetone volume used in the IDP method and observed from the results were found to be critical for PGA coatings on IONPs. An experiment was designed to investigate effect on coating particles size the amounts of PGA with a constant a volume of acetone and different volumes of acetone with constant amounts of PGA to coat IONPs. The effect of organic solvent volume and amount of polymer was studied using the IDP method. Firstly, decreasing amounts of polymer were used in the presence of 1 ml acetone with different amount of polymers 1, 0.5, 0.2 and 0.1 mg. Figures 4.5a indicate that using 1ml acetone with 1 mg PGA 0% to coat IONPs led to very large nanoparticles. The mean PGA 0%–IONPs size in diameter was approximately 176 nm in diameter. So, a range of

amounts of acetone was used with a constant amount of polymer (1 mg). Acetone (1 ml) with different amounts of polymer led to very large particles.

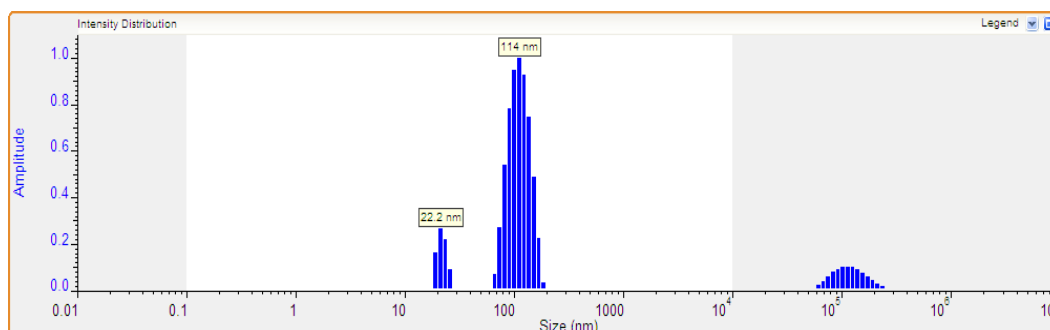
The results are shown in Fig. 4.5. In the range 1.0 mg and 0.5 mg of PGA 0% coat IONPs, a increase in the size from 176 nm and 227 nm in diameter respectively were observed (Fig. 4.5a and 4.5 b), while with 0.2 mg PGA 0% coated IONPs the mean diameter was 200 nm (Fig. 4.5c). Nanoparticles with a large mean diameter of 201 nm in diameter were obtained with 1 ml of acetone and 0.1 mg of PGA 0% to coat IONPs (Fig. 4.5d).

Figure 4-5: Different amounts of polymer with constant volume of acetone.



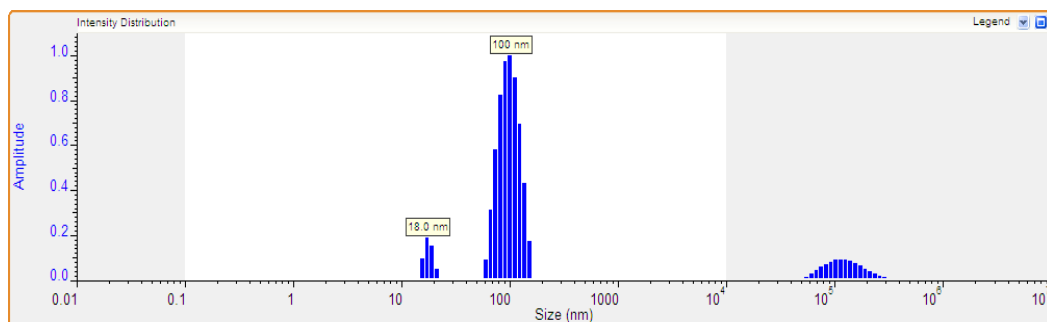
	Area %	Rh (nm)	Std Dev	% RSD
1	1.7	11.67	0.82	7.0
2	98.3	88.27	22.58	25.6

Figure 4.5a: The particle size distribution of 1 mg PGA 0%-IONPs by DLS (1 ml of acetone).



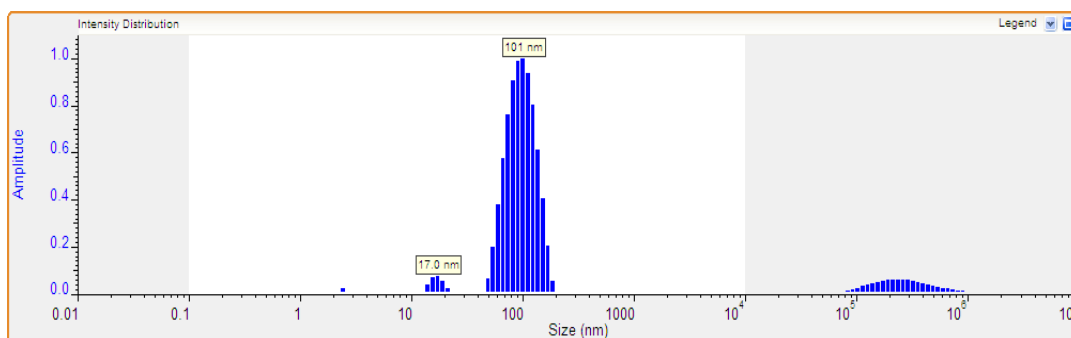
	Area %	Rh (nm)	Std Dev	% RSD
1	10.5	22.18	2.18	9.8
2	89.5	113.73	25.00	22.0

Figure 4.5b: The particle size distribution of 0.5 mg PGA 0%-IONPs by DLS (1 ml of acetone).



	Area %	Rh (nm)	Std Dev	% RSD
1	7.0	18.01	1.64	9.1
2	93.0	100.46	21.76	21.7

Figure 4.5c: The particle size distribution of 0.2 mg PGA 0%-IONPs by DLS (1 ml acetone).

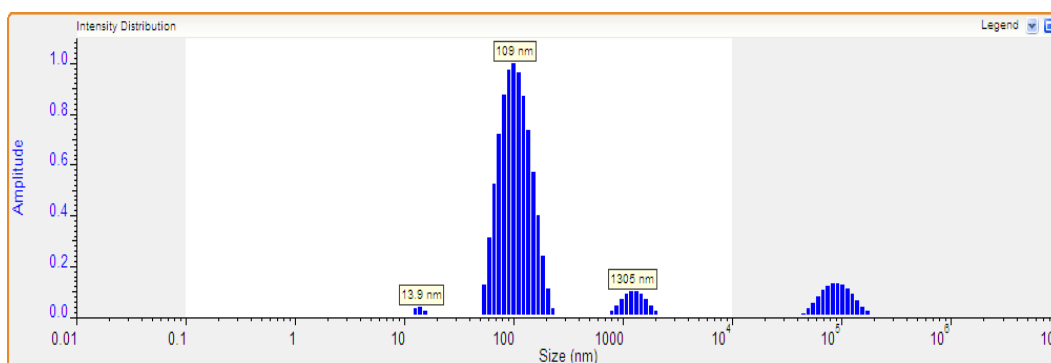


	Area %	Rh (nm)	Std Dev	% RSD
1	2.6	17.04	1.96	11.5
2	97.4	100.54	28.92	28.8

Figure 4.5d: The particle size distribution of 0.1 mg PGA 0%-IONPs by DLS (1 ml of acetone).

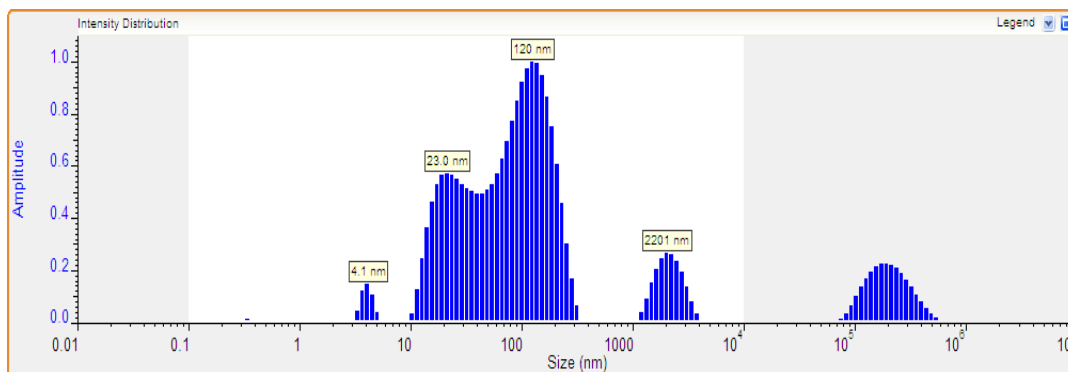
Increasing the amount of acetone (1.5, 2, 2.5 and 3 ml) with a constant amount of PGA 0% (1.0 mg) resulted in an optimum small size of polymers using 2 ml of acetone, with a subsequent increase again to bigger particles with larger volumes of acetone (Figs. 4.6 a-d, and 4.6 c). Nanoparticles made using 1mg of PGA 0% with 3 ml of acetone (Fig 4.6a) shows mono modal size distribution with peak at 218 nm in diameter, a very large particle. DLS analysis of nanoparticles made from 2.5 ml of acetone with 1 mg of PGA 0% (Fig. 4.6b) show a bimodal distribution with peaks at 46 nm in diameter and large particles about 240 nm in diameter with aggregates. . For the batch with 2 ml acetone (Fig 4.6c), mono modal particle size distribution was shown, with the majority of particles averaging 130 nm in diameter. A DLS graph showing the size distribution of particles made from 1.5 ml of acetone with 1 mg of PGA 0% (Fig 4.6d) gave a multi modal distribution, with main peak of 64 nm in diameter and some populations with nearly 2 μm sizes. Also, even a small population of 17 μm size.

Figure 4-6 : Different volumes of acetone with constant amount of the polymer.



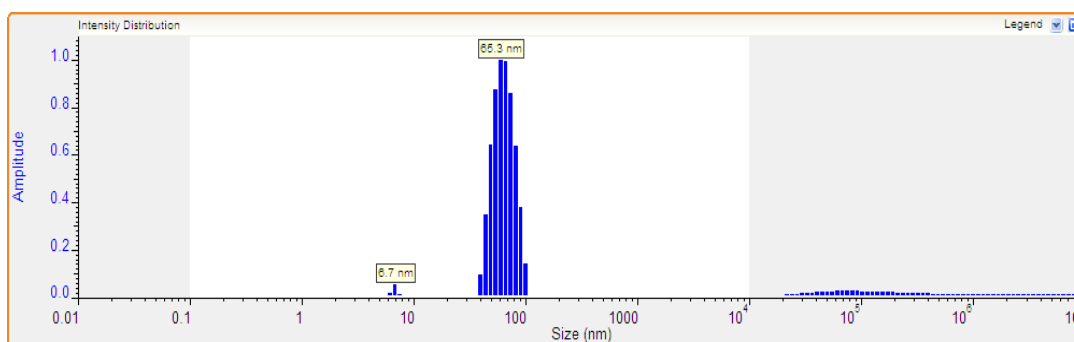
	% Area	Rh (nm)	Std Dev	% RSD
1	0.7	13.88	1.03	7.4
2	93.1	109.15	34.65	31.7

Figure 4.6a: The particle size distribution of 1 mg PGA0 %-IONPs with by DLS (3 ml of acetone).



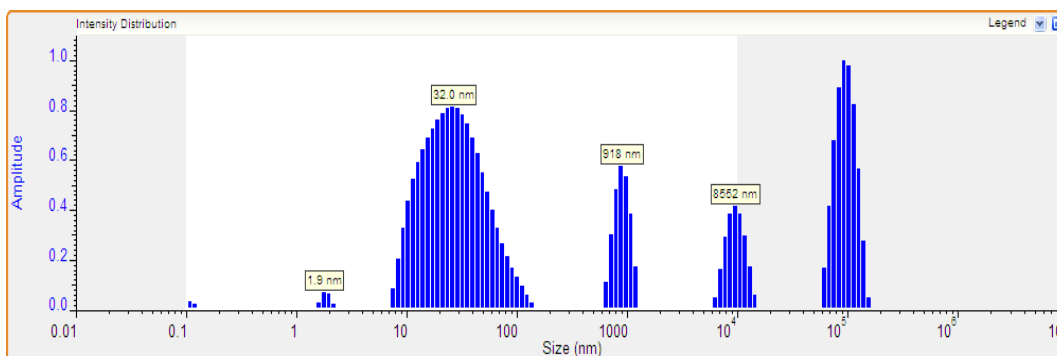
	% Area	Rh (nm)	Std Dev	% RSD
1	1.9	4.08	0.45	10.9
2	25.8	23.01	7.1	30.8
3	63.6	120.38	59.3	49.3
4	8.6	2200.56	572.75	26

Figure 4.6b: The particle size distribution of 1 mg PGA 0%-IONPs by DLS with (2.5 ml of acetone).



	Area %	Rh (nm)	Std Dev	% RSD
1	0.9	6.73	0.27	4
2	99.1	65.29	14.12	21.6

Figure 4.6c: The particle size distribution of 1 mg PGA 0%-IONPs by DLS with (2 ml of acetone).



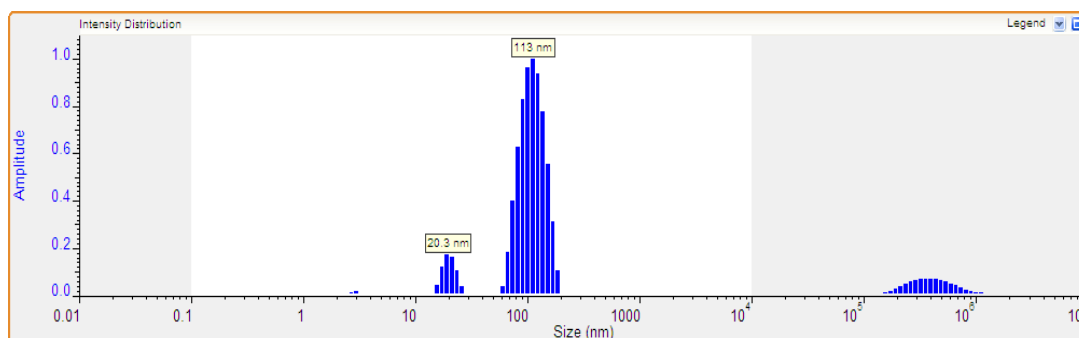
	Area %	Rh (nm)	Std Dev	% RSD
1	0.8	1.86	0.16	8.4
2	77.6	32.05	21.56	67.3
3	14.4	918.19	146.64	16
4	7.2	8551.57	966.46	11.3

Figure 4.6d: The particle size distribution of 1 mg PGA 0%-IONPs by DLS with (1.5 ml of acetone).

Clearly, both approaches were inefficient in their own right in terms of producing small size nanoparticles. However, an additional experiment, using a range of decreasing polymer amounts and 2 ml of acetone resulted in smaller particles with decreasing polymer amounts.

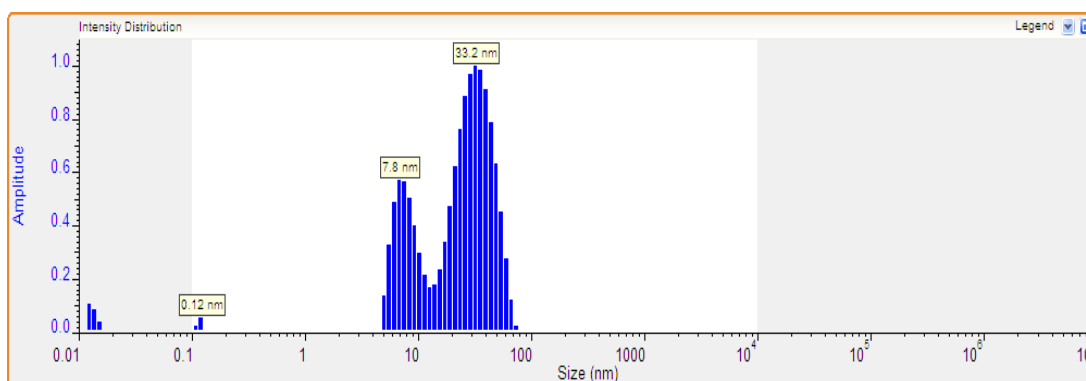
Using 1mg of the PGA 0% with the 2 ml of acetone to coat IONPs results in a large average diameter of the NPs with a bimodal size distribution, with major peak at 226 nm in diameter (Fig. 4.7a). The mean particle size was observed to fall significantly as smaller amounts of PGA 0% were used with a constant 2 ml amount of acetone. For example, in Fig. 4.7b the decrease of the amount of PGA 0% to 0.5 mg resulted in small PGA 0%-IONPs in bimodal size distribution with one peak at 66 nm in diameter and a small one at 15 nm in diameter. With 0.2 mg of PGA 0% coated IONPs a distribution of particle sizes and small size of 57 nm in diameter were obtained and a subsequent reduced risk of unwanted larger nanoparticles (Fig. 4.7c). By using 2 ml of acetone and 0.1 mg of PGA 0% to coat IONPs the majority of the PGA 0%-IONPs size was 85 nm in diameter with some small nanoparticles 9 nm in diameter (Fig. 4.7d).

Figure 4-7: Range of amounts of polymer with constant volume of acetone (2 ml).



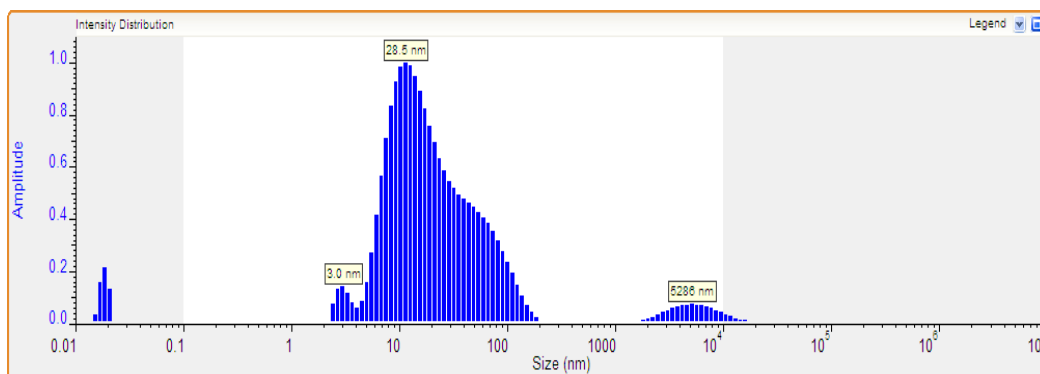
	% Area	Rh (nm)	Std Dev	% RSD
1	8.1	20.34	2.66	13.1
2	91.9	113.37	27.84	24.6

Figure 4.7a: The particle size distribution of 1 mg PGA 0%-IONPs by DLS (2 ml of acetone).



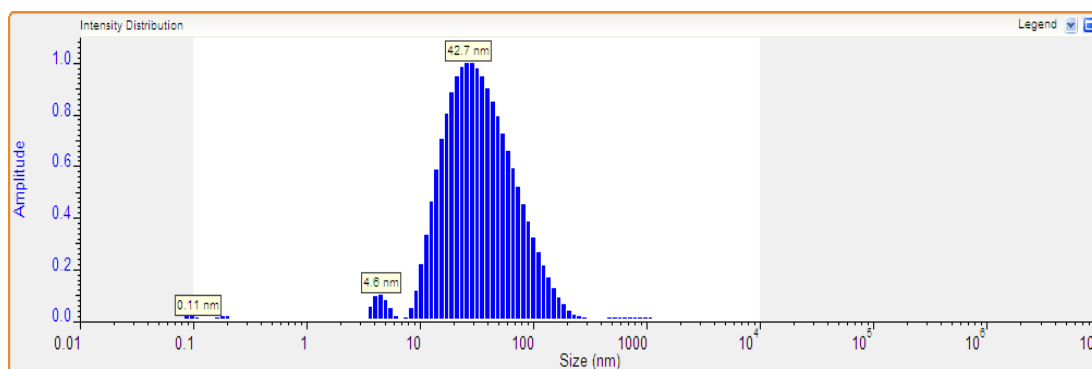
	%Area	Rh (nm)	Std Dev	% RSD
1	0.4	0.12	0	4.1
2	26	7.76	1.72	22.2
3	73.5	33.25	12.11	36.4

Figure 4.7b: The particle size distribution of 0.5 mg PGA 0%-IONPs by DLS (2 ml of acetone).



	% Area	Rh (nm)	Std Dev	% RSD
1	2.6	3	0.39	12.9
2	93.8	28.55	28.15	98.6
3	3.7	5285.7	2025.56	38.3

Figure 4.7c: The particle size distribution of 0.2 mg PGA 0%-IONPs by DLS (2 ml of acetone).



	% Area	Rh (nm)	Std Dev	% RSD
1	0	0.11	0	0
2	2	4.56	0.62	13.6
3	98	42.74	32.42	75.9

Figure 4.7d: The particle size distribution of 0.1 mg PGA 0%-IONPs by DLS (2 ml of acetone).

4.4.3 Morphology

Fig. 4.8 shows the transmission electron microscopy images of IONPs coated with 1mg of PGA 0% with 2 ml of acetone. This Figure shows that there is a distribution over a range of particle sizes 83 ± 55 nm. It can be seen there are many large particles with a few small particles. Particles appeared to be spherical.

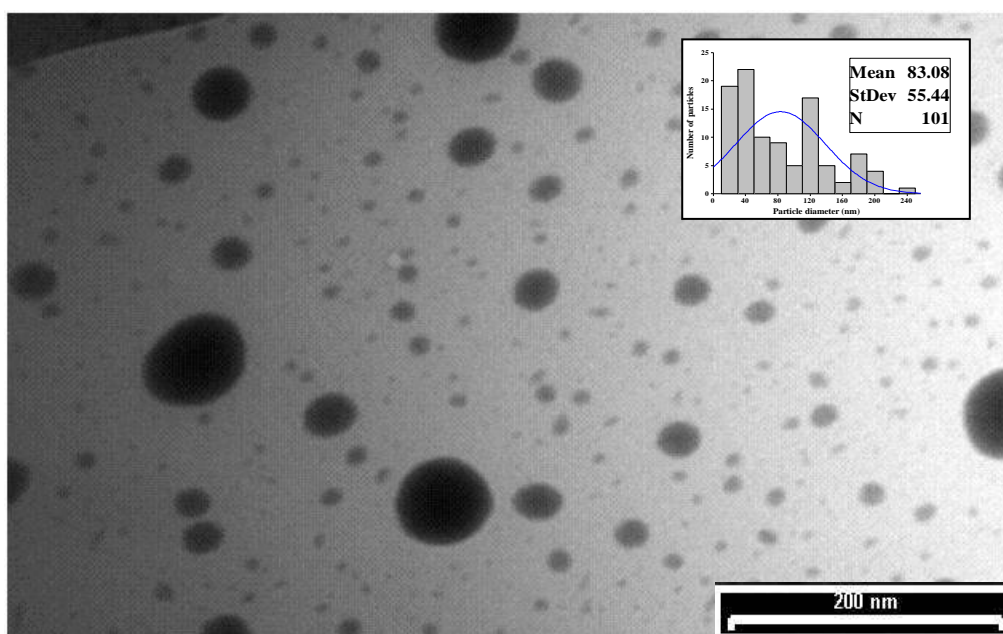


Figure 4-8 : TEM image of PGA 0% (1 mg) with (2 ml) of acetone-IONPs. Which is showing a large number of large particles, fewer small particles (Average size 83 ± 55 nm) (Scale bar 200 nm).

In Fig. 4.9, the IONPs coated with 0.5 mg of PGA 0% showed a fairly narrow size distribution with many large particles. The mean particle size ranged was 194 ± 81 nm in diameter. In the background a small particles can be seen.

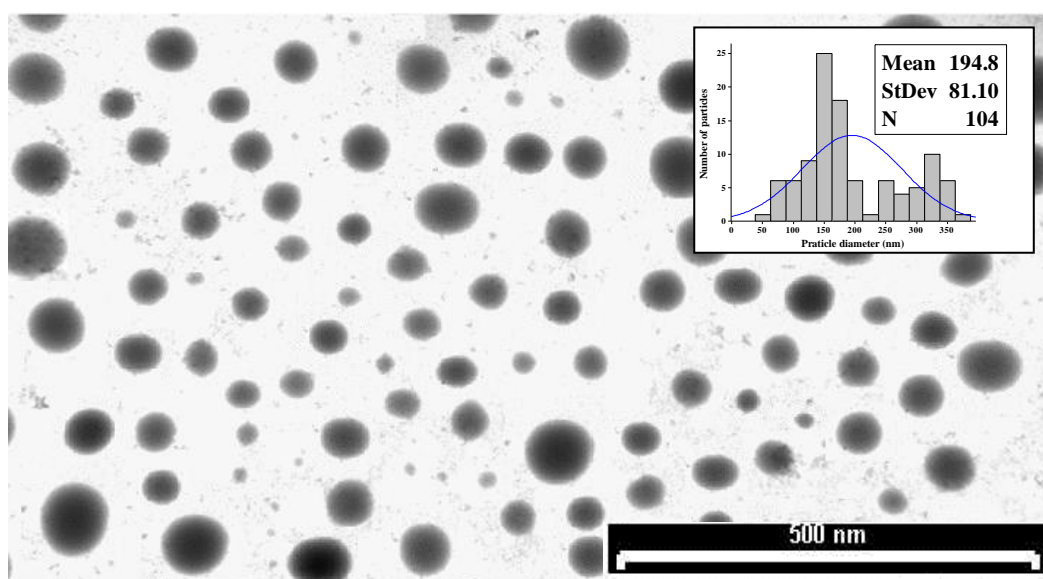


Figure 4-9: TEM image of PGA 0% (0.5 mg) with (2 ml) of acetone-IONPs. Which Showing large particles, many fewer small particles (Average size 194 ± 81 nm) (Scale bar 5000 nm).

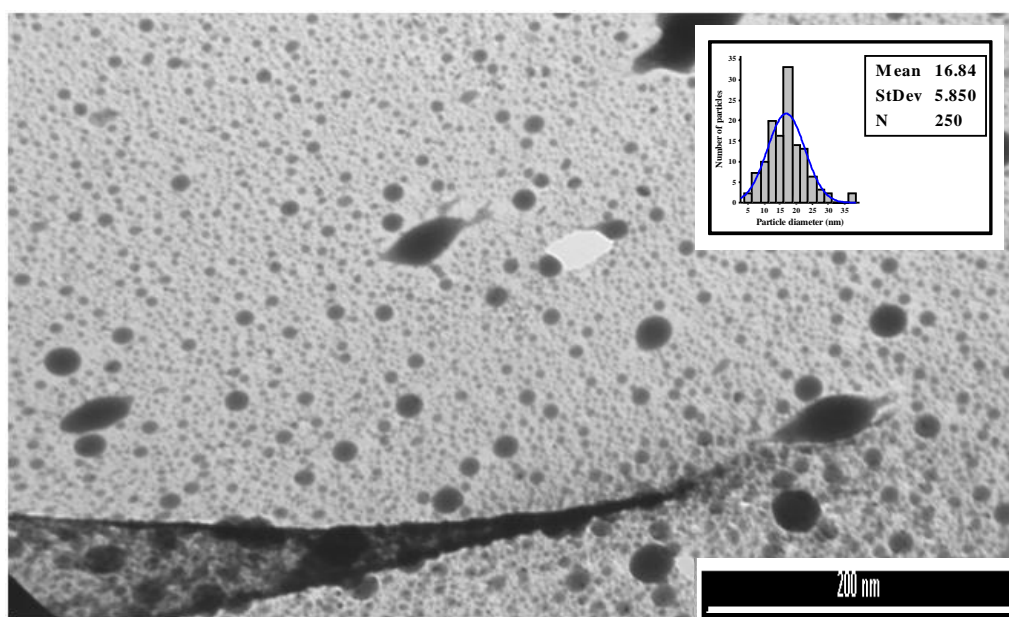


Figure 4-10: TEM images of PGA 0% (0.2 mg) with (2 ml) of acetone – IONPs. Which Showing fewer large particles, many very small particles (Average size 16 ± 5 nm) (Scale bar 200 nm).

IONPs coated with 0.2 mg of PGA 0% with 2 ml of acetone are shown in the TEM image presented in Fig. 4.10. The micrograph depicts a large number of smooth, small size spherical particles well dispersed in the polymer. The size of the particles was uniform with most of the small coated particles in particle size 16 ± 5 nm in diameter.

IONPs coated with 0.1 mg of PGA 0% prepared in this study, the shape of particles was spherical with good distribution, also some large particles as coated aggregate can be seen, and the average size was 24 ± 8 nm in diameter (Fig. 4.11).

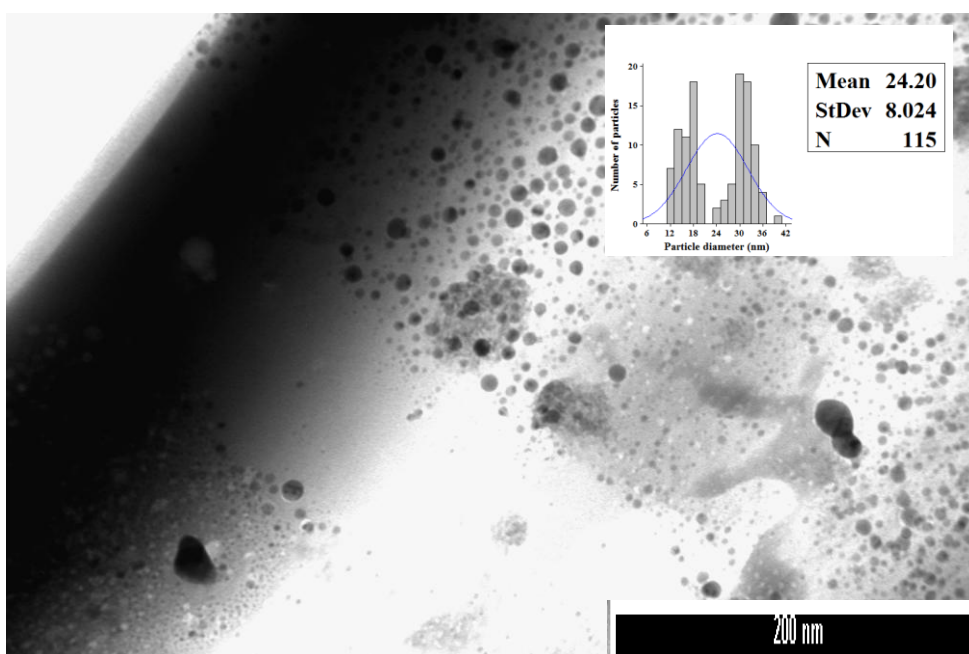


Figure 4-11: TEM image of PGA 0% (0.1 mg) with (2 ml) of acetone-IONPs. Showing a mixture of particle sizes, overall reduction in particle size (Average size 24 ± 8 nm) (Scale bar 200 nm).

4.4.3.1 Zeta potential

Zeta potential for 1 mg particles was 35.8 ± 7 mV, while 0.5 mg of PGA 0%–IONPs also exhibited a positive charge with a zeta potential of 55.6 ± 12.4 mV. For the 0.2 mg of PGA 0%–IONPs zeta potential became even more positive at 62.2 ± 11.3 mV. 0.1 mg PGA 0%–IONPs showed positive zeta potential of the particles at 39.8 ± 5.5 mV (Table 4.2).

Table 4-2: Surface charge and sizes of the best formulations with different amounts of PGA 0%–IONPs.

Nanoparticles	DLS NP diameter (nm)	TEM NP diameter (nm)	ζ -potential mV \pm SD
PGA 0% 1 mg with 2 ml of acetone–IONPs	227	83 ± 55	35.8 ± 7.0
PGA 0% 0.5 mg with 2 ml of acetone–IONPs	66	194 ± 81	55.6 ± 12.4
PGA 0% 0.2 mg with 2 ml of acetone–IONPs	46	16 ± 5	62.2 ± 11.3
PGA 0% 0.1mg with 2 ml of acetone–IONPs	84	24 ± 8	39.8 ± 5.5

4.4.4 Modification of PGA polymers

4.4.4.1 Synthesis of PGA 40% C₁₈ by acylation of backbone PGA

PGA backbone was modified to change its physicochemical characteristics in order to increase the interaction between the nanoparticles and the polymer and increase the stability of nanoparticles. The acylation was achieved by reaction of a percentage of the pendent hydroxyl group from the PGA backbone with

acid chloride using pyridine as acid scavenger and catalyst. The substitution of backbone was 40% C₁₈, i.e. poly(glycerol adipic acid), with 40% of the free hydroxyl groups substituted with an 18 carbon alkyl chain, attached via an ester linkage. The C₁₈ group provides a greater degree of hydrophobicity to the polymer. The compositions of polymer and backbone were analysed by proton NMR. Gel permeation chromatography, also provided data on the molecular weight and distribution. Following are the NMR scans of the polymer backbone (Fig. 4.13) and 40% C₁₈ substituted polymers (Fig. 4.15) together with the annotated PGA (Fig.4.12) and PGA 40% C₁₈ (Fig.4.14) structures.

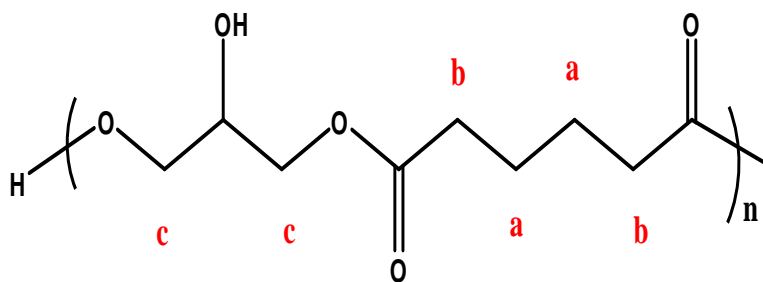


Figure 4-12: Structure of PGA backbone.

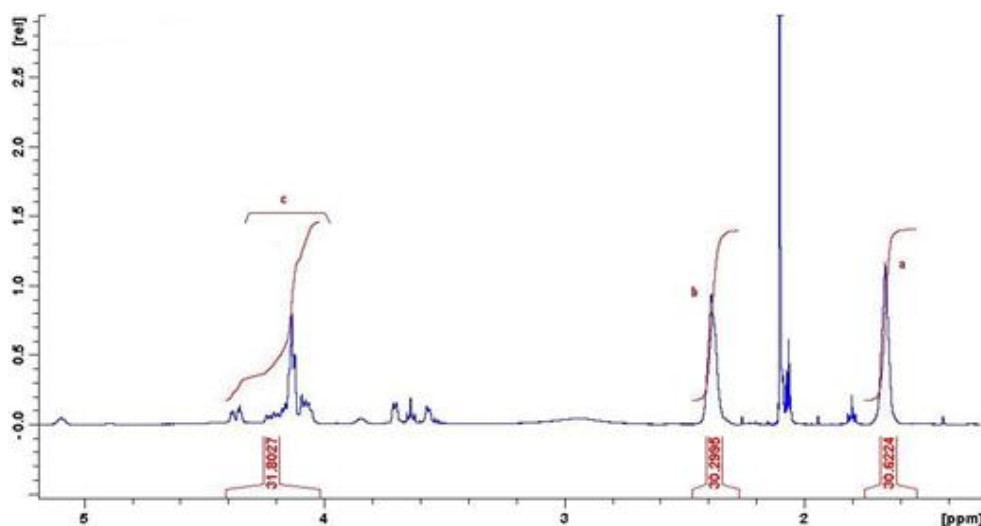


Figure 4-13: NMR spectrum for poly(glycerol adipate) backbone.

The peaks of the $\text{CH}_2\text{-CH}_2$ protons appear at δ (1.59–1.72 ppm) while the peaks of $\text{CH}_2\text{-CO}$ protons appear at δ (2.20–2.40 ppm). A broad multiplet at δ (4.02–4.27 ppm) corresponds to the $\text{CH}_2\text{-CH(OH)-CH}_2$ methylene protons.

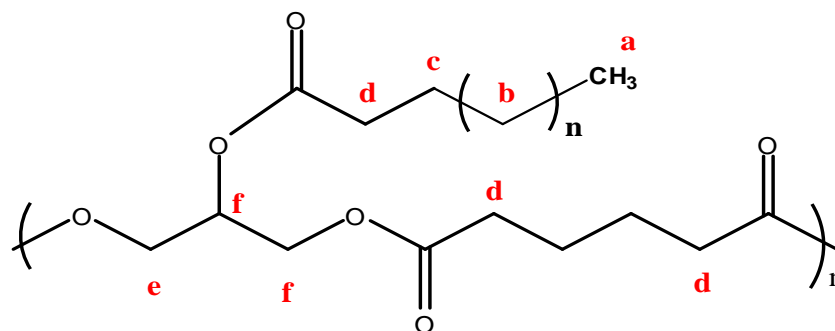


Figure 4-14: Structure of PGA 40% C_{18} .

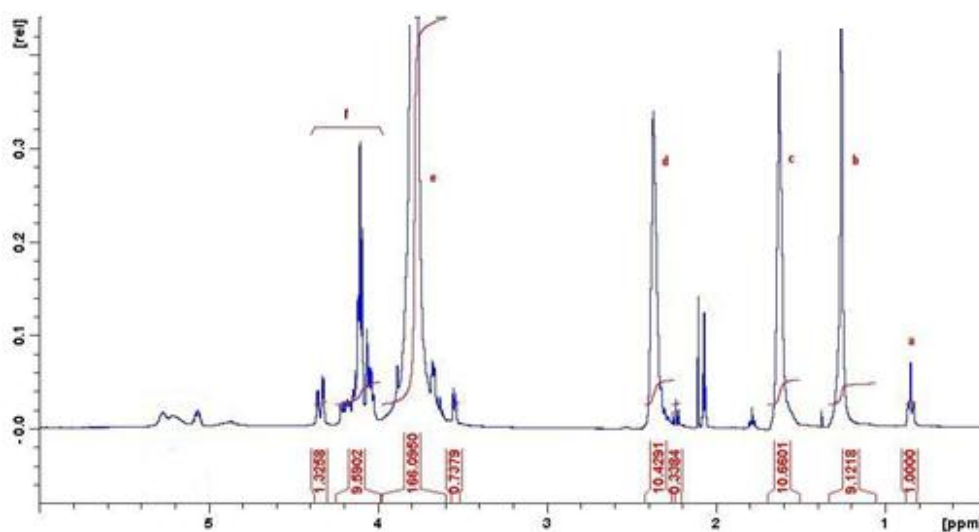


Figure 4-15: NMR spectrum for poly (glycerol adipate) 40% C_{18} .

The same peaks mentioned above are also apparent in the NMR spectrum of PGA 40% C_{18} . However, the presence of the acyl group is indicated by the peaks appearing at δ (0.81–0.89 ppm) for terminal methyl protons, δ (1.51–1.69 ppm) for $\text{OCO-CH}_2\text{-CH}_2$ protons and δ (2.26–2.42 ppm) for OCO-CH_2 protons. By NMR the proportion of hydroxyl groups substituted with acyl side

chains was estimated to be 48% in comparison to the expected 40% by comparing the single intensity of δ (1.51–1.69 ppm) for OCO-CH₂-CH₂ and δ (2.26–2.42 ppm) for OCO-CH₂. The covalent attachment of acyl group can be also confirmed by the GPC chromatograms when the Mn of PGA 0% (Fig. 4.16) increased from 10437 to 12038 for the PGA 40%C₁₈ polymer (Fig. 4.17). Assuming the molecular weight of backbone Mn at 10437 while the PGA 40%C₁₈ at 40% substitution was estimated to have an Mn of 15757. The change determined by GPC was lower than the theoretical figure. This was probably due to a structural change in the polymer, but the increase of molecular weight indicated that the acylation had occurred.

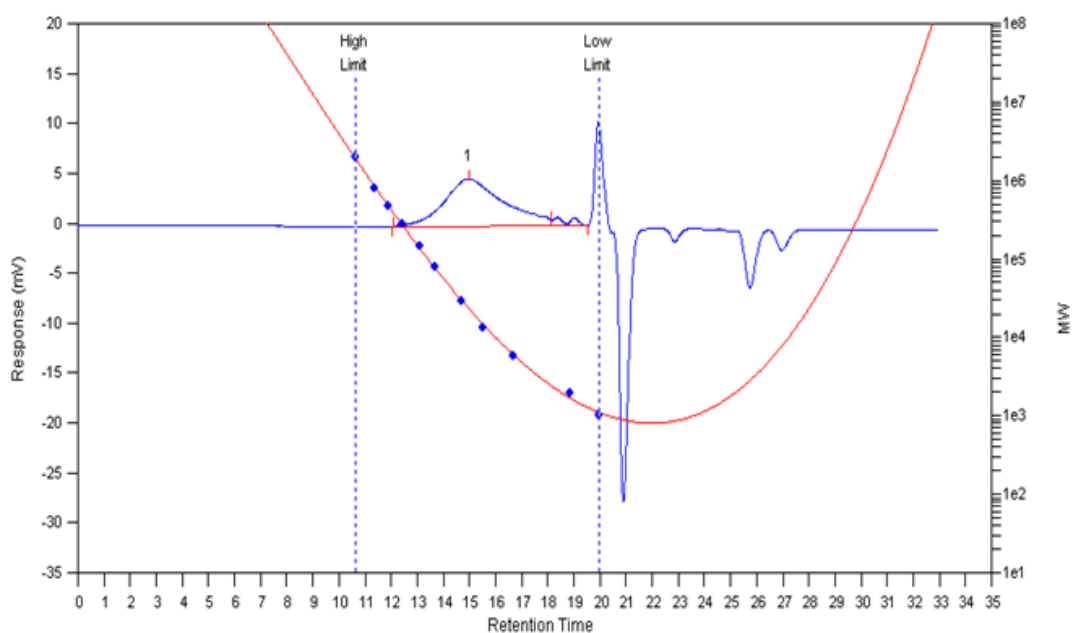


Figure 4-16: GPC elution profile for poly(glycerol adipate) backbone. The red line is the calibration curve, while peak 1 shows the retention time of the polymer. The peaks at the low limit are the solvent front.

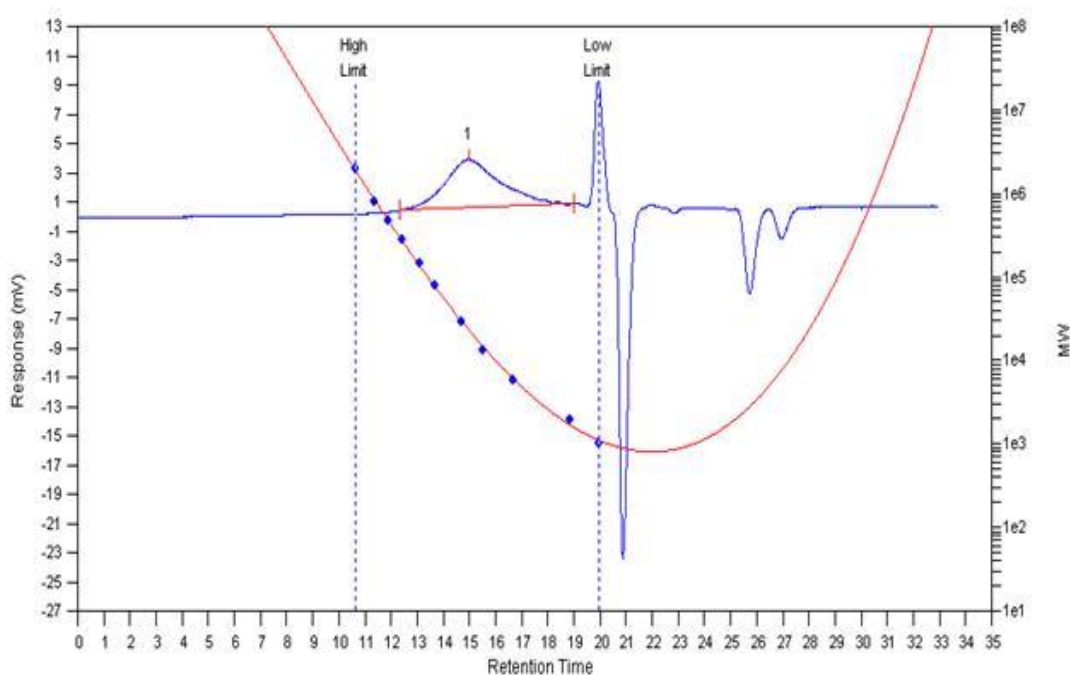


Figure 4-17: GPC elution profile for poly (glycerol adipate) 40%C₁₈. The red line is the calibration curve, while peak 1 shows the retention time of the polymer. The peaks at the low limit are the solvent front.

The FTIR of the polymer substituted with 40%C₁₈ (Fig. 4.19) further confirmed the presence of strong ester bond peaks at 1383.47 and 1462.39.50 cm⁻¹, which were absent in the scan of the unmodified polymer (Fig. 4.18). The peaks for the hydroxyl groups shifted from 2916.89 in the polymer backbone to 2360.394 m⁻¹ and OH appears at 3610.05 cm⁻¹, probably due to the involvement of some protons in an esterification reaction.

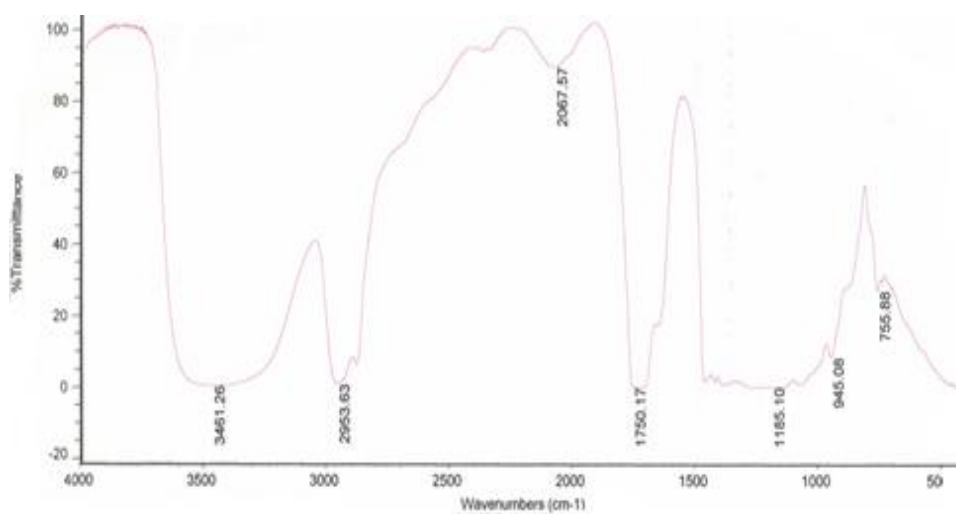


Figure 4-18: FTIR of poly(glycerol adipate) backbone.

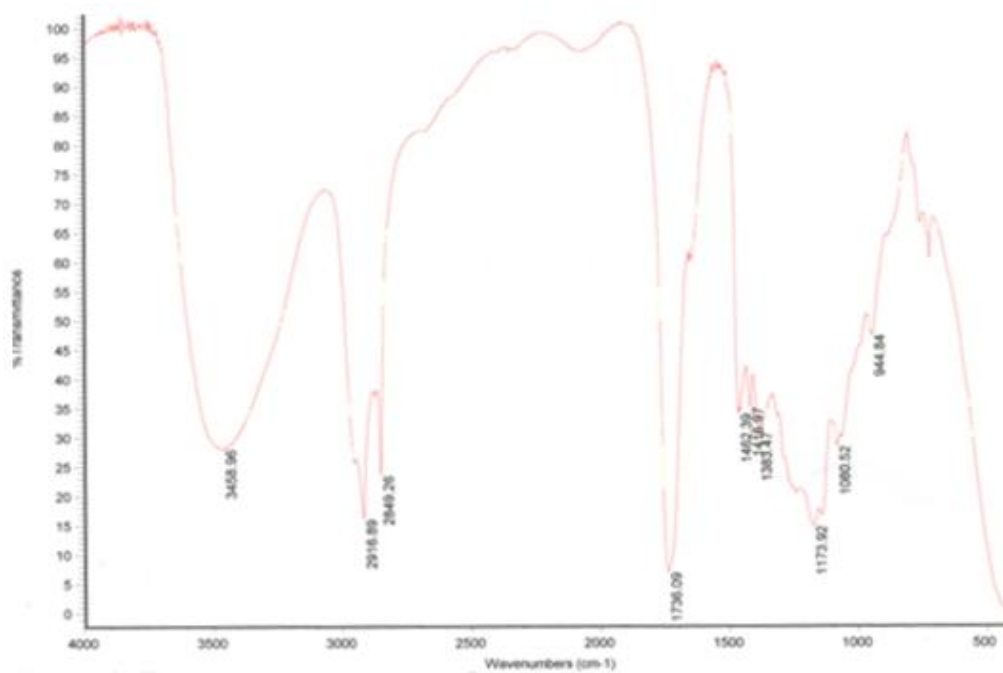


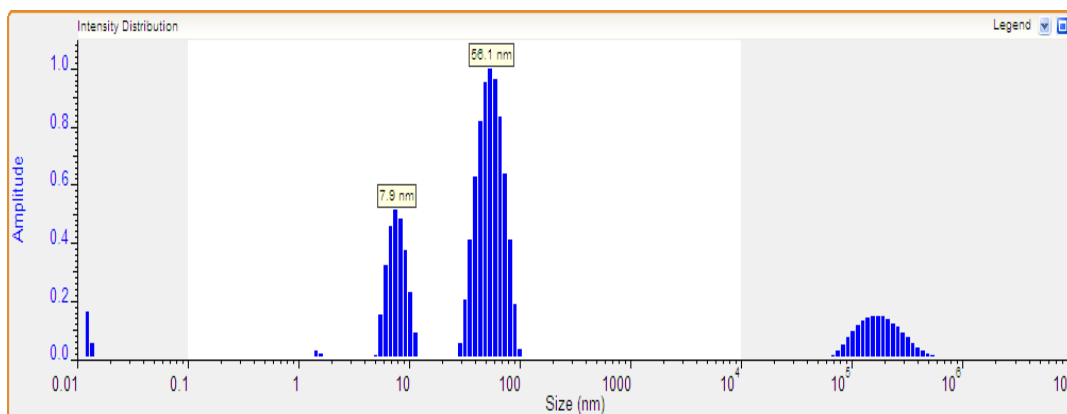
Figure 4-19: FTIR of poly(glycerol adipate) 40%C18.

4.4.5 PGA 40% C_{18} coated IONPs

IONPs were coated with PGA 40% C_{18} again using the interfacial deposition method where IONPs were dispersed in water, and we chose 0.2 mg PGA 40% C_{18} in 2 ml of acetone as the starting point for optimisation as this was the optimum from the previous experiments with PGA 0%. The IONPs were coated with polymer and dispersed in the acetone then the polymer precipitated and coated the IONPs. The PGA 40% C_{18} polymer variant is more hydrophobic and so forms nanoparticles more easily, but the presence of some free hydroxyl groups should help nanoparticles be coated because of possible interaction between the hydroxyl groups and the IONPs surface.

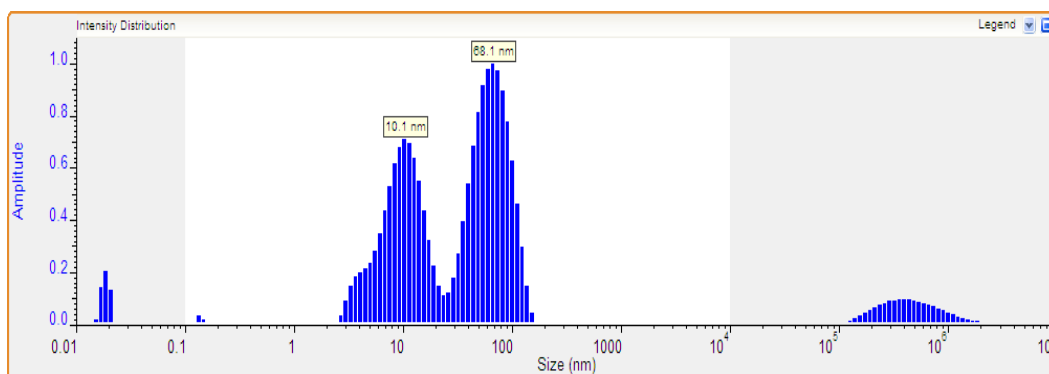
4.4.5.1 Particle size and morphology

Amounts of added polymer ranged from 0.5 to 0.1 mg PGA 40% C_{18} with constant volume of acetone (2 ml) to produce coated IONPs. The particle size distributions measured by dynamic light scattering are shown in Figures 4.20, 4.21 and 4.22, respectively. The size distribution of 0.5 mg of PGA 40% C_{18} coated IONPs shown in Fig. 4.20 showed two narrow peaks at about 15 nm and 113 nm in diameter. The size distribution of the 0.2 mg PGA 40% C_{18} -IONPs displayed two peaks and the diameter of the small particles was determined to be 20 nm in diameter and of the larger ones was 136 nm in diameter (Fig. 4.21). For Fig. 4.22, the IONPs were coated with 0.1 mg of PGA 40% C_{18} and showed a dominant peak at about 136 nm in diameter and the minor peak around 17 nm in diameter, which suggested that there was aggregation among the particles.



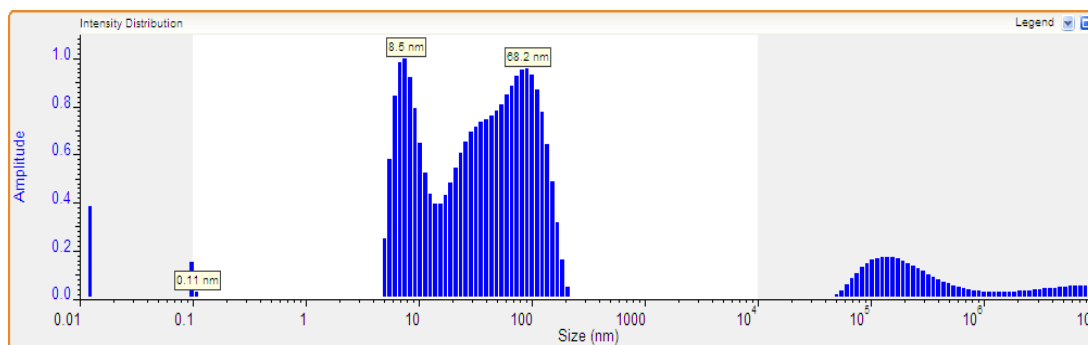
	% Area	Rh (nm)	Std Dev	% RSD
1	26.6	7.93	1.47	18.5
2	73.4	56.56	14.59	26

Figure 4-20: The particle size distribution of 0.5 mg PGA 40% C_{18} -IONPs by DLS.



	% Area	Rh (nm)	Std Dev	% RSD
1	42.8	10.11	4.29	42.4
2	57.2	68.07	25.89	38

Figure 4-21: The particle size distribution of 0.2 mg PGA 40% C_{18} -IONPs by DLS.



	% Area	Rh (nm)	Std Dev	% RSD
1	0.1	0.11	0	0
2	30.1	8.54	2.43	28.5
3	69.9	68.24	41.79	61.2

Figure 4-22: The particle size distribution of 0.1 mg PGA 40% C_{18} -IONPs by DLS.

The TEM images showed the morphology of different preparations of PGA 40% C_{18} coated IONPs (Figs. 4.23–4.25). It can be seen from the TEM image Fig. 4.23 that 0.5 mg of PGA 40% C_{18} coated IONPs showed large particles about 105 ± 32 nm. However, some small PGA 40% C_{18} coated IONPs can still be seen. TEM images showed the particles are spherical.

The image in Fig. 4.24 using 0.2 mg of PGA 40% C_{18} shows a huge number of small PGA 40% C_{18} coated IONPs of a diameter approximately 23 ± 7 nm while a few large coated nanoparticles were also present. There were very clearly separate, small coated particles. The morphology of the 0.1 mg PGA 40% C_{18} coated IONPs is shown in Figure 4.25. The particle size was large particles, 80 ± 52 nm. It was also noted that there were individual small IONPs inside surrounded by a layer of the grey polymer. Also there were large IONPs aggregates coated with PGA 40% C_{18} . By comparing with Figure 4.23 (0.5 mg PGA 40% C_{18} -IONPs.) and Figure 4.25 (0.1 mg PGA 40% C_{18} -IONPs), the IONPs coated with 0.2 mg of PGA 40% C_{18} (Fig. 4.24) were much smaller. In addition, it was observed that that nanoparticles exhibit excellent dispersion for

all the preparations, which indicated that the polymers have the function of providing a repulsive force to prevent aggregation among particles. It was also noted that the IONPs were observed as dark spots. In the images of the IONPs that had been coated, there was a mixture of small particles and big particles, which agreed with the DLS analysis table (4.3).

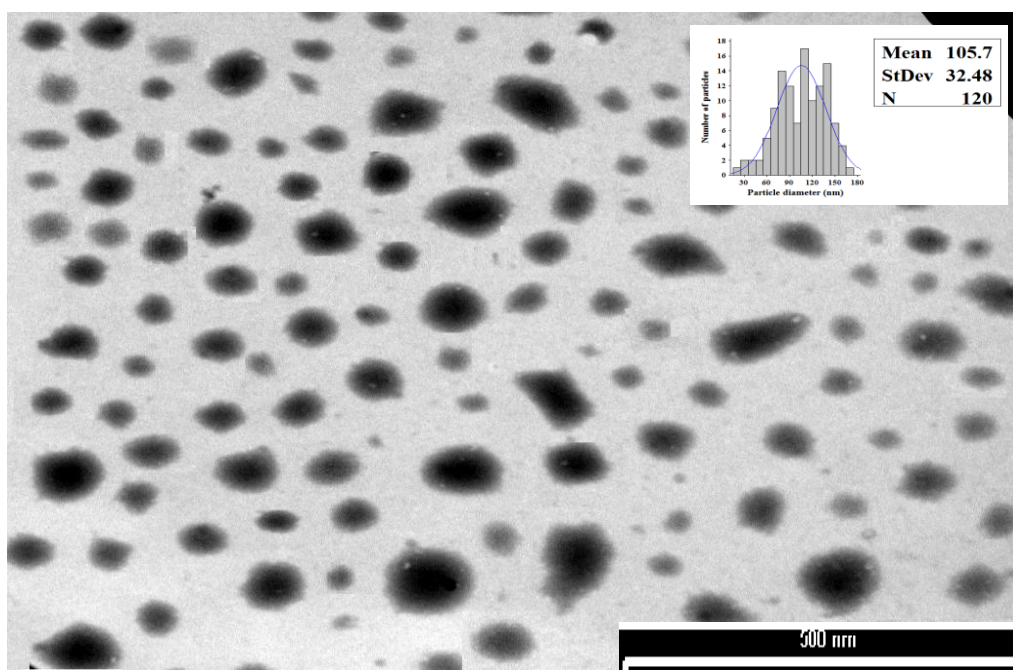


Figure 4-23: TEM images of 0.5 mg PGA 40% C_{18} -IONPs. Different sizes of larger particles are present with small coated nanoparticles (Average size 105 ± 32 nm) (Scale bar 500 nm).

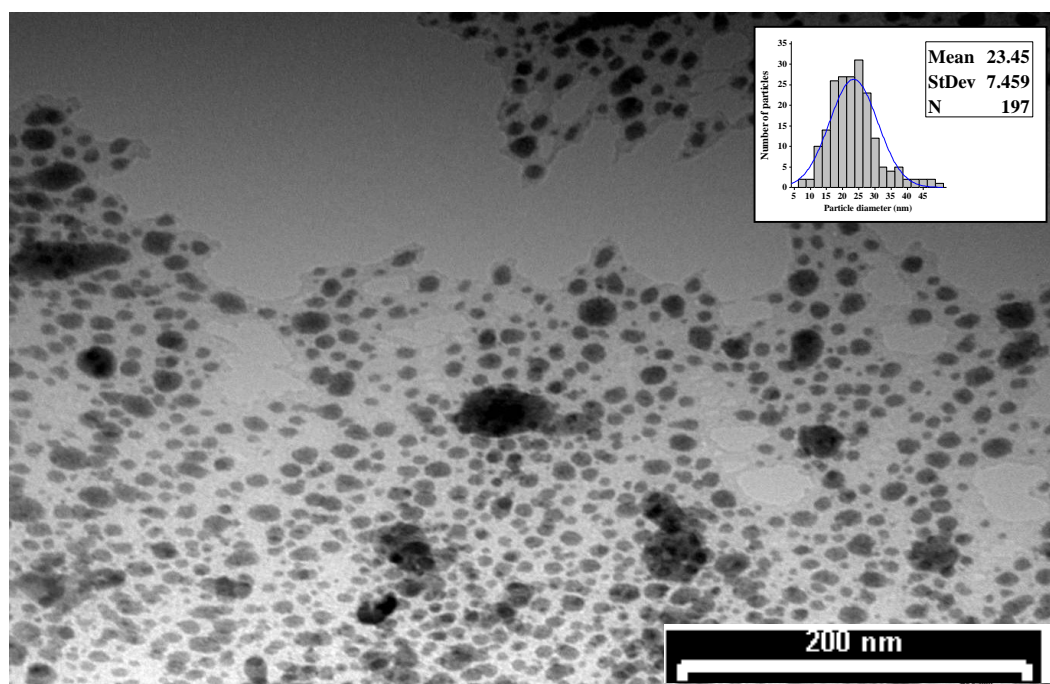


Figure 4-24: TEM images of 0.2 mg PGA 40% C_{18} -IONPs. The majority are small coated nanoparticles (Average size 23 ± 7 nm) (Scale bar 200 nm).

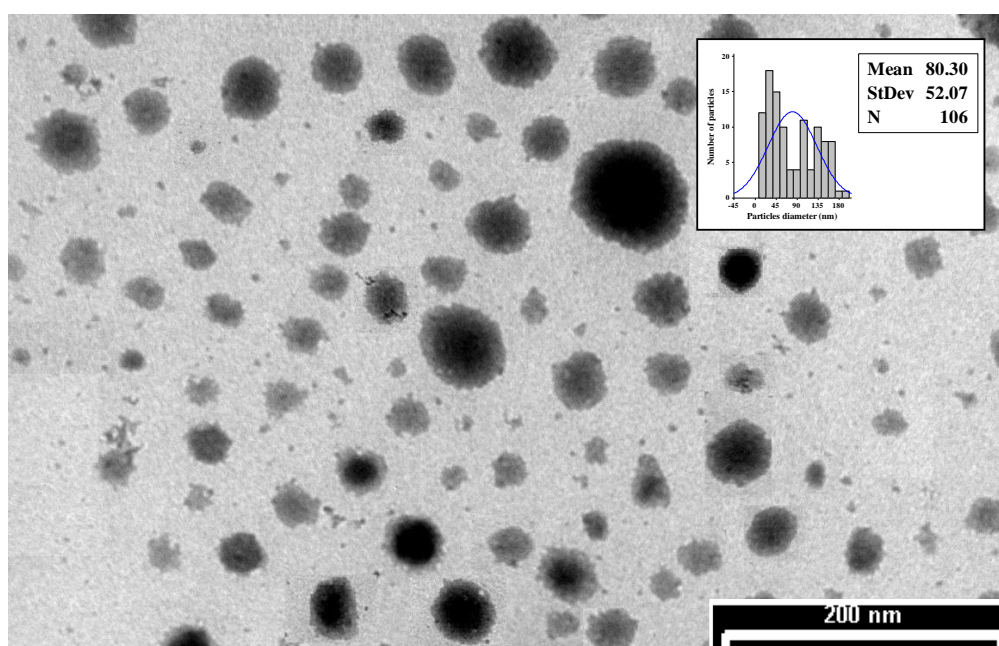


Figure 4-25: TEM images of 0.1 mg PGA 40% C_{18} -IONPs. Large particles with a few small particles (Average size 80 ± 52 nm) (Scale bar 200 nm).

Table 4-3: The surface charge and sizes of PGA 40% C_{18} -IONPs.

Nanoparticles	DLS NP diameter (nm)	TEM NP diameter (nm)	ζ -potential mV \pm S.D.
IONPs	13	13	21.2 \pm 73
0.5 mg of PGA 40% C_{18} -IONPs	14 and 122	105 \pm 32	23.5 \pm 10.5
0.2 mg of PGA 40% C_{18} -IONPs	20 and 136	23 \pm 7	67.7 \pm 118
0.1 mg of PGA 40% C_{18} -IONPs	136	80 \pm 52	50.06 \pm 17.2

4.4.5.2 Zeta potential

All formulations exhibited a net positive charge with ζ potential values ranging from 23 \pm 10.5 mV to 67.7 \pm 11.8 mV. IONPs coated with 0.5 mg of PGA 40% C_{18} showed values similar to the uncoated. In the formulations with 0.1 mg and 0.2 mg of PGA 40% C_{18} -IONPs an increase in the positive charge was observed (Table 4.3).

4.4.6 Particle Stability

The stability of nanoparticles to aggregation is an important parameter in producing useful formulations for *in vivo* use. Stability can be determined by the addition of salt and noting the concentration at which an increase in turbidity appears. Salt is capable of destabilising both electrostatic and sterically stabilised particles. Different incubation solutions were used to

determine the stabilisation of particles achieved by the adsorption of various polymer, surfactant and protein over-coatings.

4.4.6.1 0.1% Tween 80-coated PGA 0%-IONPs and PGA 40% C_{18} -IONPs

IONPs were coated with PGA polymers and, to increase the stability further, they were over-coated with the Tween 80, a PEG containing surfactant. Tween 80 has previously been used to improve the stability of PGA nanoparticles, particularly for increased stability in a biological medium.

4.4.6.2 0.1% Albumin-coated PGA coated IONPs and PGA 40% C_{18} coated IONPs

Putting particles into serum typically results in an adsorbed protein coating which can further stabilise nanoparticles. Albumin will be of great help in designing the system, as it is known to induce transcytosis of nanoparticles through the blood-brain barrier (Lu et al., 2005). Albumin-coated gold nanoparticles were used as a drug carrier to cross the blood-brain barrier and this makes them a good candidate for carrier in drug delivery (López-Viota et al., 2009). As albumin is also naturally present in serum, this may represent the coating actually present on nanoparticles in the presence of serum in cell culture and *in vivo*.

4.4.7 Colloidal Stabilisation of IONP

The turbidity of nanoparticles of different composition in the presence of increasing concentrations of NaCl is shown in Figs 4.26 and 4.27. The IONPs coated with dextran and with different formulations of PGA backbone 1.0 mg, 0.5 mg, 0.2 mg, 0.1 mg, PGA 40% C_{18} and overcoating with Tween and albumin. PGA nanoparticles (170 nm) were used as a reference because these particles have been used previously for drug delivery systems.

The IONPs and IONPs coated with these polymers were titrated with increasing concentrations of aqueous sodium chloride solution, and UV visible absorbance values at 500 nm were used to monitor the turbidity of the corresponding dispersion. Before coagulation the IONPs were stabilised by electrostatic repulsion force.

Increasing the concentration of salt can both neutralise the surface charges or cause a change in the structure of the water and affect polymer chains, causing them to become dehydrated and resulting in coagulation. Figures 4.26 and 4.27 show the relationships of the nanoparticle stabilities and the salt concentration of the medium. It can be seen that the IONPs were unstable at any salt addition. PGA 0%–IONPs showed some absorbance at very low salt concentration, suggesting some particles were poorly coated or uncoated.

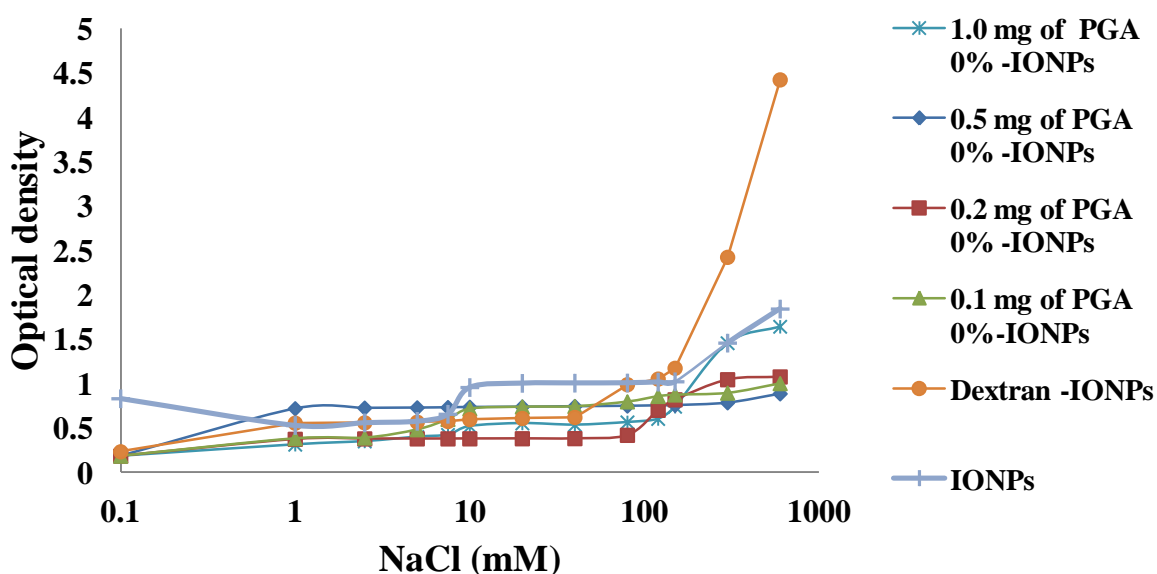


Figure 4-26 Stabilities of IONPs and IONPs coated with PGA 0% or dextran. Various PGA 0%–IONP formulations and dextran–IONPs were titrated with increasing salt concentrations and the aggregation of the formulations was monitored by optical density at 500 nm.

Dextran-IONPs became unstable at 80 mM salt concentration. However, all coated particles with 1.0 mg of PGA 0%-IONPs showed a higher stability than dextran over the range 1 mM to 120 mM salt. The IONPs coated with PGA 0% 0.5 mg and 0.1 mg-IONPs showed a similar stability. In this study, the result suggests that at some point the particles aggregate. However, this is different for different coatings. The 0.2 mg of PGA 0%-IONPs showed excellent stability when compared with the other preparations, particularly over 10-100 mM NaCl concentration range.

The stability studies have also been carried out on the optimised coated nanoparticle preparations. Particles coated with 0.2 mg of PGA 40% C_{18} -IONPs and coated with additional further coatings, such as Tween and albumin over-coatings, are shown in Figure 4.27. Note that the absorbance scale in Figure 4.27 is expanded in comparison to Figure 4.26.

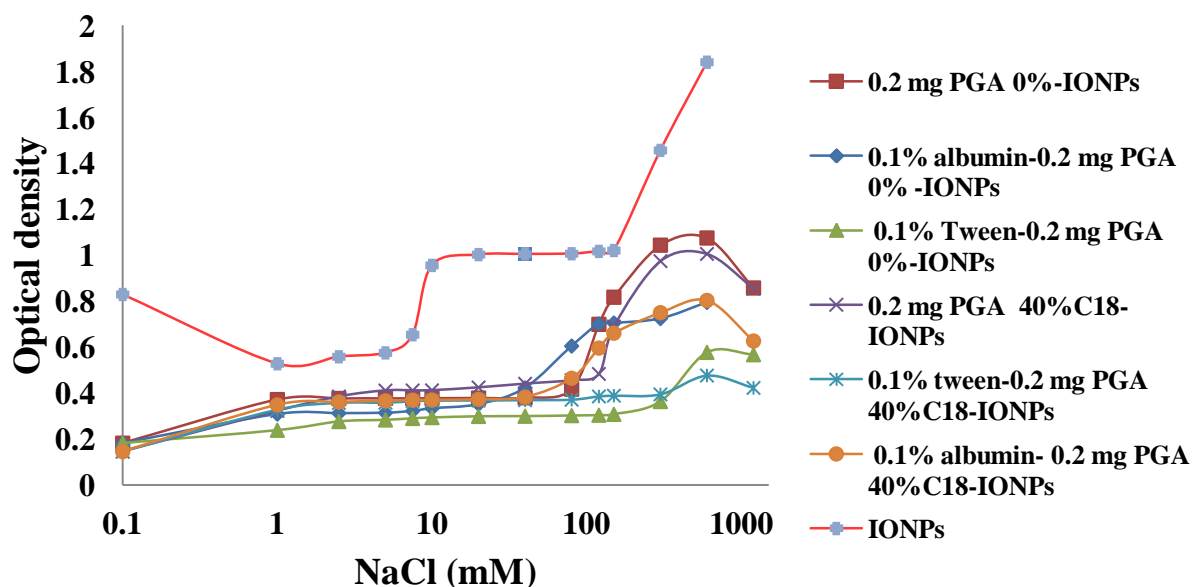


Figure 4-27: Stabilities of PGA 0%-IONPs and PGA 40% C_{18} -IONPs with different concentrations of electrolytes. Various PGA 0%-IONP and PGA 40%-IONP formulations were titrated with increasing salt concentrations and the aggregation of the formulations was monitored by optical density at 500 nm.

The stability of particle suspensions under the different salt concentrations showed an interesting set of results. The turbidity of coated particles was lower than that of IONPs before the critical flocculation point. The PGA 0%–IONPs appeared to have similar stability in the presence of NaCl with the PGA 40% C_{18} –IONPs.

The main differences between preparations were found in the range 100-1000 mM salt concentrations. It was found that the 0.2 mg PGA with 0.1% albumin–IONPs and 0.2 mg PGA 40% C_{18} –IONPs were significantly more stable than 0.2 mg PGA 0% and 0.2 mg PGA 40% C_{18} –IONPs i.e. that overcoating improved the stability further. The 0.2 mg PGA 0% with Tween–IONPs, and 0.1% and 0.2 mg PGA 40% C_{18} with 0.1% Tween–IONPs was found to have an even lower turbidity and showed stability even in very high concentration of NaCl 600 mM which gave a further improvement in stability. This result is good, showing the colloidal stability of coated particles up to and above physiological salt concentration. Further work will be needed to assess whether these formulations offer advantages for *in vivo* biodistribution as well.

4.4.8 Purification of PGA–IONPs

The stability curves above permitted an easy separation of IONPs. PGA 0% – IONPs (1 ml) were placed in a microcentrifuge tube (Fig 4.28), then a low concentration of NaCl (200 μ L, 3 mM) was added and mixed, then the mixture was centrifuged immediately at 12,000 rpm for 2 min. The supernatant was removed and was examined by TEM. IONPs are unstable and aggregate even at low salt concentration, so we can use this low salt concentration to remove uncoated nanoparticles and large coated nanoparticle aggregates.

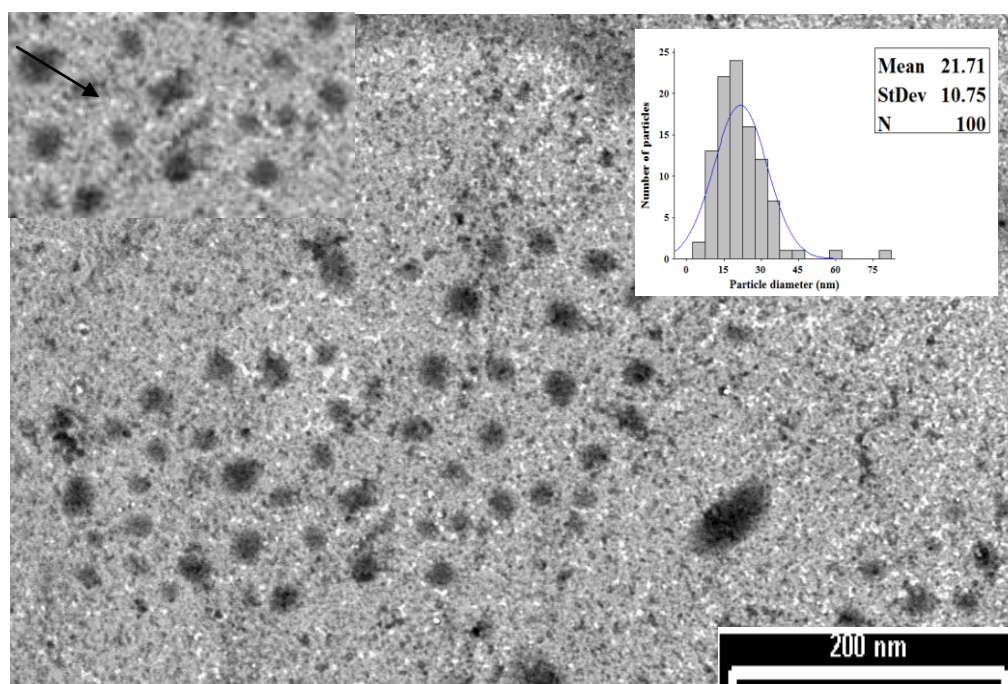


Figure 4-28: TEM image of Purification PGA 0%–IONPs. Small coated particles can be seen with a high population with just a few large particles still present and core surrounded by a grey shell shown up the image with high magnification (Average size 21 ± 10 nm) (Scale bar 200 nm).

The change induced by the salt treatment is evident in the TEM. In Figure 4.28, it is shown that most of the particles are coated and small and the sample looks a lot cleaner. The image shows the morphology of the coated particle consisting of a spherical core surrounded by a grey shell. As can be seen, the particles are well dispersed. The mean size and relative standard deviation are around 5–10 nm. These images show most of the particles with morphologies identifiable as small spherical particles. Many coated small particles, average size 21 ± 10 nm in diameter, can be seen with just a few larger particles with a flattened shape and size around 100 nm.

4.5 Discussion

4.5.1 Different PGAs-coated Iron oxide particles using two different methods.

From the literature IONPs can be readily coated with hydrophilic polymers such as PEG and PVA, but for these polymers a large excess of polymer is required to obtain a suitable coating on the nanoparticles. IONPs have been coated with biocompatible and biodegradable hydrophobic polymers such as polycaprolactone by using the spontaneous emulsification solvent diffusion method with a slight modification for coating IONPs and their characterisation, and *in vivo* MRI application has been investigated (Bae et al., 2009).

Poly(D,L-lactide-co-glycolide) has also been used as a coating IONPs material for use in MRI contrast agent (Lee et al., 2005).

PGA poly(glycerol adipate) is a novel polymer that has been developed in response to issues encountered with polymers more commonly used in the produce of nano size particles, including the release of incorporated drug, it has pendent hydroxyl groups which can be modified with a variety of pendent substituents to generate different functional groups to influence the physicochemical properties of the polymer (Kallinteri et al., 2005). PGA nanoparticles and polymers modified from PGA by the coupling of acyl chains onto the hydroxyl group on the PGA showed good incorporation of dexamethasone phosphate and cytosine arabinoside anti-cancer drugs (Puri et al., 2008).

The most common method used for the preparation of polymeric nanoparticles is the emulsification solvent evaporation technique. Preparation of sub micron poly(lactide coglycolide) composite particles loaded with magnetite/maghemite nanoparticles for intravenous drug targeting, by simple emulsion-evaporation process, has been described by (Ngaboni Okassa et al., 2005).

In emulsification/solvent evaporation the evaporation of solvent is increased by increasing the temperature, under reduced pressure or by continuous stirring (Soppimath et al., 2001).

In the IDP method the evaporation of solvent takes place by stirring overnight, which offers a chance to precipitate the polymer and coat the particles. Polymer deposition on the interface between the water and the organic solvent, caused by fast diffusion of the solvent, leads to the instantaneous formation of a colloidal suspension (Quintanar-Guerrero et al., 1998).

The evolution of nanoparticle preparation methods has been marked by three aspects: (i) the rate and the time of the solvent evaporation, (ii) the amount and the nature of the polymer and (iii) simplification of the procedure and optimisation to decrease the size and increase the coating efficiency. Parameters affecting the particle sizes of poly(DL-lactide-co-glycolide) nanospheres produced by the Emulsion Solvent Diffusion method, the mean particle diameter decreased with an increase in stirring rate. While with increase the stirring rate could improve the droplet dispersion, prevent droplet coalescence and result in the smaller apparent particle size of PLGA nanospheres (Tsukada et al., 2009). In preparation of PLA nanoparticles where acetone was used as a solvent with water as non solvent and evaporated at 35°C under pressure, it was found the amount of aggregation was high (Peltonen et al., 2002).

The size and shape of PVA coated IONPs were affected by different ratios of the polymer/iron and the stirring rate on the particles (Mahmoudi et al., 2009). There are now numerous preparation methods available for production and more investigation will be needed subsequently after producing the nanoparticles, such as into purification and preservation and residual solvent (Pinto Reis et al., 2006). The important parameters that affect particle size and synthesis are stirring time, solvent, rate of the stirring and concentration of polymer.

Composite nanoparticles made with IONPs and PLGA were produced by using the double emulsion (w/o/w) method. Under mechanical stirring the solvent was rapidly eliminated by evaporation under reduced pressure (Lee et al., 2005). The disadvantage of this method is the residual organic solvent which will have toxicological implications. It will also be difficult to remove the excess surfactant. Moreover, the surfactant must be present for preparation of nanoparticles in order to stabilise the system and scaling up is therefore difficult due to the huge amount of the organic phase required (Lin et al., 2008).

Spray drying is also used to coat or produce particles. The main problem of this method is that it produces particles that are in the micrometer size range (Kim et al., 2007). The co-precipitation method has also been used to coat nanoparticles. However, the main drawbacks of this method are the need of a large amount of water and polymer, it is not suitable for all polymers, and only those that are soluble in water can be used. The major drawback of the microemulsion technique is the adverse effects of residual surfactants on the properties of the particles, along with the difficulty in their scale-up (Teja and Koh, 2009).

In thermal decomposition methods, the presence of residual surfactant may be an obstacle to the efficiency of surface modification, besides the use of toxic solvents and surfactants could affect the biocompatibility of the particle (Majewski and Thierry, 2007 and Pinna et al., 2005). Because of by products, contamination occurs and as a result, the particles need post-treatment. This is the main disadvantage of the sol-gel method. Gas phase methods also tend to be expensive (Teja and Koh, 2009).

Initial experiments in this project took a range of PGAs with different acyl modifications and investigated coating of IONPs using two different methods, the interfacial deposition method and the sonication method. The main advantages of the interfacial deposition method are that it is reproducible, low cost and simple, can produce particles in the nanometre size range and also allows nanoparticles to be prepared without any surfactant or residual solvents

left in the system, which is important from a toxicological point of view. Nanoprecipitation does not require a source of external energy and would be easy to scale-up relative to homogenisation and sonication, which require an energy source. Moreover, in nanoprecipitation acetone used as organic solvent is considerably less toxic (Budhian et al., 2007).

In the sonication method not all the solvent evaporated immediately, resulting in a decreased precipitation of polymers leading to aggregates of the particles, therefore uncoated particles or poor coating because the polymer was still in the solvent. Slow evaporation leads to the production of spherical particles, but in this method the quick evaporation leads to produced non spherical particles. The modified emulsification solvent evaporation method (sonication method) has been used by our research group to coat the particles. Increase in the sonication to 25 min time leads to a reduction in the nanoparticles mean diameter to 255 ± 10 nm (Mainardes and Evangelista, 2005a).

On comparing the coated particles produced by the interfacial deposition method and sonication methods, a smaller size was seen for particles coated using the IDP method (Figs. 4.1 and 4.2). The nanoprecipitation method is also more flexible. Different polymers can be used to produce nanocapsules using the IDP method (Barratt et al., 1994). The most commonly used method for the preparation of PLGA nanoparticles is nanoprecipitation. Acetone dissolved polymer are added drop-wise into a continuously stirring aqueous phase with or without emulsifier/stabiliser, and consequently the organic phase is evaporated under reduced pressure (Kumari et al., 2009). To our knowledge no work has been done using the IDP method for coating iron oxide nanoparticles.

The 2 mg of PGA 40% C_{18} and backbone PGA 0% in 2 ml of acetone produced coated IONPs of a small size (Figs. 4.10 and 4.24). Also with using different acyl substitutions of polymer to increase the hydrophobicity there was no increase in particles sizes. This result was the opposite of work by Piskin et al., (1995) who reported that an increase in the number of hydrophobic domains was found to be associated with larger coated nanoparticles.

The sonication method produced large nanoparticles which could suggest that the time of stirring and the temperature are not enough to evaporate the solvent. This leads to the formation of just polymer nanoparticles which increases the size of coated aggregated iron oxide nanoparticles. The methods detailed above are the main methods extensively employed in the synthesis of nanoparticles. For different purposes, we found the best one suitable for our nanoparticles was the interfacial deposition method, but also we needed more modifications of method to improve the nanoparticle size (size reduction) and to reduce the polydispersity index based on slight modifications of standard interfacial deposition method.

4.5.2 Particle Size and Zeta Potential

The sizes of PGA–IONPs prepared using the sonication method were between 160 nm to 240 nm and with IDP method were between 126 nm to 210 nm using DLS measurements (Fig. 4.1 and 4.2). Budhian et al., (2007) have reported that sonication is better suited to produce small size nanoparticles < 300 nm diameter with a narrow size distribution.

In the interfacial deposition method, PGA–IONPs were still producing large particles, even though smaller than the particles prepared by sonication. Polymers with a large amount and long length of chain are thought to precipitate out of the water phase and aggregate to form polymer particles, which increases particle size. TEM (Fig. 4.3 and 4.4) studies showed polymer-coated nanoparticles, prepared from the various formulations of PGAs, to be spherical and discrete. The morphology of PGAs–IONPs changed both at low and high amounts of polymers and solvent. In TEM images, it was noted that the particles were spherical with a relatively narrow polydispersity. Polymer coating was demonstrated by TEM by the presence of black dots of dense iron oxide, in most cases showing a single spot inside the polymer.

In conclusion, different PGA substituted polymer–IONPs resulted in different particle sizes. The aim of this experiment was to find which method was most suitable and the particles produced were spherical to give a good coating with no aggregation. The amount of PGA polymer and the method were found to be important factors in the particles sizes and coating. A layer of polymer can be clearly seen surrounding the particles. In addition, we found that the PGA backbone was a good starting point to coat the IONPs, with the interfacial deposition method being most useful to coat the particles. Further optimisation of the coating procedure was, however, necessary.

4.5.3 Optimisation of Nanoparticle Coating Produced with PGA 0%

Based on the investigation of PGA–IONPs, the amounts and volumes of both the solvent and the polymer have major effects on the size of coated NP. We prepared PGA 0% coated IONPs from PGA 0% polymer masses between 1 mg and 0.1 mg from acetone solutions at different concentrations (1 mg/ml to 0.1 mg/ml) using different volumes of organic solvent (1 ml to 3 ml) for one volume of aqueous solution containing IONPs suspension (5 ml).

The low starting amount of PGA 0% (2 mg instead of the 20 mg reported in the literature) was based on results in this work when used different amounts of polymers showed that using a much smaller amount of PGA 0% decreased the coated IONPs size.

Poly(lactic acid) (PLA) and D- α -tocopherol polyethylene glycol 1000 succinate (TPGS) coated IONPs core with size 10 nm were prepared by two methods, first the single emulsion solvent extraction/evaporation method, and secondly the nanoprecipitation method. In the single emulsion method, 100 mg of the polymer along with 2 % loading of IONPs and 8 ml of DCM were added and the solution was the emulsified at a given concentration of TPGS of 15, 5 and 1% w/v. The sizes of particles were 352.03 ± 18.28 nm, 307.44 ± 16.46 nm and 282.2 ± 14.70 nm respectively, while in the nanoprecipitation method,

using the same amount of polymer and IONPs in an aqueous phase containing a known concentration of the emulsifier TPGS of 15,5 and 1% w/v showed different particle sizes of 302.53 ± 15.83 nm, 272.80 ± 02.53 nm and 249.43 ± 19.89 nm respectively (Prashant et al., 2010).

An increase in polymer concentration, while keeping other parameters constant, was found to increase overall nanoparticle size mainly because an increase of the shell of polymer on the coated iron oxide nanoparticles, and thus to induce a larger size and polydispersity (Hamoudeh et al., 2007).

Using a constant volume of solvent of just 1ml with different amount of PGA 0% to coat IONPs produced large coated nanoparticle sizes. This could be due to the volume of solvent not being enough to drive the polymer to coat the particle, resulting in multiple IONPs cores being coated by the PGA 0% in the same particle, while other particles were still naked or poorly coated. The increased diameters of PGA 0% coated IONPs could be due to slight aggregation caused by the reduction of negative surface charge and a reduction in repulsion forces between particles. The interaction between solvent, polymer and particle must be taken into account to improve the polymer participation and the coating of particles.

The volume of solvent used was found to be important in forming small coated IONP with a low polydispersity. The optimum was at 2 ml with both small and larger amounts being less useful. A larger amount of organic solvent was reported to prevent formation of nanoparticle coatings due to diffusion rates in the o/w emulsion (Mainardes and Evangelista, 2005b). There are a number of factors which could be involved. It could be that the amount of solvent speeds up the precipitation of polymer. In the case when the volume of solvent was increased further with a constant amount of PGA 0% the particle size of PGA 0% coated IONPs was larger. The difference in particle size may be caused by the amount of solvent in the water and the solubility of the polymer in the solvent. The physico-chemical parameters affecting the particle diameter are the viscosity and the interfacial tension of organic polymer solutions in contact with water (Chernysheva et al., 2003). Additionally acetone does cause

aggregation of the IONPs and this could also result in larger particle sizes. Also the large amount of solvent may cause a barrier between the IONPs and polymer preventing the polymer from precipitating around the IONP.

Decreasing the amount of PGA 0% to 0.2 mg with 2 ml of acetone for coating IONPs produced smaller nanoparticles which is the smallest batch, while decreasing the amount of PGA 0% still further to 0.1 mg produced larger particles. The general explanation for this phenomenon with change of the polymer amount is quite complex. In the absence of iron oxide nanoparticles, a high concentration of polymer is necessary for good nanoparticles formation and all nanoparticles are large. In the presence of IONPs, these IONPs are just incorporated into the large polymer nanoparticles, and the other parameters have little effect on particle size. There is too much polymer present to form just a small coating of polymer around the iron nanoparticles. Prozorov et al., (1999) have reported that a large amount of the polymer leads to an increase in the particle size. When the PGA 0% amount comes down to low levels (1.0 mg or lower) mixtures of both large polymer nanoparticles and individually coated IONPs.

At less than 0.2 mg the amount of PGA 0% polymer (0.1 mg of PGA 0%), is small enough just to coat all individual IONPs and at still lower amounts there is insufficient polymer to coat all nanoparticles individually, resulting in the appearance of some aggregates of particles which appear to be coated. The size and shape of polyvinyl alcohol PVA coated IONPs were affected by the amount of the polymer when the amount of iron was fixed (Mahmoudi et al., 2009).

In summary, we have shown that by adjusting the amount of PGA 0% and volume of acetone, it is possible to control the size of coated IONPs and all have been shown by TEM to have a spherical shape and uniform size.

4.5.4 Zeta Potential

The zeta potential of PGAs–IONPs was slightly positive. This was unexpected as PGA would be expected to be negative due to the free terminal carboxyl groups of the polymer. Nanoparticles made by polymers substituted with C₈ or C₁₈ acyl groups in the range between 0 % and 100 % in the absence of surfactant had a negative zeta potential (Kallinteri et al., 2005). It is possible that the carboxyl groups of the polymer could interact with the iron oxide and become non free groups, which would result in a less negative surface charge. Buffer conditions can also affect zeta potential measurement, and further work may be required to optimise the choice of buffer to obtain the expected results.

4.5.5 Modification of PGA Polymers

4.5.5.1 Synthesis of PGA 40%C₁₈ by Acylation of Backbone PGA

The synthesis of PGA 40%C₁₈ was successful as analysis by NMR, FTIR and GPS all confirm that the acylation happened. Improvements to the properties of polymers are typically limited by their chemical properties; some modifications of PLGA polymer have been reported, e.g. poly(lactic acid co-lysine) was synthesised with pendant amino groups. However, only 2 mol% lysine units were incorporated into the polymer backbone (Barrera et al., 1993). Polymerised (D, L) lactic acid or caprolactone with poly(ester amide) with pendant carboxy or amine groups was also investigated (Veld et al., 1992). Lipase which was used to produce the polymeric material, used in this study has the advantage that the enzyme catalysed reaction proceeds without the need for protection of the pendant functional groups. This advantage has been used for preparation of polyesters by polycondensation reactions (Tian et al., 1997).

The PGA pendent hydroxyl group can be modified with different pendent substituents to a functional group of great variety to improve the physicochemical properties of the polymer and influence drug incorporation

(Kallinteri et al.,2005). PGA 40% C_{18} was used to increase the hydrophobicity and stability of the nanoparticles, but still to allow the presence of some hydroxyl groups for interaction with the IONPs surface.

4.5.6 PGA 40% C_{18} Coated IONPs

More hydrophobic PGA 40% C_{18} polymer coated IONPs were produced to increase their stability in both the biological and physical state. The metallic core has been coated with a hydrophobic layer instead of surfactant coating to improve the lifetime of the nanoparticles in aqueous environments and prevent oxidation (Ge et al.,2009). The most important characteristic in the preparation of core/shell nanoparticles is their final size. This property not only affects their magnetic moment but also the biological behaviour of the particles when they are injected into the body (Arias et al., 2008b).

Different amounts of PGA 40% C_{18} were chosen to coat the IONPs to check the influence of the ratio of solvent and polymer on mean diameter. IONPs present as a suspension aqueous phase were fixed at 5 ml. As can be seen in Figures 4.20, 4.21 and 4.22 and also TEM images (fig. 4.23, 4.24 and 4.25) show that the mean diameter was noticeably affected by the ratio of polymer and solvent. The increase or decrease of PGA 40% C_{18} concentrations affect on the formation of the nanoparticles. Lee et al., (2005) have reported that the homogenisation strength and the optimal polymer concentration were the dominant factors in controlling the size for emulsification methods.

As already found with PGA backbone coated IONPs, the particle size of coated IONPs decreased as the amount of PGA 40% C_{18} decreased with a constant volume of acetone (2 ml). The acylation should increase the solubility of the PGA in organic solvent therefore, using the full amount of polymer should be available to improve the coating of the particles.

The amount of PGA 40% C_{18} 0.2 mg with 2 ml of acetone gave the best coating of IONPs. These particle sizes appear to be very good in comparison with other polymer-coated particles reported in the literature, as follows.

IONPs have been coated with different types of polyacrylates, i.e. poly(alkylcyanoacrylate), poly(ethylcyanoacrylate), poly(butylcyanoacrylate), poly(hexylcyanoacrylate) and poly(octylcyanoacrylate). Using methods based on the emulsion/polymerisation method resulted in average diameters of 160 ± 15 nm, 140 ± 20 nm, 150 ± 30 nm and 155 ± 20 nm respectively (Arias et al., 2008a).

In the literature it has been reported that other hydrophobic polymers have been used for coating iron oxide nanoparticles. PCL and PLGA have hydrolysable ester linkages which are similar to PGA. Magnetic poly ϵ -caprolactone (PCL) nanoparticles have smooth surfaces and moderately uniform size distributions (160 ± 5 nm) (Yang et al., 2006).

Magnetic poly(D,L-lactide-co-glycolide) nanospheres were prepared by a modified single oil-in-water emulsion–solvent evaporation method with a mean diameter 360–370 nm which showed high magnetisation (Liu et al., 2007).

IONPs coated with poly(ethyleneimine) (PEI) at different iron oxide to polymer weight ratios of PEI magnetite of 0.4, 0.8, 1.2, 1.6 and 2.0 resulted in a range of sizes between 200 nm to 800 nm at pH 7. When the particle coating was carried out at pH 2, the particle size decreased to 80 nm (Wang et al., 2009).

The availability of different characterisation techniques makes the detailed analysis of the nanoparticle system possible. The nanoparticle size is affected by many parameters, and researchers are continually attempting to decrease the average nanoparticle size. Considering the synthesis of PGA 40% C_{18} coated IONPs the average size over all batches was between 23 to 105 nm in diameter, and in the optimum batch (0.2 mg PGA 40% C_{18} coated IONPs) the average size was 23 ± 7 nm (Figure 4.24). Such small nanoparticles are not common by

the methods detailed above however, the advantages of smaller sizes should be studied designed for *in vitro*.

4.5.7 0.1% Tween 80% Coated PGA 0%–IONPs and PGA 40% C_{18} –IONPs

A nanoparticle coating with Tween not only prevents the uptake by the mononuclear phagocyte system (MPS) but also ensures that nanoparticles do not form aggregates in cells and also *in vivo*. Tween 80 has previously been used at Nottingham as a stabiliser for PGA nanoparticles (Meng et al., 2006) and (Puri et al., 2008), and has been shown to result in improved nanoparticle biodistribution in rats (Kallinteri and Garnett, unpublished results). Tween 80 (polysorbate 80) has also been shown to have other useful delivery properties.

Polysorbate 80 has the ability to transport nanoparticle loaded drugs across blood–brain barrier when nanoparticles are overcoated with it (Kreuter, 2001, Kreuter et al., 1995 and Olivier et al., 1999). Tween 80 has a specific role in brain targeting which relates to interaction between the Tween 80 as coating and brain micro-vessel endothelial cells (Sun et al., 2004b). Polysorbate 80 coated poly(butylcyanoacrylate) (PBCA) nanoparticles and polysorbate-80 coated poly(methyl methacrylate (PMMA) showed an ability to cross and increase uptake across the blood brain barrier (Ambruosi et al., 2006 and Borchard et al., 1994).

Tween plays an important role as surfactant to penetrate the cell membrane. Polysorbate80 coated Polyethylcyanoacrylate nanoparticles with a particle size of 240 nm had an effect on drug permeation across the biological membrane (Cavallaro et al., 1994). However, to the best of our knowledge, Tween 80 overcoated IONPs have not been reported yet.

4.5.8 0.1% Albumin Coated PGA 0% Coated-IONPs and PGA 40% C₁₈ Coated IONPs.

Albumin has the ability to interact with cell and cell membrane when nanoparticles are administered *in vitro* and *in vivo* and increase the stability of the particles. Albumin can also improve the ability of nanoparticles to cross cell and tissue barriers and protect the particles from biodegradation and agglomeration. Albumin is nontoxic. Magnetic nanoparticles are generally surface-modified with hydrophilic polymers such as albumin (Perry et al., 1986). Surface-modified albumin nanoparticles offer the potential of being able to avoid uptake by the Reticuloendothelial system (RES) and being used as drug carriers to target sites outside the vascular circulation. (Lu et al., 2005). Human serum albumin has been used *in vitro* and *in vivo* and was shown to overcome some problems with transfection (Orson et al., 2002 and Orson et al., 2000).

Wilhelm et al., (2003) have also reported that albumin coating of particles can inhibit the interaction with cell membrane. It has been reported that with 3-aminopropyltriethoxysilane APTES coated iron oxide nanoparticles, human serum albumin was covalently immobilised on the particles and showed high saturation magnetisation (Can et al., 2009). In a study performed by Xia et al., (2008) albumin was shown to be a good stabiliser for aqueous fluids with low viscosity and useful for gene therapy. Chunfu et al., (2004) suggested that human serum albumin-coated iron oxide was stable up to 72 h in Bovine serum albumin (BSA) and was promising for magnetically targeted radiotherapy. Pan et al., (2005) studied the effect of serum albumin binding with the dendrimer-coated IONPs with amino surface groups. All these studies showed the potential for using albumin as a coating or overcoating for IONPs.

4.5.9 Stability of IONPs Coated with Polymers

This part of the work was carried out to examine the ability of polymers and the surfactant Tween 80 and the serum protein albumin to provide an effective coating and as steric barriers to prevent aggregation. The turbidity of iron oxide particles in different concentrations of NaCl studies were investigated. This study not only mimics the stability in a physiological environment but also provides data on the general stability of these coated nanoparticles.

With increasing concentrations of NaCl, the PEG moieties of the coating become more dehydrated by releasing the water molecules, and the interaction between the layers increasingly leads to flocculation. At the critical flocculation point (CFPT) the PEG chains become dehydrated, chain-chain interactions become attractive and flocculation occurs (Riley et al., 1999). Polymeric chains on the surface of nanoparticles have a very important role in colloidal stability, especially at a high ionic strength, therefore the polymeric chains act as steric barriers against aggregation (Rotureau et al., 2008).

The normal salt concentration in blood is 150 mM, while the range of NaCl was varied from 0.1 mM to 600 mM in the experiment in this chapter. Uncoated particles were not stable even in very low salt concentration and this is likely to be due to the significant van der Waals attraction between the iron oxide cores. All the PGA coated nanoparticles showed high stability, and aggregation only occurred at high salt concentration. The explanation for the instability of nanoparticles at the high concentration is a less than complete surface coverage of PGA chains, leading to a different stability of particles according to the amount of coating. The coated IONPs with PGA 0 % and PGA 40 %, along with those overcoated with 0.1 % albumin and 0.1 % Tween, showed high stability overall, better than IONPs coated with dextran where the Tween and albumin with 0.2 mg PGA 40% C₁₈-IONPs showed the best stability. Barrera et al., (2009), have reported that PEG-silane coated IONPs were stable in NaCl concentration from 38 mM to 320 mM with no precipitation. All our coated nanoparticles with PGAs and with overcoatings

showed high stability up to 120 mM, which means the particles were well covered and the modifications maintained the repulsive force between the particles. The increased stability of PGAs–IONPs and with the overcoatings compared to dextran–IONPs under conditions mimicking the physiological environment could make them a useful candidate as a contrast agent in MRI.

4.5.10 Purification of PGA 0% Coated IONPs

Even after optimisation of the coating process, there may still be some uncoated nanoparticles present, as well as small numbers of particle aggregates. To remove these uncoated nanoparticles, a simple method involving addition of a low salt concentration and centrifugation can be used to purify the coated nanoparticles. The small PGA0%–IONPs could clearly be seen in the TEM image (Fig.4.28). However, the excess polymers coated IONPs and large coated IONPs were removed, and the polymer shell did not collapse when the coated IONPs were centrifuged.

4.6 CONCLUSIONS

The interfacial deposition method allowed us to easily obtain PGA–IONPs with a good yield with size smaller than particles prepared by sonication method. This chapter has examined the size and surface charge of nanoparticles coated with PGA polymer backbone and the substituted PGA 40% C_{18} . Also particles were over-coated with Tween 80 (0.1%) and albumin in order to increase the stability. Purification of coated IONP was also investigated.

The preparation of coated IONPs with PGA 0% under optimum conditions is important. In terms of the physicochemical properties of coated nanoparticles, the amount of polymer and the amount of solvent ratio used were two of the parameters with the greatest effect on the coated nanoparticles size.

By choosing the right method small coated nanoparticles can be produced with small amount of polymers. The coated IONPs prepared using 0.2 mg of PGA 0% with 2 ml of acetone were found to be an average size 16 ± 5 nm which is smaller than the other formulations in the particle size study. Transmission electron micrographs showed nanoparticles were spherical and smooth with very few aggregates and separate in the nanometre size range. PGA 0% was substituted by C₁₈ chains and coated IONPs with small size were still obtained using the IDP method. The IONPs were clearly detected in the PGA 0% and PGA 40% C₁₈ by TEM. Depending on the preparation conditions, individual IONPs coated with the or aggregates of IONPs coated with polymers could be seen. The analysis of the TEM pictures correlates very well with the data obtained by dynamic light scattering. The zeta potential study showed that the surface charge of the IONPs changed when coating had occurred.

The stability of the IONP and coated IONP in biological medium were investigated. The PGA 0% coated IONPs and PGA 40% C₁₈ coated IONPs were remarkably stable even in high sodium chloride concentration and showed more stability than dextran coated IONPs. It was shown that the stability of the coated nanoparticles increased further when overcoated with Tween or albumin. The overcoatings were found to be stable under conditions mimicking physiological medium. Thus, 0.2 mg of PGA 0% and PAG 40% C₁₈ coated IONPs and 0.1% Tween and 0.1 % albumin would be useful to stabilize the nanoparticles *in vivo*. Treatment of PGA 0%–IONPs with a low concentration of NaCl followed by a brief centrifugation particle removed large and poorly coated nanoparticle, this technique seems to be suitable for the purification of coated nanoparticle.

CHAPTER 5

5. PEGYLATED POLY (GLYCEROL ADIPATE) 40% C_{18} COATED IRON OXIDE NANOPARTICLES

5.1 INTRODUCTION

Many studies have reported that the biodistribution of different contrast agents depends on the size, charge and thickness of the coating of the particles (Chouly et al., 1996b). Poly(ethylene glycol) (PEG) is now the most common material to modify particle surfaces in order to avoid recognition by cells of the MPS. The attachment of these polymers onto the particle surface often involves physical adsorption (Storm et al., 1995).

Particles made from or coated with hydrophobic polymers tend to be opsonised by protein adsorption and rapidly cleared from systemic circulation by the phagocytic system, ending up in the liver or the spleen. The level of protein absorption can be decreased by changing the density and molecular weight of PEG on the surface (Gref et al., 2000). The presence of a PEG coating on the surface of nanoparticles enhances their specific uptake by minimizing the RES recognition and consequently increases the time of nanoparticle circulation in the blood (Akerman et al., 2002). PEG is a widely used polymer, having many beneficial properties, such as being non-toxic (Hern and Hubbell, 1998) .

Particle size and surface properties have a strong effect on the pharmacokinetics of particles, and the main disadvantages for *in vivo* applications of magnetic nanoparticles are large particle size, quick blood clearance and non-specific uptake by macrophages. Small particles (< 50 nm) and poly(ethylene glycol) (PEG) surfaces have been shown to be effective in extending blood circulation time (Acar et al., 2005). The disadvantage of dextran as a coating seems to be the high cost and huge

amount of polymer needed to coat the particles. Also dextran is less effective than PEG as a coating for this purpose. Dextran coated liposomes showed shorter circulation time than PEG coated liposomes (Pain et al., 1984).

Dextran-coated poly(butyl cyanoacrylate) nanoparticles failed to prevent the nanoparticles accumulating in the RES, and were found mainly in the liver (Douglas et al., 1986).

5.2 Aims of the Chapter

In Chapter 3 it was shown that PGA coated IONPs could be manufactured with both PGA 0% with size 16 ± 5 nm and PGA 40% C_{18} 23 ± 7 nm This process was optimised in order to produce small particles. It was also shown that coating nanoparticles with copolymer can have a dramatic effect on the colloidal stability of the nanoparticles.

The PEGylation of PGA 40% C_{18} is desirable for the assessment of uptake of particles into cells, for the stability of the particles and to increase the circulation time. In this chapter the preparation and use of PEGylated PGA 40% C_{18} (PEG–PGA 40% C_{18}) in a coating procedure will be developed to produce nanoparticles with a small size and acceptable morphology. A PEGylated PGA copolymer is expected to arrange into two layers on the nanoparticle surface, the inner layer being composed of the hydrophobic acylated PGA covering the surface of the iron oxide core, the outer layer being composed of the hydrophilic polymer PEG that provides stabilisation through steric repulsion through the hydrated polymer chains. Having synthesised PGA 40% C_{18} , the next stage was to couple it to the PEG. PEG MW 2000 functionalised with an amine group was commercially available. This permitted the coupling of the PEG to the core polymer via carbonyldiimidazole to activate the PGA carboxyl group for coupling with the amine group.

5.3 Methods

PEGylated PGA 40% C_{18} (see 2.2.13).

PEGylated PGA 40% C_{18} coated IONPs (see 2.2.14).

Stability of IONPs coated with PEG–PGA 40% C_{18} (see 2.2.15).

5.4 Results

5.4.1 PEGYLATED PGA 40% C_{18}

The reaction between the free NH_2 of the PEG and the carboxyl group of the PGA was used to synthesise the PEG-PGA 40% C_{18} . The reaction scheme is shown below in Fig 5.1. The product of synthesis of PEG-PGA 40% C_{18} was then characterised by NMR, FTIR and GPC.

The NH_2 -PEG was added at 1: 1 molar ratio to the PGA 40% C_{18} and the yield was 77% (366 mg). Polymer molecular weight was measured using GPC. Figures 5.2 and 5.3 show that the molecular weight was increased from Mn 12,038 to Mn 16,331 implying that 2 molecules of PEG 2000 were added per molecule of PGA.

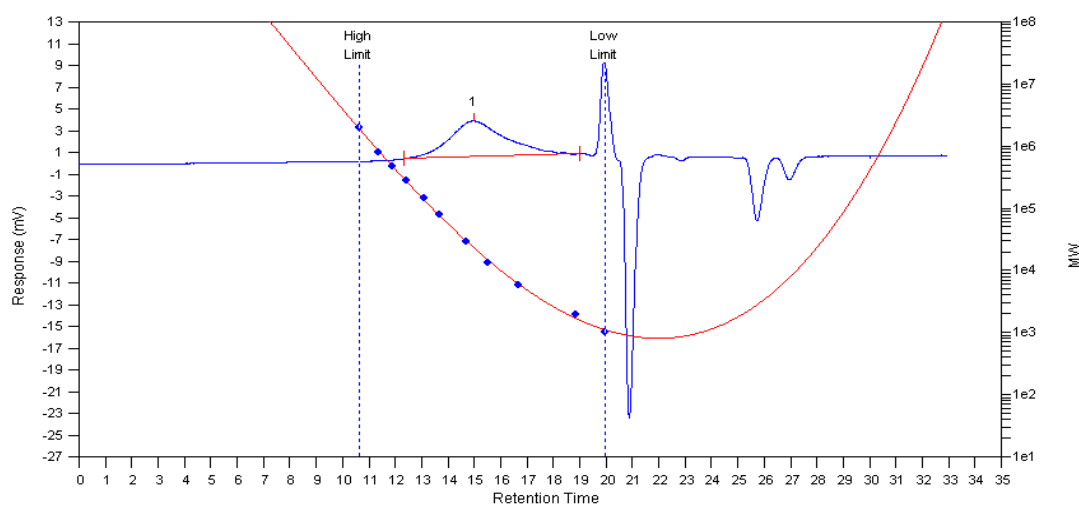


Figure 5-2: GPC elution profile for poly(glycerol adipate) substituted with 40%C₁₈. The red line is the calibration curve, while the peaks (1 and 2) are related to the polymer retention time.

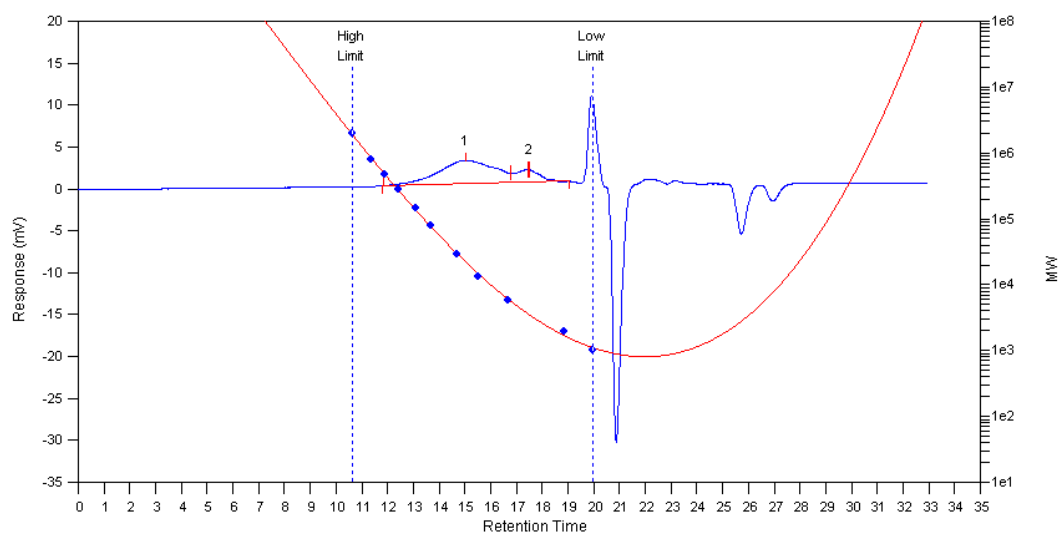


Figure 5-3: GPC elution profile for poly(ethylene glycol) coupled to poly(glycerol adipate) substituted with 40%C₁₈. The red line is the calibration curve, while the peaks (1 and 2) are related to the polymer retention time.

The PGA 40%C₁₈ polymer is expected to have an average of one carboxyl group per polymer, but some of the polymers will have 2 carboxyl termini and some will have two hydroxyl termini, suggesting that the ratio of PEG to PAA may be a little high.

5.4.2 NMR Analysis

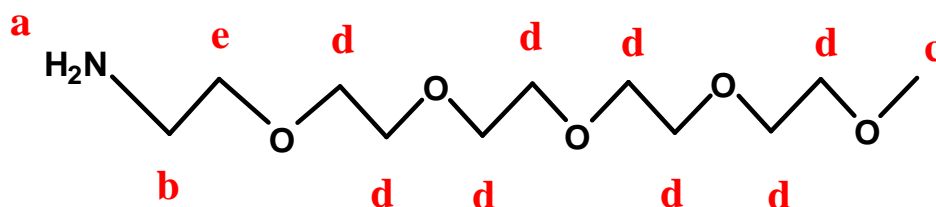


Figure 5-4: Structure of poly (ethylene glycol) (PEG).

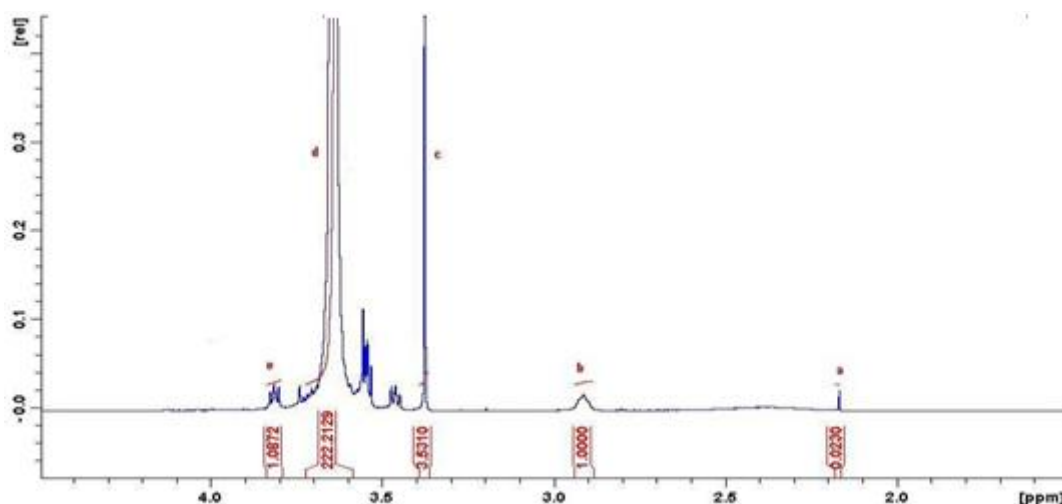


Figure 5-5: NMR spectrum for poly (ethylene glycol) (PEG).

Figure 5.4 shows the annotated structure for PEG and Figure 5.5 the NMR trace. The amine protons appear at δ (2.17) while $\text{CH}_2\text{-NH}_2$ protons appear as a broad multiplet at δ (2.80–2.95). Methoxy protons appear as a sharp singlet at δ (3.40) and ethylene oxide protons at δ (3.43–3.78). The peak of $\text{NH}_2\text{-CH}_2\text{-CH}_2\text{-O}$ protons appear as a triplet at δ (3.78–3.85).

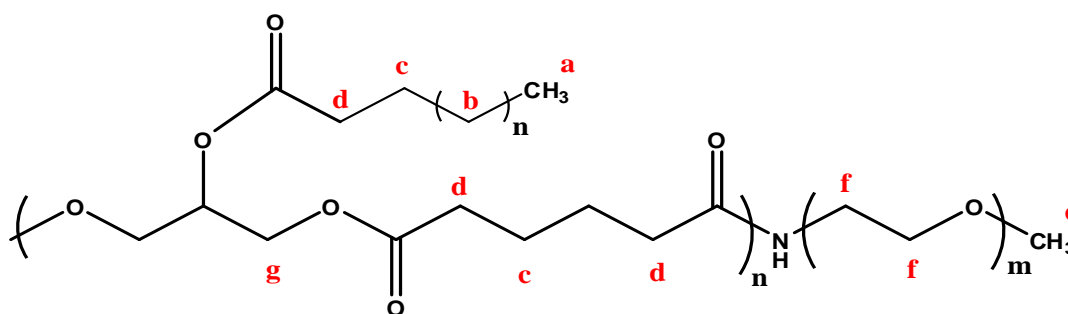


Figure 5-6: Structure of poly(ethylene glycol)-PGA 40% C_{18} .

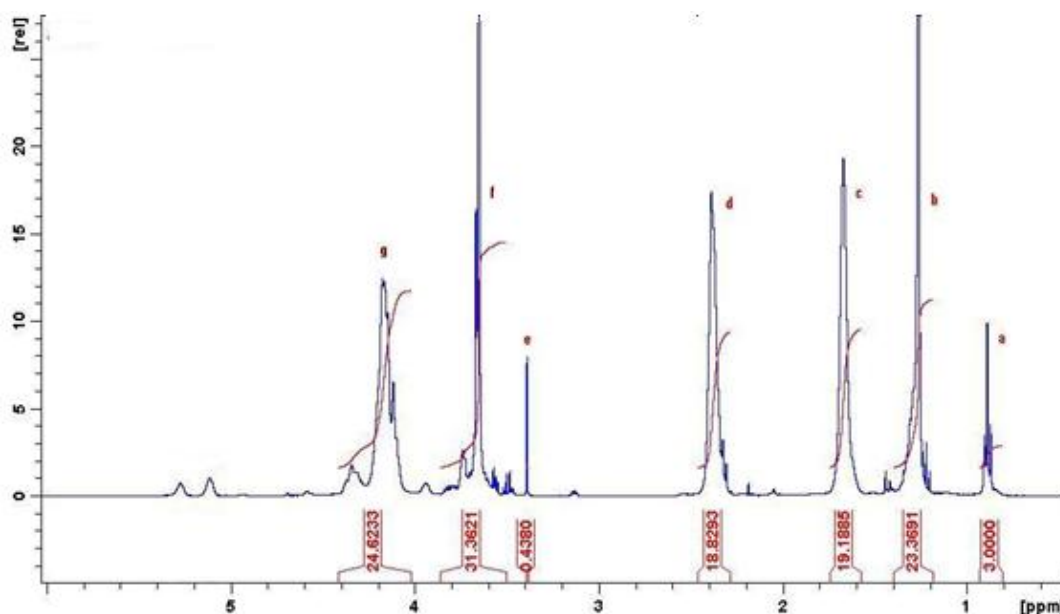


Figure 5-7: NMR spectrum for PEG-PGA 40% C_{18} .

Figure 5.6 shows the annotated structure for PEG-PGA 40% C_{18} . In Figure 5.7 the peaks annotated as a, b, c, d and g correspond to the same groups discussed for PGA 40% C_{18} , the peak of methoxy protons appear as a sharp singlet at δ (3.40), while ethylene glycol $\text{CH}_2\text{-CH}_2\text{-O}$ protons show up at δ (3.40–3.86). These two groups indicate the presence of PEG which was covalently attached to PGA chains. ^1H NMR confirmed the presence of the PGA and PEG. Comparing the area of the PEG peaks 4.9–4.16 with that of the PGA 0.5–1.31 revealed a coupling ratio of PEG to the PGA 40% C_{18} of approximately 0.7 PEG moieties per PGA moiety.

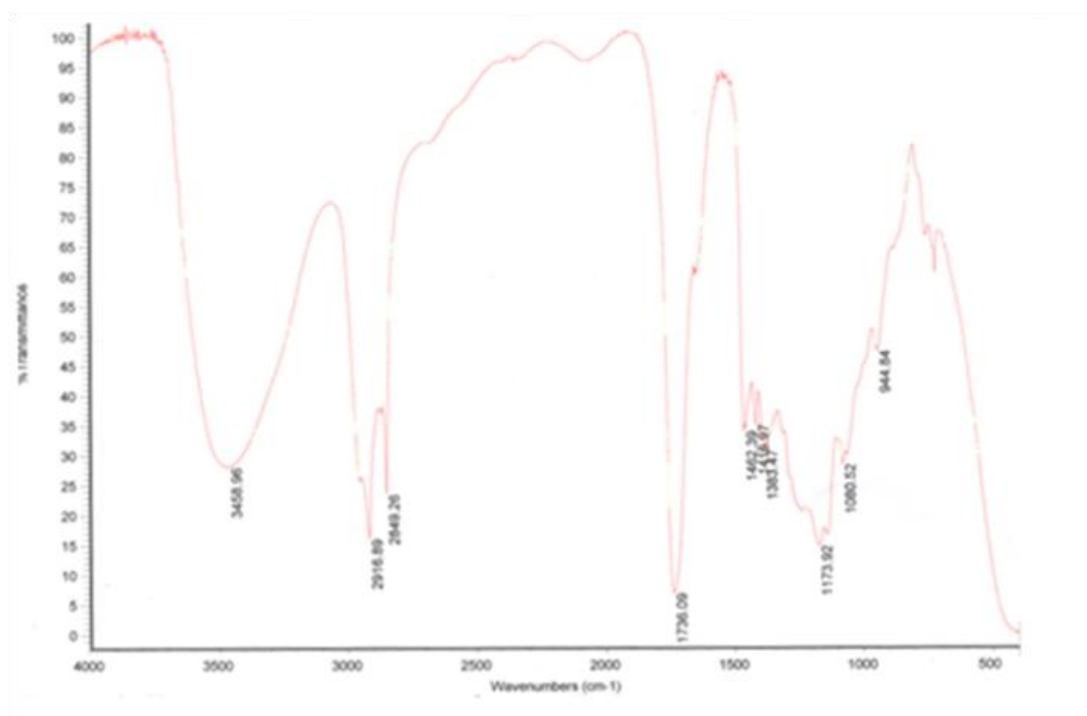


Figure 5-8 : FTIR for PGA 40%C₁₈.

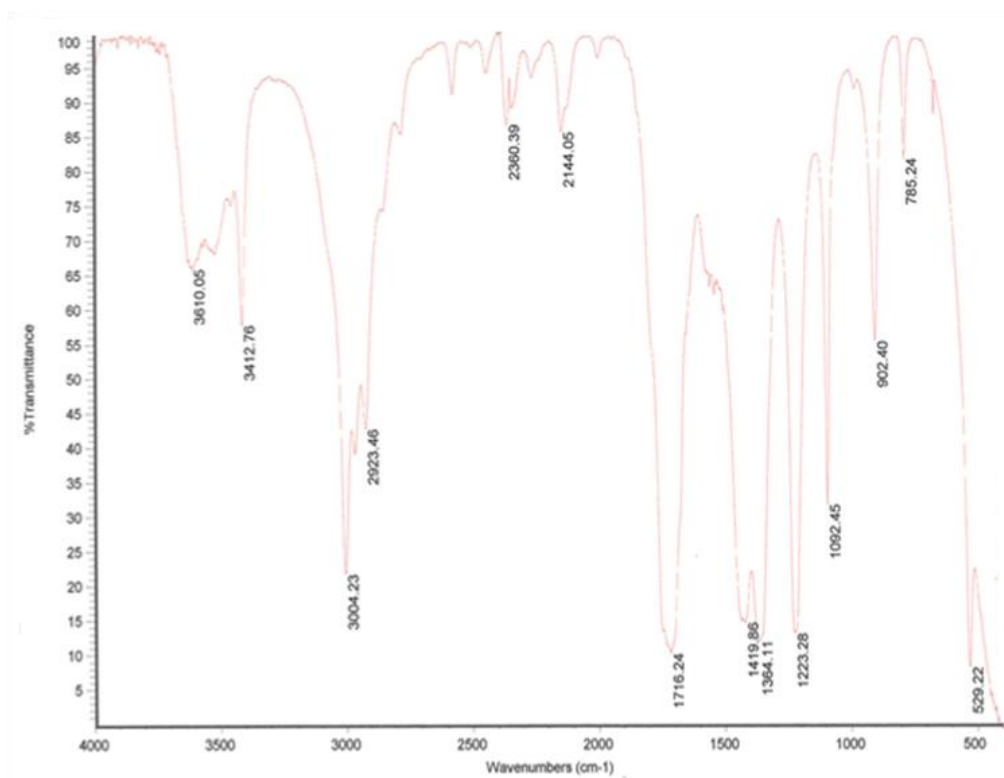


Figure 5-9: FTIR of PEG-PGA 40%C₁₈.

FTIR confirmed the amine group at 2916.68 cm^{-1} and 3004.23 cm^{-1} shifted to 3412.76 cm^{-1} and 3610.05 cm^{-1} as the amine was converted to amide (Figs. 5.8 and 5.9).

5.4.3 PEGylated PGA 40% C_{18} -IONPs

The coating of IONPs with PEG may offer advantages over other delivery systems. PEG-coated IONPs are expected to increase the blood circulation time of nanoparticles. The formulation strategies are to control the size of PEG-PGA 40% C_{18} -IONPs during synthesis. The ability to control NPs size may be broadly important to their use in various clinical applications, allowing for the optimisation of NPs delivery vehicles for systemic administration. IONPs were coated by different amounts of PEG-PGA 40% C_{18} (0.2 mg, 0.1 mg and 0.05 mg) and characterised by TEM and DLS.

5.4.3.1 TEM photomicrographs and DLS analysis

The TEM photomicrograph from batches using 0.2 mg, 0.1 mg and 0.05 mg copolymer PEG-PGA 40% C_{18} coated IONPs are shown in (Figs. 5.10, 5.11 and 5.12) and the DLS results in (Figs. 5.13, 5.14 and 5.15). These images show both the size and morphology of the particles formed in each batch.

The relatively spherical structure and the narrow size distribution of the small particles in the 0.2 mg PEG-PGA 40% C_{18} -IONPs batch can be seen in the TEM image (Fig. 5.10). Here the polymer appears as a translucent layer on the coated IONPs (the dark core). All the particles are formed into a spherical shape with a size around $16 \pm 4\text{ nm}$, which is still very small.

According to chapter 3 the nanoparticles size of IONPs is $13 \pm 9\text{ nm}$ (Fig. 3.2), while that of the coated ones shown here is $41 \pm 19\text{ nm}$ with CMD and $40 \pm 12\text{ nm}$ with dextran (Figs. 3.9 and 3.12).

The TEM image in Figure 5.11 shows the particles coated with 0.1 mg of PEG-PGA 40% C_{18} -IONPs. In this case, particle diameter increased to a plateau value at 46 ± 13 nm. The particles were spherical in shape and uniform. Both aggregates of IONPs coated by polymer and also individual coated nanoparticles were seen, however, they are well-formed particles.

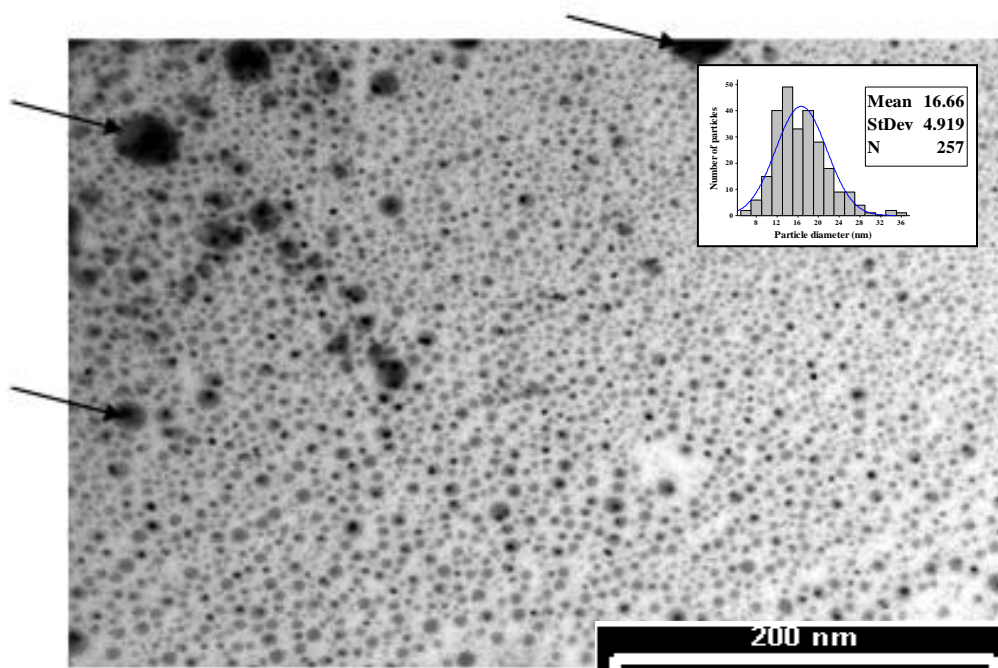


Figure 5-10: TEM image of 0.2 mg PEG-PGA 40% C_{18} – IONPs. The majority of the particles are small (Average size 16 ± 4 nm) with some aggregates forming, but only rarely (arrow). The particles highlighted by the arrows in the figure may just be small particles stuck together. (Scale bar 200 nm).

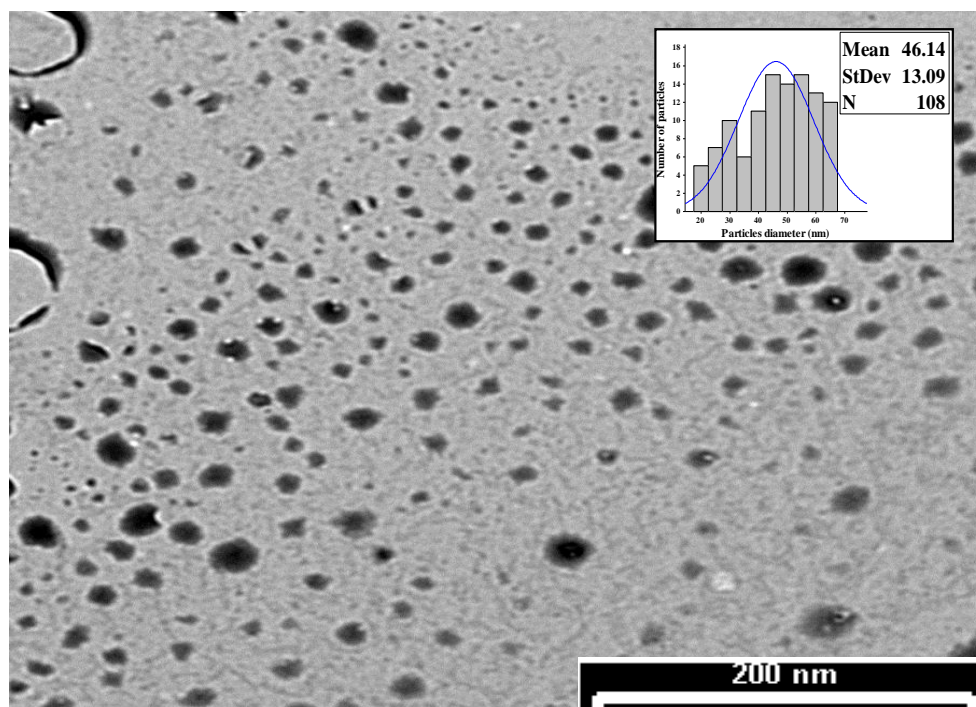


Figure 5-11 : TEM image of 0.1 mg PEG–PGA 40% C_{18} –IONPs. Both small and large particle sizes are present, but with an increased number of larger particles. (Average size 46 ± 13 nm), and it can be seen that the IONPs have been coated and that the larger particles contain aggregates of IONPs. (Scale bar 200 nm).

The typical TEM image of nanoparticles in 0.05 mg of PEG–PGA 40% C_{18} –IONPs is shown in Figure (5.12). The image revealed that the PEG–PGA 40% C_{18} –IONPs dispersed as individual NPs with a well-defined spherical shape and homogeneously distributed around 20 ± 14 nm in diameter. The image showed different range sizes of PEG–PGA 40% C_{18} –IONPs, small and large, a large number of IONPs coated with PEG–PGA 40% C_{18} as aggregates, and a huge number of small PEG–PGA 40% C_{18} –IONPs.

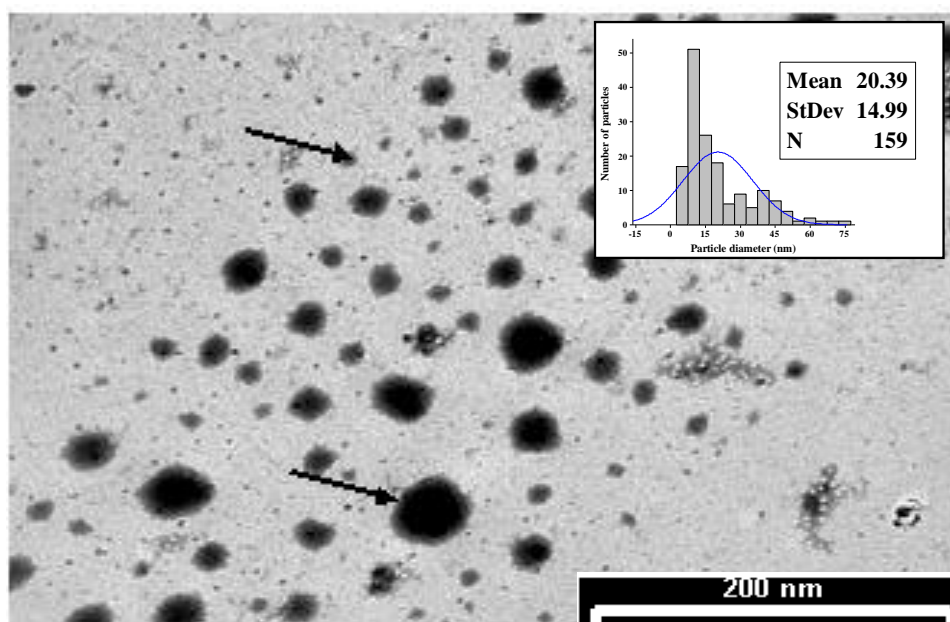
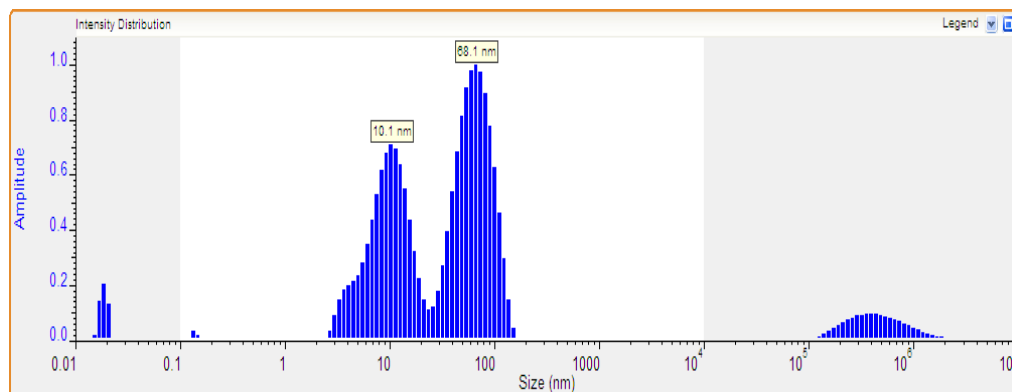


Figure 5-12 : Image of 0.05 mg PEG–PGA 40% C_{18} –IONPs. Ranges of particle sizes are displayed. Many small coated particles can be seen in the background, but also coated aggregates are present (shown by arrows) (Average size 20 ± 14 nm). (Scale bar 200 nm).

The layer of polymer was very clearly seen in TEM images in all the PEG–PGA 40% C_{18} –IONP formulations and well-formed particles of an optimum size. They have a good morphology and are not aggregated, and it is very easy to see individual particles which are clean.

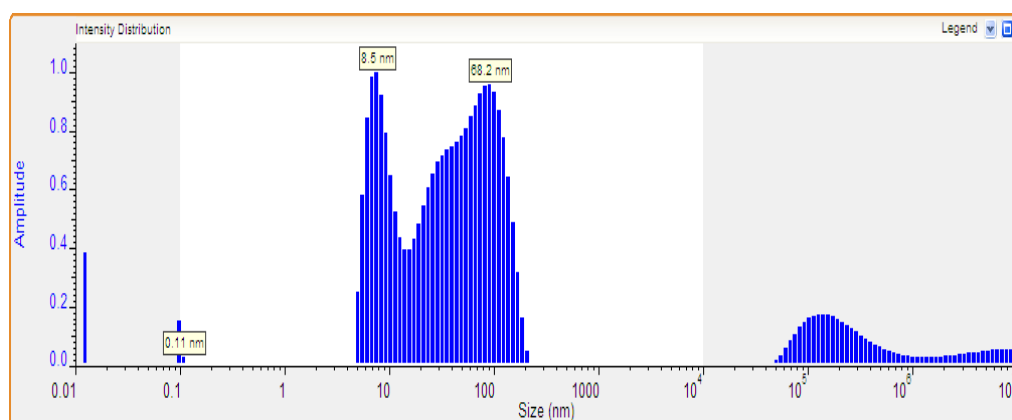
The DLS showed the different sizes of the formulations. Figures 5.13, 5.14 and 5.15 show a mixture of sizes. The 0.2 mg of PEG–PGA 40% C_{18} –IONPs batch (Fig.5.13) had a bimodal distribution of nanoparticles. There was a large amount of PEG-PGA 40% C_{18} –IONPs around 136 nm in diameter, but there were also many small particles with size of 22 nm in diameter, with the size range of the particles in the 0.2 mg of PEG-PGA 40% C_{18} –IONPs batch between 22 and 136 nm in diameter. The 0.1 mg of PEG–PGA 40% C_{18} –IONPs batch (Fig.5.14) also had a bimodal size distribution, with a majority of the nanoparticles being large (about 136 nm in diameter) and a high proportion of these being less than 50 nm. The size range of nanoparticles in the 0.1 mg PEG–PGA 40% C_{18} –IONPs batch was between 17 and 136 nm in diameter. The majority of the nanoparticles formed in the 0.05 mg of PEG–PGA 40% C_{18} –IONPs batch (Fig. 5.15) were about 112 nm in diameter, though

there are some small particles at 15 nm in diameter, a reflected in the TEM image. The particle size distribution of this batch was 15 and 122 nm.



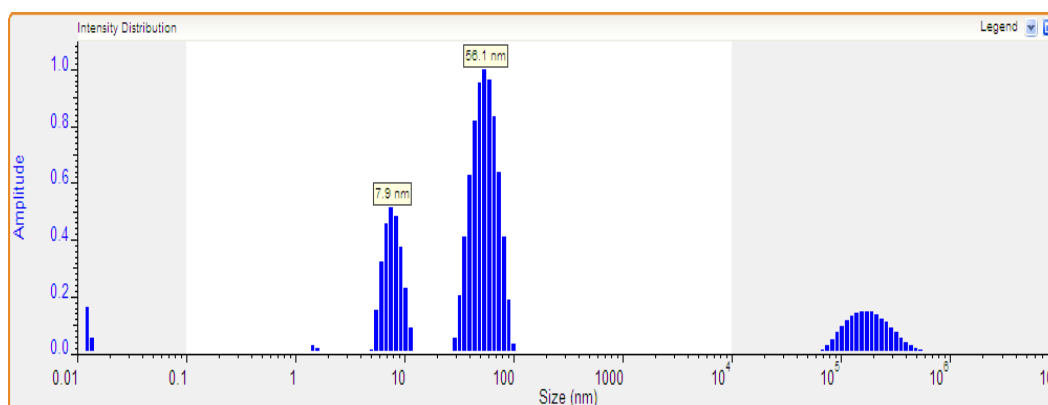
	% Area	Rh (nm)	Std Dev	% RSD
1	42.8	10.11	4.29	42.4
2	57.2	68.07	25.89	38

Figure 5-13: The particle size distribution of 0.2 mg PEG-PGA 40% C_{18} -IONPs by DLS.



	% Area	Rh (nm)	Std Dev	% RSD
1	0.1	0.11	0	0
2	30.1	8.54	2.43	28.5
3	69.9	68.07	41.79	61.2

Figure 5-14 : The particle size distribution of 0.1 mg PEG-PGA 40% C_{18} -IONPs by DLS.



	% Area	Rh (nm)	Std Dev	% RSD
1	26.6	7.93	1.47	18.5
2	73.4	56.05	14.59	26

Figure 5-15 : The particle size distribution of 0.05 mg PEG-PGA 40% C_{18} -IONPs by DLS.

The sizes of the nanoparticles determined by the DLS technique were slightly bigger than seen in the TEM photomicrographs. The reason for this larger diameter is that DLS measures the diameter of hydrated particles including the surface adsorbed water molecules, while TEM shows the unhydrated size of dry particles.

In conclusion, all the formulations showed small particles overall with minimum aggregation. The change of the amount of polymer with the different formulations affects the formation of smaller nanoparticles. These particle sizes for the different formulations are summarised in Table 5.1.

Table 5-1: Sizes of PEG-PGA 40% C_{18} -IONPs measured by DLS and TEM.

Nanoparticles	DLS NP diameter (nm)	TEM NP diameter (nm)
0.2 mg PEG-PGA 40% C_{18} -IONPs	20 and 136	16 ± 4
0.1 mg PEG-PGA 40% C_{18} -IONPs	17 and 136	46 ± 13
0.05 mg PEG-PGA 40% C_{18} -IONPs	15 and 122	20 ± 14

5.4.3.2 Zeta potential

The results of zeta potential measurements showed the surface charge of nanoparticles was increased compared to the uncoated nanoparticles where the buffer was water (Table 5.2). Increasing the amount of added polymer resulted in an increase in the zeta potential. The increase was relatively small for the 0.05 mg amount of PEG–PGA 40% C_{18} –IONPs and not very different from the IONPs, and was maximal after a 0.2 mg polymer addition of PEG–PGA 40% C_{18} coated IONPs.

Table 5-2: Zeta potential of different formulations of PEG-PGA 40% C_{18} –IONPs.

Nanoparticles	ζ potential mV\pm S.D
IONPs	21.2 \pm 7.3
0.2 mg PEG–PGA 40% C_{18} –IONPs	67.7.7 \pm 11.8
0.1 mg PEG–PGA 40% C_{18} –IONPs	50.6 \pm 17.2
0.05 mg PEG–PGA 40% C_{18} –IONPs	23.5 \pm 10.5

5.4.4 Stability of PEG–PGA 40% C_{18} Coated IONPs

The stability of the coated nanoparticle dispersions was determined at NaCl concentrations varying from 1mM to 600 mM, as shown in Figure 5.16. The iron oxide nanoparticles were coated with different amounts of PEG–PGA 40% C_{18} coated IONPs (0.2 mg, 0.1 mg, and 0.05 mg). UV visible absorbance spectra were used to monitor the turbidity of the corresponding dispersion solutions containing polymer-coated IONPs. With the change in sodium chloride concentration. All the samples showed high stability over all the concentrations of the NaCl, with no significant differences. The 0.1 mg of PEG–PGA 40% C_{18} coated IONPs batch, which has relatively low polymer content, was highly resistant to NaCl induced aggregation and gave slightly lower absorbances than either the 0.2 mg or 0.05 mg formulations PEG–PGA 40% C_{18} coated IONPs. In conclusion, all three formulations showed the high stability suitable for use with biological media.

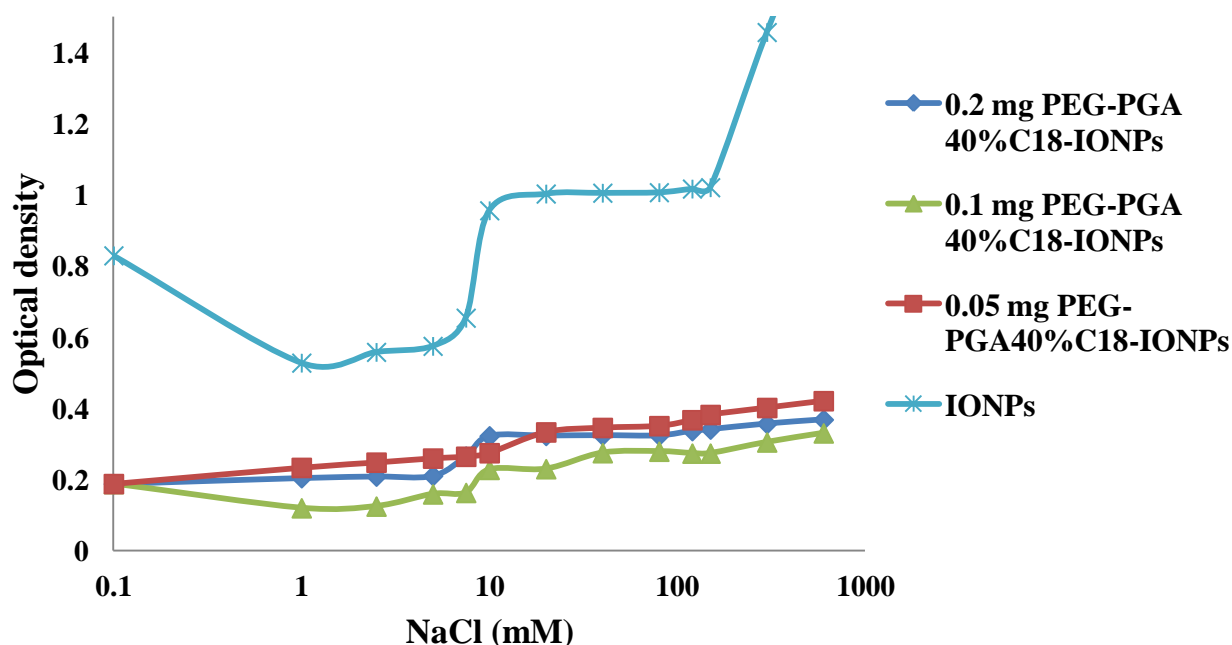


Figure 5-16 : Stabilities of different formulations of PEG-PGA 40% C_{18} -IONPs. Various PEG–PGA 40% C_{18} -IONP formulations were titrated with increasing salt concentrations and the aggregation of the formulations was monitored by optical density at 500 nm.

5.5 Discussion

5.5.1 PEGYLATED PGA 40% C_{18}

PEGylated PGA 40% C_{18} was successfully synthesised. Analysis by NMR, FTIR and GPC confirmed that PEGylated polymer was formed successfully, resulting in a final yield of 78%. The reaction was between the amine group of PEG and the COOH of PGA, using carbonyldiimidazole (CDI) to produce a stable carbamate bond linking the PEG and the 40% C_{18} substituted PGA. CDI is a well-known coupling reagent. Oster et al., (2004) have reported that it had been used to attach an amine functionalised chemical to a poly(vinyl alcohol) through a hydroxyl group.

CDI has the ability to react with amino groups and carboxylic acid to give reactive carbonyl imidazole intermediates, which are more easily handled and can be isolated. The carbonyl imidazole might consequently undergo selective reaction with primary amines or alcohol to form amide, carbonate or ester derivatives (Rannard and Davis, 2000 and Rannard and Davis, 1999). The PGA would be expected to consist of 50% monocarboxyl, 25% dicarboxyl and 25% with no carboxy termini. The yield of 78% would suggest that the carboxy terminal is the preferred site of coupling.

From the yield and from the proportion of PGA which cannot react, which is expected to be 25%, the maximum ratio achievable is 1.25 PEG: 1 PGA 40% C_{18} , where the results of GPC suggest 2 PEG: 1 PGA 40 % C_{18} and NMR 0.7 PEG: 1 PGA 40% C_{18} . It seems most likely that the PEG-PGA ratio achieved is between that determined by GPC and NMR.

PEGylated polymers may improve the stability of the drug delivery system in the blood by preventing protein absorption and uptake by the reticuloendothelial system (RES). To provide further functionality on the coated IONPs surface, PGA 40% C_{18} was chosen as it is very hydrophobic and forms good nanoparticles and because it is biodegradable and non-toxic. PEG was chosen as the hydrophilic segment, acting as a modifier for preparing surfaces with protein adsorption resistance, it is also a non-ionic, highly hydrophilic and flexible polymer (Sofia et al., 1998 and Kim et al.,

2005b). PEG has a range of chain lengths and with its functionalised termini makes the chemical coupling to another polymer simple. A PEG chain with M.W 2000 functionalised with an amine group at one terminus was commercially available, and was coupled to the core polymer via amine activation using CDI. In the ^1H , NMR was clearly both peaks of the PEG and PGA. Comparing the areas of the PEG and PGA gave an estimate of the PGA: PEG ratio. Copolymers could increase the time in circulation and increasing the chance to avoid the defence system in the body when they are hydrophilic and hydrophobic.

5.5.2 PEGylated PGA 40% C₁₈-IONPs

There have been many reports of nanoparticulate drug delivery with PEG surfaces to improve biodistribution and drug delivery. It has been reported that PEG stabilises poly(lactic acid) nanoparticles in the presence of lysozyme (Vila et al., 2002).

The physicochemical characteristics of the different formulations prepared with a PEG-PGA 40% C₁₈ coating were investigated. The size of the nanoparticles characterised by TEM was approximately 20–59 nm over all the formulations and showed spherical-shaped particles with a narrow size distribution. Unlike the PGA coatings, there was no population of bigger particles when an excess of polymer was added to the iron oxide nanoparticles. When the copolymer solution was added dropwise into iron nanoparticles in water under magnetic stirring the organic solvent would diffuse into the water, and phase separation occurs in this system. The PEG block is soluble in water but not in the organic phase, and the hydrophobic PGA block is not water soluble but is highly soluble in organic solvent. Consequently, the acetone goes out while the water goes in as result the droplet breaks up and the polymer is precipitated. The solvent evaporates and the core solidifies, and the core-shell structured nanoparticles are formed. The presence of the PEG prevents the layer from getting too thick. The TEM clearly shows a layer of the PEG-PGA 40% C₁₈ is coating the IONPs in all batches. PEG attachment to nanoparticles can be carried out either by physical adsorption or by covalent grafting (Stolnik et al., 1995 and Jaeghere et al., 2000).

IONPs coated with PEG-polyanion block copolymer via electrostatic interaction had a longer half-life in the blood stream compared to dextran-IONPs, allowing the improved MR imaging of the liver by their intravenous administration (Thünemann et al., 2006 and Lutz et al., 2006). PEG coating and stability make these particles suitable for *in vivo* applications. Particle sizes were affected by the method of preparation and dictated by the quantity of the copolymer-coated particles. Work was done by Gref et al., (1994a) who prepared PEG-PLGA nanoparticles smaller than 200 nm using a nanoprecipitation method.

Work that was done by Hu et al., (2007) also used a nanoprecipitation method to obtain polycaprolactone poly(ethylene glycol) PCL-PEG. The morphology and size of nanoparticles were measured by field emission scanning electron microscopy (FESEM) and laser light scattering (LLS). All the nanoparticles were spherical in shape and the sizes were less than 200 nm. The sizes of the nanoparticles increased with increasing PCL segment length. The PEG outer shell of the nanoparticles reduced surface absorption of proteins and escape from reticuloendothelial system (RES) after intravenous administration (Jones and Leroux, 1999 and Zambaux et al., 1999).

Using IONPs coated with PEG silane copolymer, MR imaging of solid tumour has recently been demonstrated (Lee et al., 2006). The coating of iron nanoparticles should be an adsorption mechanism other than simple electrostatic interaction, The PEG chain may affect the hydrodynamic size and hydrophilicity as well as the anti-opsonisation properties of the particles (Xie et al., 2009, Xie et al., 2007 and Harris and Chess, 2003).

Decuzzi et al., (2006) produced models suggesting that smaller sized, spherical NPs observed higher diffusion rates, increasing the NP concentration at the centre of a blood vessel, thus limiting interactions with endothelial cells and prolonging the NP blood circulation time. For the PEG-PGA 40% C₁₈-IONPs described in this chapter, a remarkably small size was witnessed, which is rarely reported for IONPs with other types of biodegradable polymer coatings.

Veiseh et al., (2009) reviewed many studies reporting that the hydrodynamic size plays a very important role in the NPs clearance from circulation. Small particles around 20 nm are excreted renally while medium size particles from 30–150 nm accumulate in the bone marrow, stomach, kidney, liver and spleen. On the other hand, large sizes from 150 nm to 300 nm have been found in spleen and liver.

In conclusion, the size and shape of the PEG-PGA 40% C_{18} -IONPs were perfect and small, and these parameters can be tuned to achieve the enhanced biodistribution of the coated nanoparticles.

5.5.2.1 Zeta potential

Increase of zeta potential seems to be an indicator for the PEGPGA 40% C_{18} -IONPs. The 0.05 mg of PEG-PGA 40% C_{18} -IONPs were similar to the IONPs, while the other formulations were more positive. The continued increase in the zeta potential may indicate that the thickest coating was achieved with the highest amount of polymer. However, the PEG-PGA 40% C_{18} -IONPs should have given a more negative or neutral rather than positive potential, and this could be due to the use of water rather than a low concentration of buffer for this measurement.

5.5.3 Stability of PEG-PGA 40 % C_{18} -IONPs

The PEG-PGA 40% C_{18} -IONPs showed excellent stability due to steric stabilisation. Electrostatic and steric stabilisation are now extensively accepted as being two mechanisms by which it is possible to generate colloidal stability (Napper, 1977 and Vincent, 1974). The 0.1 mg PEG-PGA 40% C_{18} coating produced very stable particles and contrary to the zeta potential results appeared to be more stable than even the 0.2 mg and 0.05 mg coatings, but there was not a great difference between them. The 0.1 mg polymer coating also seemed to be even more effective than the 0.1% Tween coated PGA 0%-IONPs reported in the previous chapter. Steric stabilisers have long been used to achieve greater stability of colloidal particles or to prevent capture by phagocytic cells (Illum et al., 1987). The flocculation of the

particles at high concentration of the salt NaCl is attributed to the dehydration effects and the high stability of the coated nanoparticles attributed to a good coating and the reaction between the particles and the polymer to enhance the stability, strong interactions between the PGA chains and the nanoparticle. The surface can produce anchoring at many points in the stabilisation (Napper, 1977).

The study shows that a range of IONPs coated with a thin PEG–PGA 40% C_{18} layer demonstrated significant colloidal stability and the layer coating was enough to prevent aggregation. If the thickness of the polymer is large enough, the van der Waals attraction between the particles is unimportant in comparison to the Brownian thermal energy. This is the origin of the term ‘steric’ stabilisation (Vincent, 1974 and Napper, 1977).

PEGylated PGA 40% C_{18} increased the stability of the nanoparticles in comparison to the stability of PGA and PGA 40% C_{18} also those with Tween 80 and albumin overcoating as described in chapter 4.

Bazile et al., (1995) reported the advantage of PEGylated poly(d,l-lactic acid) PLA in comparison with colloidal systems like PLA nanoparticles by covalently coupling the PEG to PLA, thus minimising uptake by the MPS.

5.6 CONCLUSION

The aim of this chapter was to synthesise PEGylated PGA 40% C_{18} with PEG 2000 to give surface modified layer of IONPs with PGA 40% C_{18} to the surface of the IONPs. PEG–PGA 40% C_{18} –IONPs were prepared using our modified interfacial deposition method to determine the optimum conditions resulting in a small size. The best condition was found to be 0.2 mg polymer, which produced clean and smooth particles with only rare aggregates. Decreasing the amount of the polymer used caused an increase of the size of PEG-PGA 40% C_{18} –IONPs. The best particle size was determined by both TEM and DLS. All the formulations had a small size approximately from 20 to 59 nm diameter. The PEGylated PGA 40% C_{18} –IONPs was shown to be an effective stabiliser at high concentrations of NaCl (600 mM) which

makes these particles suitable for both *in vitro* and *in vivo* applications. Small size of PEG-PGA 40% C₁₈-IONPs can be produced by a simple coating method which is the modified interfacial deposition method

CHAPTER 6

6. INTERACTION OF COATED NANOPARTICLES WITH CELLS IN CULTURE

6.1 INTRODUCTION

IONPs have been used widely in studies for potential applications in biology and medicine such as enzyme and protein immobilisation, magnetic resonance imaging (MRI), RNA and DNA purification, magnetic cell separation, purification, magnetically controlled transport of anticancer drugs, and also hyperthermia generation (Matsunaga et al., 1999 and Reetz et al., 1998).

Many factors affect the efficacy of the IONPs as contrast agent, such as the size of the iron oxide crystals. Also, the charge, the nature of the coating, and the hydrodynamic size of the coated particle affect the stability, biodistribution, opsonisation and metabolism of different contrast agents (Corot et al., 2006). IONPs should have a narrow size distribution, and be coated with biocompatible non-toxic and biodegradable polymer to provide stability in a physiological medium and biological environment. Also these properties will affect cellular uptake and hence biodistribution.

For polymer-coated IONPs with a diameter larger than 50 nm, the NPs would be trapped in the liver or spleen. However, smaller than 30 nm would rapidly circulate in almost the whole body. Normally, these small 30 nm NPs are more likely to enter the lymphatic system and be eliminated slowly. The properties of nanoparticles coated with a layer of polymer are important. Coated nanoparticles with a hydrophobic surface may improve the uptake of the nanoparticles by the liver or spleen, while with a hydrophilic surface they may increase the time of circulation in the blood and increase the chance to penetrate into marrow and enter the lymph (Li et al., 2005).

Cell labelling with magnetic nanoparticles is a common method which has been widely used for *in vitro* cell separation and also for *in vivo* imaging because of their properties to improve the signal in magnetic resonance imaging (Wilhelm et al., 2003 and Lok, 2001). Two current cell labelling nanoparticle techniques can use either internalisation of the nanoparticles by fluid phase endocytosis, receptor mediated endocytosis or phagocytosis, or alternatively by attaching magnetic nanoparticles to the cell surface (Weissleder et al., 2000 and Tzu-Chen et al., 1993).

MR contrast agents are used increasingly to detect diseased and defective cells and to increase and enhance the resolution of the image, but they are dependent on their particle size and coating. Using drug delivery techniques it should be possible not only to deliver diagnostic agents to the target site with maximum uptake by target cells, but also to minimise the side-effects. Understanding the cellular uptake of nanoparticles is therefore important in both cell labelling and for MRI contrast agents.

In this study, we incorporated a rhodamine B isothiocyanate RBITC label into our PGA 40% C_{18} -IONPs with size 23 ± 7 nm and PEG-PGA 40% C_{18} -IONPs with size 16 ± 4 nm for labelling cells to investigate the intracellular uptake of nanoparticles with different coatings in cell monolayers and cell aggregates using the C6 brain glioma cell line. Particles were examined using a range of techniques, such as TEM, fluorescence microscopy, confocal microscopy and flow cytometry.

The aim of the present investigation is to determine the uptake of small coated IONPs to get some idea of how these properties may be used for detecting morphological and physiological tissue *in vitro* and can be a good contrast agent for MR images.

The cell culture studies investigated the two best formulations developed during this project, i.e IONP produced as described in chapter 3 and subsequently coated with either PGA 40% C_{18} as described in chapter 4 or PEG-PGA 40% C_{18} as described in chapter 5.

6.2 Methods

Routine monolayer cell culture (see 2.2.18.4).

RBITC labelled PGA-coated iron oxide nanoparticles (see 2.2.16).

Determination of fluorescent dye loading (see 2.2.17).

Preparation of the nanoparticles for cell work (see 2.2.18.1).

Qualitative Nanoparticle uptake by cells study (see 2.2.18.9).

Qualitative uptake of nanoparticles in C6 cells (see 2.2.18.10).

Qualitative uptake and metabolism of nanoparticles in C6 cell (see 2.2.18.11).

Evaluation of time-dependent uptake of NPs by cells growing in monolayer culture using TEM (see 2.2.18.12).

Quantitative NP uptake study dependent on dose and time (see 2.2.18.14).

Quantitative determination of loss of nanoparticles from cells (see 2.2.18.15).

Aggregate cultures (see 2.2.18.16).

Cell aggregate uptake of RBITC NPs (see 2.2.18.17).

6.3 Results

6.3.1 Qualitative Nanoparticle Uptake Study: Dose-dependent uptake of RBITC labelled NPs by cells

6.3.1.1 0.1 % Tween–PGA 40% C_{18} coated IONPs

As shown in Figure 6.1, the uptake level progressively increased with increased dose of RBITC labelled NPs and did not reach saturation up until the highest dose of the polymer coated IONPs. To confirm the uptake resulted from cellular uptake of fluorescently labelled NPs, untreated cells as a control with 2 h incubation time were also used. The controls in Figure 6.1e show, firstly that in cells not incubated with NPs there was no significant autofluorescence. After 2 h incubation time of cells with medium with serum containing NPs, fluorescence was seen to increase with dose, clearly confirming that nanoparticle uptake occurred into cells. These nanoparticles are too fine to be resolved individually in the light microscope, but the fine distribution suggests that the particles were not significantly aggregated on uptake.

Cells incubated with PGA 40% C_{18} –IONPs show very fine particles distribution all across the cell and over the nuclei. However, there was an apparent difference in subcellular localisation shown by all doses and the PGA 40% C_{18} –IONPs were located mainly on the periphery of the nuclei.

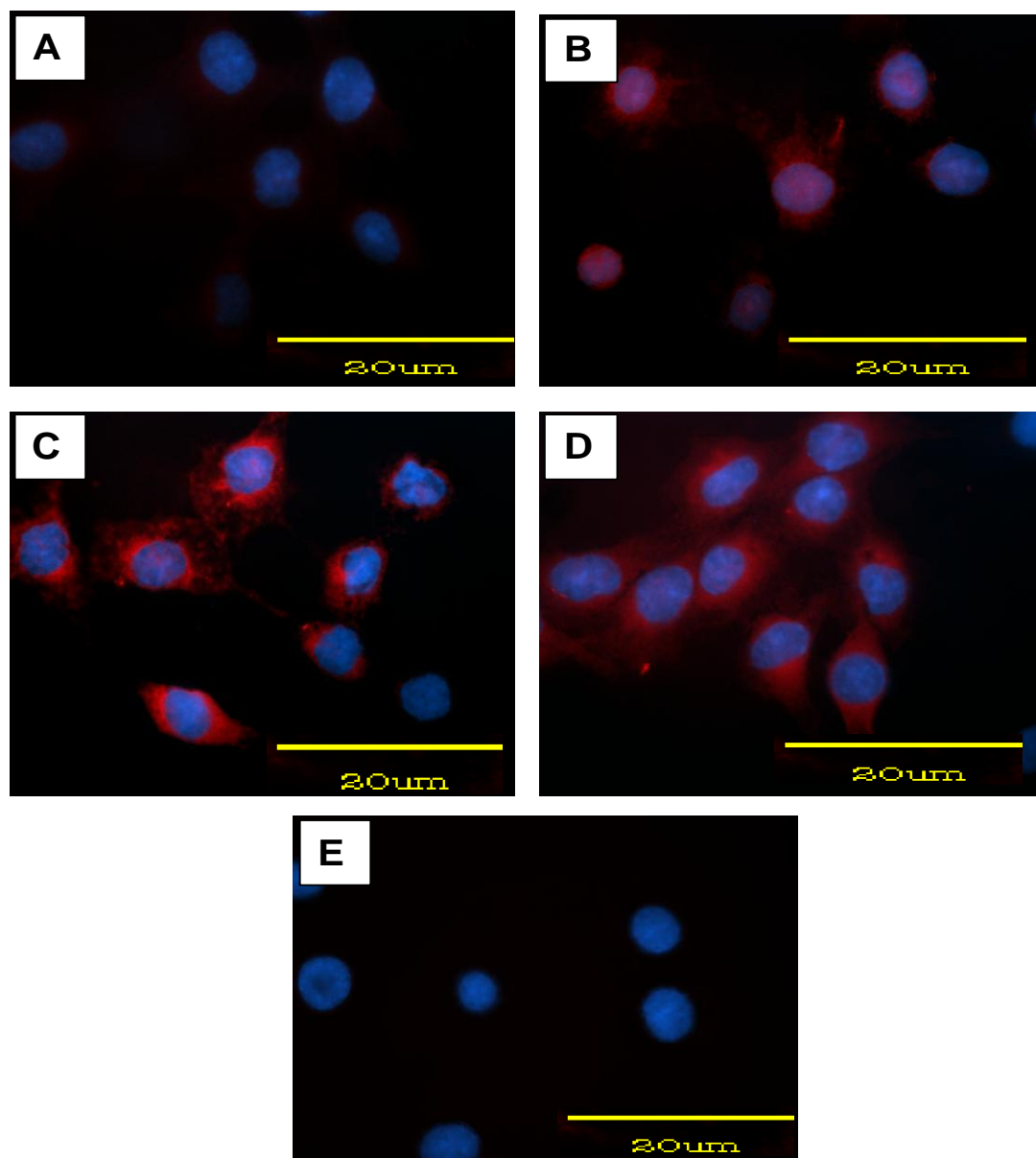


Figure 6-1: Fluorescence microscopy images of PGA 40% C_{18} -IONPs without Tween incubated with C6 cell for 2 h in the presence of serum. (A) 0.1 ml, (B) 0.2 ml, (C) 0.5 ml, (D) 1 ml and (E) control untreated cells. (Scales bar 20 μ m).

Different conditions were used in this experiment to see how it affects the uptake, the blue is DAPI which stained the cell nuclei while the red is the fluorescence labelling the PGA 40% C_{18} -IONPs. Our experiment above showed that the uptake of RBITC labelled PGA 40% C_{18} -IONPs in the presence of the serum in the medium is high. To further investigate the effect of overcoating on the surface of the PGA 40% C_{18} -IONPs on the uptake we tested the cellular uptake of different NPs. Figures 6.2 and 6.3 show the typical images of PGA 40% C_{18} -IONPs overcoated with 0.1% Tween in

the presence of serum and PGA 40% C_{18} -IONPs without Tween and in the absence of serum in the cell medium respectively.

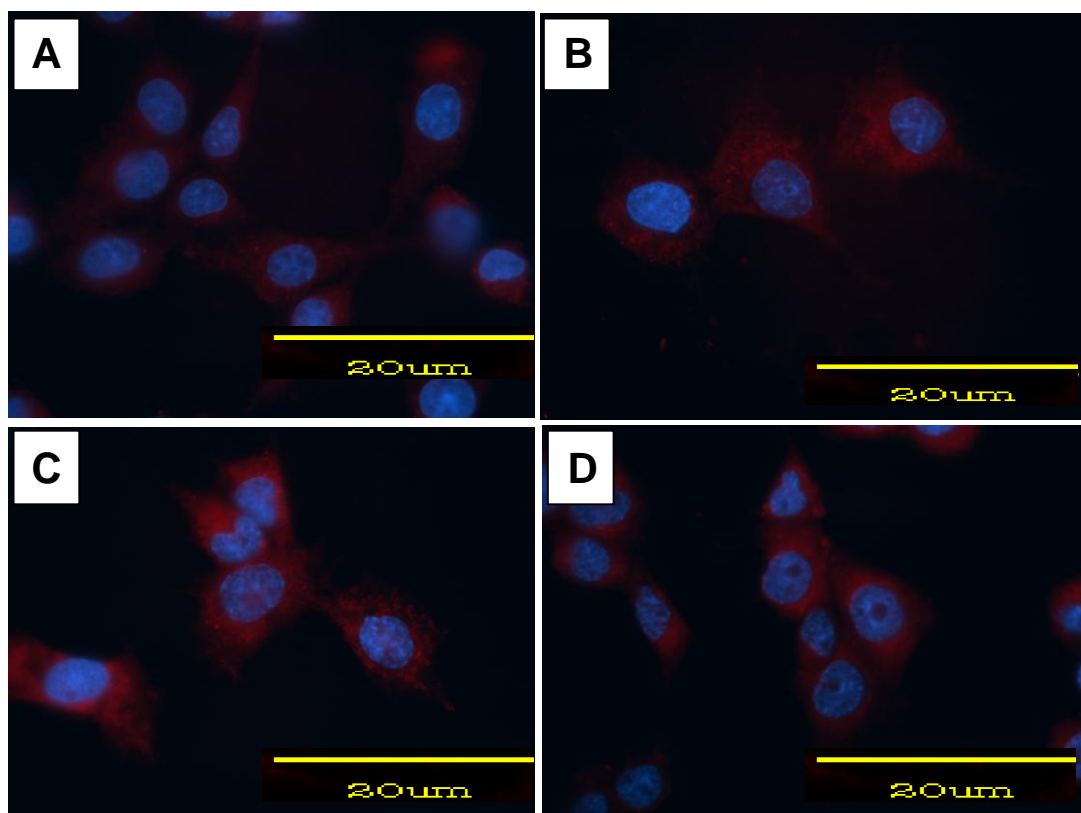


Figure 6-2 : Fluorescence microscopy images of PGA 40% C_{18} -IONPs with Tween 0.1% incubated with C6 cell for 2 h in the presence of serum. (A) 0.1 ml, (B) 0.2 ml, (C) 0.5 ml and (D) 1 ml. (Scales bar 20 μ m).

The uptake here again increased with increasing dose for both of the two experiments. In all doses the fine particles were across the cell and throughout the cytoplasm. Cell uptake of nanoparticles was shown as highly fluorescent patterns, preferentially distributed in the cytoplasm or around nucleus but without the obvious perinuclear distribution frequently seen with larger particles. There are spots on the nuclei but it is difficult to see if these are in or merely above the nuclei. The presence of Tween seemed to reduce the uptake of the nanoparticles. In Figure 6.3, PGA 40% C_{18} -IONPs appeared to be taken up to a greater extent in the absence of serum without Tween. There also appeared to be less effect of the dose, but the nanoparticles showed very high concentration and accumulation. This may be partly due to the cells having a more rounded up appearance, possibly due to the absence of

serum. Figure 6.3e showed untreated cells again demonstrating the lack of background fluorescence.

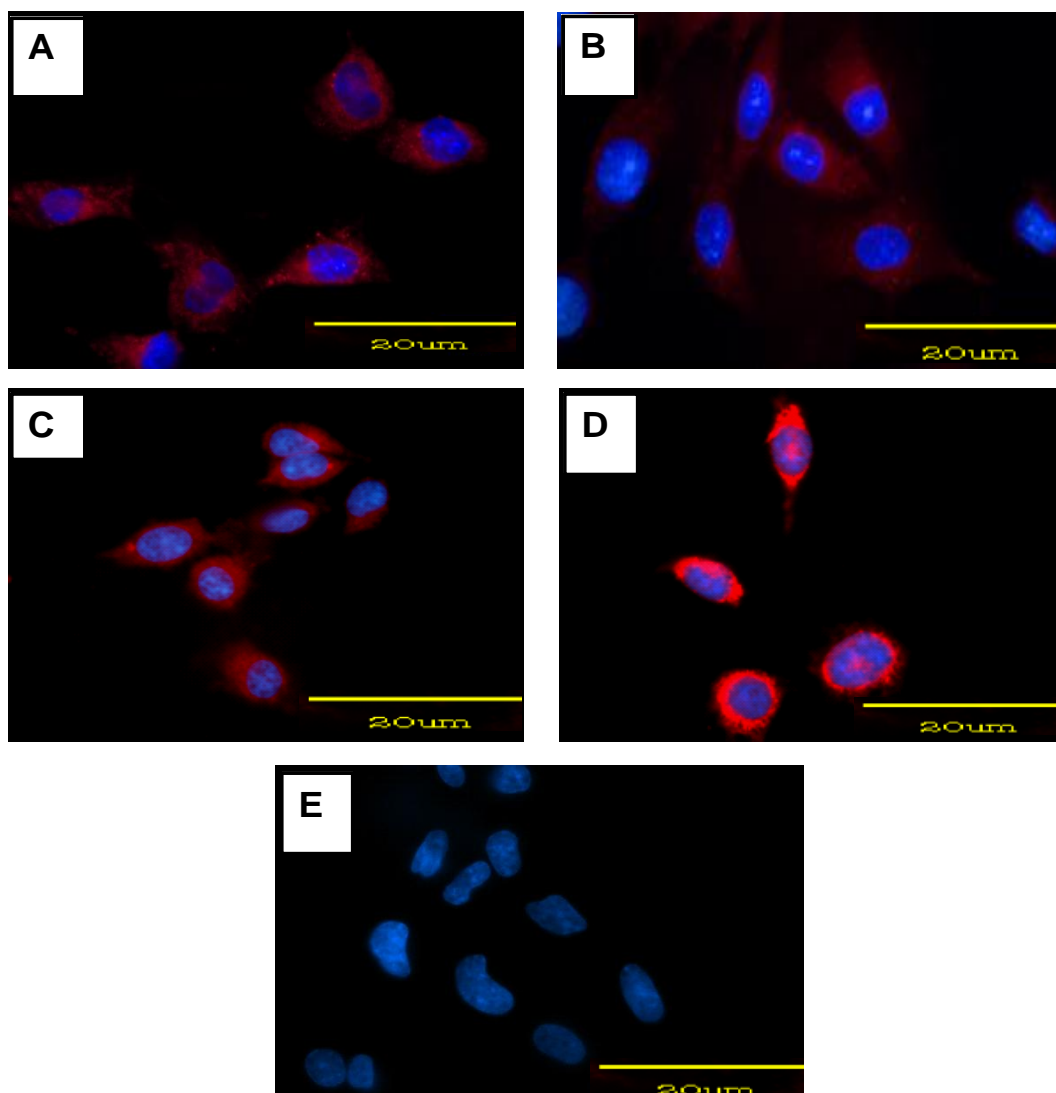


Figure 6-3 : Fluorescence microscopy images of PGA 40% C_{18} -IONPs without Tween incubated with C6 cells for 2 h in the absence of serum. (A) 0.1 ml, (B) 0.2 ml, (C) 0.5 ml, (D) 1 ml and (E) control untreated cells. (Scales bar 20 μ m).

6.3.1.2 PEG-PGA 40% C_{18} coated IONPs

In order to visualise the distribution of the modified IONPs, the PEG-PGA 40% C_{18} coated IONPs were fluorescently labelled by RBITC. Here (Fig.6.4) four samples of C6 cell cultures in the presence of serum, each containing PEG-PGA 40% C_{18} -IONPs at different doses, were incubated under the same conditions (2 h, 37°C).

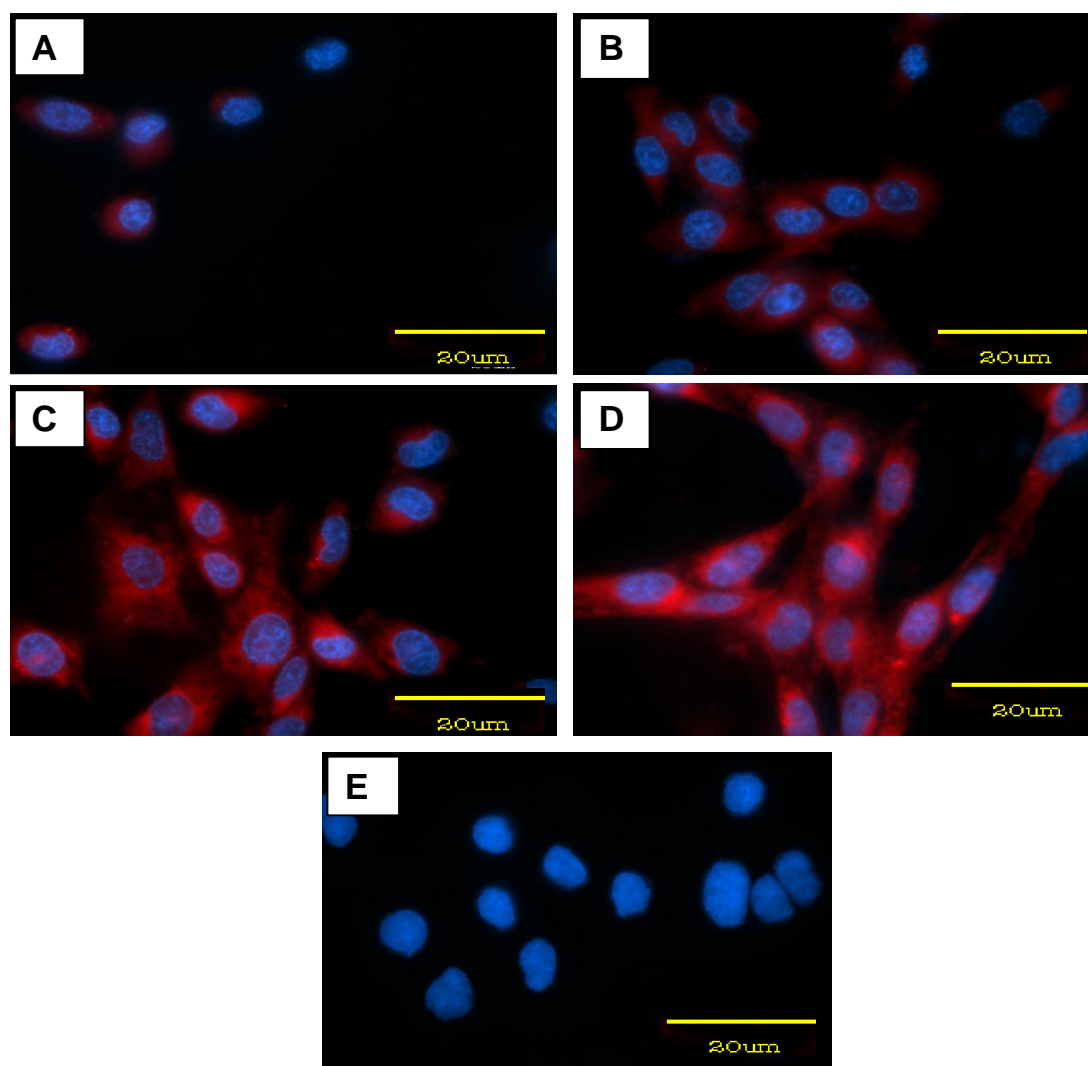


Figure 6-4 : Fluorescence microscopy images of PEG-PGA 40% C_{18} -IONPs in different concentration incubated with C6 Cell for 2 h in the presence of serum. (A) 0.1 ml, (B) 0.2 ml, (C) 0.5 ml, (d) 1 ml and (E) control untreated cells. (Scales bar 20 μ m).

It can be seen from Figure 6.4 that the fluorescence intensity gradually increased with increasing concentration of the labelled nanoparticles. From the lowest dose (0.1 ml) fine particles were clearly visible in the cytoplasm.

One can see from Fig 6.4d that the fluorescence of the 1 ml loaded PEG-PGA 40% C_{18} -IONPs is closely located around the nuclei area, which indicates that the PEG-PGA 40% C_{18} -IONPs have been taken up by the cells. The signal in the nuclear area was very strong, particularly at the 0.5 ml dose. The PEG-PGA 40% C_{18} -IONPs overall showed a higher fluorescence than the particles without

PEG, whether PGA 40% C_{18} -IONPs with Tween or in the presence or absence of serum. However, cells incubated with the control showed no fluorescence.

6.3.2 Time-dependent Uptake of RBITC Labelled NPs by Cells

6.3.2.1 0.1% Tween-PGA 40% C_{18} -IONPs

Cells were treated with labelled particles over different time periods from 2 h to 24 h before washing and fixing the cells after the end of the incubation time. Figure 6.5 shows the fluorescence images of 0.1% Tween-PGA 40% C_{18} -IONPs for different times without washing. The uptake increased with increasing time. The distribution was clear from the early time incubation and the fine particles can be seen around the nuclei. High accumulation was observed in the longer incubation times at 12 h and 24 h, with very intense fluorescence observed at 24 h incubation time (Fig. 6.5 f).

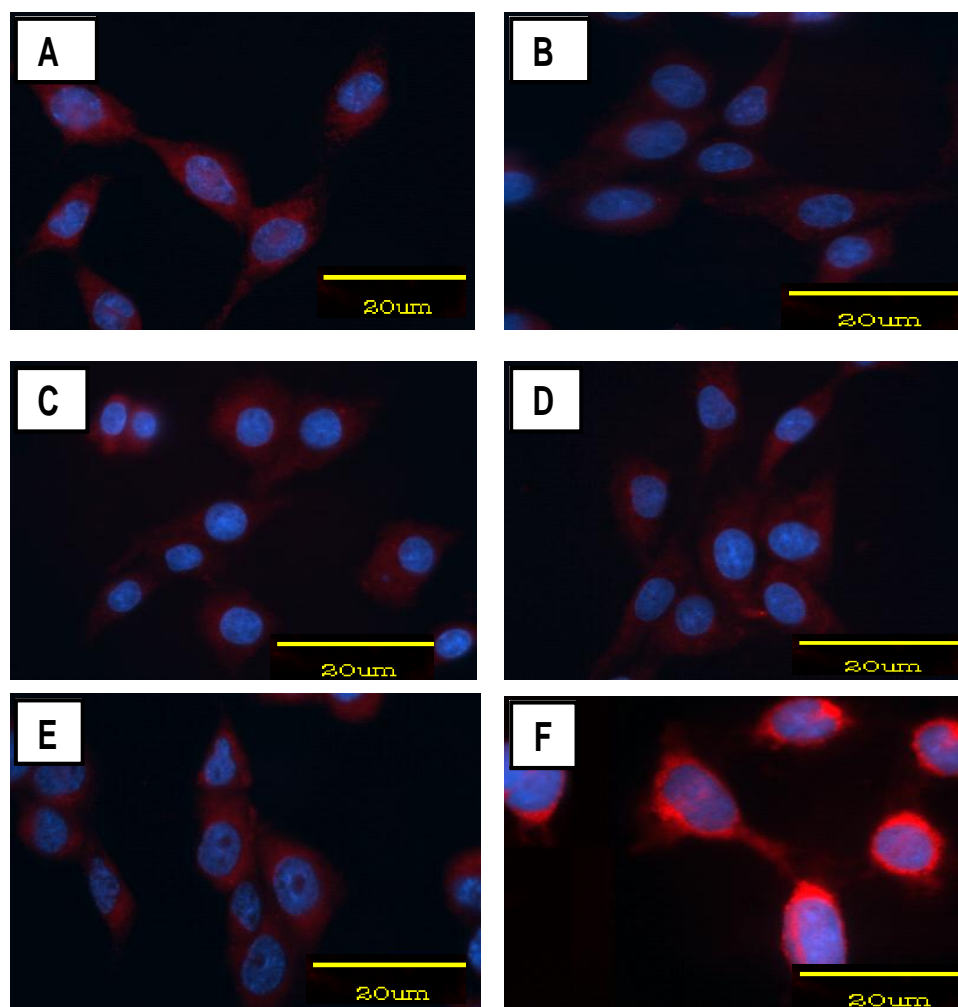


Figure 6-5: Fluorescence microscopy images of 0.1% Tween-PGA 40% C_{18} -IONPs incubated with C6 cells for different time periods without washing. (A) 2 h, (B) 4 h, (C) 6 h, (D) 8 h, (E) 12 h and (F) 24 h. (Scales bar 20 μ m).

6.3.2.2 PEG-PGA 40% C_{18} -IONPs

The uptake of PEG-PGA 40% C_{18} -IONPs was monitored by fluorescence microscopy Figure 6.6, over time. Up to the shortest practical incubation time of about 2 h, uptake had occurred already and a good distribution with very fine particles was seen. All of the nanoparticles with different time incubation had a uniform distribution in what is most likely the cytoplasm. Accumulation increased significantly from 6–8 hours onwards (Figure 6.6c and d), with a very intense accumulation by 24 h.

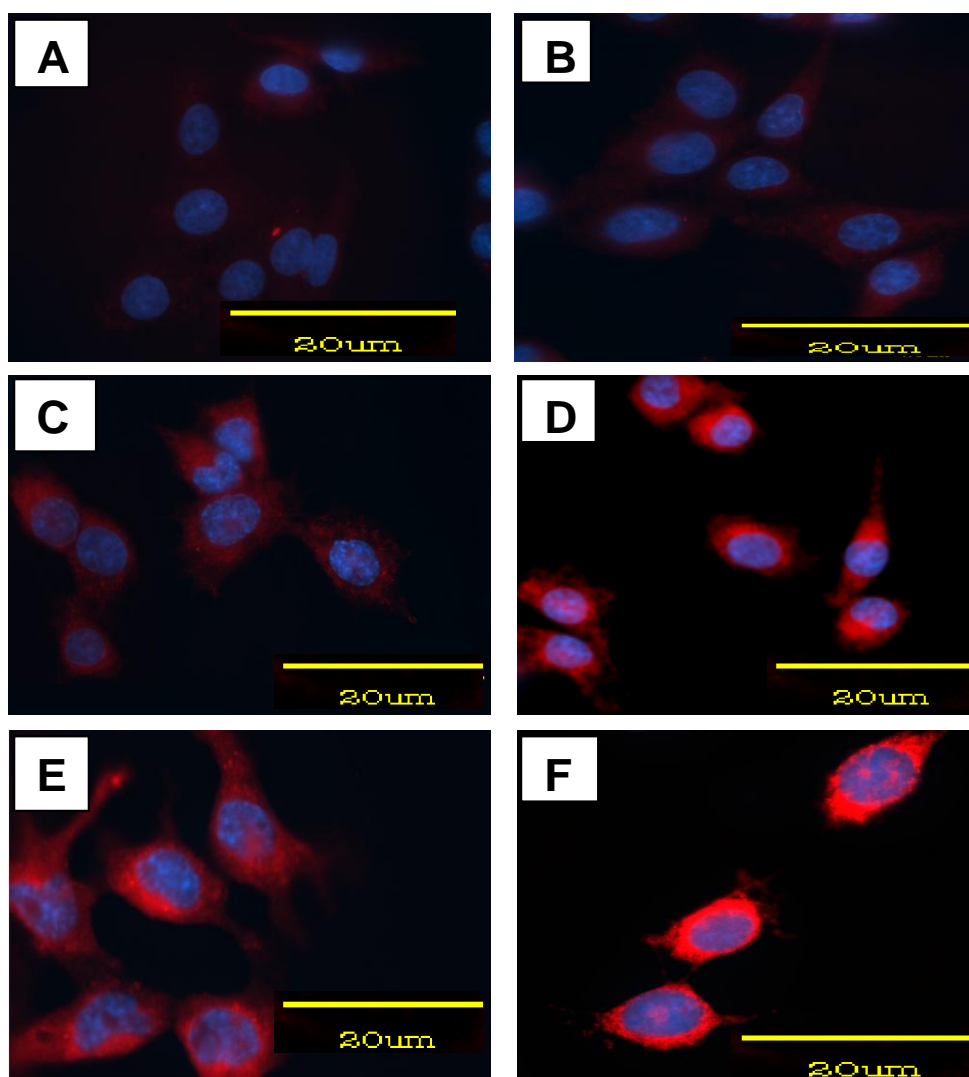


Figure 6-6: Fluorescence microscopy images of PEG-PGA 40% C_{18} -IONPs incubated with C6 cells for different time periods without washing. (A) 2 h, (B) 4 h, (C) 6 h, (D) 8 h, (E) 12 h, and (F) 24 h. (Scales bar 20 μ m).

6.3.3 Time-dependent Metabolism of RBITC Labelled NPs by Cells.

6.3.3.1 0.1 % Tween-PGA 40% C_{18} coated IONPs

The uptake of the 0.1% Tween-PGA 40% C_{18} -IONPs by C6 cells with incubation times of 1 to 24 h was visualised using fluorescence microscopy, after incubation of 2 h and then reincubation for varying periods. This experiment shows the retention of

fluorescence with time after exposure of cells to labelled 0.1% Tween-PGA 40% C_{18} -IONPs. The effect of incubation time on the cellular uptake is clearly shown in (Fig. 6.7). The images showed that the cells started with a surprisingly even labelling of the cells throughout the cytoplasm. Fluorescence was not detected in control cells that had not been exposed to the RBITC labelled nanoparticles.

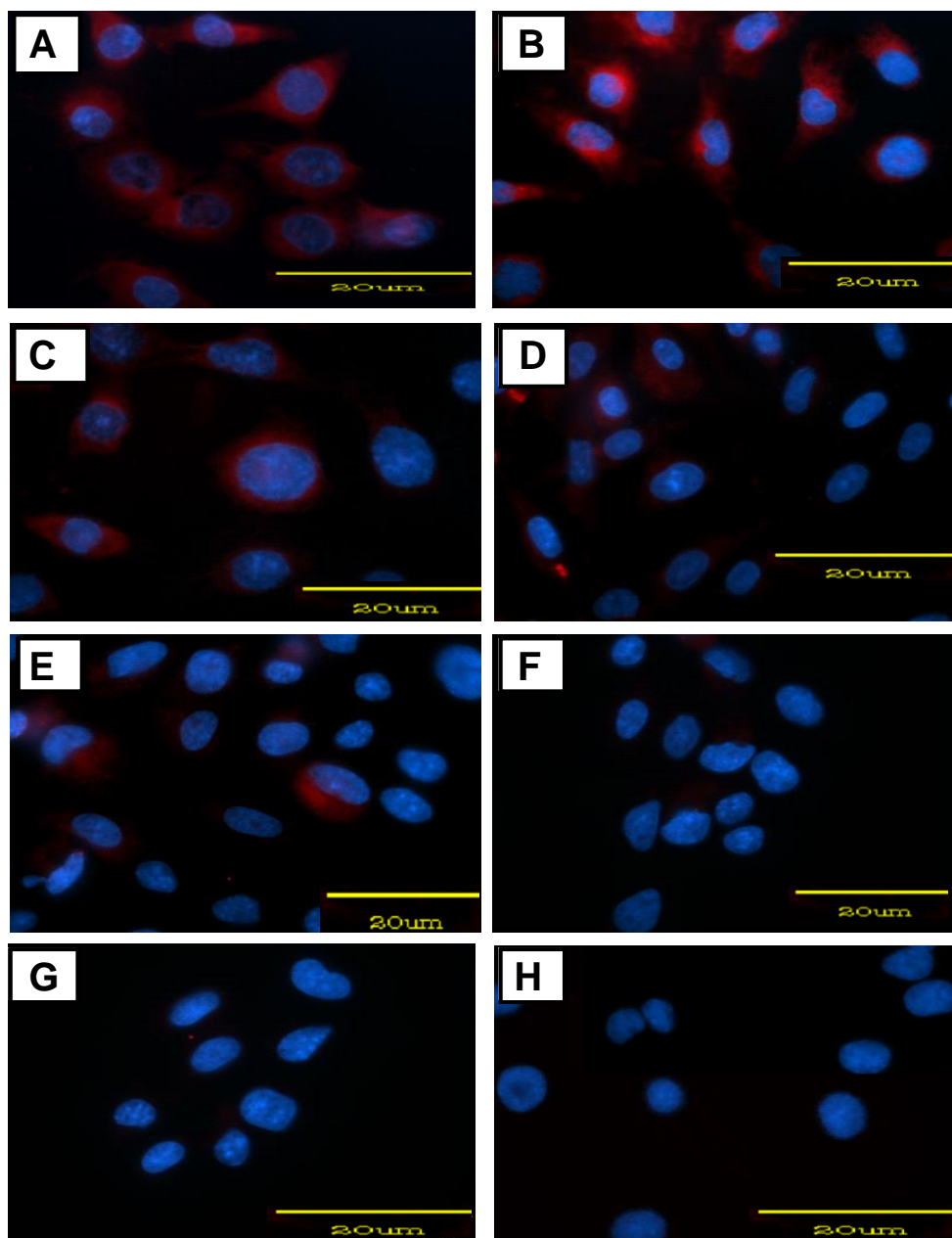


Figure 6-7 : Fluorescence microscopy images of 0.1% Tween-PGA 40% C_{18} -IONPs incubated with C6 cells for different time periods in presence of serum. (A) 1 h, (B) 2 h, (C) 4 h, (D) 6 h, (E) 8 h, (F) 12 h, (G) 18 h and (H) 24 h. (Scale bar 20 μ m).

The images in the early time periods 1 to 2 h show that in the cells the highest concentration was in the perinuclear area and in some cases overlying the nucleus. Red fluorescence intensity was only retained for the first two hours but had started to disappear by 4 h incubation although it can be still detected inside the cells (Fig. 6.7c).

In the case of 6h and 8 hr, most of the cells showed no fluorescent patches but some fluorescence was retained in a few cells as a small amount of fine particles (Fig. 6.7d and e). In the case of 12 h, 18 h and 24 h the fluorescence had disappeared entirely.

Cells in this case must be investigated by TEM to determine whether it is the fluorescence or the iron particles which have disappeared.

6.3.3.2 PEG–PGA 40% C_{18} –IONPs

Figure 6.9 shows the cellular disappearance for different incubation time using C6 cells treated with 1 ml of PEG–PGA 40% C_{18} –IONPs

Figure 6.9 a, b and c clearly shows the nanoparticle presence in C6 cells as a widespread and fine distribution throughout the cytoplasm but with some perinuclear accumulation. Significant fluorescence also appeared over the nucleus.

The fluorescence intensity MFI of PEG–PGA 40% C_{18} –IONPs was high for the initial 30 min to 1 h of incubation time. After that, fluorescence started to disappear. The disappearance again being higher in some cells than others, it remained relatively stable over the next few hours. Then the fluorescence started disappearing at 8 h. In Figure 6.9d, the fluorescence still appears in just a part of the cell and in the majority of the cells the fluorescence has disappeared.

No red fluorescence was detected in the cell in 12 h and 24 h time of incubation (Fig.6.9 g and h). Sample control (Fig. 6.8) was used for both experiments as control.

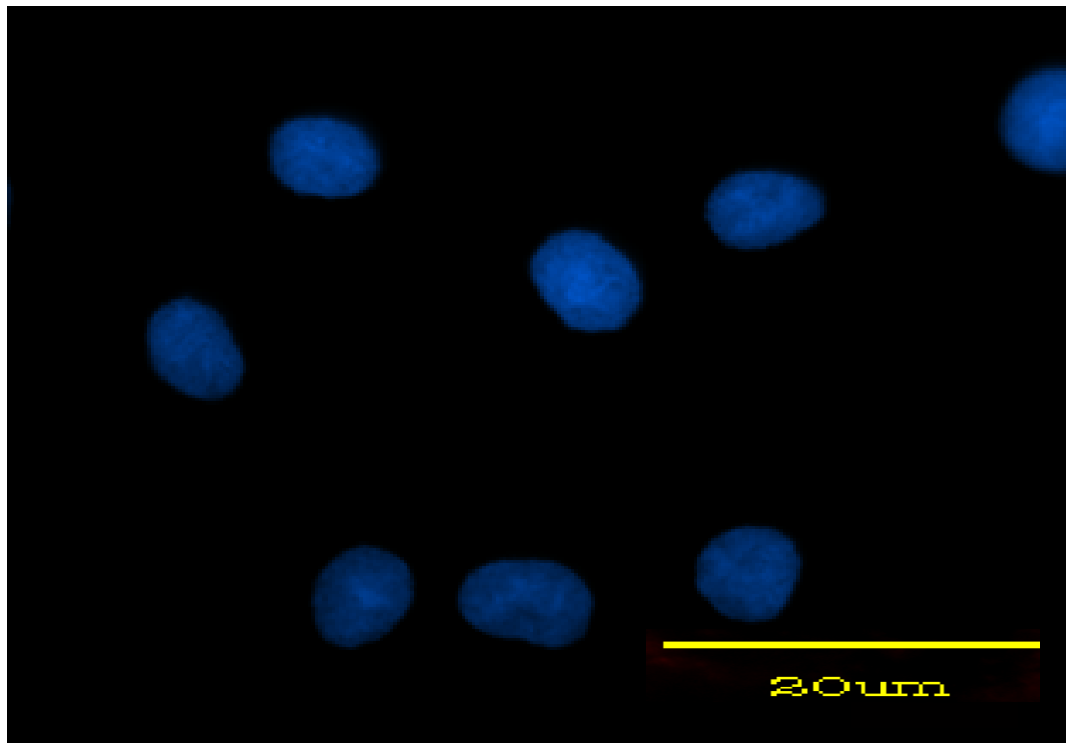


Figure 6-8: Fluorescence microscopy images of untreated C6 cells as control for both 0.1% Tween-PGA 40% C_{18} and PEG-PGA 40% C_{18} coated IONPs time-dependent metabolism studies. (Scale bar 20 μ m).

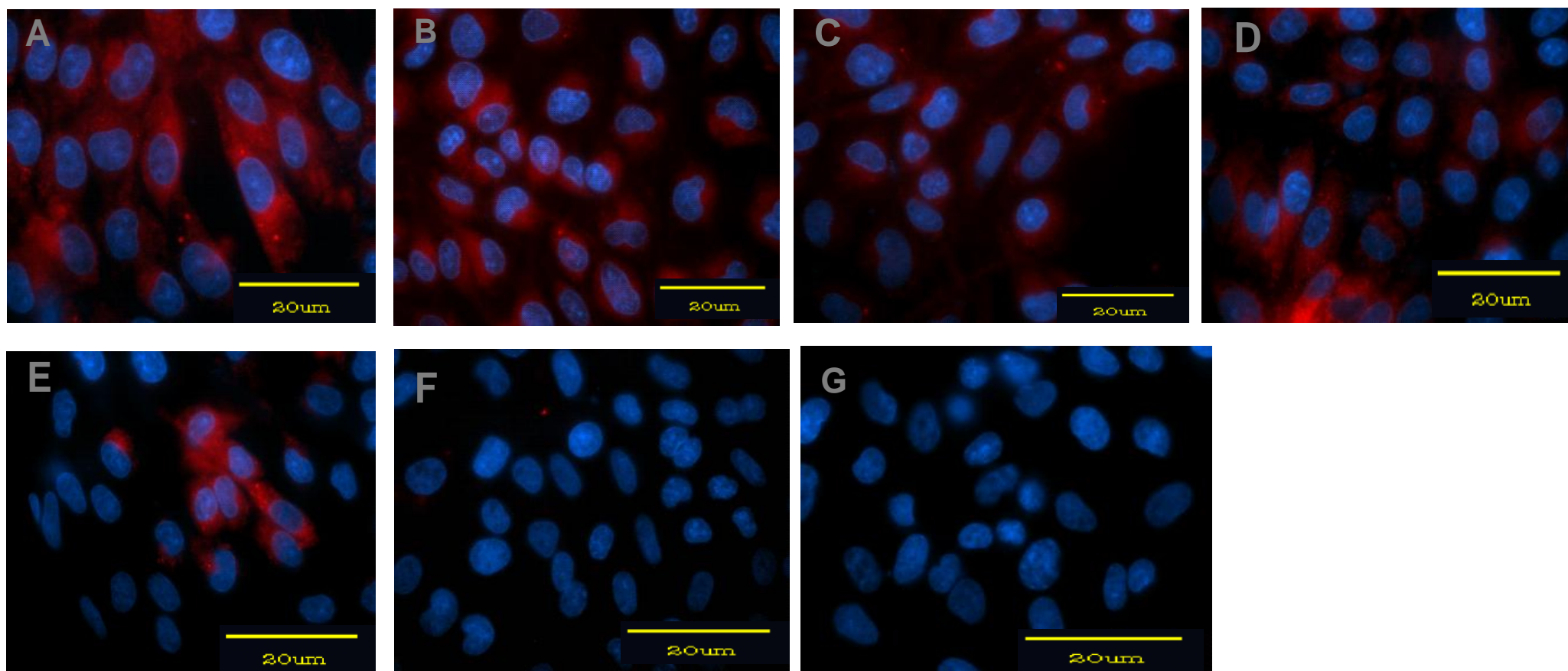


Figure 6-9 : Fluorescence microscopy images of PEG-PGA 40% C_{18} -IONPs incubated with C6 cells for different time periods. (A) 0.5 h, (B) 1 h, (C) 2 h, (D) 4h, (E) 6 h, (F) 12 h and (G) 24 h. (Scales bar 20 μ m).

6.3.4 Dose-dependent uptake of RBITC Labelled NPs by Monolayer using Confocal Fluorescence Microscope

6.3.4.1 0.1% Tween-PGA 40% C_{18} -IONPs

Confocal microscopy was employed to visualise the interaction of fluorescently labelled NPs within cells in RBITC labelled NPs uptake studies. Figure 6.10 shows confocal images of C6 cells incubated with different doses 0.1 ml, 0.5 and 1 ml of RBITC labelled PGA 40% C_{18} -IONPs for 2 h.

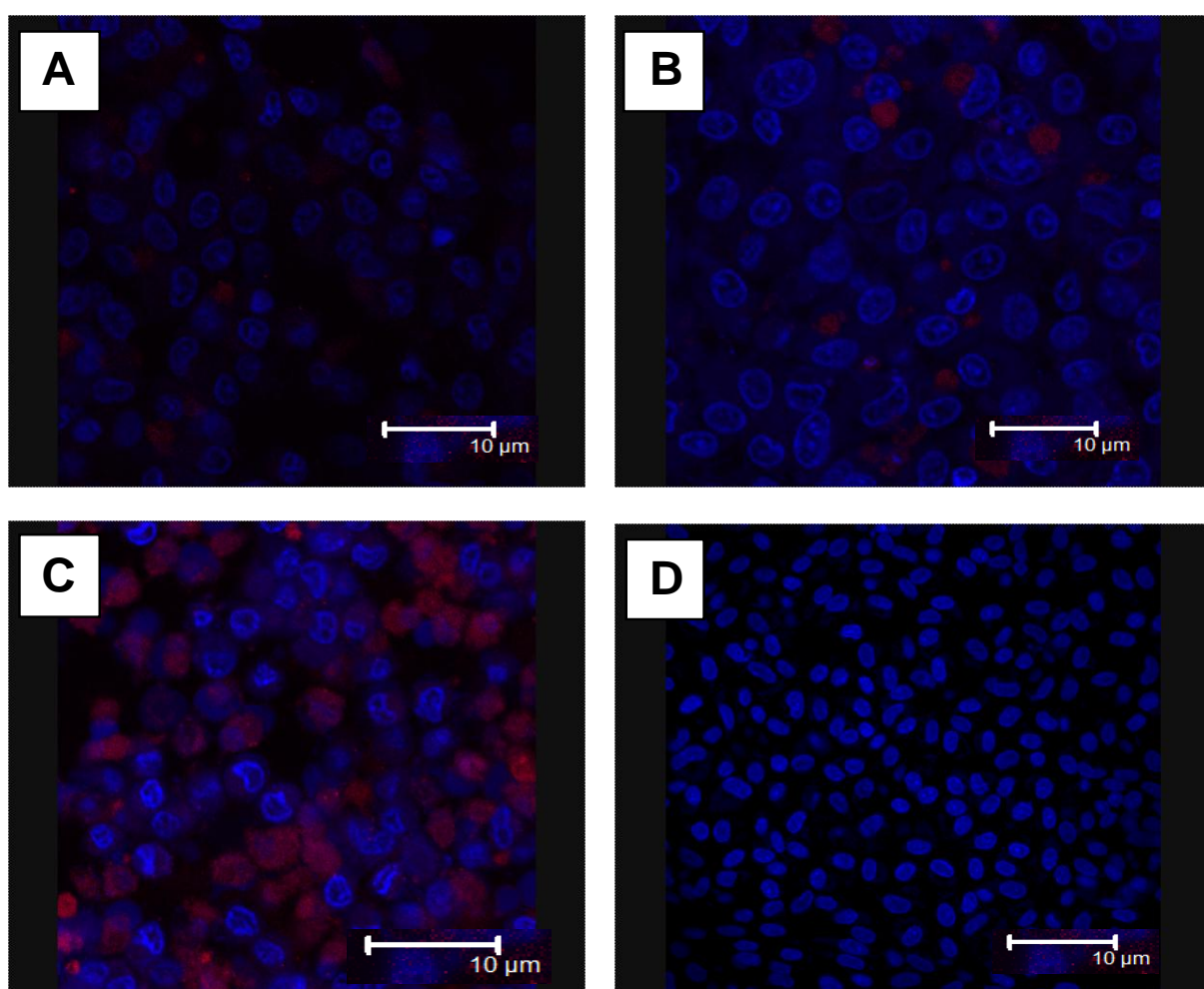


Figure 6-10 : Confocal laser micrograph of C6 cell monolayer incubated with 0.1 % Tween-PGA 40% C_{18} -IONP for 2 h. (A) 0.1 ml, (B) 0.5 ml, (C) 1 ml and (D) control. (Scales bar 10 µm).

The spherical bright red fluorescent spots could be observed in cytoplasm and in discrete areas surrounding the nucleus. It should be noted that, as the size of PGA 40% C_{18} -IONP are below 30 nm in diameter, fine PGA 40% C_{18} -IONP would appear very small under confocal microscopy. There are many small dots and some large red fluorescent spots representing large collections of PGA 40% C_{18} -IONP. The latter almost certainly indicate an intracellular location and the intercellular localisation increased with increasing doses. When comparing the three doses, uptake was visibly more extensive for the cells treated with 1ml rather than the 0.1 and 0.5 ml PGA 40% C_{18} -IONP suspension (Fig. 6.10a and b). In Figure 6.10c showing the 1.0 ml dose, there was extensive localisation of the PGA 40% C_{18} -IONP around the nucleus, but also in some cells some dark patches could be inside the nucleus indicating uptake into the nucleus itself. Figure 6.10d shows the control was clear, there were no dark patches, just the DAPI which stained nuclei.

6.3.4.2 PEG-PGA 40% C_{18} -IONPs

C6 cells were incubated with different doses also of PEG-PGA 40% C_{18} -IONPs and visualised using confocal microscopy (Fig. 6.11). In general, uptake with the PEG-PGA 40% C_{18} -IONPs appeared to be lower than the PGA 40% C_{18} -IONPs. PEG-PGA 40% C_{18} -IONPs uptake into the cytoplasm was only clear at the 0.2 ml dose with the nanoparticles distributed through the cytoplasm and around nuclei (Fig. 6.11a). At the highest 1.0 ml dose, some nuclei exhibited some significant dark areas and this may represent some PEG-PGA 40% C_{18} -IONPs uptake. The control sample showed just cells stained with DAPI in (Fig. 6.11d).

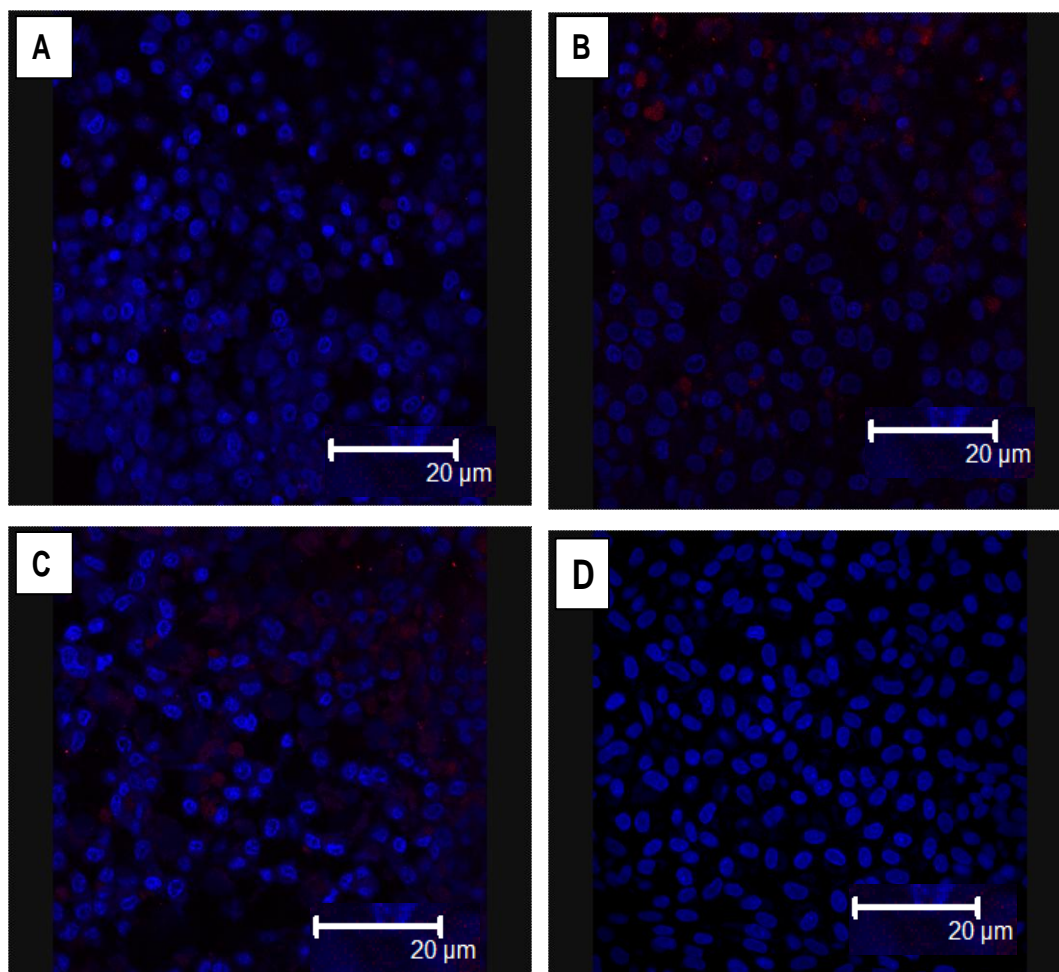


Figure 6-11: Confocal laser micrograph of C6 cell monolayer incubated with PEG-PGA 40% C_{18} -IONPs for 2 h. (A) 0.1 ml, (B) 0.5 ml, (C) 1 ml and (D) control without labelled PEG-PGA 40% C_{18} -IONPs. (Scales bar 20 μ m).

6.3.5 Metabolism and Redistribution of RBITC Labelled NPs by C6 Cell Monolayers using Confocal Fluorescence microscopy

The intracellular uptake of nanoparticles by cell was estimated by using different incubation times for the cells at 1 h, 4 h and 24 h using monolayer cells.

6.3.5.1 0.1% Tween–PGA 40% C_{18} –IONPs

Confocal microscope images showed that 0.1% Tween–PGA 40% C_{18} –IONPs were initially internalised into the cells and mainly stayed in the cytoplasm. The appearance of the cells was different each time and exhibited a strong dependence on the length of the observation period (Fig. 6.12). Images showed that huge numbers of nanoparticles were present in the cell at 1 h with a wide distribution in the cytoplasm and distributed around the nuclei. There were some small dark patches within the nuclei. By 4 h and 24 h (Figs. 6.12b and 6.12c) there was less fluorescence visible in the cytoplasm and the fluorescence present was more localised into one place in the cytoplasm. Also the DAPI was less visible in the nucleus, with the whole centre of nuclei appearing black suggesting nanoparticle uptake into the nucleus.

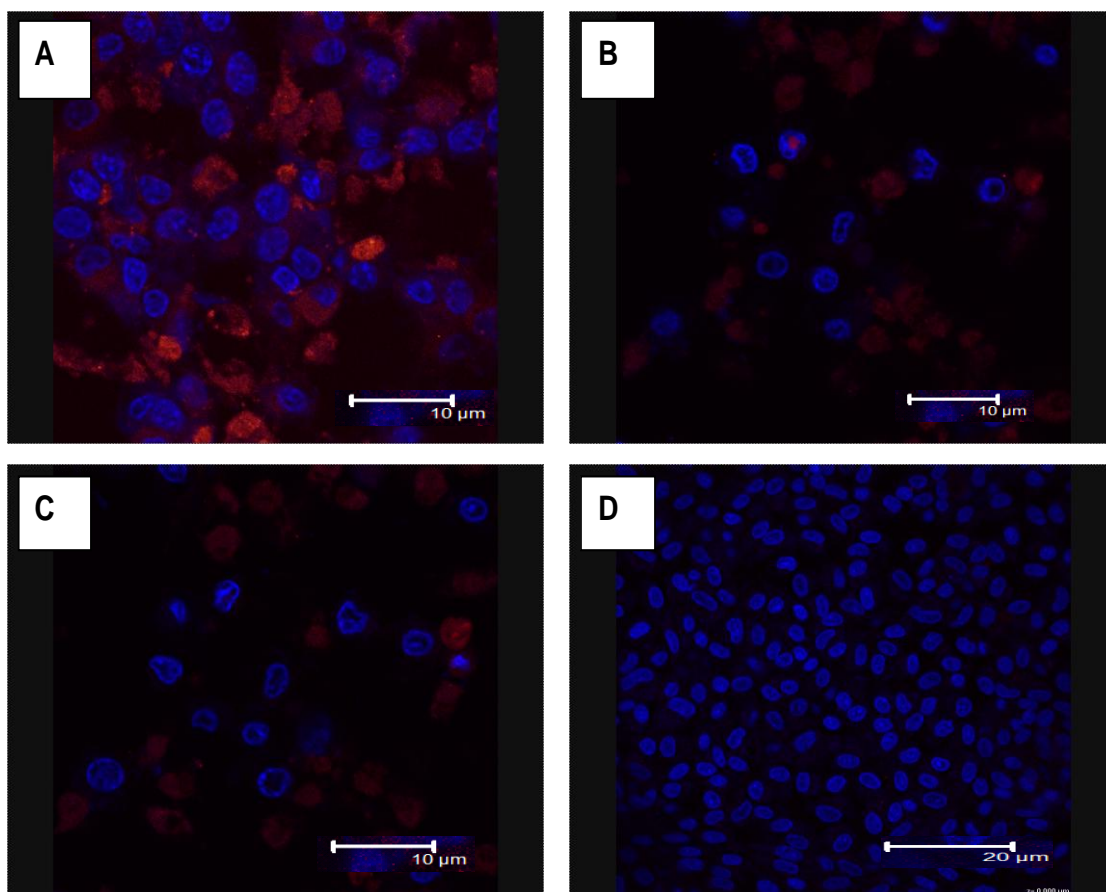


Figure 6-12: Confocal laser micrograph of C6 cell monolayer incubated with 0.1% Tween–PGA 40% C_{18} –IONPs for different time periods. (A) 1 h (Scale bar 10 μ m), (B) 4 h (Scale bar 10 μ m), (C) 24 h with (Scale bar 10 μ m) and (D) control with (Scale bar 20 μ m).

6.3.5.2 PEG–PGA 40% C_{18} –IONPs

The metabolism and redistribution of PEG–PGA 40% C_{18} –IONPs into C6 cells was monitored by confocal laser scanning microscopy Figure 6.13. The PEG–PGA 40% C_{18} –IONPs localisation was time-dependent. After 1 h of incubation, PEG–PGA 40% C_{18} –IONPs identified as many fluorescent spots, were observed on the periphery of the cells (Fig. 6.13a).

Figure 6.13b shows the image obtained by the second period of 4 h. It can be observed from this Figure that the fluorescence of PEG–PGA 40% C_{18} –IONPs are closely located around the nuclei in very small, evenly distributed and punctate patches of fluorescence. Also seen were dark spots and fine particles in nuclei which are likely to be nanoparticles. It was evident that many more particles had entered the nuclei and on the periphery by the cells after 24 h incubation (Fig.6.13c) than after 1 h and 4 h because of the extended exposure time.

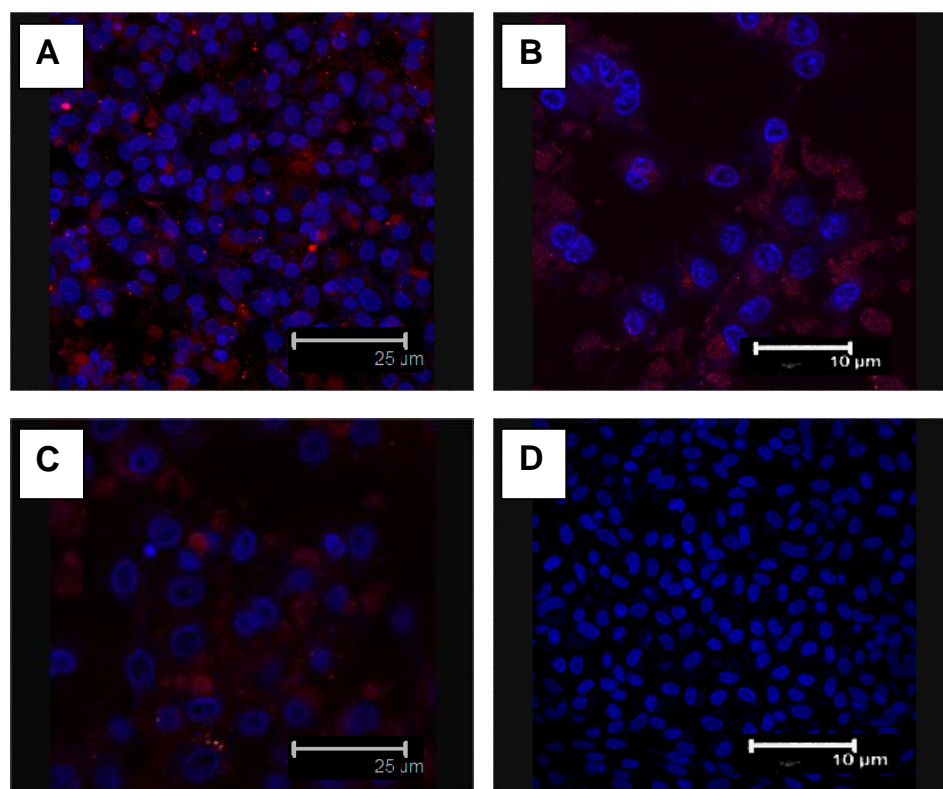


Figure 6-13: Confocal laser micrograph of C6 cell monolayer incubated with PEG–PGA 40% C_{18} –IONPs for different time periods. (A) 1 h (Scale bar 25 μm), (B) 4 h (Scale bar 10 μm), (C) 24 h (Scale bar 25 μm) and (D) control (scale bar 10 μm).

6.3.6 Uptake of RBITC Labelled NPs by C6 Cells Cultured as a Spherical Aggregate using Confocal microscopy

After harvesting C6 monolayer cells, cell suspensions were seeded at 1×10^6 cells/ml in rotation culture. In this culture the cells formed spherical aggregates within 24 h. To visualise aggregates under the confocal microscope, aggregates were transferred into a 24-well plate with PDL-coated coverslips after 1 day of culture by the rotation method, and then cultured for 24 h in a 24-well plate (Fig. 6.14 a, b). As can be seen, the aggregates were well formed and individual cells could still be distinguished in the periphery of the aggregates. C6 aggregates appeared larger in size and denser with less translucence under a light microscope. The mean diameter of the aggregates was 150 μm . Some cells on the edge of the aggregate grew onto the coverslip, in which the shape of single cells could be clearly seen (Fig. 6.14b), and cells in the middle of the aggregate stayed within the spheroid shape.

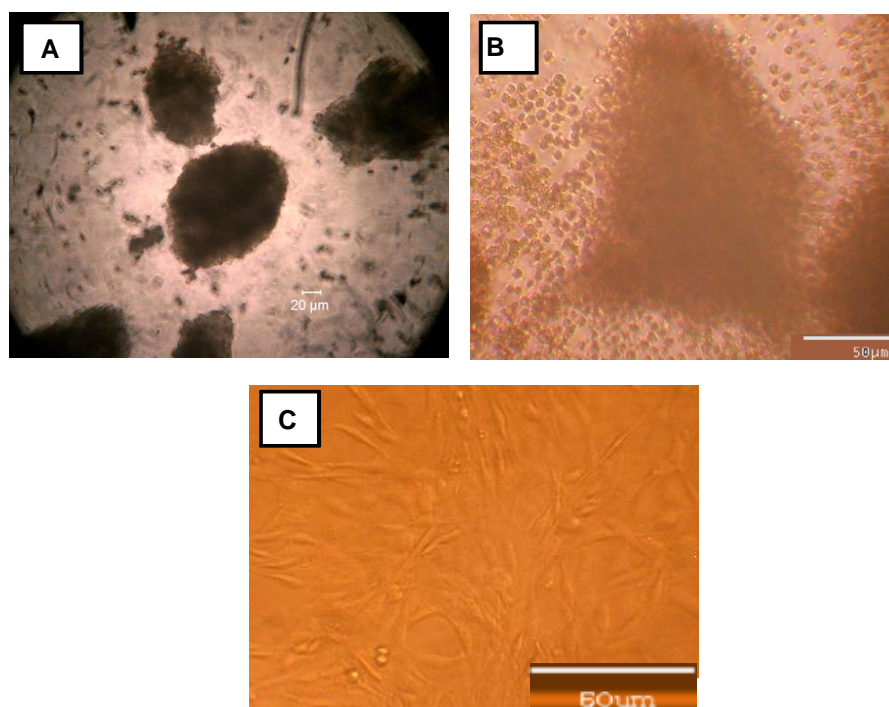


Figure 6-14 : Phase-contrast micrographs illustrating the aggregates formed by the rotation method and C6 monolayer cells. (A) and (B) a phase-contrast micrographs showing C6 cells in aggregates formed from (C) using rotation method (Scale bars 20 μm and 50 μm); (C) a phase-contrast micrograph illustrating C6 cells in monolayer culture (Scale bar 50 μm).

6.3.7 Time-dependent Uptake of RBITC Labelled NPs by C6 cell Aggregates Using Confocal Fluorescence microscope

6.3.7.1 0.1% Tween–PGA 40% C_{18} –IONPs

Confocal fluorescence micrographs (Fig. 6.15) show cell aggregates incubated with 1 ml of 0.1 % Tween–PGA 40% C_{18} –IONPs. The micrographs, which were taken from the middle of aggregates (Fig. 6.15a, b and c), and (Fig. 6.16 a1, b1 and c1) revealed the influence of the increasing diffusion distance of NPs on intracellular fluorescence intensity and the fluorescence activity in the different parts of the C6 through a series of z-sections of the C6 cells. In the first hour of incubation time, the intensity of fluorescence in the periphery of aggregates was high (Fig. 6.15a,) and the nanoparticles penetrated at least 15 micrometres into the aggregates. With increased incubation time, the intensity of fluorescence in the centre of aggregates was increased. Compared with 4 h and 24 h incubation time, it was found that the difference in intracellular fluorescence intensity between them in the periphery of the aggregates and in the centre of the aggregates was greater as shown in (Fig. 6.15b and c). Also the images gallery (Fig. 6.16 a1, b1 and c1) showed the level of the uptake in all the doses, whereas in 0.1 ml showed a low level while the other doses showed the penetration of the nanoparticles throughout the layers of the aggregates. The fluorescence intensity level was much higher after 24 h incubation time than either 1 h or 4 h. The control sample clearly showed no fluorescence when cells were incubated without any labelled NPs (Fig. 6.15d). Compared with the images of monolayer by confocal (Fig. 6.12), it was found that there was a large increase in intracellular fluorescence intensity in the aggregates compared to the monolayer experiments. The galleries of pictures show the fluorescence in different slices through the spheroids etc.

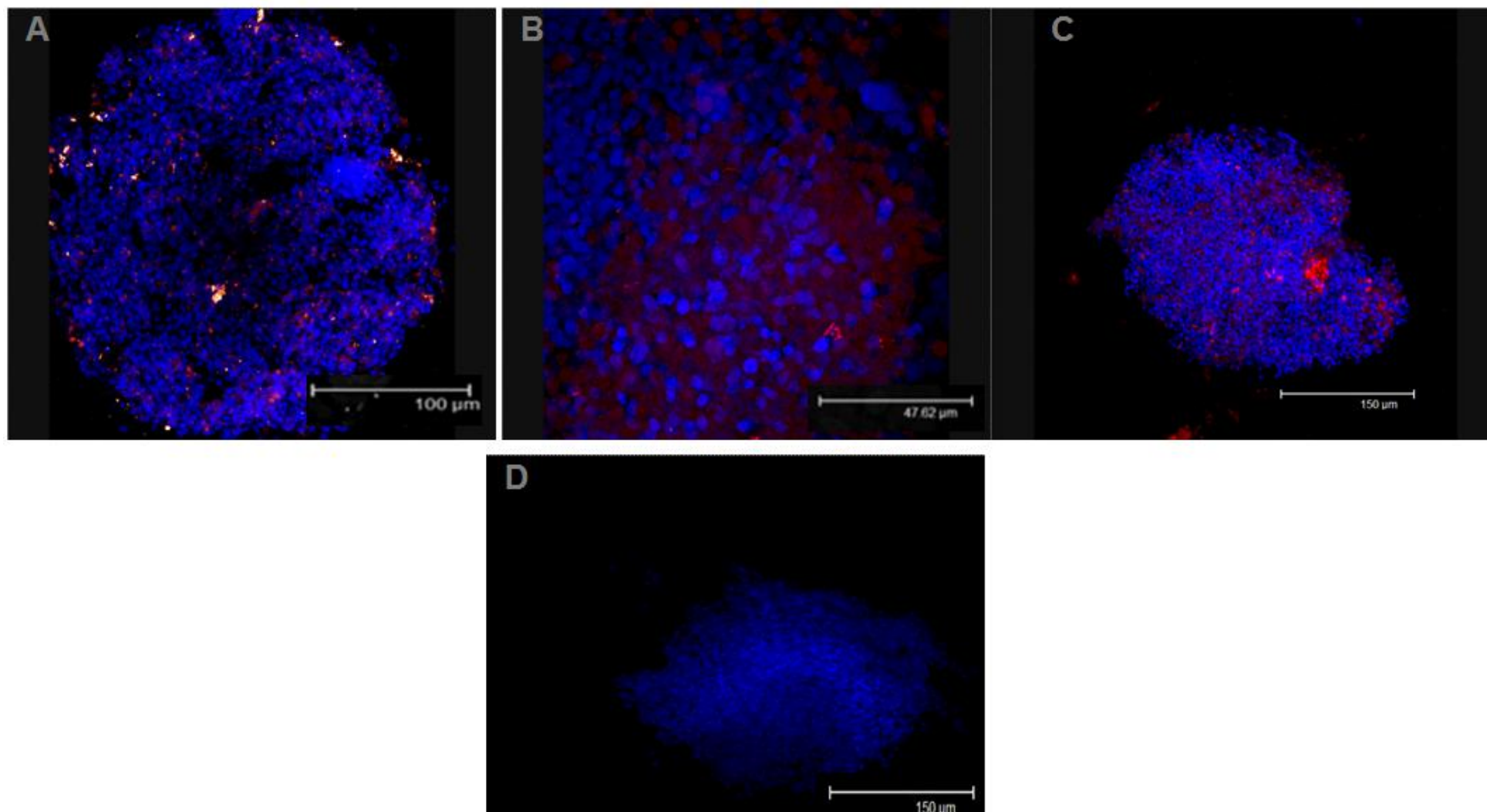
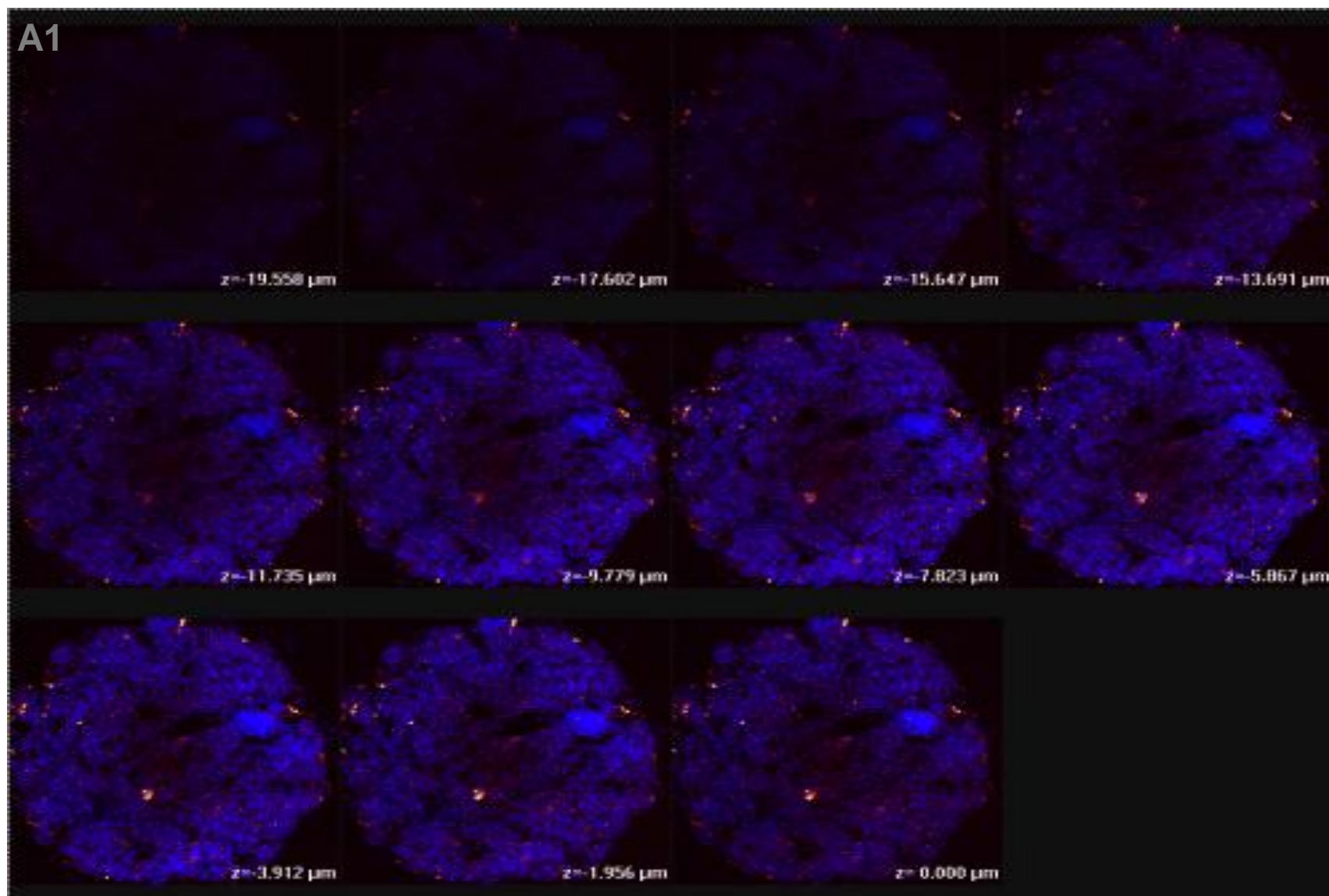
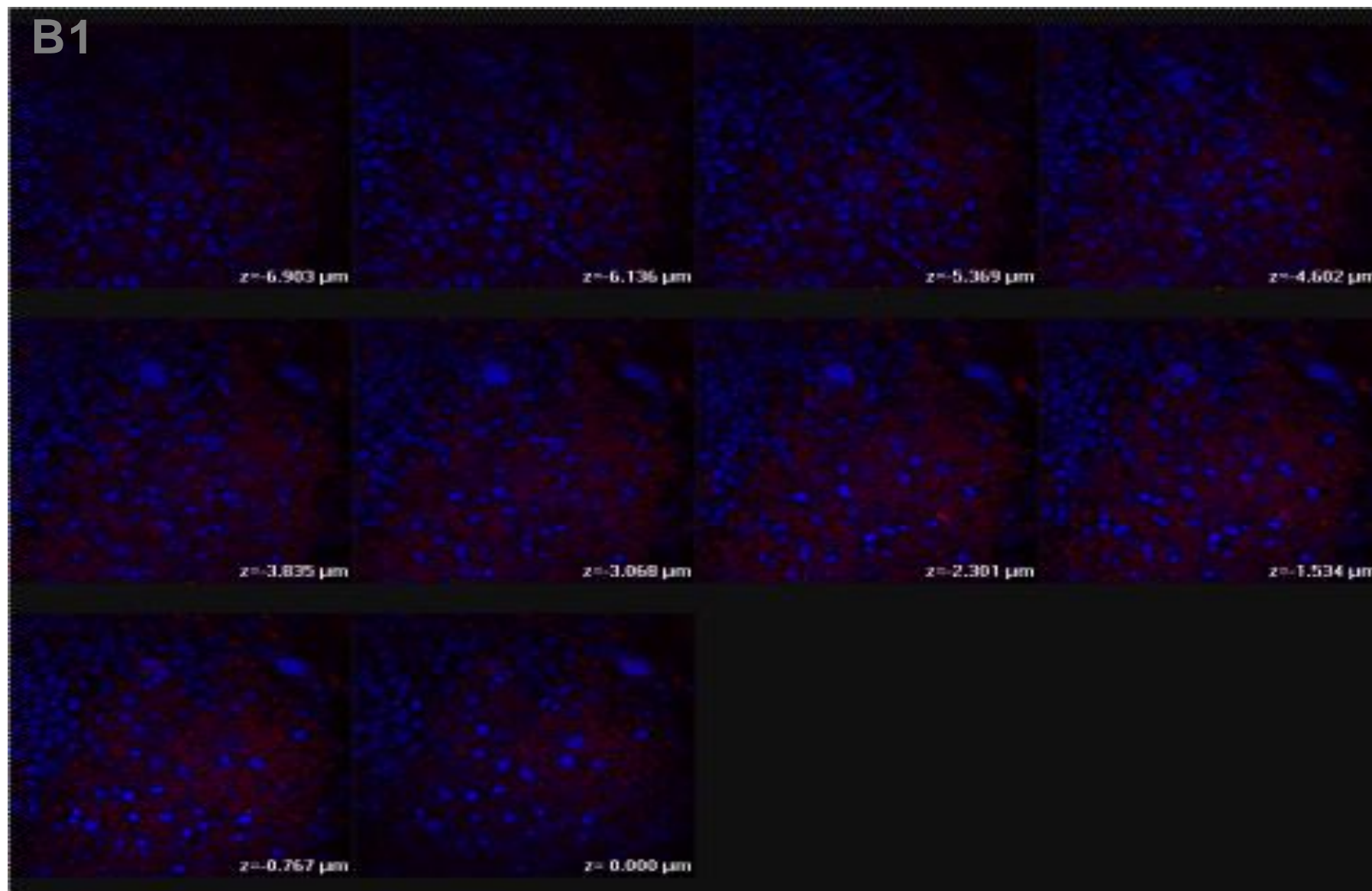


Figure 6-15 : Confocal fluorescence microscopy images of 0.1 % Tween–PGA 40% C_{18} –IONPs incubated with C6 cells aggregates for different time periods. (A) 1 h (Scale bar 100 μm), (B) 4 h (Scale bars 47.2 μm), (C) 24 h (Scale bar 150 μm) and (D) control (Scale bars 150 μm).





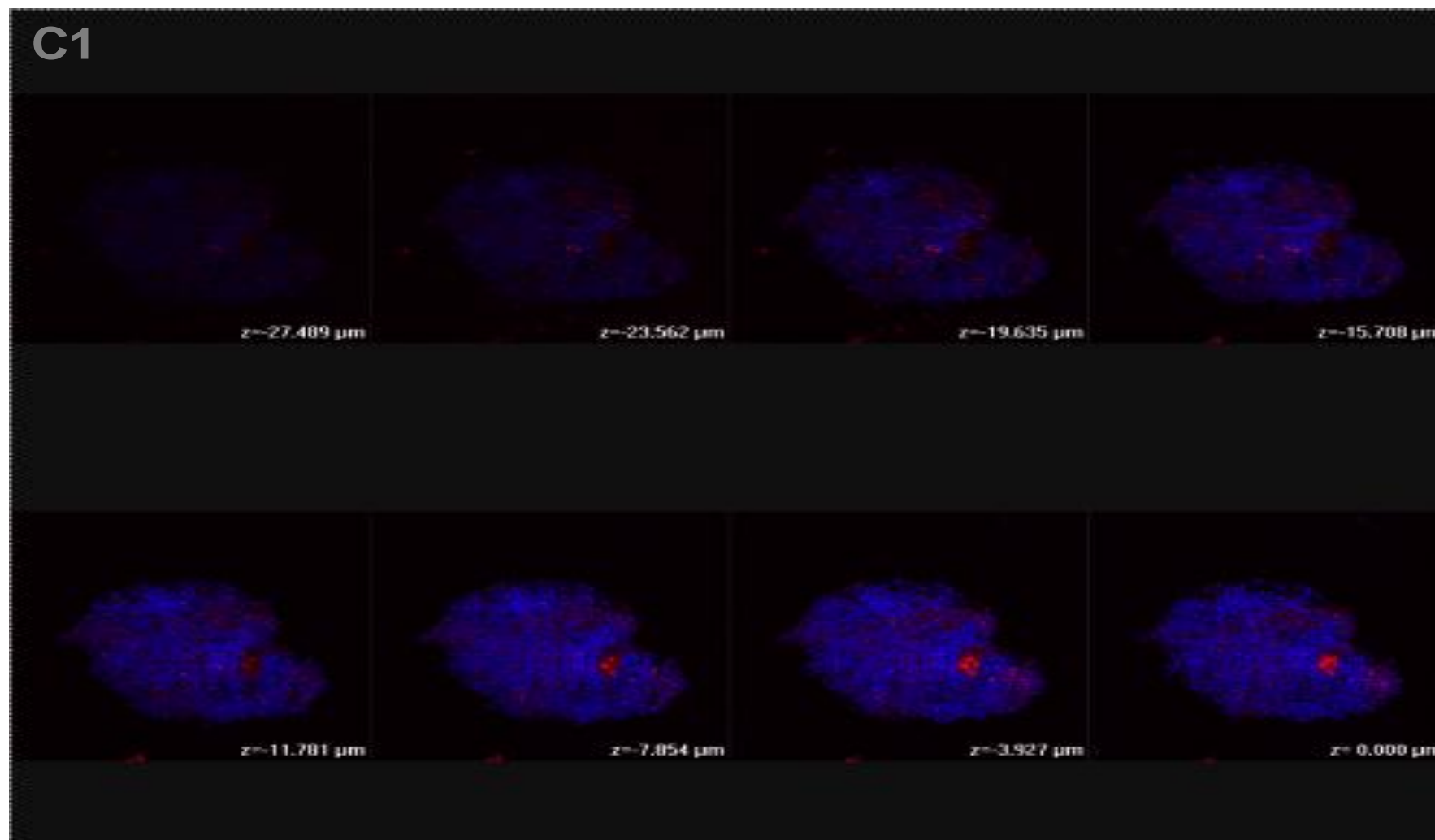


Figure 6-16 : Confocal fluorescence microscopy images gallery of 0.1 % Tween-PGA 40% C_{18} - IONPs incubated with C6 cells aggregates for different time periods. 1 h (A1), 4 h (B1) and 24 h (C1); each section is 1.956 μm thick for A1, 0.767 μm thick for B1 and 3.927 μm thick for C1 illustrates the fluorescence activity in all the sections of the cells.

6.3.7.2 PEG–PGA 40% C_{18} –IONPs

In order to analyse the cellular and subcellular localisation of the particles, confocal fluorescence microscopy was performed.

The images of C6 cell aggregates incubated with PEG–PGA 40% C_{18} –IONPs for different times of 1 h, 4 h and 24 h showed that all PEG–PGA 40% C_{18} –IONPs were located intracellularly (Fig. 6.17). In the first 1 h, we observed intracellular uptake (red clusters inside of cells) (Fig. 6.17a). Also the gallery showed the fluorescence in the centre of the aggregate and the stages of the uptake level. For 4 h particles showed an increase in the number of particles that were taken up (Fig. 6.17b). In the case of 24 h incubation time (Fig. 6.17c) there is a large increase in uptake of particles with more particles in cells, some of them completely stuffed full of PEG–PGA 40% C_{18} –IONPs.

The gallery of confocal fluorescence microscopy images (Fig.6.18 c1) showed that most of the red fluorescence can be seen in the middle of the spontaneously formed aggregates. It was found that the red fluorescence intensity in some areas was higher than that of other areas. The gallery of confocal fluorescence microscopy images (Fig.6.18) showed that most PEG–PGA 40% C_{18} –IONPs were localised in the middle of the aggregates and many PEG–PGA 40% C_{18} –IONPs penetrate through the whole of the aggregates after 24 h incubation time.

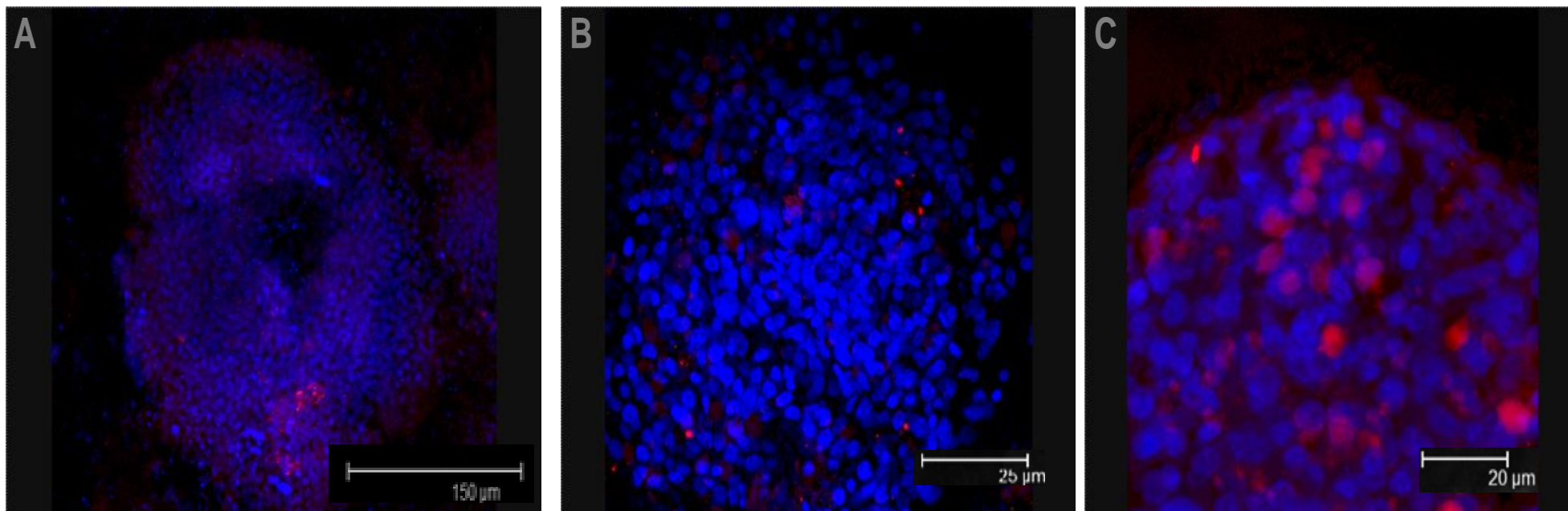
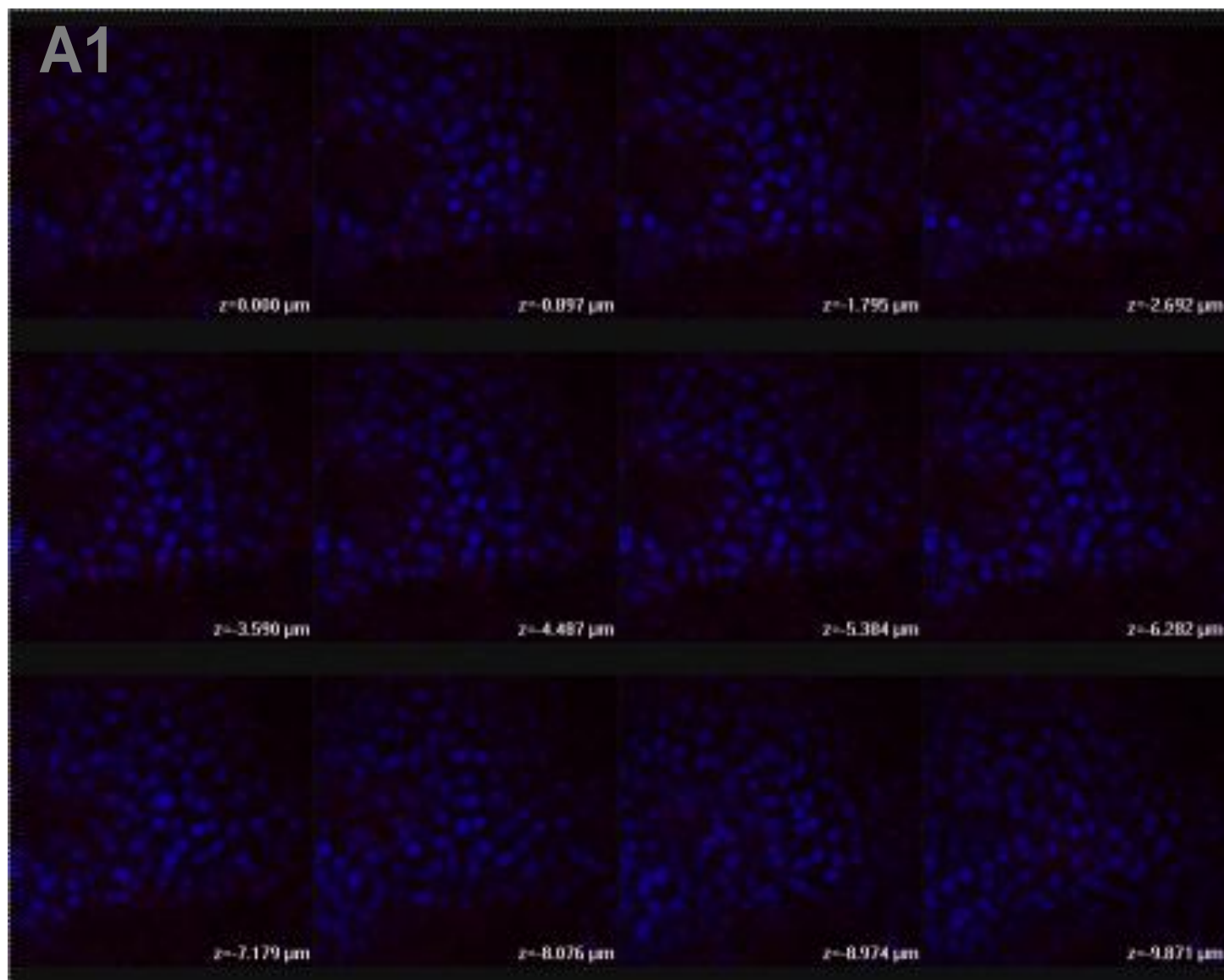
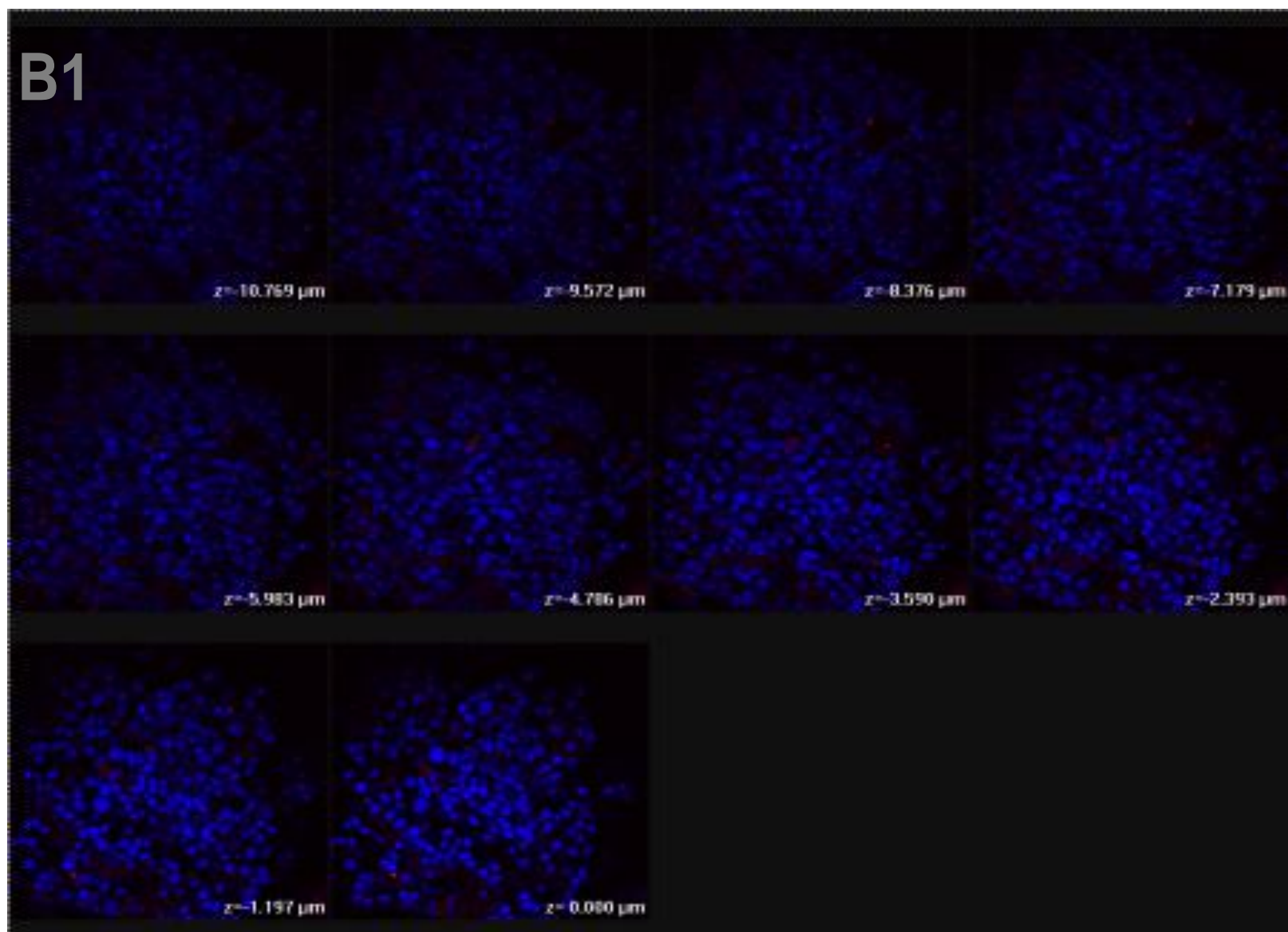


Figure 6-17: Confocal fluorescence microscopy images of PEG-PGA 40% C_{18} -IONPs incubated with C6 cells aggregates for different time periods. (A) 1 h (Scale bar 150 μm), (B) 4 h (Scale bar 25 μm) and (C) 24 h (Scale bar 20 μm).





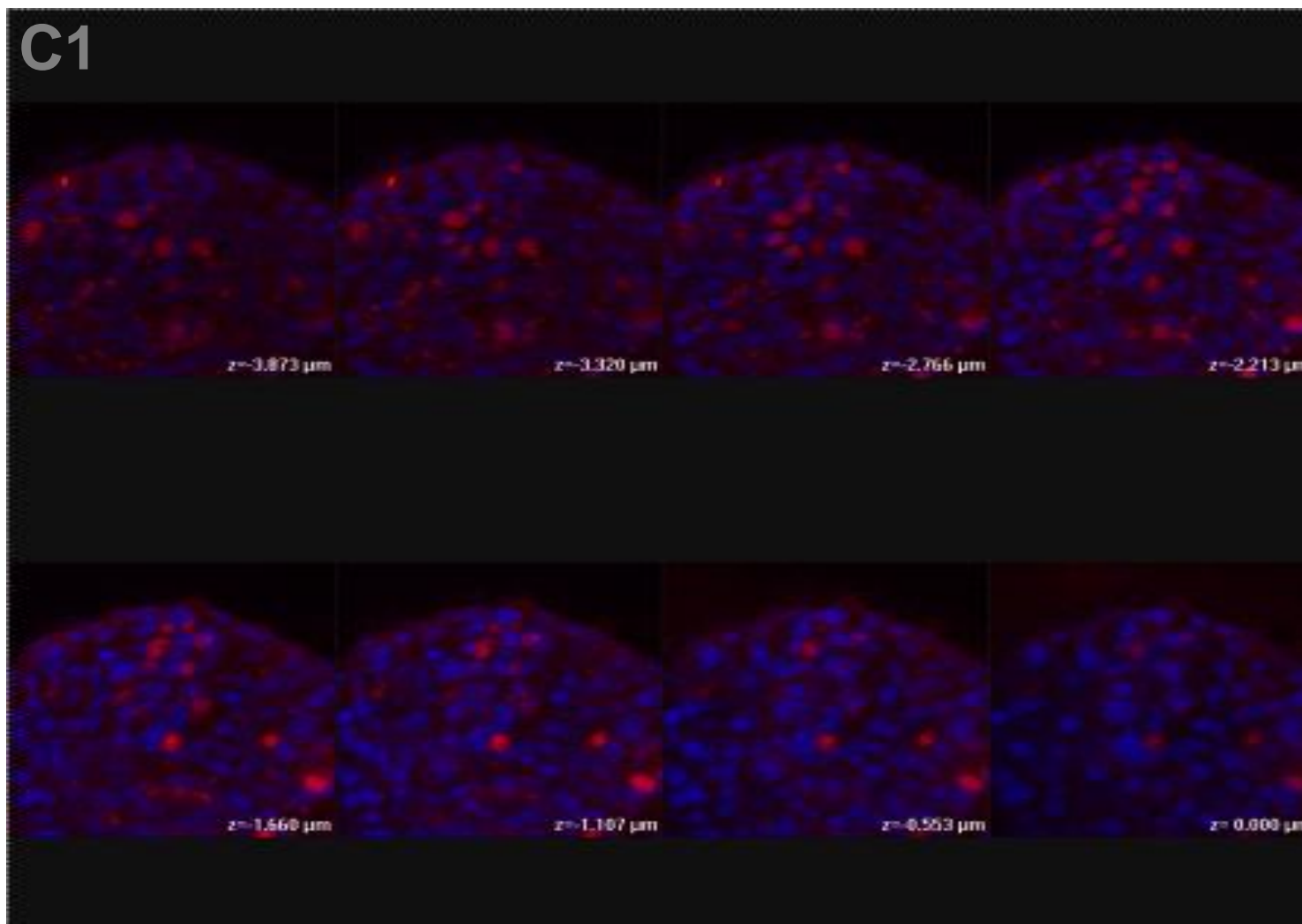


Figure 6-18: Confocal fluorescence microscopy images gallery of PEG-PGA 40% C_{18} -IONPs incubated with C6 cells aggregates for different time periods. (A1) 1 h, (B1) 4 h and (C1) 24 h; each section is $0.897 \mu\text{m}$ thick for A1, $1.197 \mu\text{m}$ thick for B1 and $0.553 \mu\text{m}$ thick for C1 illustrates the fluorescence activity in all the sections of the cells.

6.3.8 cytometry Investigation of Uptake of RBITC Labelled NPs by C6 Monolayer cell cultures.

6.3.8.1 Dose-dependent uptake of RBITC labelled PGA 40% C_{18} -IONPs and PEG-PGA 40% C_{18} -IONPs by cells

Quantitative evaluation of cellular uptake of fluorescently labelled NPs was performed using flow cytometry. Flow cytometry is a means of measuring certain physical and chemical characteristics of cells or particles as they travel in suspension one by one past a laser beam. Thus flow cytometry can measure the fluorescence intensity of every single cell or particle. As shown in (Figure 6.19), the cellular level of mean fluorescence intensity (MFI) progressively increased with doses of RBITC labelled NPs for both PGA 40% C_{18} -IONPs and PEG-PGA 40% C_{18} -IONPs. Uptake of the PGA 40% C_{18} -IONPs appeared lower than uptake for the PEG-PGA 40% C_{18} -IONPs, but the difference was not statistically significant. While uptake had started to plateau due to the addition of 1 ml of particles, saturation had not yet been achieved using either coating. This result reflects the result of the labelled NPs in fluorescence microscopy.

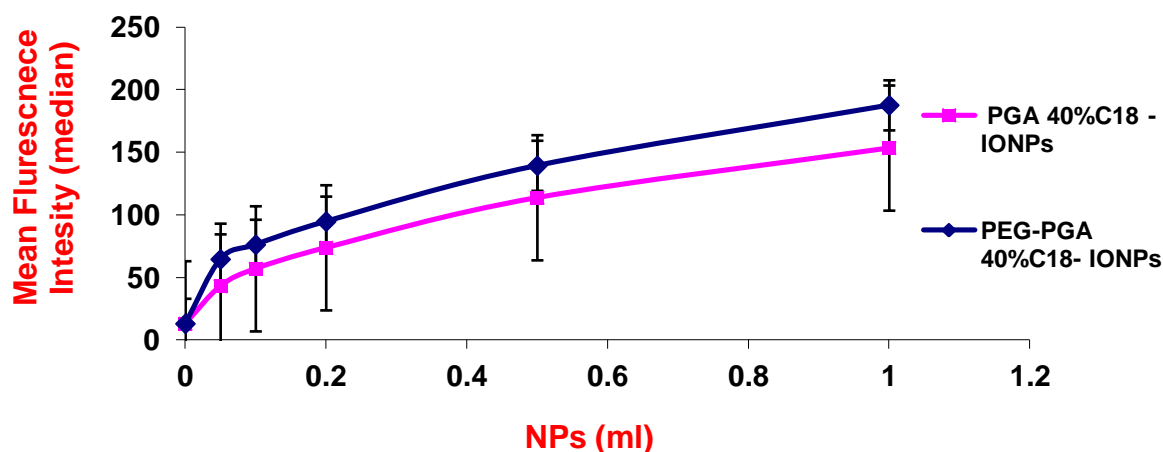


Figure 6-19: RBITC labelled PGA 40%C₁₈-IONPs and PEG-PGA 40%C₁₈-IONPs taken up by C6 cells monolayer depended on dose using flow cytometry.

6.3.8.2 Time-dependent uptake of RBITC labelled PGA 40%C₁₈-IONPs and PEG-PGA 40%C₁₈-IONPs by cells

Briefly, cells were incubated with nanoparticle suspensions in tubes for different time periods of 1, 4 and 24 h, then cells were washed three times with PBS, they were fixed in 4% fresh prepared paraformaldehyde (PFA) and the last washing of PFA was just prior to measurement using flow cytometry.

Figure 6.20 shows that the uptake of both RBITC labelled PGA 40%C₁₈-IONPs and PEG-PGA 40%C₁₈-IONPs were also dependent on the incubation time. Studies of flow cytometry in cells show the MFI increased sharply within 1h of incubation time and then increased gradually. In this assay the rate of uptake of PEG-PGA 40%C₁₈-IONPs was greater than that of the PGA 40%C₁₈-IONPs (statistical significance $P < 0.049$ by Student *t*-test). This was particularly apparent over longer time periods when further uptake of PGA 40%C₁₈-IONPs had virtually stopped increasing, but the PEG-PGA 40%C₁₈-IONPs continued to accumulate.

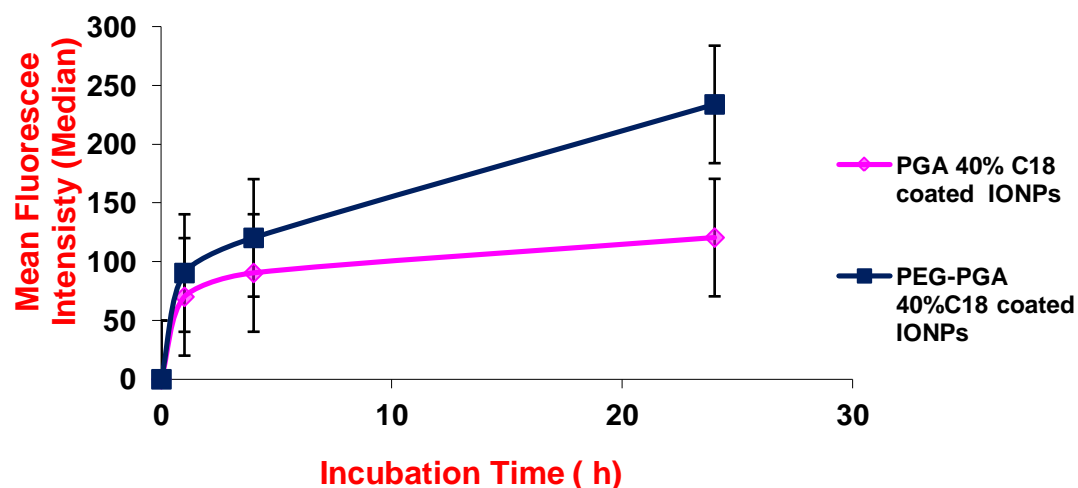


Figure 6-20 : Time-dependent uptake of RBITC labelled PGA 40% C_{18} -IONPs and PEG-PGA 40% C_{18} -IONPs by cells in monolayer culture using flow cytometry.

6.3.8.3 Time-dependent uptake of RBITC labelled PGA 40% C_{18} -IONPs and PEG-PGA 40% C_{18} -IONPs by C6 cells using flow cytometry studies to investigate retention of RBITC labelled nanoparticles within C6 cells

Briefly, cells were incubated with NPs suspension for 2 h, washed and incubated in new culture medium with serum for up to 24 h, and then were measured by using flow cytometry.

Flow cytometry studies showed a decrease in MFI with an increased incubation time (Fig. 6.21). Decrease in cellular fluorescence levels with long incubation time confirmed the pattern seen in the fluorescence microscopy studies. The percentage of cells that internalised RBITC-labelled NPs and their fluorescence intensity were quantified by flow cytometry. As shown in (Fig. 6.21), the fluorescence intensity of the cells was found to continuously decrease over the time up to 24 h. A similar rate of loss of fluorescence was seen for both PEG-PGA 40% C_{18} -IONPs and PGA 40% C_{18} -IONPs.

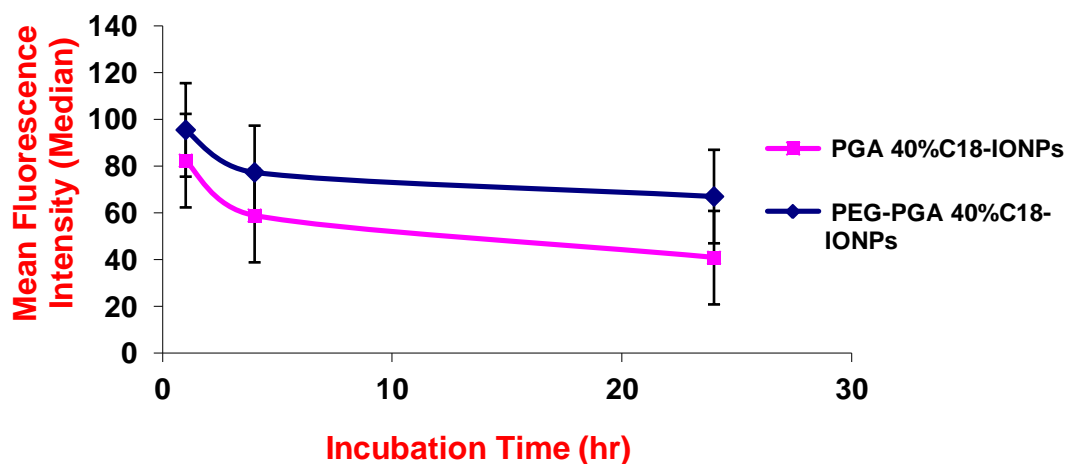


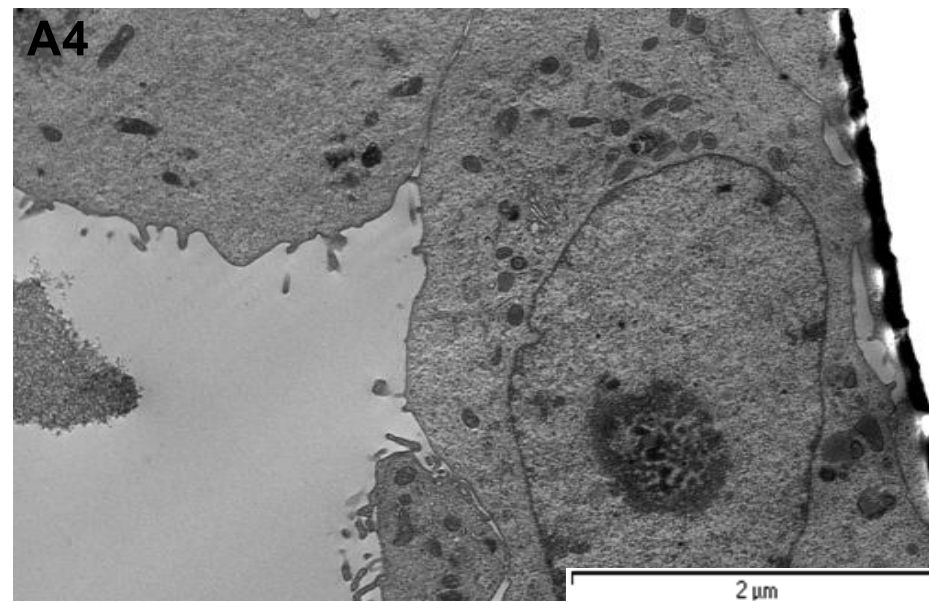
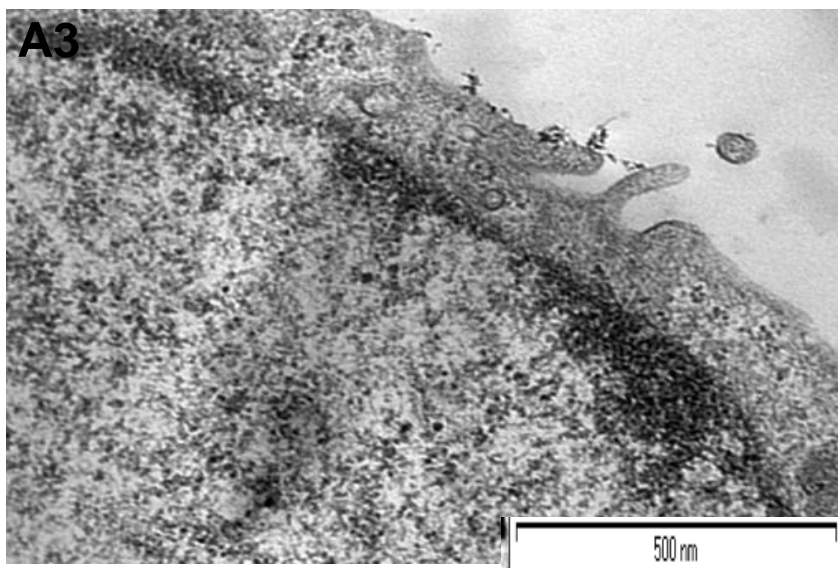
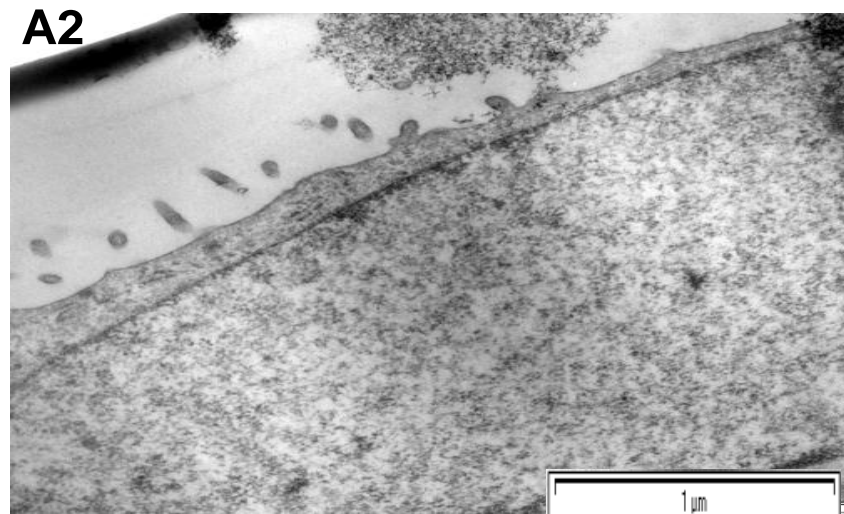
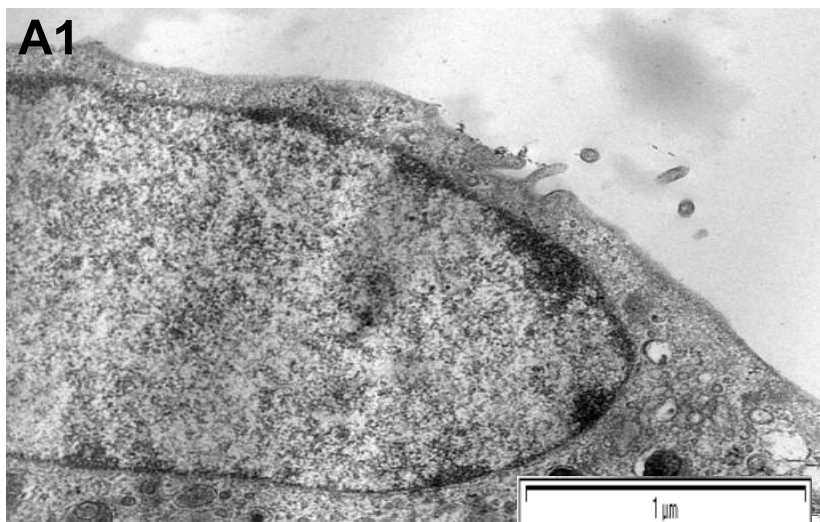
Figure 6-21 : Retention study of RBITC labelled PGA 40%C₁₈-IONPs and PEG-PGA 40%C₁₈-IONPs within C6 cells using flow cytometry.

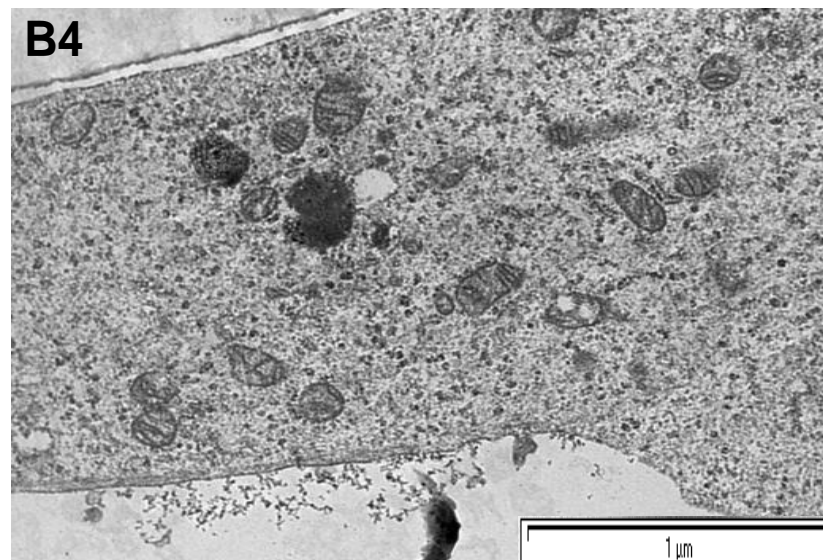
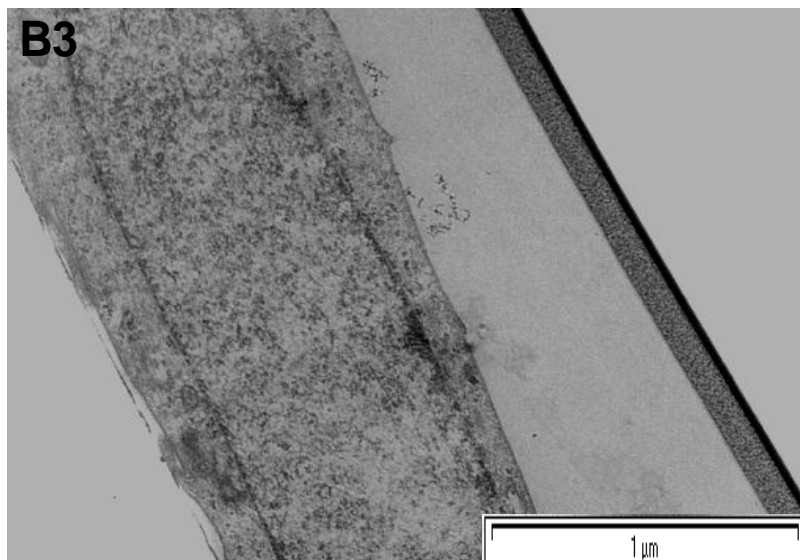
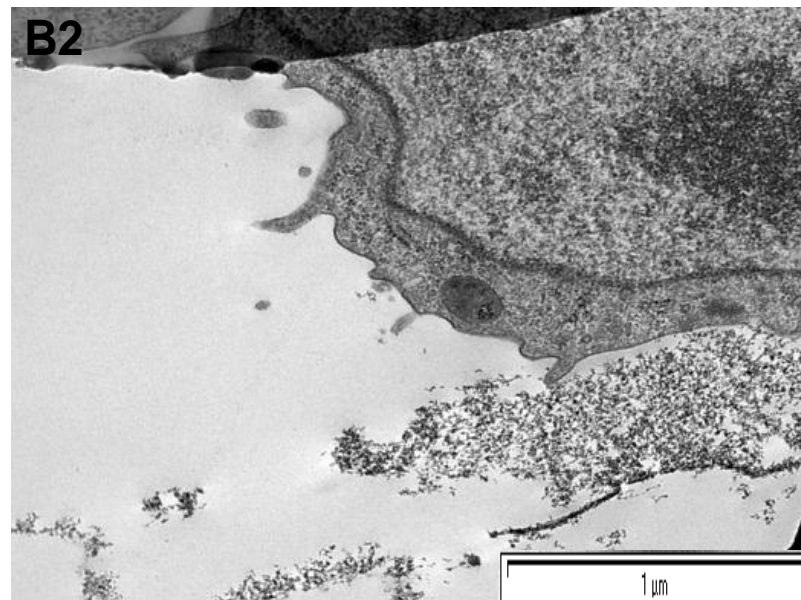
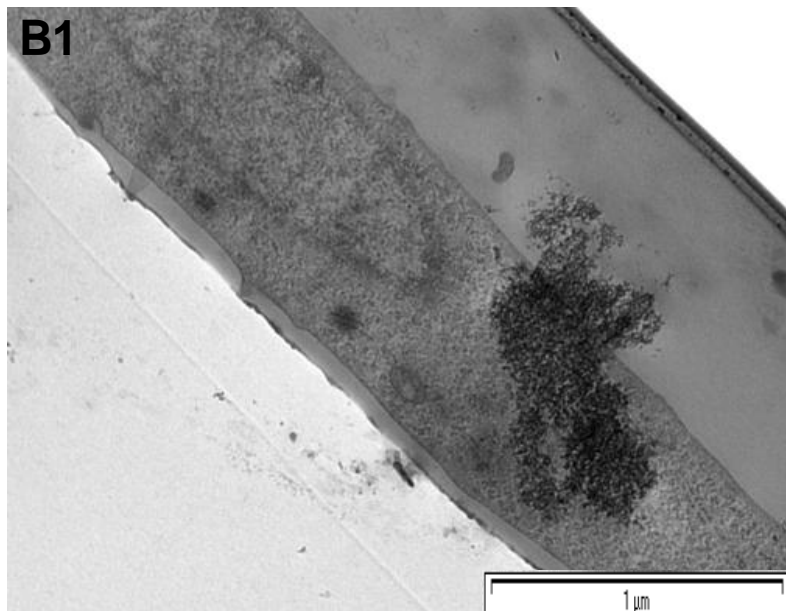
6.3.9 Localisation NPs in C6 cells using TEM

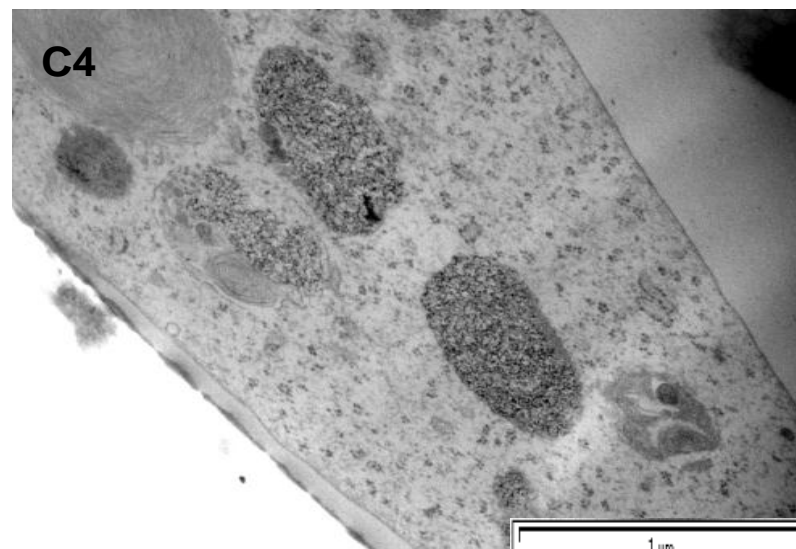
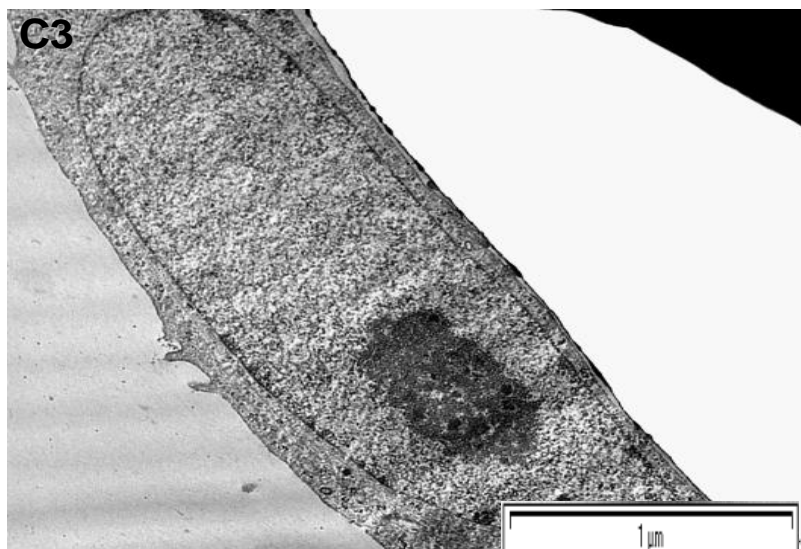
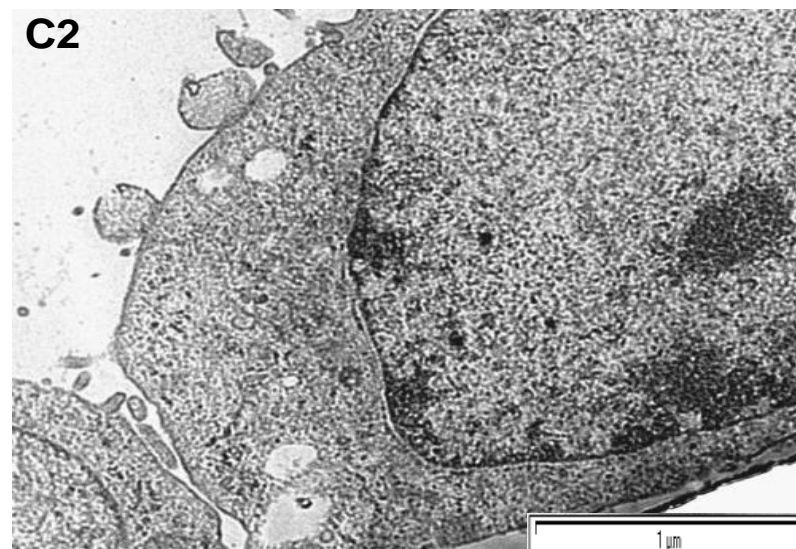
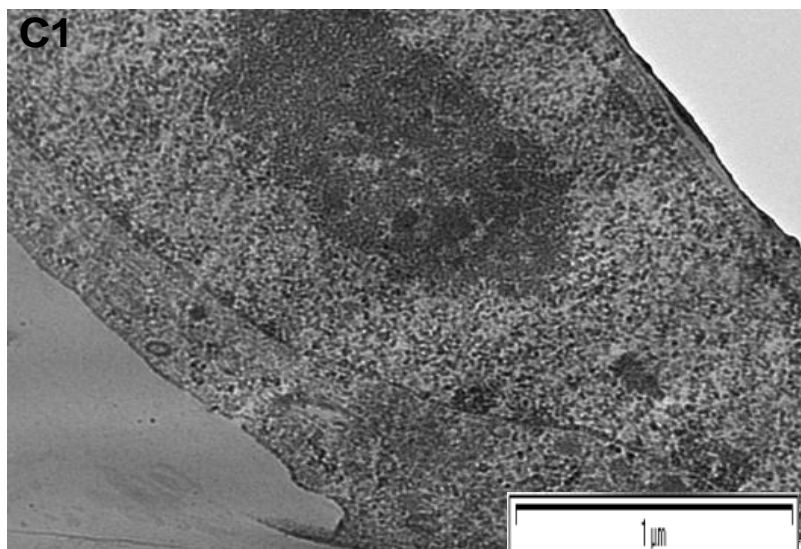
6.3.9.1 Time-dependence uptake of PGA 40%C₁₈-IONPs by C6 cells and localisation in cells using TEM

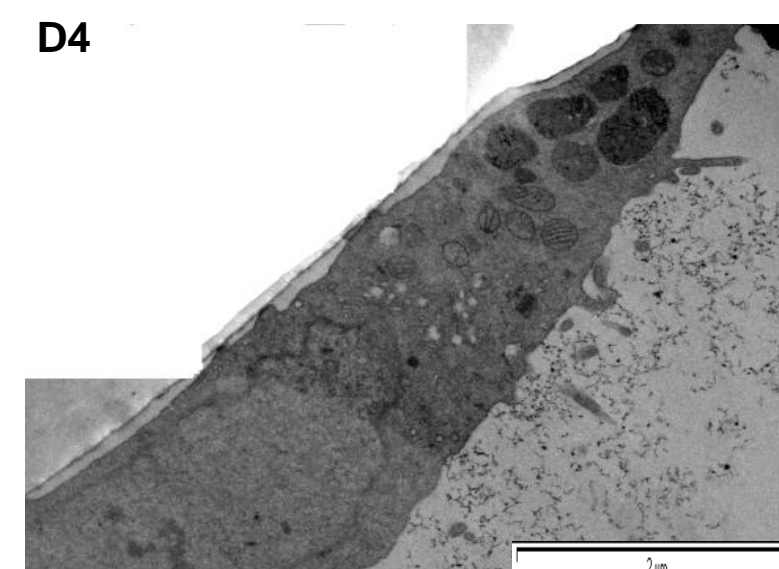
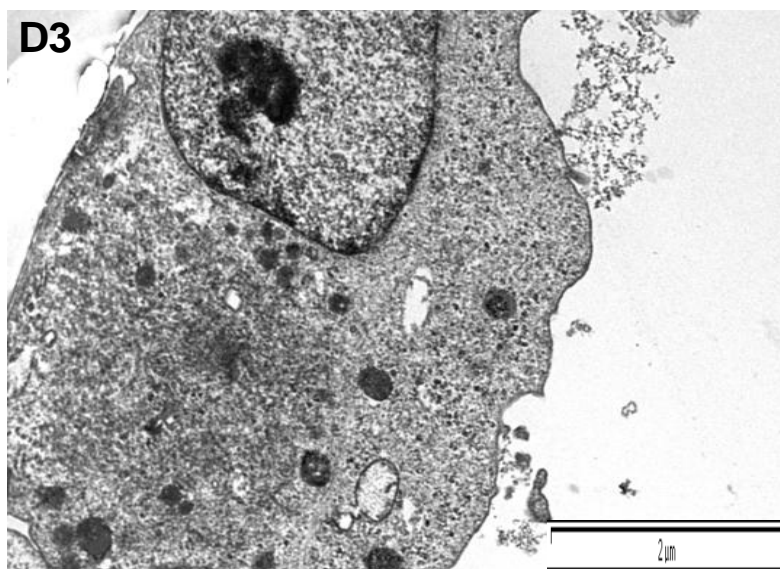
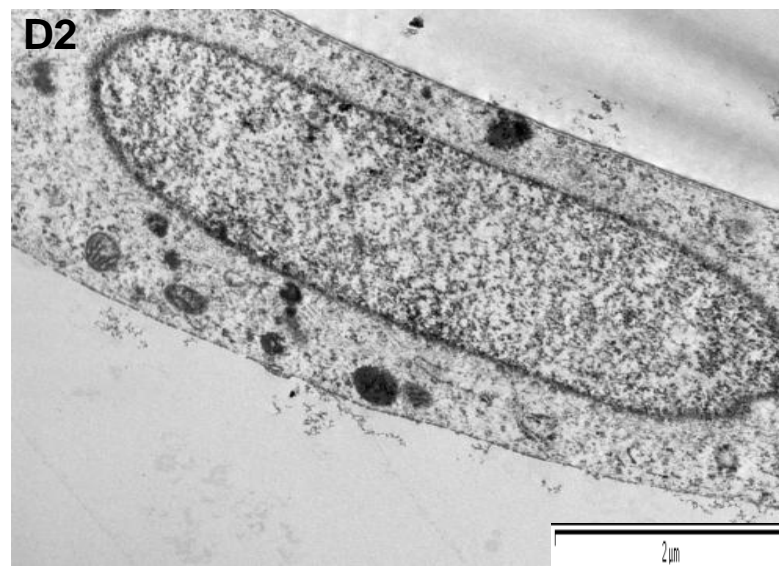
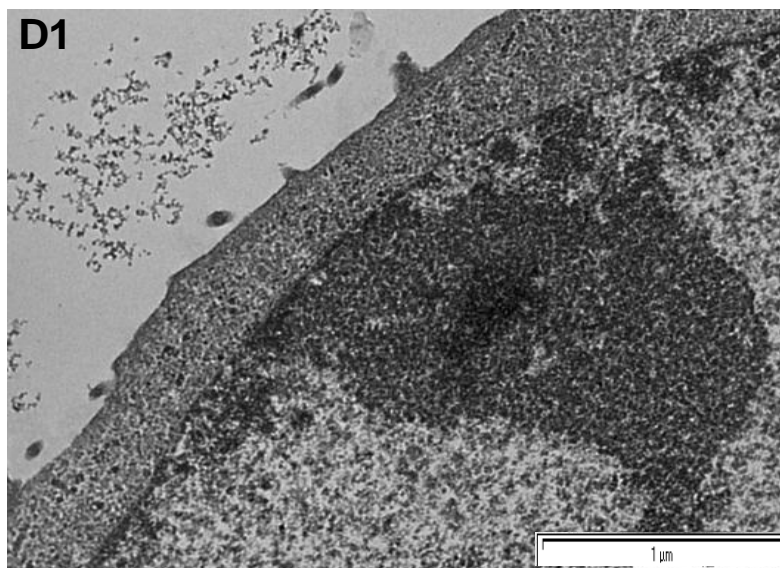
TEM was utilised to determine the sub-cellular localisation of coated IONPs in C6 cells. A cumulative experimental protocol was used where cells were incubated with nanoparticles for varying periods up to 24 h before washing. Samples were then post-fixed, stained, dehydrated, embedded, and sectioned (see 2.2.18.13) for TEM analysis. Figure 6.22 shows a high magnification image for PGA 40%C₁₈-IONPs incubated with cells for different time periods of 1 h, 4 h, 12 h and 24 h.

At 1h incubation time (Fig 6.22a1, a2, a3 and a4), numerous particles were detected forming clusters inside the cells and can be seen throughout the cell in nuclei and in mitochondria, endosomes and cytoplasm. Mostly, particles were seen in dense collections, but also in small groups or as individual particles. Nanoparticles can also be seen outside the cell. There was quite a lot of variation between cells, but a similar distribution and intensity of particles were seen at all the time points investigated. By contrast, the control image shows virtually no contrast or obvious black dots as seen in the experimental pictures.









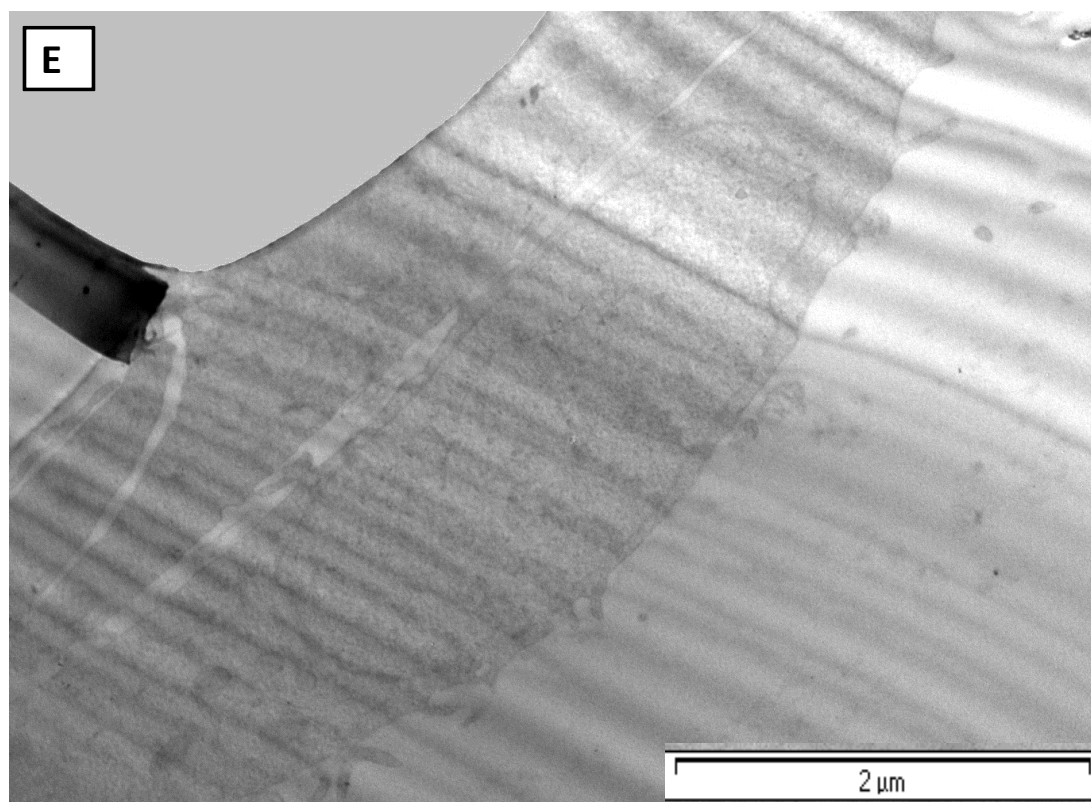
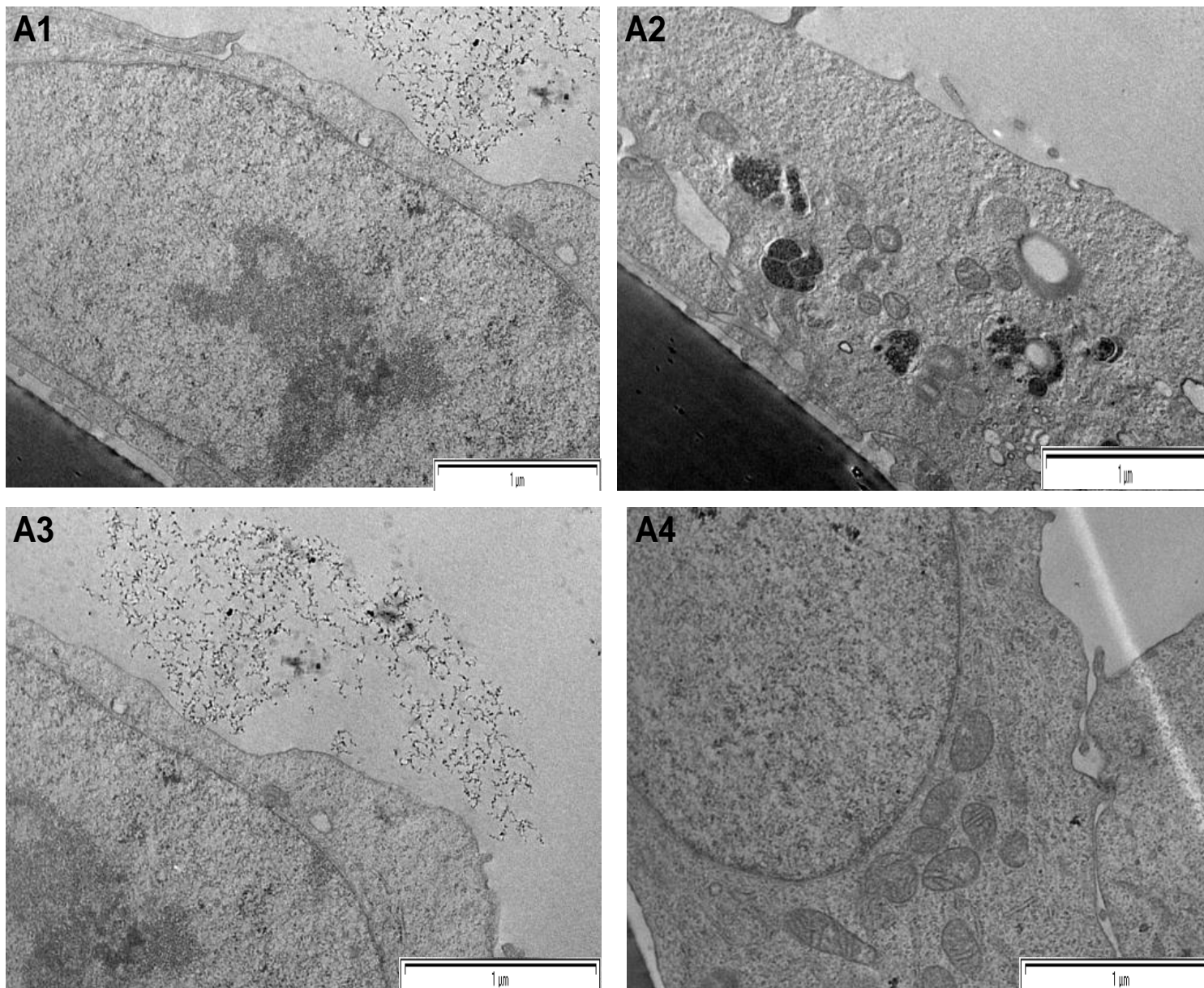
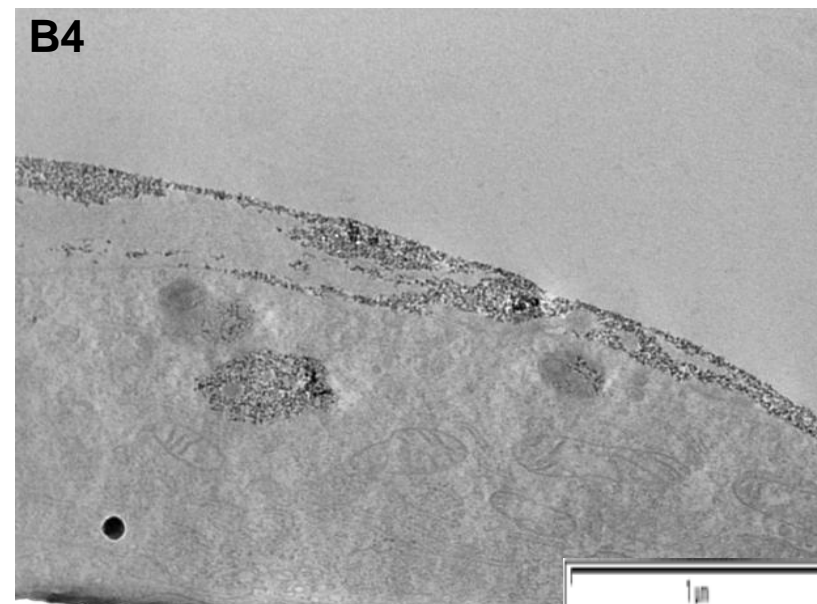
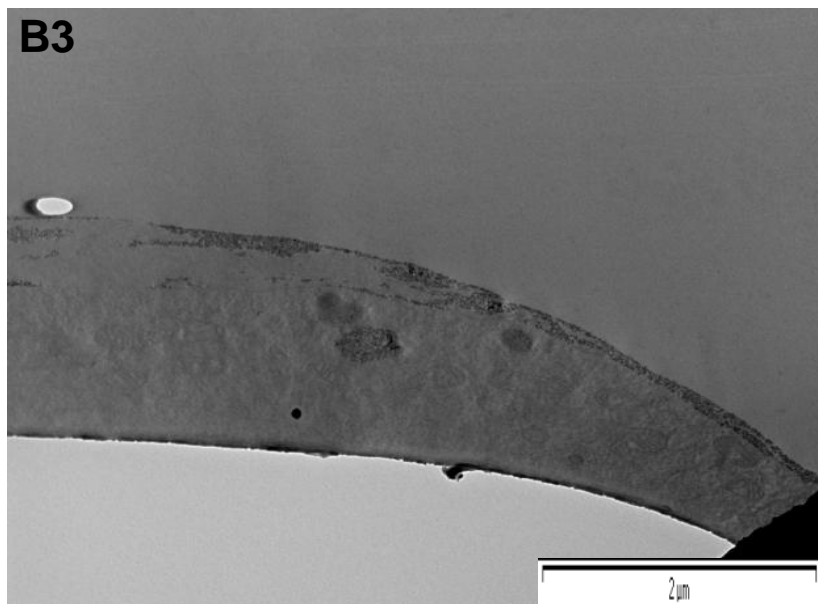
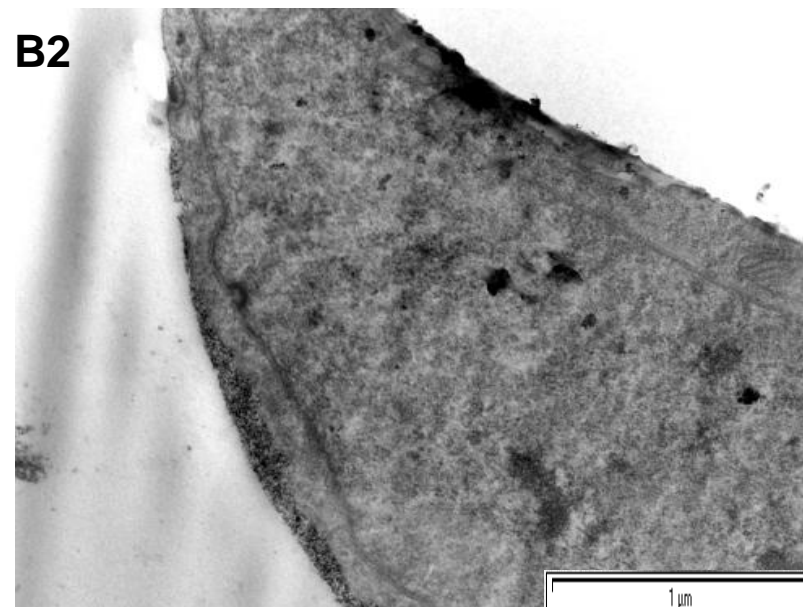
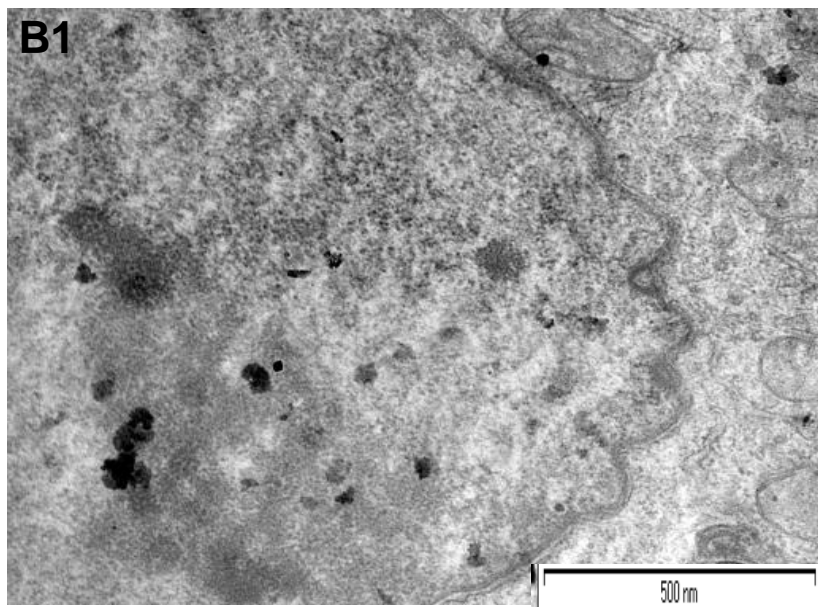


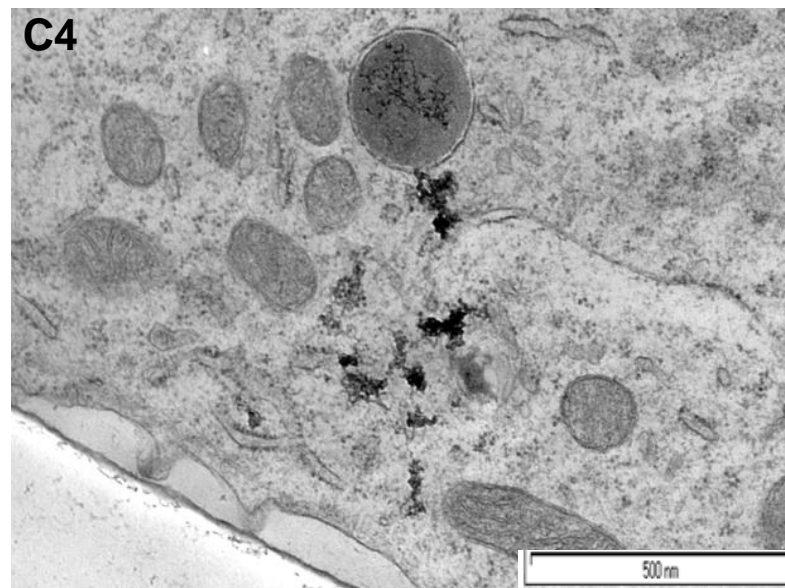
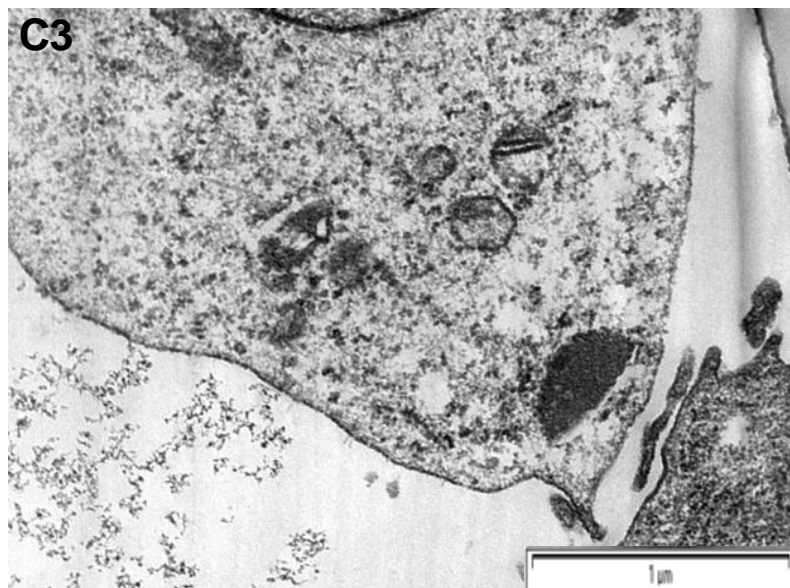
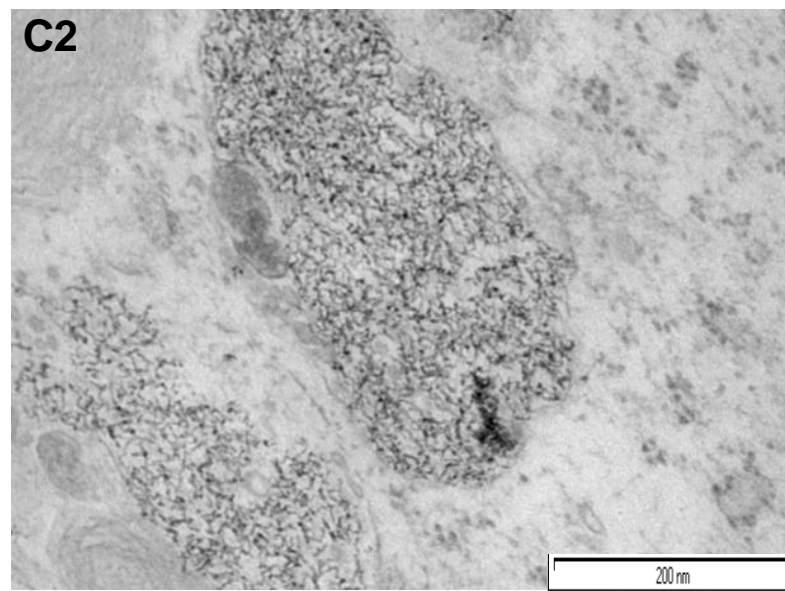
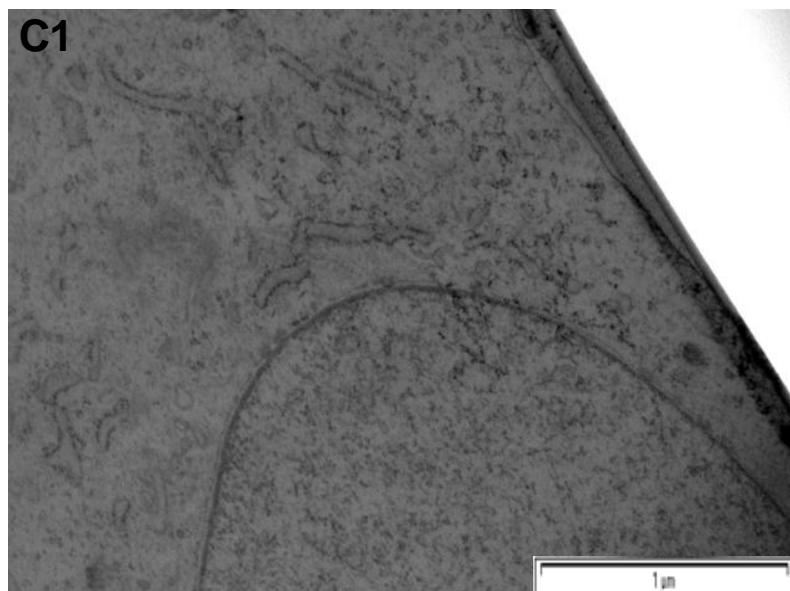
Figure 6-22 : Electron micrographs for PGA 40% C_{18} -IONPs. Incubated with C6 for different time periods (A) 1 h, (B) 4 h, (C) 12 h, (D) 24 h and (E) untreated cell control.

6.3.9.2 PEG-PGA 40% C_{18} -IONPs

To observe with TEM, the cells were incubated for different times of 1 h, 4 h, 12 h and 24 h with PEG-PGA 40% C_{18} -IONPs and the representative TEM images are presented in Figure 6.23. After 1h incubation time (Fig. 6.23a1, a2, a3 and a4) PEG-PGA 40% C_{18} -IONPs were seen outside the cells, near the plasma membrane and inside the endosome, in mitochondria, and the nanoparticles can also be seen in the nuclei. This phenomenon indicated that the uptake of PEG-PGA 40% C_{18} -IONPs was very high and in all the compartments of the cell. After 4 h of incubation, PEG-PGA 40% C_{18} -IONPs were already inside the cells, while others were about to enter, as shown in b1, b2, b3, and b4 of Figure 6.23. The PEG-PGA 40% C_{18} -IONPs were internalised and taken up as individual particles in 12 h incubation time. As shown in Figure 6.23 c1 and c2, interestingly some of PEG-PGA 40% C_{18} -IONPs lined up on membrane surfaces in the cytoplasm in mitochondria and apparently adsorbed onto structures in the nucleus. Figure 6.23 c3 and c4 showed the nanoparticles







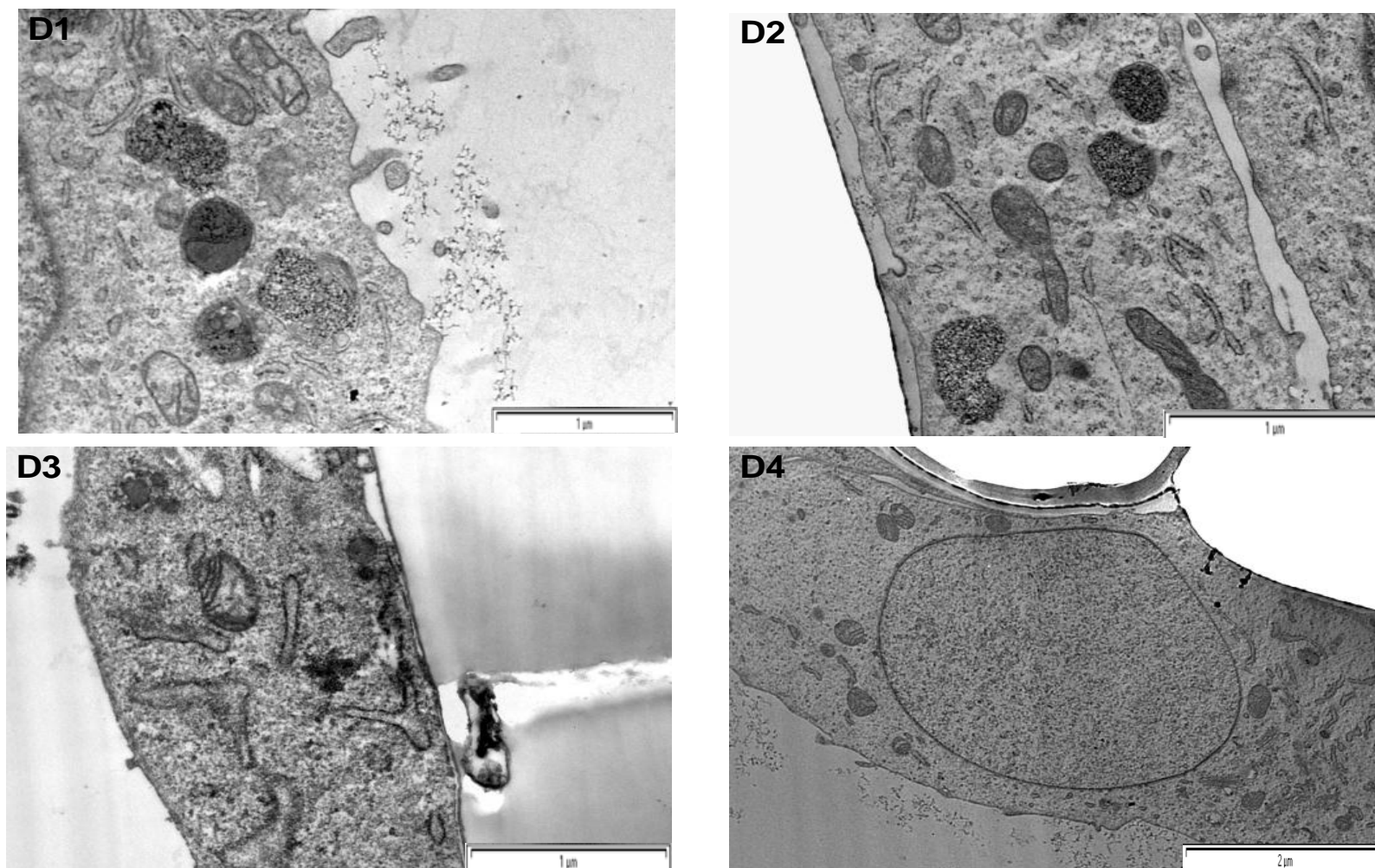


Figure 6-23 : Electron micrographs for PEG-PGA 40% C_{18} -IONPs. Incubated with C6 cells for different time periods (A) 1 h, (B) 4 h, (C) 12 h, and (D) 24 h.

in nuclei in very tiny groups or individually. In 24 h time incubation Figure 6.23d1, d2, d3 and d4 shows the particles in individual form and as groups inside the cell and also the many nanoparticles lined up adsorbed to various subcellular membranes. The control (Fig. 6.22 e) also here shown without nanoparticles for comparison to show the change in contrast seen with these very small IONPs.

For both PGA 40% C_{18} -IONPs and PEG-PGA 40% C_{18} -IONPs, the subcellular biodistribution was more widespread at later times, but nanoparticles could be seen in many cellular compartments even at early time points. In addition, there was no obvious collection of nanoparticles mainly in endosomal type compartments at early time points. It is therefore not clear whether initial uptake was by endosomal pathways.

6.4 DISCUSSION

The normal pathway and mechanism of drug absorption is by partition and diffusion, but with nanoparticles, other processes such as phagocytosis and endocytosis take place.

For use of iron oxide nanoparticles in a variety of applications, studying uptake is very important in order to find out if the nanoparticles had been taken up by the cells, how long it takes and whether or not the nanoparticles are retained in the cells. Also the effect of time and dose on the accumulation and distribution and the way the nanoparticles entered into the cells.

In this chapter, uptake of nanoparticles by cells and the effects of time or dose were evaluated in two types of cell models: monolayer culture and aggregate culture, using fluorescence microscopy and confocal microscopy. To determine where the nanoparticles were localised in cells, NPs were incubated with cells for different periods of time and TEM images acquired.

6.4.1 Uptake into Monolayers

Cell culture monolayers were incubated with both PGA 40% C_{18} -IONPs and PEG-PGA 40% C_{18} -IONPs were studied using fluorescence microscopy, confocal microscopy and TEM. The aim of these studies was to find out the uptake of the nanoparticles into cells, also the sub-cellular localisation of nanoparticles, and how the nanoparticles entered the cells.

The fluorescence micrographs of nanoparticles with both coatings appeared to show NP uptake by the cells with a broad distribution of fluorescence across the cell. The nanoparticles appeared to show a very fine fluorescence without strong points of light even after prolonged incubation. They were seen throughout the entire cell cytoplasm and tended to be near the nucleus where they were more concentrated, forming a highly fluorescent region. All of the nanoparticles with their different coatings and overcoatings gave a similar picture of distribution by fluorescence microscopy (Figs. 6.1, 6.2, 6.3 and 6.4). While the pictures are similar to most other particle uptake studies in showing a cytoplasmic uptake, in these studies the pictures were subtly different. Typically, particle uptake shows a much more punctate fluorescence due to the accumulation of particles in endosomes and lysosomes. Also at later time points (2–4 h) a typical horseshoe shaped perinuclear pattern of highly fluorescent spots of high concentration delineating the late endosome/lysosome accumulation is seen. However, unusually in this work these patterns were absent, suggesting some unusual features to the uptake. A further difference was the appearance of fluorescent patches over the nuclei. This was particularly noticeable in cells with high particle uptake, but it was unclear whether this represented particles actually in the nucleus or merely fluorescence in the cytoplasm overlying the nucleus.

PGA 40% C_{18} -IONPs and PEG-PGA 40% C_{18} -IONPs also showed a higher uptake in the presence of serum and in the absence of the serum with Tween overcoated nanoparticles. The uptake, however, was still very strong with all the coatings. There were some relative differences in the level of uptake with the different coatings (presence and absence of serum, Tween 0.1% and PEG-PGA 40% C_{18} -IONPs, but apparent differences in subcellular distribution were quite small. When particles were

without Tween in the presence of serum (Fig. 6.1), the accumulation was high and concentrated in the cytoplasmic region and showed higher uptake than with Tween in the presence of serum (Fig. 6.2). Using just PGA 40% C_{18} -IONPs without Tween and in the absence of serum (Fig. 6.3), the uptake was high and the fine particles could be seen in the cytoplasm and around the nuclei. The apparently high level of fluorescence in these cells could have been exaggerated because the cells tended to be more rounded up in the absence of serum. Very high uptake was also shown with PEG-PGA 40% C_{18} -IONPs (Fig. 6.4). The relative levels of uptake for the serum and Tween coatings was in the same order to that shown for the stability of particles in the presence of salt in chapter 4. However, surprisingly the PEG-PGA 40% C_{18} -IONPs, which showed even greater stability, do not fit this pattern. PGA particles in the absence of serum are hydrophobic and so should bind to cells and be taken up well. Incubation of PGA 40% C_{18} -IONPs with serum should result in protein adsorption and a hydrophilic surface leading to lower uptake. Tween coating could result in a thin layer of hydrophobic PEG on the surface of cells, reducing protein uptake and also reducing nanoparticle uptake. This theory fits well to the observed effects. However, PEG-PGA 40% C_{18} -IONPs could result in a much more hydrophilic surface, with a much lower uptake of particles. This was not seen in my experiments.

Confocal fluorescence micrographs of C6 monolayer appeared to show NPs within the cytoplasm for both PGA 40% C_{18} -IONPs and PEG-PGA 40% C_{18} -IONPs (Fig.6.10, 6.11, 6.12 and 6.13). Dark patches were also seen in the DAPI stained nuclei in the nanoparticle treated cells which were not apparent in the control (Fig. 6.10 d, Fig.11d, Fig.12d and Fig.13d). In these images, the PGA 40% C_{18} -IONPs appeared to be taken up better than the PEG-PGA 40% C_{18} -IONPs. The exact localisation of nanoparticles with both coatings was still not clear. The majority of the particles were in the cytoplasm, but again not in an obvious perinuclear location and the nuclear localisation was still unclear. The confocal microscopy confirmed that nanoparticles were definitely taken up into the cells.

The TEM studies confirmed that the nanoparticles were internalised by the cells (Fig. 6.22 and 6.23) confirming the above fluorescence microscopy work. The subcellular localisation of the nanoparticles was surprising. Large amounts of

nanoparticles were seen inside the cells and particles were everywhere in the cell and in the nuclei even after incubation times as short as one hour. The size of nanoparticles was clearly very small and there were no large aggregates. A few nanoparticles were observed outside of the cells and which may have been exocytosed. Almost all of the particles appeared to have been taken up as individual particles rather than as aggregates. Inside the cells the particles were sometimes arranged as individual particles in small groups or in many cases in lines adsorbed to various membrane structures inside the cell.

Looking at the results and the huge number of nanoparticles, the mechanism of entry into the cells was not clear. With nanoparticles in all subcellular compartments, nuclei, endosomes, mitochondria and cytoplasm, it is clear that particles have somehow been able to cross various intracellular membranes. It is only possible to pick out a few possible candidates for coated pits and caveolae on cell membranes, and these do not contain obvious accumulations of nanoparticles. Uptake could therefore have involved either a translocation of nanoparticles across membranes or could also have involved the usual endocytic pathways. A similar picture was seen for both the PGA 40% C_{18} -IONPs and PEG-PGA 40% C_{18} -IONPs. Despite the large numbers of nanoparticles taken up into all areas of the cells, there was no obvious change in the morphology of the cells observed compared with the control.

It is difficult to find any evidence in the literature for uptake even by very small nanoparticles either directly into cells or passing across membranes. In this study there is no direct evidence that the nanoparticles were taken up by one of these mechanisms. But the evidence of both the fluorescence microscopy and the TEM suggests quite strongly that the normal endocytic mechanisms were not the main uptake route.

Uptake of 200 nm particles in both serum-free and serum containing medium was low and could be attributed to the particle size improving the mode of nanoparticle-cell interaction and/or a smaller particle surface area available for serum protein adsorption (Johnston et al., 2010). It was reported that nanoparticles with sizes between 100 to 200 nm size acquired the best properties for cellular uptake (Panyam et al., 2003). Also, Jo et al., (2010) have reported that nanoparticles of a large size between 100 and 160 nm were aggregated in the culture media, therefore interaction

with serum proteins could cause the elimination of cell internalisation. Nanoparticles with a positive surface interacted with cell surfaces, which are negatively charged, resulting in improved cell internalisation of nanoparticles.

It has been reported that the size has an important role in their adhesion and interaction with the biological cell (Foster et al., 2001). Also Zhang et al., (2008) have showed that better cellular uptake can be achieved by smaller particle size 198.5 ± 131.1 nm.

The characteristics of the nanoparticles themselves are likely to play a very important role in the uptake, particularly the size of nanoparticles. In this study, the particle size was about 20–40 nm and this is likely to have some effect on the high uptake and wide distribution of the nanoparticles in cells.

In previous work within our group on larger nanoparticles made from PGA, Meng et al., (2006) investigated cell uptake. She showed a high uptake of these Tween-coated PGA nanoparticles into DAOY cells by fluorescence microscopy. This uptake showed a perinuclear distribution in the cells typical of lysosomal accumulation of particles. Uptake was time and concentration dependent. This work by Meng therefore demonstrates that the distribution seen with the smaller PGA nanoparticles results from the size, or the size in combination with the coating, rather than from the coating of the nanoparticles. Also, the charge of nanoparticles could be another factor to increase the uptake and distribution of nanoparticles.

Jun-ichiro Jo et al., (2009) reported that nanoparticles of large size between 100 and 160 nm were aggregated in the culture media, therefore interaction with serum proteins caused the elimination of cell internalisation. Nanoparticles with a positive surface charge interacted with the cell surface, which is negatively charged, resulting in improved cell internalisation of nanoparticles.

Nam et al., (2009) reported that the formulation of nanoparticles with different surface properties could improve their cellular uptake and intracellular distribution. magnetite I nanoparticles were synthesised using spermine with a zeta potential of 9.4 mV and magnetite II with hexanediamine with a zeta potential of -8.3 mV, magnetite I showed a higher uptake than that of magnetite II when the cells were

incubated with cancer cells or normal cells which have negative surface charge (Osaka et al., 2009).

Other factors, which may have effects on the uptake, are the type of coatings, particularly coatings to reduce nonspecific protein adsorption and clearance by macrophages. The type of coating used could indeed be directed towards cell interaction (Berry et al., 2004).

Polymeric surface coats may be functional in themselves through their influence on particle size and *in vivo* properties (Sébastien et al., 2006). Nanoparticle size, shape, surface properties, incubation temperature and time and concentration in the medium influenced the uptake of nanoparticles (Torchilin, 2000a and Rowland et al., 2005). Yang et al., (2008) used aminopropyl triethoxysilane (APTS) modified IONPs and adapted a tumour-targeting nanoimmunoliposome platform technology. Nanoparticles were labelled with sulfo-NHS-LC-biotin. Cells grown in monolayer were incubated with the ligand targeted scL- superparamagnetic IONPs complex with a size of 157.4 ± 12.5 nm compared with either the liposome-SPIO or free SPIO with a size of about 10 nm at 70 nmol for 4.5 h. The result showed the NPs were delivered to the tumour specifically and more efficiently when incorporated into a complex than as free SPIO.

Epidermal growth factor (EGF) was conjugated with carboxymethyldextran (CMD) coated iron oxide magnetic nanoparticles. Both CMD coated IONPs and EGF modified nanoparticles were incubated for 1 h with CaCo-2 cancer cells, and visualised using confocal microscopy. After 1 h of incubation, IONPs coated by CMD-EGF were present in both the cell membrane and cytoplasm. Internalised nanoparticles that appear in the cytoplasm seemed to accumulate in small vesicles, while after 1 h of incubation time, no presence of CMD coated IONPs was observed in the cells (Creixell et al., 2010).

In the present work IONPs were coated with different coatings and showed high uptake over the whole time period studied, also showing different levels of uptake and different distribution.

The increased intracellular uptake by using PEG as coating to IONPs could result from the possibility that the nanoparticles with the PEGylated functionalised surface could interact with the cell membrane to a greater extent, because of the capability of PEG dissolved in both polar and non-polar solvents and having high solubility in cell membranes (Yamazaki and Ito, 1990).

Many studies have reported a route of uptake of nanoparticles which did not involve a huge number of the nanoparticles. Wilhelm and Gazeau, (2008) have reported the incubation of anionic monomer-coated IONPs with cells. After 1 h incubation time, all the nanoparticles were confined within late endosomes or lysosomes dispersed throughout the cytoplasm, and did not behave as single particles, but were clustered into aggregates decorating the endosomal membrane and/or homogeneously dispersed in the endosome.

In this study, the nanoparticles that were shown in individual particles formed as single particles rather than in groups, and this could be attributed to the efficiency of the coatings. Work done by Stroh et al., (2004) used different concentrations of citrate-coated small superparamagnetic iron oxide particles of 1.5 or 3.0 mM incubated with the rat macrophages (RAW) cells for 90 min and viewed by CLSM. This work clearly demonstrated iron oxide particles seemed to be incorporated via endocytosis, as indicated by the observation of aggregates in vesicles and surrounded by membranes.

After the adsorption of the nanoparticles on the cellular membrane, the uptake occurs via several possible mechanisms, like pinocytosis, non-specific or receptor-mediated endocytosis or phagocytosis. The attachment of the particles to the cell membrane as the first step seems to be most affected by the surface charge of the particles (Lorenz et al., 2006).

Ge et al., (2009) used three different coatings with meso-2, 3-dimercaptosuccinic acid (DMSA), chitosan (CS) and (CS-DMSA) on IONPs incubated with the KB cells for 24h incubation. The higher cellular uptake of CS-DMSA-MNPs compared with CS-MNPs results from the high surface charge (positive zeta potential) and also showed higher cellular uptake compared to DMSA-MNPs with negative zeta potential. After 24 h most of the particles were endocytosed by cells and were

eventually sequestered in digestive vacuoles in the cell, some of them being taken up as agglomerates. According to my results, the uptake was by none of these routes mentioned above and could be by another way altogether. It has been demonstrated that particles with PEG-modified surfaces cross cell membranes, in non-specific cellular uptake (Caliceti et al., 1989). The possible mechanism for this uptake is that PEG can dissolve in both polar and nonpolar solvents and have high solubility in cell membranes (Yamazaki and Ito, 1990 and Boni et al., 1984).

Other studies agree with my result about the uptake of the particles located in cells but there is no evidence as to how the particles have been taken up. Häfeli et al., (2009) reported that when IONPs with size about 10 nm were coated with poly(ethyleneoxide) triblock copolymer (PEO-COOH-PEO) the size was increased to 100–200 nm. Uptake of particles was observed in three cell types: prostate cancer cell lines (PC3 and C4–2), human umbilical vein endothelial cells (HUVECs), and human retinal pigment epithelial cells (HRPEs) were investigated. The particles were located inside the cells after uptake, and the locations were defined by staining the lysosomes with LysoTracker. The result of the confocal image showed the particles did not locate inside these vesicles. Other results reported by Panyam et al., (2002) showed PLGA nanoparticles of 70 nm diameter escaped from the endo-lysosomal compartment, and it was postulated that this could be attributed to the selective surface charge reversal in acidic endo-lysosomes.

The other finding in this project was that the PGA 40% C_{18} -IONPs and PEG-PGA 40% C_{18} -IONPs showed high uptake in the presence of serum. Normally serum adsorption on the nanoparticles reduces uptake. Work reported by Petri-Fink et al., (2008) showed the presence of serum strongly inhibited the uptake of vinyl alcohol/vinyl amine copolymer (A-PVA) coated iron oxide nanoparticles, because of adsorption of serum on the particle surface. Berry et al., (2004) have reported that FITC labelled dextran-derivatised IONPs appear to be in clusters in the cell cytoplasm, possibly located in endocytic vesicles. Studies reported that the commercial dextran-IONPs, such as Feridex and Resovist, showed poor intracellular uptake, especially for cells lacking substantial phagocytic capacity (Dodd et al., 1999 and Ralph et al., 1997).

In the presence of the serum the PGA 40% C_{18} -IONPs and PEG-PGA 40% C_{18} -IONPs, however, showed wide distribution and high uptake by TEM and fluorescence microscopies (Figs. 6.1, 6.2, 6.4, 6.22 and 6.23).

6.4.2 Effects of Time and Dose

Two further factors have been investigated in this chapter, which are the time and the dose and how they affect the uptake. These have been determined using fluorescence microscopy, confocal microscopy and flow cytometry. Two coatings were used here, PEG-PGA 40% C_{18} -IONPs and PGA 40% C_{18} -IONPs. Fluorescence microscopy micrographs showed the uptake increased with an increase in the dose. The uptake was high even with a low dose of nanoparticles. Also, both of the coatings showed very high uptake but uptake of PEG-PGA 40% C_{18} -IONPs was higher than PGA 40% C_{18} -IONPs. The uptake was carried out in the presence of serum but this did not affect the uptake.

Confocal fluorescence micrographs of cells appeared to show fluorescence intensity increased with an increase of nanoparticle concentration (Figs. 6.10 and 6.11). However, in these experiments the PGA 40% C_{18} -IONPs appeared to be taken up more effectively than the PEG-PGA 40% C_{18} -IONPs.

The quantification of nanoparticles uptake was carried out by flow cytometry. As shown in Fig. 6.19, RBITC labelled uptake by C_6 cells was dependent on the dose of NPs. The results of flow cytometry revealed that at early time points the uptake of PGA 40% C_{18} -IONPs and PEG-PGA 40% C_{18} -IONPs was very similar, but that at later time points PEG-PGA 40% C_{18} -IONPs uptake was higher than PGA 40% C_{18} -IONPs and continued increasing steadily. The results corresponded with the fluorescence microscopy dose uptake.

The goal was to find out how time and dose had affected the uptake and the required time and dose that could be used for *in vitro* studies. Wang et al., (2010) studied the uptake of the poly(DL-lactic acid-co-a,b-malic acid) coated IONPs by cells incubated for different times: 2, 4, 8, 12, 24 and 48 h. He showed that the uptake increased with increasing incubation time and the highest iron uptake was obtained after 24 h

incubation with a medium containing 0.2 mg/mL nanoparticles. In my studies, a range of 0.1 to 1 ml of nanoparticles was used. The concentration of coated IONPs was 0.07 M (3.92 mg/ml) and after dilution into cell culture medium was 1.96 mg/ml giving amounts down to 0.2 mg/ml for the '0.1 ml' amount. This lowest amount used in my studies was therefore similar to the amount used in the study reported above. In my studies, the highest were 10x this amount, and even at this was not a saturating amount for uptake.

6.4.3 Metabolism and Retention of Nanoparticles Uptake with time

The metabolism of particles in the cells was followed by changes in fluorescence over time after incubation of the cells with particles for 2 h followed by washing and further incubation of cells. The fluorescence micrographs showed that PGA 40% C_{18} -IONPs (Figs. 6.7 and 6.9) remained in the cells over the early hours, i.e. from 1 to 4 hr, and then started to disappear after that, while with PEG-PGA 40% C_{18} -IONPs the fluorescence started to disappear after 6 h incubation time. The time series fluorescence images over the 24 h incubation time showed that the intracellular fluorescence intensity level decreased with increased incubation time. The fluorescence had completely disappeared at 24 h.

Flow cytometry studies of the two coatings showed the drop in MFI (Fig. 6.21) and agreed with the fluorescence images. By 24 h the fluorescence levels were close to background levels. The explanation could be attributed to the fluorescence disappearing but the nanoparticles still remaining in the cells. The PGA 40% C_{18} could be degraded by lysosome and the RBITC diffused out of the cells, while the IONPs may have either been metabolised or still be in the cells. Previous studies by Meng et al. (2006) with 200 nm PGA nanoparticles have shown that the PGA is degraded rapidly in the lysosomal compartment, leading to a loss of RBITC fluorescence. PGA backbone is synthesised by an enzymic reaction, and so the ester bonds would be expected to be particularly labile in the lysosomal environment.

The uptake of Streptavidin-fluorescein labelled iron oxide incubated with cells for 24 h was investigated by using flow cytometry and fluorescence microscopy.

The particles were shown to be in the lysosomal compartment of the cells, which suggested a receptor-mediated uptake mechanism (Becker et al., 2007).

Corot et al., (2006) explained the disappearance of iron oxide nanoparticles. Cells showed a gradual decline of intracellular iron particles with increasing time after incubation, which can be attributed to cell division and exocytosis or release of iron from non-viable cells over a period of 3 days.

The gradual disappearance of magnetic labelling may be because of the incorporation of iron into metabolic pathways, which constitutes a major pathway in non-dividing cells. This is a longer time period than investigated in these studies.

6.4.4 Uptake into Aggregates

Work was carried out using 3D cell aggregates because they are a much better model of the *in vivo* environment. This matters for two reasons. Firstly, the penetration of small nanoparticles across tissues is very important when considering the possible *in vivo* localisation of these nanoparticles if used as contrast agents, and this cannot be investigated using monolayers. Secondly the uptake of nanoparticles in cells grown in 3D is different to that of cells grown in monolayer (Meng et al., 2007a). This work was carried out using confocal microscopy.

A very high uptake of PGA 40% C_{18} -IONPs and PEG-PGA 40% C_{18} -IONPs was observed in the periphery of aggregates but there were still substantial amounts of nanoparticles penetrating into the centre of the aggregates (Figs. 6.15, 6.16, 6.17 and 6.18). Uptake, particularly penetration into the aggregates, increased with time, with very high levels of uptake observed at 24 h. PEG-PGA 40% C_{18} -IONPs appeared to show a higher penetration than the PGA 40% C_{18} -IONPs. The pattern of intracellular uptake was more difficult to see in these lower magnification pictures, but appeared to be similar to that seen in monolayer culture. The amount of uptake subjectively looked higher than in monolayer culture as reported for larger PGA nanoparticle (Meng et al., 2006).

The percentage of carboxylated polystyrene nanoparticles that were taken up by the spheroid core was affected by the particle size, i.e. the uptake decreased with increased particle size, where particles with size 20 and 40 nm penetrated more effectively than the nanoparticles with sizes about 100 and 200 nm (Goodman et al., 2007). With the nanoparticles in this study, which had a similar size to the smaller particles as reported above, the uptake and penetration was high. Also the surface charge has an effect on the uptake with aggregates. Liposomes with different surface charge were investigated. The results showed liposomes with neutral or low surface charge penetrated to the centre of spheroids, whereas with higher particle surface charge they remained more towards the outer layer of the aggregates (Saga et al., 1995). In chapters 4 and 5 it was shown that the IONPs coated with PGA 0%, PGA 40% C_{18} and PEG–PGA 40% C_{18} showed low surface charge and were nearly neutral.

Insufficient uptake of nanoparticles in solid tumours and extravasation because of the binding within tumour tissue increased the interstitial fluid pressure caused by leaky vasculature and poor lymphatic drainage, and tortuosity and hindered diffusion due to cell packing and the extracellular matrix (ECM) (Netti et al., 2000, Jain, 2001, Kuppen et al., 2001, Davies et al., 2001 and Grantab et al., 2006). At Nottingham, previous work by Meng (2006) using PGA nanoparticles with size about 170 nm showed limited uptake in aggregates because of the size, while with PGA 40% C_{18} -IONPs and PEG–PGA 40% C_{18} -IONPs in this project the uptake was higher. Studies reported that the smaller particles showed an ability to transport across and diffuse between organised collagen fibrils. The spacing of the fibrils was measured in poorly organised tumour ECM where the small space was about 20–40 nm and the larger spaces between 75–130 nm (Pluen et al., 2001).

6.4.5 Overview

Coated IONPs have been evaluated as a possible candidate for contrast agent for MRI by cellular uptake, distribution in the cell, retention, metabolism and localisation of RBITC labelled nanoparticles in cells.

Microscopy studies illustrated that when the IONPs coated with both PGA 40% C_{18} and PEG–PGA 40% C_{18} were taken up by the cells, the uptake was very high.

The nanoparticles showed a very fine distribution in cytoplasm and around the nuclei. The uptake of PEG–PGA 40% C_{18} –IONPs was similar to or higher than the PGA 40% C_{18} –IONPs, depending on the conditions used. Flow cytometry studies showed cellular uptake of PGA 40% C_{18} –IONPs and PEG-PGA 40% C_{18} –IONPs were dependent on the dose and incubation time of nanoparticles. The study showed agreement with the microscopy studies and the higher cellular uptake in cells was with PEG–PGA 40% C_{18} –IONPs, but also the PGA 40% C_{18} –IONPs showed very high uptake. This was in contrast to many other studies using IONPs reported in the literature where uptake was usually poor.

The retention and metabolism of nanoparticles were studied and showed a loss of fluorescence with time. Further work is necessary to show whether this was a loss of particle coating and fluorescence or also a loss of iron oxide core. Distribution, penetration and intracellular uptake were studied in 3-D cell cultures and it was found that intracellular uptake of the nanoparticles was dependent on the incubation time. The confocal microscopy micrographs demonstrated that penetration of nanoparticles into aggregates was very effective, giving high fluorescence intensity even towards the centre of the aggregates.

TEM studies demonstrated the subcellular localisation of nanoparticles. TEM images illustrated the massive uptake into cells and showed that the nanoparticles were located in nuclei and every other subcellular compartment in the cells. The nanoparticles did not show any aggregation after uptake, although some small groups of particles were seen as well as nanoparticle adsorption to membranes. This distribution is unusual as most studies show uptake by an endosomal route and confinement of nanoparticles to the endosomal/lysosomal system. TEM investigations were unable to determine the route of uptake that needs more investigation. There was no change in the morphology of the cell as a result of even high levels of nanoparticle uptake. The results in this chapter suggest the capability of these small particles to be taken up with very broad subcellular distribution and the power to penetrate into cell aggregates. These novel PEG–PGA 40% C_{18} –IONPs and PGA 40% C_{18} –IONPs could therefore be useful for medical applications of both drug delivery and as MRI contrast agents.

CHAPTER 7

7. SUMMARY AND CONCLUSIONS

7.1 Aims and objectives

In this project, coated IONPs have been produced and their properties examined. IONPs with size 13 ± 9 nm in diameter as determined by TEM were synthesised by the co-precipitation method. The IONPs tend to aggregate and form large particles which can easily be eliminated by defence systems in the body. Coating particles was necessary to prevent aggregation and provide biological stability.

The early stage of the research project focused on the synthesis of small nanoparticles coated with the most common polymers used in this field, dextran and carboxymethyl dextran (CMD). Characterisation of each of the products was investigated using the complementary techniques of DLS, zeta potential and TEM.

Throughout this study we were also trying to understand the effect of the type of the polymer, the amount of polymer coating nanoparticles, the amount of solvent and the method on the coated particles size. Polymers such as CMD and dextran have been extensively used as coating for nanoparticle formulations.

The bulk of this project has concentrated on developing coatings using biodegradable polymers. The idea is to exploit existing knowledge on drug delivery systems to deliver contrast agents. PGA was chosen for this work because this polymer backbone can be modified with acyl groups to give polymers with different properties. The 40% C_{18} acylated polymer has been previously shown to have excellent properties for this work. Particles made with these polymers have been shown to be taken up by cells and readily degraded within the cells. They also have high drug entrapment efficiency for labelling with fluorescent dyes. These polymers

were used for coating the nanoparticles. This thesis describes the development of suitable coatings using these polymers.

To improve the stability of the nanoparticles, PEG was coupled to the acylated 40% C₁₈ by using a monoamine PEG to couple to a terminal carboxyl group on the PEG. This reaction gave a yield of 77%, and the copolymer has been characterised. The copolymer has been used to coat the nanoparticles.

The stability of the nanoparticles with different coatings, including overcoatings such as albumin and Tween 80%, has been assessed using a range of different concentrations of NaCl. The coated particles show a very good stability to aggregation up to physiological levels.

Intracellular uptake of RBITC labelled PGA 40% C₁₈ and PEG–PGA 40% C₁₈ coated IONPs by the C6 cell line, and C₆ cell aggregates, have been carried out. Retention of RBITC labelled NPs within cells was evaluated. Uptake was determined and confirmed using fluorescence microscopy, confocal microscopy and flow cytometry. Finally, cells were also used to examine the intracellular location of the uptake of NPs using TEM.

7.2 Overall Summary

7.2.1 Iron Oxide Nanoparticle Manufacture

We have presented a controlled co-precipitation method which produced iron oxide nanoparticles. The pH of IONPs was a crucial factor to control the particle size. Particle sizes 13 nm in diameter, a narrow size distribution, were measured by TEM and DLS. Small particle sizes can be prepared by changing the operational parameters, e.g. optimum pH, which was established at pH 0.5. The particle showed high stability when stored for 7 days as a formal experiment, but my records show up to 1 year without any change of the particle size.

7.2.2 Dextran–Coated Iron Oxide Nanoparticles

7.2.2.1 Synthesis of Carboxymethyl dextran

The carboxymethyl dextran derivative was obtained by statistical substitution of the dextran hydroxyl groups on the glycosyl unit. The degree of substitution of carboxymethyl groups was determined by acidic titration. The dextran derivative with high degree of substitution with carboxymethyl group was 0.49, a result similar to that reported by other groups for this reaction.

CMD–IONPs and dextran–IONPs about 40 nm in size with narrow distribution measured by TEM have been synthesised using a co-precipitation method, either in the presence of the polymer or in the absence of the polymer. The two methods for coating nanoparticles gave a similar final nanoparticle size. Zeta potential was negative for all preparations of CMD nanoparticles made. This could be attributed to the carboxyl group on the polymer.

7.2.3 Different Substitutions of PGA–coated IONPs using two different Methods

This chapter has examined coated nanoparticles with PGA polymer backbone and its substituted acylated 40% variant. Particles were coated with Tween 80 (0.1%) and albumin in order to increase the stability. The purification of nanoparticles was also investigated.

On comparing the particles prepared by the IDP and sonication methods, the modified interfacial deposition method allowed us easily to obtain PGAs–coated IONPs nanoparticles with a good yield and with a smaller size than particles

prepared by the sonication method. The nanoprecipitation method is more flexible and can be modified (Alonso, 1996).

Using PGA polymers with acyl groups of varying chain lengths, it was observed that the chain length of the acyl group and the degree of acylation seemed to be less important for enhanced coatings. The preparation of coated nanoparticles under optimum conditions is important in terms of the physicochemical properties of nanoparticles. The polymer and solvent ratios were two of the parameters with the greatest effect on size.

By choosing the right method, small PGA 0% coated IONPs can be produced with a small amount of polymers (0.2 mg) and 2 ml of acetone. The small particles were found to be under about 20 nm, which is smaller than other formulations reported in the literature with biodegradable hydrophobic polymers. Transmission electron micrographs showed nanoparticles were spherical and with very little aggregates and in the nanometre size range 16 ± 5 nm.

Poly(glycerol adipate) is a water insoluble polyester. The presence of hydrophilic groups confers some hydrophilic characteristics on the backbone. The addition of acyl groups led to an increase in polymer hydrophobicity by decreasing the number of free OH groups on the backbone. Substituting the pendant hydroxyl groups of the backbone with hydrophobic acyl groups (C_{18}) increases the stability of the nanoparticles. The acyl groups and the chain lengths were determined using the traditional analysis techniques such as FTIR, NMR and GPC and confirmed the acylation of PGA backbone with high yield. The acylation of PGA backbone is simple, flexible and efficient.

Polymer was substituted by C_{18} chains, and coated IONPs with small size were still obtained using the nanoprecipitation method. The iron oxide particles were clearly detected in the polymer by TEM. Many nanoparticles were separately coated with the polymer and some polymer-coated aggregates were also found. These TEM results correlate very well with the data obtained by dynamic light scattering.

Treatment of coated nanoparticles with a low concentration of NaCl followed by a brief centrifugation removed large and poorly coated nanoparticles. This technique seems to be suitable for the purification of coated nanoparticles.

7.2.4 PEGylated PGA 40% C_{18}

An easy and favourable approach had been developed to prepare PEGylated PGA 40% C_{18} by activating the COOH group on the PGA by the CDI and bio-orthogonal reaction of the N terminus of the monoamine PEG molecule. The coupling of monoamine group on the PEG to the PGA 40% C_{18} was successful and gave a yield of 78%. The coupling between the polymers has been confirmed by GPC, NMR and FTIR.

7.2.4.1 PEGylated PGA 40% C_{18} coated iron oxide nanoparticles

In this work demonstrated the possibility of synthesising PEGylated–PGA 40% C_{18} . PEGylation with PEG 2000 gave surface modified layer with PGA 40% C_{18} precipitated around the surface of the nanoparticles. On the basis of the result, it is concluded that the physicochemical characteristics of PGA–IONPs could be controlled by altering several experimental conditions, such as the amount of the polymer and the amount of the solvent.

IONPs coated with a layer of PEG–PGA 40% C_{18} were prepared using our modified ID method to determine the optimum conditions for preparing small nanoparticles. The best conditions were found to be using 0.2 mg of polymer and 2 ml of acetone which gave clean and smooth particles with only very rare aggregates with average size 16 ± 4 nm. Decreasing the amount of the polymer to 0.1 mg caused an increase of the particle size. The TEM images indicated that the optimised nanoparticles with 0.2 mg of polymers (PGA 0% ,PGA 40% C_{18} and PEG–PGA 40% C_{18}) with 2 ml of acetone coated IONPs were spherical in shape without any aggregation, and smooth, and that the particle size was small 16 ± 5 nm, 23 ± 7 nm and 16 ± 4 nm respectively.

Zeta potential showed a positive charge. In any case, for all the formulations the smallest size was with 0.2 mg of polymer addition for all the polymers (PGA, PGA 40% C_{18} and PEG–PGA 40% C_{18}) with 2 ml of acetone coated IONPs.

7.2.5 Stability of Coated Iron Oxide Nanoparticles.

The investigation on the stability of NPs coated with different polymers and overcoating showed differences in the turbidity of NP suspensions with different concentrations of NaCl before the critical flocculation point occurred. To increase the stability of the nanoparticles in a biological medium, the surface of nanoparticles was coated with either 0.1% Tween or 0.1% albumin.

The PGA–IONPs were remarkably stable even in high sodium chloride concentration and showed more stability than dextran-coated IONPs. It was shown that the stability of the coated nanoparticles increased after overcoating with either Tween or albumin. The overcoatings were found to be stable under conditions mimicking the physiological medium. Thus, 0.2 mg of polymers (PGA 0% and PGA 40% C_{18}) coated IONPs and 0.1% Tween and albumin would be useful to stabilise the nanoparticles *in vivo*. Overcoating with albumin would be equivalent to providing the surface characteristics which would be expected by putting the particles into serum. PEGylated PGA 40% C_{18} –IONPs were also effectively stabilised at high concentrations of NaCl, making these particles suitable for *in vitro* and *in vivo* use.

7.2.6 Coated IONPs Uptake by Cells

To evaluate IONPs as a useful delivery system for medical applications, cellular uptake, intracellular distribution and localisation, the retention and metabolism of RBITC labelled NPs have been examined in C6 cells. NP uptake has been determined over different time periods and with different doses. Both the quantitative and qualitative evaluation of NP uptake was performed by using flow cytometry and fluorescence microscopy following the uptake of fluorescently labelled NPs. Uptake

has also been investigated in cell aggregates. Observation of cultures by confocal microscope and TEM images have confirmed the uptake and the localisation into cells.

Firstly, studies of NP distribution and intracellular distribution were carried out in monolayer culture mode using fluorescence microscopy. Those studies demonstrated that, in contrast to many other studies, the uptake was very high and dependent on both time and dose. Both in the presence and absence of serum the nanoparticles also showed high uptake. Similarly, PGA 40% C_{18} coatings based on either Tween or PEGylation of PGA 40% C_{18} also showed high uptake of particles into cells. In all of these conditions there was a surprising intracellular distribution. These findings were confirmed by confocal fluorescence microscopy. Uptake studies were also performed by using flow cytometry studies. Intracellular uptake of NPs was dependent on the incubation time and NP concentration. Flow cytometry studies also showed cells had high nanoparticle uptake.

From the TEM images can be concluded that the nanoparticles were internalised in cells entering the cytoplasm, subcellular organelles and nuclei. The number of individual nanoparticles taken up was huge, and nanoparticles were found to be present in nuclei and in all subcellular compartments throughout the cell. The invasion of nanoparticles into all areas of the cell was very surprising. As transport across membranes has clearly taken place, it is unclear whether or not uptake is mediated by endocytosis or direct uptake. This unusual behaviour must be attributed to two factors: the small size of the particles and the high protection to stability given by the coatings.

The time-series fluorescence images of cells incubated with both NPs showed that the intracellular fluorescence intensity level decreased with the incubation time of cells with fresh culture medium. These results were confirmed with quantitative flow cytometry, suggesting either loss of nanoparticle coating or disappearance of the nanoparticles from cells. Further experiments are needed to resolve this question.

Uptake of nanoparticles into spherical aggregates was evaluated by confocal microscopy studies in 3-D cell aggregates which were formed spontaneously by using a high individual cell concentration. The penetration of NPs in aggregates was rapid and occurred deep into the aggregates. These aggregate models have not so far been used much by other workers in this field, but they supply very important information that may help us with further future research into medical applications such as drug delivery.

7.3 FUTURE WORK

In this thesis, a new system of manufacturing small coated IONPs with unmodified PGA, C₁₈ acylated PGA and PEGylated PGA has been established. This work has helped in understanding and identifying a range of key factors that primarily contributed to the successful production of small monodisperse coated nanoparticles.

Use of analytical techniques like DLS, Zeta potential and TEM was sufficient to find out the important properties of the nanoparticles, but needs to be explored further in order to quantify other important properties using X-ray diffraction techniques and magnetic measurements. More study is needed to capture further information about the zeta potential of the particles using a range of buffers.

The excellent results in cell work showed a different uptake behaviour by these very small coated nanoparticles. Further investigation of the uptake of nanoparticles in different types of cell and different cultures, such as co-culture models, would be particularly useful. Also, further investigation into the effects of different surface coatings would be valuable. Further work is also required on the uptake of the nanoparticles into cellular aggregates examined by TEM.

PGA has a very flexible chemistry, and these coated nanoparticles could be very useful for more research in the development of drug delivery systems. In addition to loading with conventional drugs, loading with DNA, siRNA and binding with a

range of ligands and incorporating different types of proteins, enzymes, antibodies, or nucleotides on the particle surfaces is possible.

With the preparation and characterisation of these coated nanoparticles almost completed, *in vivo* studies would now be useful to determine their biodistribution and in the assessment of the effects of the nanoparticles as contrast agents to detect defective and diseased cells. Also for the possible tracking of stem cells *in vitro* and *in vivo*.

REFERENCES

- Acar, H. Y. C., Garaas, R. S., Syud, F., Bonitatebus, P. & Kulkarni, A. M. 2005. Superparamagnetic nanoparticles stabilized by polymerized PEGylated coatings. *Journal of Magnetism and Magnetic Materials*, **293**, 1-7.
- Ahniyaz, A., Seisenbaeva, G. A., Häggström, L., Kamali, S., Kessler, V. G., Nordblad, P., Johansson, C. & Bergström, L. 2008. Preparation of iron oxide nanocrystals by surfactant-free or oleic acid-assisted thermal decomposition of a Fe(III) alkoxide. *Journal of Magnetism and Magnetic Materials*, **320**, 781-787.
- Akerman, M. E., Chan, W. C., Laakkonen, P., Bhatia, S. N. & Ruoslahti, E. 2002. Nanocrystal targeting *in vivo*. *Proceedings of the National Academy of Sciences USA*, **99**, 12617-21.
- Allkemper, T., Bremer, C., Matuszewski, L., Ebert, W. & Reimer, P. 2002. Contrast-enhanced Blood-Pool MR Angiography with Optimized Iron Oxides: Effect of Size and Dose on Vascular Contrast Enhancement in Rabbits¹. *Radiology*, **223**, 432-438.
- Alonso, M., J. 1996. Nanoparticulate Drug Carrier Technology, in Pharmaceutical Dosage Forms: Disperse Systems. *Marcel Dekker: New York.*, 203-242.
- Ambruosi, A., Khalansky, A. S., Yamamoto, H., Gelperina, S. E., Begley, D. J. & Kreuter, J. 2006. Biodistribution of polysorbate 80-coated doxorubicin-loaded [14C]-poly(butyl cyanoacrylate) nanoparticles after intravenous administration to glioblastoma-bearing rats. *Journal of Drug Targeting*, **14**, 97-105.
- Arias, J. L., Gallardo, V., Gomez-Lopera, S. A., Plaza, R. C. & Delgado, A. V. 2001. Synthesis and characterization of poly(ethyl-2-cyanoacrylate) nanoparticles with a magnetic core. *Journal of Controlled Release*, **77**, 309-21.
- Arias, J. L., Gallardo, V., Ruiz, M. A. & Delgado, A. V. 2008a. Magnetite/poly(alkylcyanoacrylate) (core/shell) nanoparticles as 5-Fluorouracil delivery systems for active targeting. *European Journal of Pharmaceutics and Biopharmaceutics*, **69**, 54-63.
- Arias, J. L., López-Viota, M., López-Viota, J. & Delgado, A. V. 2009. Development of iron/ethylcellulose (core/shell) nanoparticles loaded with diclofenac sodium for arthritis treatment. *International Journal of Pharmaceutics*, **382**, 270-276.

-
- Arias, J. L., López-Viota, M., Ruiz, M. A., López-Viota, J. & Delgado, A. V. 2007. Development of carbonyl iron/ethylcellulose core/shell nanoparticles for biomedical applications. *International Journal of Pharmaceutics*, **339**, 237-245.
- Ashtari, P., He, X., Wang, K. & Gong, P. 2005. An efficient method for recovery of target ssDNA based on amino-modified silica-coated magnetic nanoparticles. *Talanta*, **67**, 548-554.
- Babes, L., Denizot, B., Tanguy, G., Le jeune, J. J. & Jallet, P. 1999. Synthesis of Iron Oxide Nanoparticles Used as MRI Contrast Agents: A Parametric Study. *Journal of Colloid and Interface Science*, **212**, 474-482.
- Bae, S.-J., Park, J.-A., Lee, J.-J., Lee, G.-H., Kim, T.-J., Yoo, D.-S. & Chang, Y. 2009. Ultrasmall iron oxide nanoparticles: Synthesis, physicochemical, and magnetic properties. *Current Applied Physics*, **9**, S19-S21.
- Baker, I., Zeng, Q., Li, W. & Sullivan, C. R. Year. Heat deposition in iron oxide and iron nanoparticles for localized hyperthermia. In, 2006. *Journal of Applied Physics*, **08H106-3**.
- Bala, I., Hariharan, S. & Kumar, M. N. 2004. PLGA nanoparticles in drug delivery: the state of the art. *Critical reviews in therapeutic drug carrier systems*, **21**, 387-422.
- Barratt, G., Puisieux, F., Yu, W. P., Foucher, C., Fessi, H. & Devissaguet, J. P. 1994. Anti-metastatic activity of MDP-L-alanyl-cholesterol incorporated into various types of nanocapsules. *International Journal of Immunopharmacology*, **16**, 457-461.
- Barrera, C., Herrera, A. P. & Rinaldi, C. 2009. Colloidal dispersions of monodisperse magnetite nanoparticles modified with poly(ethylene glycol). *Journal of Colloid and Interface Science*, **329**, 107-113.
- Barrera, D. A., Zylstra, E., Lansbury, P. T. & Langer, R. 1993. Synthesis and rgd peptide modification of a new biodegradable copolymer - poly(lactic acid-co-lysine). *Journal of the American Chemical Society*, **115**, 11010-11011.
- Bazile, D., Prud'Homme, C., Bassoullet, M. T., Marlard, M., Spenlehauer, G. & Veillard, M. 1995. Stealth Me.PEG-PLA nanoparticles avoid uptake by the mononuclear phagocytes system. *Journal of Pharmaceutical Sciences*, **84**, 493-498.
-

-
- Becker, C., Hodenius, M., Blendinger, G., Sechi, A., Hieronymus, T., Müller-Schulte, D., Schmitz-Rode, T. & Zenke, M. 2007. Uptake of magnetic nanoparticles into cells for cell tracking. *Journal of Magnetism and Magnetic Materials*, **311**, 234-237.
- Belleville, P., Jolivet, J.-P., Tronc, E. & Livage, J. 1992. Crystallization of ferric hydroxide into spinel by adsorption on colloidal magnetite. *Journal of Colloid and Interface Science*, **150**, 453-460.
- Bergemann, C., Müller-Schulte, D., Oster, J., Brassard, L. & Lübke, A. S. 1999. Magnetic ion-exchange nano- and microparticles for medical, biochemical and molecular biological applications. *Journal of Magnetism and Magnetic Materials*, **194**, 45-52.
- Berry, C. C. & Curtis, A. S. G. 2003. Functionalisation of magnetic nanoparticles for applications in biomedicine. *Journal of Physics D: Applied Physics*, **36**, R198-R206.
- Berry, C. C., Wells, S., Charles, S., Aitchison, G. & Curtis, A. S. G. 2004. Cell response to dextran-derivatised iron oxide nanoparticles post internalisation. *Biomaterials*, **25**, 5405-5413.
- Berry, C. C., Wells, S., Charles, S. & Curtis, A. S. G. 2003. Dextran and albumin derivatised iron oxide nanoparticles: influence on fibroblasts *in vitro*. *Biomaterials*, **24**, 4551-4557.
- Blankenberg, F. G., Katsikis, P. D., Storrs, R. W., Beaulieu, C., Spielman, D., Chen, J. Y., Naumovski, L. & Tait, J. F. 1997. Quantitative Analysis of Apoptotic Cell Death Using Proton Nuclear Magnetic Resonance Spectroscopy. *Blood*, **89**, 3778-3786.
- Bonadonna, G., Gianni, L., Santoro, A., Bonfante, V., Bidoli, P., Casali, P., Demicheli, R. & Valagussa, P. 1993. Drugs ten years later: epirubicin. *Annals of Oncology*, **4**, 359-69.
- Boni, L. T., Hah, J. S., Hui, S. W., Mukherjee, P., Ho, J. T. & Jung, C. Y. 1984. Aggregation and fusion of unilamellar vesicles by poly(ethylene glycol). *Biochimica et Biophysica Acta (BBA) - Biomembranes*, **775**, 409-418.
- Borchard, G., Audus, K. L., Shi, F. & Kreuter, J. 1994. Uptake of surfactant-coated poly(methyl methacrylate)-nanoparticles by bovine brain microvessel endothelial cell monolayers. *International Journal of Pharmaceutics*, **110**, 29-35.
-

-
- Budhian, A., Siegel, S. J. & Winey, K. I. 2007. Haloperidol-loaded PLGA nanoparticles: Systematic study of particle size and drug content. *International Journal of Pharmaceutics*, **336**, 367-375.
- Bulte, J. W. & Kraitchman, D. L. 2004. Iron oxide MR contrast agents for molecular and cellular imaging. *NMR in Biomedicine*, **17**, 484-99.
- Bulte, J. W. M., Cuyper, M. D., Despres, D. & Frank, J. A. 1999. Preparation, relaxometry, and biokinetics of PEGylated magnetoliposomes as MR contrast agent. *Journal of Magnetism and Magnetic Materials*, **194**, 204-209.
- Bumb, A., Brechbiel, M. W., Choyke, P. L., Fugger, L., Eggeman, A., Prabhakaran, D., Hutchinson, J. & Dobson, P. J. 2008. Synthesis and characterization of ultra-small superparamagnetic iron oxide nanoparticles thinly coated with silica. *Nanotechnology*, **19**, 335601.
- Büscher, K., Helm, C. A., Gross, C., Glöckl, G., Romanus, E. & Weitschies, W. 2004. Nanoparticle Composition of a Ferrofluid and Its Effects on the Magnetic Properties. *Langmuir*, **20**, 2435-2444.
- Cabrera, L., Gutierrez, S., Menendez, N., Morales, M. P. & Herrasti, P. 2008. Magnetite nanoparticles: Electrochemical synthesis and characterization. *Electrochimica Acta*, **53**, 3436-3441.
- Cai, W. & Wan, J. 2007. Facile synthesis of superparamagnetic magnetite nanoparticles in liquid polyols. *Journal of Colloid and Interface Science*, **305**, 366-70.
- Can, K., Ozmen, M. & Ersoz, M. 2009. Immobilization of albumin on aminosilane modified superparamagnetic magnetite nanoparticles and its characterization. *Colloids and Surfaces B: Biointerfaces*, **71**, 154-159
- Carl, E. S., Karen, B.-S., Maj, H. & Christer, J. 1994. Magnetic characterization of iron oxides for magnetic resonance imaging. *Magnetic Resonance in Medicine*, **31**, 268-272.
- Carmen Bautista, M., Bomati-Miguel, O., Del Puerto Morales, M., Serna, C. J. & Veintemillas-Verdaguer, S. 2005. Surface characterisation of dextran-coated iron oxide nanoparticles prepared by laser pyrolysis and coprecipitation. *Journal of Magnetism and Magnetic Materials*, **293**, 20-27.

-
- Cavallaro, G., Fresta, M., Giammona, G., Puglisi, G. & Villari, A. 1994. Entrapment of β -lactams antibiotics in polyethylcyanoacrylate nanoparticles: Studies on the possible *in vivo* application of this colloidal delivery system. *International Journal of Pharmaceutics*, **111**, 31-41.
- Chang, W., Skandan, G., Danforth, S. C., Kear, B. H. & Hahn, H. 1994a. Chemical vapor processing and applications for nanostructured ceramic powders and whiskers. *Nanostructured Materials*, **4**, 507-520.
- Chang, W., Skandan, G., Hahn, H., Danforth, S. C. & Kear, B. H. 1994b. Chemical vapor condensation of nanostructured ceramic powders. *Nanostructured Materials*, **4**, 345-351.
- Chaubet, F., C. J., Maïga, O., Mauray, S., Jozefonvicz, J. 1995. Synthesis and structure--anticoagulant property relationships of functionalized dextrans: CMDBS. *Carbohydrate Polymers*, **28**, 145-152.
- Chen, C.-W. 1986. Magnetism and metallurgy of soft magnetic materials, *New York, Dover Publications*.
- Chen, D. X., Sun, N. & Gu, H. C. 2009. Size analysis of carboxydextran coated superparamagnetic iron oxide particles used as contrast agents of magnetic resonance imaging. *Journal of Applied Physics*, **106**, 063906-9.
- Chen, Z. P., Zhang, Y., Zhang, S., Xia, J. G., Liu, J. W., Xu, K. & Gu, N. 2008. Preparation and characterization of water-soluble monodisperse magnetic iron oxide nanoparticles via surface double-exchange with DMSA. *Colloids and Surfaces A: Physicochemical and Engineering Aspects*, **316**, 210-216.
- Cheng, F.-Y., Su, C.-H., Yang, Y.-S., Yeh, C.-S., Tsai, C.-Y., Wu, C.-L., Wu, M.-T. & SHIeh, d.-B. 2005. Characterization of aqueous dispersions of Fe₃O₄ nanoparticles and their biomedical applications. *Biomaterials*, **26**, 729-738.
- Chernysheva, Y. V., Babak, V. G., Kildeeva, N. R., Boury, F., Benoit, J. P., Ubrich, N. & Maincent, P. 2003. Effect of the type of hydrophobic polymers on the size of nanoparticles obtained by emulsification-solvent evaporation. *Mendeleev Communications*, **13**, 65-67.
- Chin, A. B. & Yaacob, I. I. 2007. Synthesis and characterization of magnetic iron oxide nanoparticles via w/o microemulsion and Massart's procedure. *Journal of Materials Processing Technology*, **191**, 235-237.
-

-
- Chouly, C., Pouliquen, D., Lucet, I., Jeune, J. J. & Jallet, P. 1996b. Development of superparamagnetic nanoparticles for MRI: effect of particle size, charge and surface nature on biodistribution. *Journal of Microencapsulation*, **13**, 245-55.
- Chunfu, Z., Jinqian, C., Duanzhi, Y., Yongxian, W., Yanlin, F. & Jiaju, T. 2004. Preparation and radiolabeling of human serum albumin (HSA)-coated magnetite nanoparticles for magnetically targeted therapy. *Applied Radiation and Isotopes*, **61**, 1255-9.
- Chung, H. J., Go, D. H., Bae, J. W., Jung, I. K., Lee, J. W. & Park, K. D. 2005. Synthesis and characterization of Pluronic® grafted chitosan copolymer as a novel injectable biomaterial. *Current Applied Physics*, **5**, 485-488.
- Claus, F. & Hans-Otto, J. 2001. Polyol-Mediated Preparation of Nanoscale Oxide Particles13. *Angewandte Chemie International Edition*, **40**, 359-362.
- Conner, S. D. & Schmid, S. L. 2003. Regulated portals of entry into the cell. *Nature*, **422**, 37-44.
- Cormode, D. P., Jarzyna, P. A., Mulder, W. J. M. & Fayad, Z. A. 2010. Modified natural nanoparticles as contrast agents for medical imaging. *Advanced Drug Delivery Reviews*, **62**, 329-338.
- Corot, C., Robert, P., Idée, J.-M. & Port, M. 2006. Recent advances in iron oxide nanocrystal technology for medical imaging. *Advanced Drug Delivery Reviews*, **58**, 1471-1504.
- Cotton, F. A. 1988. *Advanced inorganic chemistry*, New York :, Wiley.
- Creixell, M., Herrera, A. P., Ayala, V., Latorre-Esteves, M., Pérez-Torres, M., Torres-Lugo, M. & Rinaldi, C. 2010. Preparation of epidermal growth factor (EGF) conjugated iron oxide nanoparticles and their internalization into colon cancer cells. *Journal of Magnetism and Magnetic Materials*, **322**, 2244-2250.
- Dale, L. H. 2005. Synthesis, Properties, and Applications of Iron Nanoparticles. *Small*, **1**, 482-501.
- Davies, C. D. L., Engesaeter, B. O., Haug, I., Ormberg, I. W., Halgunset, J. & Brekken, C. 2001. Uptake of IgG in osteosarcoma correlates inversely with interstitial fluid pressure, but not with interstitial constituents. *British Journal of Cancer*, **85**, 1968-1977.

-
- Decuzzi, P., Causa, F., Ferrari, M. & Netti, P. A. 2006. The effective dispersion of nanovectors within the tumor microvasculature. *Annals of Biomedical Engineering*, **34**, 633-41.
- Del Pozo-Rodriguez, A., Solinis, M. A., Gascon, A. R. & Pedraz, J. L. 2009. Short- and long-term stability study of lyophilized solid lipid nanoparticles for gene therapy. *European Journal of Pharmaceutics and Biopharmaceutics*, **71**, 181-9.
- Deng, Y.-H., Wang, C.-C., Hu, J.-H., Yang, W.-L. & Fu, S.-K. 2005. Investigation of formation of silica-coated magnetite nanoparticles via sol-gel approach. *Colloids and Surfaces A: Physicochemical and Engineering Aspects*, **262**, 87-93.
- Deng, Y., Wang, L., Yang, W., Fu, S. & Elaïssari, A. 2003. Preparation of magnetic polymeric particles via inverse microemulsion polymerization process. *Journal of Magnetism and Magnetic Materials*, **257**, 69-78.
- Dilnawaz, F., Singh, A., Mohanty, C. & Sahoo, S. K. 2010. Dual drug loaded superparamagnetic iron oxide nanoparticles for targeted cancer therapy. *Biomaterials*, **31**, 3694-3706.
- Dodd, S. J., Williams, M., Suhan, J. P., Williams, D. S., Koretsky, A. P. & Ho, H. 1999. Detection of single mammalian cells by high-resolution magnetic resonance imaging. *Biophysical Journal*, **76**, 103-109.
- Douglas, S. J., Davis, S. S. & Illum, L. 1986. Biodistribution of poly(butyl 2-cyanoacrylate) nanoparticles in rabbits. *International Journal of Pharmaceutics*, **34**, 145-152.
- Duan, H., Kuang, M., Wang, X., Wang, Y. A., Mao, H. & Nie, S. 2008. Reexamining the Effects of Particle Size and Surface Chemistry on the Magnetic Properties of Iron Oxide Nanocrystals: New Insights into Spin Disorder and Proton Relaxivity. *Journal of Physical Chemistry C*, **112**, 8127-8131.
- Duan, H. L., Shen, Z. Q., Wang, X. W., Chao, F. H. & Li, J. W. 2005. Preparation of immunomagnetic iron-dextran nanoparticles and application in rapid isolation of E.coli O157:H7 from foods. *World Journal of Gastroenterol*, **11**, 3660-4.
- Dumitrache, F., Morjan, I., Alexandrescu, R., Ciupina, V., Prodan, G., Voicu, I., Fleaca, C., Albu, L., Savoiu, M., Sandu, I., Popovici, E. & Soare, I. 2005. Iron-iron oxide core-shell nanoparticles synthesized by laser pyrolysis followed by superficial oxidation. *Applied Surface Science*, **247**, 25-31.
-

-
- Dutz, S., Andrä, W., Hergt, R., Müller, R., Oestreich, C., Schmidt, C., Töpfer, J., Zeisberger, M. & Bellemann, M. E. 2007. Influence of dextran coating on the magnetic behaviour of iron oxide nanoparticles. *Journal of Magnetism and Magnetic Materials*, **311**, 51-54.
- Elliott, S. R. 1998. The physics and chemistry of solids, Chichester, West Sussex, England; New York, NY, USA, *John Wiley & Sons*.
- Enochs, W. S., Schaffer, B., Bhide, P. G., Nossiff, N., Papisov, M., Bogdanov, A., Brady, T. J. & Weissleder, R. 1993. MR Imaging of Slow Axonal Transport *in Vivo*. *Experimental Neurology*, **123**, 235-242.
- Evgenov, N. V., Medarova, Z., Dai, G., Bonner-Weir, S. & Moore, A. 2006. *In vivo* imaging of islet transplantation *Nature Medicine*, **12**, 144-148.
- Fahlvik, A. K., Holtz, E. & Klaveness, J. 1990. Relaxation efficacy of paramagnetic and superparamagnetic microspheres in liver and spleen. *Magnetic Resonance Imaging*, **8**, 363-9.
- Felton, N. & Pileni, M. P. 1997. New Technique for Synthesizing Iron Ferrite Magnetic Nanosized Particles. *Langmuir*, **13**, 3927-3933.
- Feng, B., Hong, R. Y., Wang, L. S., Guo, L., Li, H. Z., Ding, J., Zheng, Y. & Wei, D. G. 2008. Synthesis of Fe₃O₄/APTES/PEG diacid functionalized magnetic nanoparticles for MR imaging. *Colloids and Surfaces A: Physicochemical and Engineering Aspects*, **328**, 52-59.
- Fessi, H., Puisieux, F., Devissaguet, J. P. & Ammoury, N. 1989. Nanocapsule formation by interfacial polymer deposition following solvent displacement. *International Journal of Pharmaceutics*, **55**, R1-R4.
- Fievet, F., Lagier, J. P., Blin, B., Beaudoin, B. & Figlarz, M. 1989a. Homogeneous and Heterogeneous Nucleations in The Polyol PROCESS for The Preparation of Micron and Sub-micron Size Metal Particles. *Solid State Ionics*, **32-3**, 198-205.
- Figuerola, A., Di corato, R., Manna, L. & Pellegrino, T. 2010. From iron oxide nanoparticles towards advanced iron-based inorganic materials designed for biomedical applications. *Pharmacological Research*, **2**, 126-143.
- Finotelli, P. V., Morales, M. A., Rocha-Leão, M. H., Baggio-Saitovitch, E. M. & Rossi, A. M. 2004. Magnetic studies of iron(III) nanoparticles in alginate polymer for drug delivery applications. *Materials Science and Engineering: C*, **24**, 625-629.
-

-
- Foster, K. A., Yazdanian, M. & Audus, K. L. 2001. Microparticulate uptake mechanisms of in-vitro cell culture models of the respiratory epithelium. *Journal of Pharmacy and Pharmacology*, **53**, 57-66.
- Frank, M. M. & Fries, L. F. 1991. The role of complement in inflammation and phagocytosis. *Immunology Today*, **12**, 322-326.
- Franssen, O., Vos, O. P. & Hennink, W. E. 1997. Delayed release of a model protein from enzymatically-degrading dextran hydrogels. *Journal of Controlled Release*, **44**, 237-245.
- Gaihre, B., Khil, M. S., Lee, D. R. & Kim, H. Y. 2009. Gelatin-coated magnetic iron oxide nanoparticles as carrier system: Drug loading and *in vitro* drug release study. *International Journal of Pharmaceutics*, **365**, 180-189.
- Gast, A. P. & Leibler, L. 1986. Interactions of sterically stabilized particles suspended in a polymer solution. *Macromolecules*, **19**, 686-691.
- Ge, Y., Zhang, Y., Xia, J., Ma, M., He, S., Nie, F. & Gu, N. 2009. Effect of surface charge and agglomerate degree of magnetic iron oxide nanoparticles on KB cellular uptake *in vitro*. *Colloids and Surfaces B: Biointerfaces*, **73**, 294-301.
- Gilchrist, R. K., Medal, R., Shorey, W. D., Hanselman, R. C., Parrott, J. C. & Taylor, C. B. 1957. Selective inductive heating of lymph nodes. *Annals of Surgery*, **146**, 596-606.
- Gnanaprakash, G., Mahadevan, S., Jayakumar, T., Kalyanasundaram, P., Philip, J. & Raj, B. 2007. Effect of initial pH and temperature of iron salt solutions on formation of magnetite nanoparticles. *Materials Chemistry and Physics*, **103**, 168-175.
- Goetze, T., Gansau, C., Buske, N., Roeder, M., Görnert, P. & Bahr, M. 2002. Biocompatible magnetic core/shell nanoparticles. *Journal of Magnetism and Magnetic Materials*, **252**, 399-402.
- Gómez-Lopera, S. A., Arias, J. L., Gallardo, V. & Delgado, Á. V. 2006. Colloidal Stability of Magnetite/Poly(lactic acid) Core/Shell Nanoparticles. *Langmuir*, **22**, 2816-2821.
- Gómez-Lopera, S. A., Plaza, R. C. & Delgado, A. V. 2001. Synthesis and Characterization of Spherical Magnetite/Biodegradable Polymer Composite Particles. *Journal of Colloid and Interface Science*, **240**, 40-47.
-

-
- Gonzales-Weimuller, M., Zeisberger, M. & Krishnan, K. M. 2009. Size-dependant heating rates of iron oxide nanoparticles for magnetic fluid hyperthermia. *Journal of Magnetism and Magnetic Materials*, **321**, 1947-1950.
- González-Carreño, T., Morales, M. P., Gracia, M. & Serna, C. J. 1993. Preparation of uniform [gamma]-Fe₂O₃ particles with nanometer size by spray pyrolysis. *Materials Letters*, **18**, 151-155.
- Goodman, T. T., Olive, P. L. & Pun, S. H. 2007. Increased nanoparticle penetration in collagenase-treated multicellular spheroids. *International Journal of Nanomedicine*, **2**, 265-274.
- Gou, M., Qian, Z., Wang, H., Tang, Y., Huang, M., Kan, B., Wen, Y., Dai, M., Li, X., Gong, C. & Tu, M. 2008. Preparation and characterization of magnetic poly(ε-caprolactone) poly(ethylene glycol)-poly(ε-caprolactone) microsphere. *Journal of Materials Science: Materials in Medicine*, **19**, 1033-1041.
- Grantab, R., Sivanathan, S. & Tannock, I. F. 2006. The Penetration of Anticancer Drugs through Tumor Tissue as a Function of Cellular Adhesion and Packing Density of Tumor Cells. *Cancer Research*, **66**, 1033-1039.
- Gref, R., Lück, M., Quellec, P., Marchand, M., Dellacherie, E., HARNISCH, S., Blunk, T. & Müller, R. H. 2000. 'Stealth' corona-core nanoparticles surface modified by polyethylene glycol (PEG): influences of the corona (PEG chain length and surface density) and of the core composition on phagocytic uptake and plasma protein adsorption. *Colloids and Surfaces B: Biointerfaces*, **18**, 301-313.
- Gref, R., Minamitake, Y., Peracchia, M. T., Trubetskoy, V., Torchilin, V. & Langer, R. 1994a. Biodegradable long-circulating polymeric nanospheres. *Science*, **263**, 1600-1603.
- Gupta, A. K. & Curtis, A. S. 2004a. Lactoferrin and ceruloplasmin derivatized superparamagnetic iron oxide nanoparticles for targeting cell surface receptors. *Biomaterials*, **25**, 3029-3040.
- Gupta, A. K. & Gupta, M. 2005. Synthesis and surface engineering of iron oxide nanoparticles for biomedical applications. *Biomaterials*, **26**, 3995-4021.
- Gupta, A. K. & Wells, S. 2004. Surface-Modified Superparamagnetic Nanoparticles for Drug Delivery: Preparation, Characterization, and Cytotoxicity Studies. *IEEE transactions on nanobioscience*, **3**, 66-73.

-
- Hadjipanayis, G. C. & Siegel, R. W. Year. Nanophase materials, synthesis, properties, applications : proceedings of the NATO Advanced Study Institute on Nanophase Materials, Synthesis, Properties, Application. *In*, 1994 1993 *Dordrecht; Boston. Kluwer Academic Publishers*.
- Häfeli, U. O., Riffle, J. S., Harris-Shekhawat, L., Carmichael-Baranauskas, A., Mark, F., Dailey, J. P. & Bardenstein, D. 2009. Cell Uptake and *in Vitro* Toxicity of Magnetic Nanoparticles Suitable for Drug Delivery. *Molecular Pharmaceutics*, **6**, 1417-1428.
- Hamoudeh, M., Faraj, A. A., Canet-Soulas, E., Bessueille, F., Léonard, D. & Fessi, H. 2007. Elaboration of PLLA-based superparamagnetic nanoparticles: Characterization, magnetic behaviour study and *in vitro* relaxivity evaluation. *International Journal of Pharmaceutics*, **338**, 248-257.
- Hanns-Joachim, W., Wolfgang, E., Bernd, M. & Heribert, S.-W. 2003. Tissue-specific MR contrast agents. *European journal of radiology*, **46**, 33-44.
- Harisinghani, M. G., Saini, S., Weissleder, R., Halpern, E. F., Schima, W., Rubin, D. L., Stillman, A. E., Sica, G. T., Small, W. C. & Hahn, P. F. 1997. Differentiation of liver hemangiomas from metastases and hepatocellular carcinoma at MR imaging enhanced with blood-pool contrast agent Code-7227. *Radiology*, **202**, 687-91.
- Harris, J. M. & Chess, R. B. 2003. Effect of pegylation on pharmaceuticals. *Nature Reviews Drug Discovery*, **2**, 214-221.
- Hergt, R., Hiergeist, R., Hilger, I., Kaiser, W. A., Lapatnikov, Y., Margel, S. & Richter, U. 2004. Maghemite nanoparticles with very high AC-losses for application in RF-magnetic hyperthermia. *Journal of Magnetism and Magnetic Materials*, **270**, 345-357.
- Hern, D. L. & Hubbell, J. A. 1998. Incorporation of adhesion peptides into nonadhesive hydrogels useful for tissue resurfacing. *Journal of Biomedical Materials Research*, **39**, 266-276.
- Herrmann, J. & Bodmeier, R. 1998. Biodegradable, somatostatin acetate containing microspheres prepared by various aqueous and non-aqueous solvent evaporation methods. *European Journal of Pharmaceutics and Biopharmaceutics*, **45**, 75-82.
- Hildebrandt, N., Hermsdorf, D., Signorell, R., Schmitz, S. A. & Diederichsen, U. 2007. Superparamagnetic iron oxide nanoparticles functionalized with peptides by electrostatic interactions. *Arkivoc*, 79-90.

-
- Hindle, A. J. & Perkins, A. C. 1995. History and basic principle of echo-contrast media. *Ultrasound in Medicine & Biology*, **3**, 17-23.
- Hong, R. Y., Li, J. H., Qu, J. M., Chen, L. L. & Li, H. Z. 2009. Preparation and characterization of magnetite/dextran nanocomposite used as a precursor of magnetic fluid. *Chemical Engineering Journal*, **150**, 572-580.
- Horák, D., Petrovský, E., Kapicka, A. & Frederichs, T. 2007. Synthesis and characterization of magnetic poly(glycidyl methacrylate) microspheres. *Journal of Magnetism and Magnetic Materials*, **311**, 500-506.
- Hoste, K., Bruneel, D., Demarre, A., Deschrijver, F. & Schacht, E. 1994. Synthesis and Characterization of Poly(oxyethylene) Modified Dextrans. *Macromolecular Rapid Communications*, **15**, 697-704.
- Hu, F. X., Neoh, K. G. & Kang, E. T. 2006. Synthesis and *in vitro* anti-cancer evaluation of tamoxifen-loaded magnetite/PLLA composite nanoparticles. *Biomaterials*, **27**, 5725-5733.
- Hu, L., Hach, D., Chaumont, D., Brachais, C. H. & Couvercelle, J. P. 2008. One step grafting of monomethoxy poly(ethylene glycol) during synthesis of maghemite nanoparticles in aqueous medium. *Colloids and Surfaces A: Physicochemical and Engineering Aspects*, **330**, 1-7.
- Hu, Y., Xie, J., Tong, Y. W. & Wang, C.-H. 2007. Effect of PEG conformation and particle size on the cellular uptake efficiency of nanoparticles with the HepG2 cells. *Journal of Controlled Release*, **118**, 7-17.
- Huang, H., Xie, Q., Kang, M., Zhang, B., Zhang, H., Chen, J., Zhai, C., Yang, D., Jiang, B. & Wu, Y. 2009. Labeling transplanted mice islet with polyvinylpyrrolidone coated superparamagnetic iron oxide nanoparticles for *in vivo* detection by magnetic resonance imaging. *Nanotechnology*, **20**, (9.pp)
- Huber, D. L. 2005. Synthesis, properties, and applications of iron nanoparticles. *Small*, **1**, 482-501.
- Hume, D. A. 2006. The mononuclear phagocyte system. *Current Opinion in Immunology*, **18**, 49-53.
- Ibrahim, M., Serrano, K. G., Noe, L., Garcia, C. & Verelst, M. 2009. Electro-precipitation of magnetite nanoparticles: An electrochemical study. *Electrochimica Acta*, **55**, 155-158.
-

-
- Illum, L., Church, A. E., Butterworth, M. D., Arien, A., Whetstone, J. & DAVIS, S. S. 2001. Development of systems for targeting the regional lymph nodes for diagnostic imaging: *in vivo* behaviour of colloidal PEG-coated magnetite nanospheres in the rat following interstitial administration. *Pharmaceutical Research*, **18**, 640-5.
- Illum, L., Davis, S. S., Müller, R. H., Mak, E. & West, P. 1987. The organ distribution and circulation time of intravenously injected colloidal carriers sterically stabilized with a blockcopolymer - poloxamine 908. *Life Sciences*, **40**, 367-374.
- Illum, L., Davis, S. S. & Wilson, C. G. 1982. Blood clearance and organ deposition of intravenously administered colloidal particles. The effects of particle size, nature and shape. *International Journal of Pharmaceutics*, **12**, 135-146.
- Jaeghere, F., Allemann, E., Feijen, J., Kissel, T., Doelker, E. & Gurny, R. 2000. Cellular Uptake of PEO Surface-Modified Nanoparticles: Evaluation of Nanoparticles Made of PLA: PEO Diblock and Triblock Copolymers. *Journal of Drug Targeting*, **8**, 143-153.
- Jafari, T., Simchi, A. & Khakpash, N. 2010. Synthesis and cytotoxicity assessment of superparamagnetic iron-gold core-shell nanoparticles coated with polyglycerol. *Journal of Colloid and Interface Science*, **345**, 64-71.
- Jain, R. K. 2001. Delivery of molecular and cellular medicine to solid tumors. *Advanced Drug Delivery Reviews*, **46**, 149-168.
- Jain, T. K., Richey, J., Strand, M., Leslie-Pelecky, D. L., Flask, C. A. & Labhasetwar, V. 2008a. Magnetic nanoparticles with dual functional properties: drug delivery and magnetic resonance imaging. *Biomaterials*, **29**, 4012-21.
- Jain, T. K., Richey, J., Strand, M., Leslie-Pelecky, D. L., Flask, C. A. & Labhasetwar, V. 2008b. Magnetic nanoparticles with dual functional properties: Drug delivery and magnetic resonance imaging. *Biomaterials*, **29**, 4012-4021.
- Jang, J. H. & Lim, H. B. 2010. Characterization and analytical application of surface modified magnetic nanoparticles. *Microchemical Journal*, **94**, 148-158.
- Jarrett, B., Frendo, M., Vogan, J. & Louie, A. 2007. Size-controlled synthesis of dextran sulfate coated iron oxide nanoparticles for magnetic resonance imaging. *Nanotechnology*, **18**, 035603.
-

-
- Jeong, B., Bae, Y. H., Lee, D. S. & Kim, S. W. 1997. Biodegradable block copolymers as injectable drug-delivery systems. *Nature*, **388**, 860-2.
- Jeong, J., Ha, T. H. & Chung, B. H. 2006. Enhanced reusability of hexa-arginine-tagged esterase immobilized on gold-coated magnetic nanoparticles. *Analytica chimica acta.*, **569**, 203.
- Jiu, J., Ge, Y., Li, X. & Nie, L. 2002. Preparation of Co₃O₄ nanoparticles by a polymer combustion route. *Materials Letters*, **54**, 260-263.
- Jo, J.-I., Aoki, I. & Tabata, Y. 2010. Design of iron oxide nanoparticles with different sizes and surface charges for simple and efficient labeling of mesenchymal stem cells. *Journal of Controlled Release*, **142**, 465-473.
- Johnston, H. J., Semmler-Behnke, M., Brown, D. M., Kreyling, W., Tran, L. & Stone, V. 2010. Evaluating the uptake and intracellular fate of polystyrene nanoparticles by primary and hepatocyte cell lines *in vitro*. *Toxicology and Applied Pharmacology*, **242**, 66-78.
- Jolivet, J.-P., Henry, M. & Livage, J. 2000. Metal oxide chemistry and synthesis : from solution to solid state, Chichester, John. Wiley & sons.
- Jolivet, J. P., Belleville, P., Tronc, E. & Livage, J. 1992. Influence of Fe(II) on The Formation of The Spinel Iron-Oxide in Alkaline-Medium. *Clays and Clay Minerals*, **40**, 531-539.
- Jolivet, J. P., Chanéac, C., Vayssières, L. & Tronc, E. 1997. Wet chemistry of spinel iron oxide nanoparticles. *Journal of Physical*, IV, 481-7.
- Jolivet, J. P. & Massart, R. F., J.-M 1983. Synthesis and non-magnetic colloids physicochemical surfactant environment aqueous. *New Journal of Chemistry.*, **7**, 325–331.
- Jones, M.-C. & Leroux, J.-C. 1999. Polymeric micelles - a new generation of colloidal drug carriers. *European Journal of Pharmaceutics and Biopharmaceutics*, **48**, 101-111.
- Jordan, A., Scholz, R., Wust, P., Fähling, H. & Roland, F. 1999. Magnetic fluid hyperthermia (MFH): Cancer treatment with AC magnetic field induced excitation of biocompatible superparamagnetic nanoparticles. *Journal of Magnetism and Magnetic Materials*, **201**, 413-419.
-

-
- Jordan, A., Wust, P., Fahling, H., John, W., Hinz, A. & Felix, R. 1993. Inductive heating of ferrimagnetic particles and magnetic fluids: physical evaluation of their potential for hyperthermia. *International Journal of Hyperthermia*, **9**, 51-68.
- Kallinteri, P., Higgins, S., Hutcheon, G. A., ST Pourcain, C. B. & Garnett, M. C. 2005. Novel functionalized biodegradable polymers for nanoparticle drug delivery systems. *Biomacromolecules*, **6**, 1885-94.
- Kang, Y., Risbud, S., Rabolt, J. & Stroeve, P. 1996. Synthesis and Characterization of Nanometer-Size Fe₃O₄ and γ -Fe₂O₃ Particles. *Chemistry of Materials*, **8**, 2209-2211.
- Kawaguchi, T., Hanaichi, T., Hasegawa, M. & Maruno, S. 2001. Dextran-magnetite complex: conformation of dextran chains and stability of solution. *Journal of Materials Science-Materials in Medicine*, **12**, 121-127.
- Kayal, S. & Ramanujan, R. V. 2010. Doxorubicin loaded PVA coated iron oxide nanoparticles for targeted drug delivery. *Materials Science and Engineering: C*, **30**, 484-490.
- Khosroshahi, M. E. & Ghazanfari, L. 2010. Preparation and characterization of silica-coated iron-oxide bionanoparticles under N₂ gas. *Physica E: Low-dimensional Systems and Nanostructures*, **42**, 1824-1829.
- Kiessling-Cooper, A. & Anderson, S. 2003. Human embryonic stem cells : an introduction to the science and therapeutic potential, *Sudbury, Mass., Jones and Bartlett*.
- Kim, D. K., Mikhaylova, M., Wang, F. H., Kehr, J., Bjelke, B., Zhang, Y., Tsakalacos, T. & Muhammed, M. 2003a. Starch-Coated Superparamagnetic Nanoparticles as MR Contrast Agents. *Chemistry of Materials*, **15**, 4343-4351.
- Kim, D. K., Mikhaylova, M., Zhang, Y. & Muhammed, M. 2003b. Protective Coating of Superparamagnetic Iron Oxide Nanoparticles. *Chemistry of Materials*, **15**, 1617-1627.
- Kim, D. K., Zhang, Y., Voit, W., Rao, K. V. & Muhammed, M. 2001. Synthesis and characterization of surfactant-coated superparamagnetic monodispersed iron oxide nanoparticles. *Journal of Magnetism and Magnetic Materials*, **225**, 30-36.
-

-
- Kim, E. H., Ahn, Y. & Lee, H. S. 2007. Biomedical applications of superparamagnetic iron oxide nanoparticles encapsulated within chitosan. *Journal of Alloys and Compounds*, **434-435**, 633-636.
- Kim, S. H., Won, C. Y. & Chu, C. C. 1999. Synthesis and characterization of dextran-maleic acid based hydrogel. *Journal of Biomedical Materials Research*, **46**, 160-70.
- Kim, T., Reis, L., Rajan, K. & Shima, M. 2005a. Magnetic behavior of iron oxide nanoparticle-biomolecule assembly. *Journal of Magnetism and Magnetic Materials*, **295**, 132-138.
- Kim, Y. W., Shick Ahn, W., Kim, J. J. & Ha Kim, Y. 2005b. In situ fabrication of self-transformable and hydrophilic poly(ethylene glycol) derivative-modified polysulfone membranes. *Biomaterials*, **26**, 2867-75.
- Kneuer, C., Sameti, M., Haltner, E. G., Schiestel, T., Schirra, H., Schmidt, H. & Lehr, C.-M. 2000. Silica nanoparticles modified with aminosilanes as carriers for plasmid DNA. *International Journal of Pharmaceutics*, **196**, 257-261.
- Koenig, S. H. & Kellar, K. E. 1995. Theory of 1/T1 and 1/T2 NMRD profiles of solutions of magnetic nanoparticles. *Magnetic Resonance in Medicine*, **34**, 227-33.
- Kresse M, W. S., Pfefferer D, Lawaczeck R, Elste V, Semmler W. 1998. Targeting of ultrasmall superparamagnetic iron oxide (USPIO) particles to tumor cells *in vivo* by using transferrin receptor pathways. *Magnetic Resonance in Medicine*, **40**, 236-242.
- Kreuter, J. 1983. Evaluation of nanoparticles as drug-delivery systems. I.Preparation methods. *Pharmaceutica Acta Helvetiae*, **58**, 196-209.
- Kreuter, J. 2001. Nanoparticulate systems for brain delivery of drugs. *Advanced Drug Delivery Reviews*, **47**, 65-81.
- Kreuter, J., Alyautdin, R. N., Kharkevich, D. A. & Ivanov, A. A. 1995. Passage of peptides through the blood-brain barrier with colloidal polymer particles (nanoparticles). *Brain Research*, **674**, 171-4.
- Kryszewski, M. & Jeszka, J. K. 1998. Nanostructured conducting polymer composites -- superparamagnetic particles in conducting polymers. *Synthetic Metals*, **94**, 99-104.
-

-
- Kubaska, S., Sahani, D. V., Saini, S., Hahn, P. F. & Halpern, E. 2001. Dual contrast enhanced magnetic resonance imaging of the liver with superparamagnetic iron oxide followed by gadolinium for lesion detection and characterization. *Clinical Radiology*, **56**, 410-5.
- Kumagai, M., Kano, M. R., Morishita, Y., Ota, M., Imai, Y., Nishiyama, N., Sekino, M., Ueno, S., Miyazono, K. & Kataoka, K. 2009. Enhanced magnetic resonance imaging of experimental pancreatic tumor *in vivo* by block copolymer-coated magnetite nanoparticles with TGF- β inhibitor. *Journal of Controlled Release*, **140**, 306-311.
- Kumari, A., Yadav, S. K. & Yadav, S. C. 2009. Biodegradable polymeric nanoparticles based drug delivery systems. *Colloids and Surfaces B: Biointerfaces*, **75**, 1-18.
- Kuppen, P. J. K., Van Der Eb, M. M., Jonges, L. E., Hagenaars, M., Hokland, M. E., Nannmark, U., Goldfarb, R. H., Basse, P. H., Fleuren, G. J., Hoeben, R. C. & Van De Velde, C. J. H. 2001. Tumor structure and extracellular matrix as a possible barrier for therapeutic approaches using immune cells or adenoviruses in colorectal cancer. *Histochemistry and Cell Biology*, **115**, 67-72.
- Laconte, L., Nitin, N. & Bao, G. 2005. Magnetic nanoparticle probes. *Materials Today*, **8**, 32-38.
- Laurent, S., Forge, D., Port, M., Roch, A., Robic, C., Vander Elst, L. & Muller, R. N. 2008. Magnetic Iron Oxide Nanoparticles: Synthesis, Stabilization, Vectorization, Physicochemical Characterizations, and Biological Applications. *Chemical Reviews*, **108**, 2064-2110.
- Le Renard, P.-E., Jordan, O., Faes, A., Petri-Fink, A., Hofmann, H., Rüfenacht, D., Bosman, F., Buchegger, F. & Doelker, E. 2010. The *in vivo* performance of magnetic particle-loaded injectable, in situ gelling, carriers for the delivery of local hyperthermia. *Biomaterials*, **31**, 691-705.
- Lee, C. M., Jeong, H. J., Kim, E. M., Cheong, S. J., Park, E. H., Kim, D. W., Lim, S. T. & Sohn, M. H. 2009. Synthesis and Characterization of Iron Oxide Nanoparticles Decorated with Carboxymethyl Curdlan. *Macromolecular Research*, **17**, 133-136.
- Lee, E. S. M., Shuter, B., Chan, J., Chong, M. S. K., Ding, J., Teoh, S.-H., Beuf, O., Briguet, A., Tam, K. C., Choolani, M. & Wang, S.-C. 2010. The use of microgel iron oxide nanoparticles in studies of magnetic resonance relaxation and endothelial progenitor cell labelling. *Biomaterials*, **31**, 3296-3306.
-

-
- Lee, H., Lee, E., Kim, D. K., Jang, N. K., Jeong, Y. Y. & Jon, S. 2006. Antibiofouling Polymer-Coated Superparamagnetic Iron Oxide Nanoparticles as Potential Magnetic Resonance Contrast Agents for *in Vivo* Cancer Imaging. *Journal of the American Chemical Society*, **128**, 7383-7389.
- Lee, J., Isobe, T. & Senna, M. 1996. Preparation of Ultrafine Fe₃O₄ Particles by Precipitation in the Presence of PVA at High pH. *Journal of Colloid and Interface Science*, **177**, 490-494.
- Lee, K., Kim, S.-G., Kim, W.-S. & Kim, S. 2002. Properties of iron oxide particles prepared in the presence of dextran. *Korean Journal of Chemical Engineering*, **19**, 480-485.
- Lee, S.-J., Jeong, J.-R., Shin, S.-C., Kim, J.-C., Chang, Y.-H., Chang, Y.-M. & Kim, J. D. J.-D. 2004. Nanoparticles of magnetic ferric oxides encapsulated with poly(D,L lactide-co-glycolide) and their applications to magnetic resonance imaging contrast agent. *Journal of Magnetism and Magnetic Materials*, **272-276**, 2432-2433.
- Lee, S.-J., Jeong, J.-R., Shin, S.-C., Kim, J.-C., Chang, Y.-H., Lee, K.-H. & Kim, J.-D. 2005. Magnetic enhancement of iron oxide nanoparticles encapsulated with poly(d,l-lactide-co-glycolide). *Colloids and Surfaces A: Physicochemical and Engineering Aspects*, **255**, 19-25.
- Lesot, P., Chapuis, S., Pierre Bayle, J., Rault, J., Lafontaine, E., Campero, A. & Judeinstein, P. 1998. Structural-dynamical relationship in silica PEG hybrid gels. *Journal of Materials Chemistry*, **8**, 147-151.
- Li, Z., Wei, L., Gao, M. Y. & Lei, H. 2005. One-Pot Reaction to Synthesize Biocompatible Magnetite Nanoparticles. *Advanced materials*, **17**, 1001.
- Lien, Y.-H. & Wu, T.-M. 2008. Preparation and characterization of thermosensitive polymers grafted onto silica-coated iron oxide nanoparticles. *Journal of Colloid and Interface Science*, **326**, 517-521.
- Lin, H.-Y., Chen, Y.-W. & Wang, W.-J. 2005. Preparation of nanosized iron oxide and its application in low temperature CO oxidation. *Journal of Nanoparticle Research*, **7**, 249-263.
- Lin, M. M., Kim Do, K., El Haj, A. J. & Dobson, J. 2008. Development of superparamagnetic iron oxide nanoparticles (SPIONS) for translation to clinical applications. *IEEE Trans Nanobioscience*, **7**, 298-305.

-
- Lin, S.-Y., Ho, L.-T. & Chiou, H.-L. 1985. Microencapsulation and Controlled Release of Insulin from Polylactic Acid Microcapsules. **13**, 187-201.
- Liu, H., Hou, P., Zhang, W. & Wu, J. 2010. Synthesis of monosized core-shell Fe₃O₄/Au multifunctional nanoparticles by PVP-assisted nanoemulsion process. *Colloids and Surfaces A: Physicochemical and Engineering Aspects*, **356**, 21-27.
- Liu, X., Kaminski, M. D., Chen, H., Torno, M., Taylor, L. & Rosengart, A. J. 2007. Synthesis and characterization of highly-magnetic biodegradable poly(d,l-lactide-co-glycolide) nanospheres. *Journal of Controlled Release*, **119**, 52-58.
- Lobel, B., Eyal, O., Kariv, N. & Katzir, A. 2000. Temperature controlled CO₂ laser welding of soft tissues: Urinary bladder welding in different animal models (rats, rabbits, and cats). *Lasers in Surgery and Medicine*, **26**, 4-12.
- Lok, C. 2001. Picture perfect. *Nature*, **412**, 372-374.
- López-Viota, J., Mandal, S., Delgado, A. V., Toca-Herrera, J. L., Möller, M., Zanuttin, F., Balestrino, M. & Krol, S. 2009. Electrophoretic characterization of gold nanoparticles functionalized with human serum albumin (HSA) and creatine. *Journal of Colloid and Interface Science*, **332**, 215-223.
- Lopez-Quintela, M. A. & Rivas, J. 1993. Chemical-Reactions in microemulsions - a powerful method to obtain ultrafine particles. *Journal of Colloid and Interface Science*, **158**, 446-451.
- Lorenz, M. R., Holzapfel, V., Musyanovych, A., Nothelfer, K., WALTHER, P., Frank, H., Landfester, K., Schrezenmeier, H. & Mailänder, V. 2006. Uptake of functionalized, fluorescent-labeled polymeric particles in different cell lines and stem cells. *Biomaterials*, **27**, 2820-2828.
- Lu, Q. H., Yao, K. L., Xi, D., Liu, Z. L., Luo, X. P. & Ning, Q. 2006. Synthesis and characterization of composite nanoparticles comprised of gold shell and magnetic core/cores. *Journal of Magnetism and Magnetic Materials*, **301**, 44-49.
- Lu, W., Zhang, Y., Tan, Y. Z., Hu, K. L., Jiang, X. G. & Fu, S. K. 2005. Cationic albumin-conjugated pegylated nanoparticles as novel drug carrier for brain delivery. *Journal of Control Release*, **107**, 428-48.
- Lubbe, A. S., Alexiou, C. & Bergemann, C. 2001. Clinical applications of magnetic drug targeting. *Journal of Surgical Research*, **95**, 200-6.
-

-
- Lubbe, A. S., Bergemann, C., Huhnt, W., Fricke, T., Riess, H., Brock, J. W. & Huhn, D. 1996. Preclinical experiences with magnetic drug targeting: tolerance and efficacy. *Cancer Research*, **56**, 4694-701.
- Luckarift, H. R., Spain, J. C., Naik, R. R., and Stone, M. O. 2004 Enzyme Immobilization in a Biomimetic Silica Support. *Nature Biotechnology*, **22**, 211-213.
- Lutz, J.-F. O., Stiller, S., Hoth, A., Kaufner, L., Pison, U. & Cartier, R. G. 2006. One-Pot Synthesis of PEGylated Ultrasmall Iron-Oxide Nanoparticles and Their *in Vivo* Evaluation as Magnetic Resonance Imaging Contrast Agents. *Biomacromolecules*, **7**, 3132-3138.
- Ma, H.-L., Qi, X.-R., Maitani, Y. & Nagai, T. 2007. Preparation and characterization of superparamagnetic iron oxide nanoparticles stabilized by alginate. *International Journal of Pharmaceutics*, **333**, 177-186.
- Ma, H. L., Xu, Y. F., Qi, X. R., Maitani, Y. & Nagai, T. 2008. Superparamagnetic iron oxide nanoparticles stabilized by alginate: Pharmacokinetics, tissue distribution, and applications in detecting liver cancers. *International Journal of Pharmaceutics*, **354**, 217-226.
- Ma, Y.-H., Wu, S.-Y., Wu, T., Chang, Y.-J., Hua, M.-Y. & Chen, J.-P. 2009. Magnetically targeted thrombolysis with recombinant tissue plasminogen activator bound to polyacrylic acid-coated nanoparticles. *Biomaterials*, **30**, 3343-3351.
- Maaßen, S., Fattal, E., Mueller, R. H. & Couvreur, P. 1993. Cell cultures for the assessment of toxicity and uptake of polymeric particulate drug carriers. *STP Pharma Sciences*, **3**, 11.
- Mahmoudi, M., Simchi, A., Imani, M., Stroeve, P. & Sohrabi, A. 2010. Templated growth of superparamagnetic iron oxide nanoparticles by temperature programming in the presence of poly(vinyl alcohol). *Thin Solid Films*, **518**, 4281-4289.
- Mahmoudi, M., Simchi, A., Milani, A. S. & Stroeve, P. 2009. Cell toxicity of superparamagnetic iron oxide nanoparticles. *Journal of Colloid and Interface Science*, **336**, 510-8.
- Mainardes, R. M. & Evangelista, R. C. 2005a. PLGA nanoparticles containing praziquantel: effect of formulation variables on size distribution. *International Journal of Pharmaceutics*, **290**, 137-144.
-

-
- Maity, D., Choo, S.-G., Yi, J., Ding, J. & Xue, J. M. 2009. Synthesis of magnetite nanoparticles via a solvent-free thermal decomposition route. *Journal of Magnetism and Magnetic Materials*, **321**, 1256-1259.
- Majewski, P. & Thierry, B. 2007. Functionalized Magnetite Nanoparticles - Synthesis, Properties, and Bio-Applications. *Critical Reviews in Solid State and Material Sciences*, **32**, 203-215.
- Massart, R. & Cabuil, V. 1987. Effect of some parameters on the formation of colloidal magnetite in alkaline-medium - yield and particle-size control. *Journal De Chimie Physique Et De Physico-Chimie Biologique*, **84**, 967-973.
- Matsunaga, T., Sato, R., Kamiya, S., Tanaka, T. & Takeyama, H. 1999. Chemiluminescence enzyme immunoassay using ProteinA-bacterial magnetite complex. *Journal of Magnetism and Magnetic Materials*, **194**, 126-131.
- Mauzac, M., J. J. 1984. Anticoagulant activity of dextran derivatives. Part I: Synthesis and characterization *Biomaterials*, **5**, 301-304.
- Meng, W., Kallinteri, P., Walker, D. A., Parker, T. L. & Garnett, M. C. 2007a. Evaluation of Poly (Glycerol-Adipate) Nanoparticle Uptake in an *In Vitro* 3-D Brain Tumor Co-Culture *Experimental Biology and Medicine*, **232**, 1100-1108.
- Meng, W., Parker, T. L., Kallinteri, P., Walker, D. A., Higgins, S., Hutcheon, G. A. & Garnett, M. C. 2006. Uptake and metabolism of novel biodegradable poly (glycerol-adipate) nanoparticles in DAOY monolayer. *Journal of Controlled Release*, **116**, 314-321.
- Mikhaylova, M., Kim, D. K., Berry, C. C., Zagorodni, A., Toprak, M., Curtis, A. S. G. & Muhammed, M. 2004. BSA immobilization on amine-functionalized superparamagnetic iron oxide nanoparticles. *Chemistry of Materials*, **16**, 2344-2354.
- Moghimi, S. M., Hunter, A. C. & Murray, J. C. 2001. Long-Circulating and Target-Specific Nanoparticles: Theory to Practice. *Pharmacological Reviews*, **53**, 283-318.
- Moghimi, S. M., Hunter, A. C. & Murray, J. C. 2005. Nanomedicine: current status and future prospects. *The FASEB Journal*, **19**, 311-330.
-

-
- Molday, R. S. & Mackenzie, D. 1982. Immunospecific ferromagnetic iron-dextran reagents for the labeling and magnetic separation of cells. *Journal of immunological methods*, **52**, 353-67.
- Morales, M. A., Finotelli, P. V., Coaquira, J. A. H., Rocha-Leão, M. H. M., Diaz-Aguila, C., Baggio-Saitovitch, E. M. & Rossi, A. M. 2008. In situ synthesis and magnetic studies of iron oxide nanoparticles in calcium-alginate matrix for biomedical applications. *Materials Science and Engineering: C*, **28**, 253-257.
- Morales, M. P., Bomati-Miguel, O., Pérez De Alejo, R., Ruiz-Cabello, J., Veintemillas-Verdaguer, S. & O'grady, K. 2003. Contrast agents for MRI based on iron oxide nanoparticles prepared by laser pyrolysis. *Journal of Magnetism and Magnetic Materials*, **266**, 102-109.
- Morawski, A. M., Lanza, G. A. & Wickline, S. A. 2005. Targeted contrast agents for magnetic resonance imaging and ultrasound. *Current Opinion in Biotechnology*, **16**, 89-92.
- Mornet, S., Vasseur, S., Grasset, F. & Duguet, E. 2004. Magnetic nanoparticle design for medical diagnosis and therapy. *Journal of Materials Chemistry*, **14**, 2161-2175.
- Mornet, S., Vasseur, S., Grasset, F., Veverka, P., Goglio, G., Demourgues, A., Portier, J., Pollert, E. & Duguet, E. 2006. Magnetic nanoparticle design for medical applications. *Progress in Solid State Chemistry*, **34**, 237-247.
- Moroz, P., Jones, S. K. & Gray, B. N. 2002. Magnetically mediated hyperthermia: current status and future directions. *International Journal of Hyperthermia*, **18**, 267-284.
- Muller, R. H., Luck, M., Harnisch, S. E. A., IN: U. Häufeli, & Et Al. (EDS.) 1997. Scientific and Clinical Applications of Magnetic Carriers. *Plenum Press, New York*, **562**.
- Nam, H. Y., Kwon, S. M., Chung, H., Lee, S.-Y., Kwon, S.-H., Jeon, H., Kim, Y., PARK, j. H., Kim, J., Her, S., Oh, Y.-K., Kwon, I. C., Kim, K. & Jeong, S. Y. 2009. Cellular uptake mechanism and intracellular fate of hydrophobically modified glycol chitosan nanoparticles. *Journal of Controlled Release*, **135**, 259-267.
- Napper, D. H. 1977. Steric stabilization. *Journal of Colloid and Interface Science*, **58**, 390-407.
-

-
- Napper, D. H. 1989. *Polymeric Stabilization of Colloidal Dispersions*. Academic Press, London; New York
- Narita, A., Naka, K. & Chujo, Y. 2009. Facile control of silica shell layer thickness on hydrophilic iron oxide nanoparticles via reverse micelle method. *Colloids and Surfaces A: Physicochemical and Engineering Aspects*, **336**, 46-56.
- Netti, P. A., Berk, D. A., Swartz, M. A., Grodzinsky, A. J. & Jain, R. K. 2000. Role of Extracellular Matrix Assembly in Interstitial Transport in Solid Tumors. *Cancer Research*, **60**, 2497-2503.
- Neuberger, T., Schöpf, B., Hofmann, H., Hofmann, M. & Von Rechenberg, B. 2005. Superparamagnetic nanoparticles for biomedical applications: Possibilities and limitations of a new drug delivery system. *Journal of Magnetism and Magnetic Materials*, **293**, 483-496.
- Ngaboni Okassa, L., Marchais, H., Douziech-Eyrolles, L., Cohen-Jonathan, S., Soucé, M., Dubois, P. & Chourpa, I. 2005. Development and characterization of sub-micron poly(d,l-lactide-co-glycolide) particles loaded with magnetite/maghemite nanoparticles. *International Journal of Pharmaceutics*, **302**, 187-196.
- Nitin, N., Laconte, L. E. W., Zurkiya, O., Hu, X. & Bao, G. 2004. Functionalization and peptide-based delivery of magnetic nanoparticles as an intracellular MRI contrast agent. *Journal of Biological Inorganic Chemistry*, **9**, 706-712.
- Oh, J. K. & Park, J. M. 2011. Iron oxide-based superparamagnetic polymeric nanomaterials: Design, preparation, and biomedical application. *Progress in Polymer Science*, **36**, 168-189.
- Olivier, J.-C., Fenart, L., Chauvet, R., Pariat, C., Cecchelli, R. & Couet, W. 1999. Indirect Evidence that Drug Brain Targeting Using Polysorbate 80-Coated Polybutylcyanoacrylate Nanoparticles Is Related to Toxicity. *Pharmaceutical Research*, **16**, 1836-1842.
- Olsvik, O., Popovic, T., Skjerve, E., Cudjoe, K. S., Hornes, E., Ugelstad, J. & Uhlen, M. 1994. Magnetic separation techniques in diagnostic microbiology. *Clinical Microbiology Reviews*, **7**, 43-54.
- Orson, F. M., Kinsey, B. M., Hua, P. J., Bhogal, B. S., Densmore, C. L. & Barry, M. A. 2000. Genetic immunization with lung-targeting macroaggregated polyethyleneimine-albumin conjugates elicits combined systemic and mucosal immune responses. *Journal of Immunology*, **164**, 6313-21.

-
- Orson, F. M., Song, L., Gautam, A., Densmore, C. L., Bhogal, B. S. & Kinsey, B. M. 2002. Gene delivery to the lung using protein/polyethylenimine/plasmid complexes. *Gene Therapy*, **9**, 463-71.
- Osaka, T., Nakanishi, T., Shanmugam, S., Takahama, S. & Zhang, H. 2009. Effect of surface charge of magnetite nanoparticles on their internalization into breast cancer and umbilical vein endothelial cells. *Colloids and Surfaces B: Biointerfaces*, **71**, 325-330.
- Oster, C., Wittmar, M., Unger, F., Barbu-Tudoran, L., Schaper, A. & Kissel, T. 2004. Design of Amine-Modified Graft Polyesters for Effective Gene Delivery Using DNA-Loaded Nanoparticles. *Pharmaceutical Research*, **21**, 927-931.
- Pain, D., Das, P., Ghosh, P. & Bachhawat, B. 1984. Increased circulatory half-life of liposomes after conjunction with dextran. *Journal of Biosciences*, **6**, 811-816.
- Pan, B.-F., Gao, F. & Gu, H.-C. 2005. Dendrimer modified magnetite nanoparticles for protein immobilization. *Journal of Colloid and Interface Science*, **284**, 1-6.
- Panyam, J. & Labhasetwar, V. 2003. Biodegradable nanoparticles for drug and gene delivery to cells and tissue. *Advanced Drug Delivery Reviews*, **55**, 329-347.
- Panyam, J., Sahoo, S. K., Prabha, S., Bargar, T. & Labhasetwar, V. 2003. Fluorescence and electron microscopy probes for cellular and tissue uptake of poly(D,L-lactide-co-glycolide) nanoparticles. *International Journal of Pharmaceutics*, **262**, 1-11.
- Panyam, J., Zhou, W.-Z., Prabha, S., Sahoo, S. K. & Labhasetwar, V. 2002. Rapid endo-lysosomal escape of poly(DL-lactide-co-glycolide) nanoparticles: implications for drug and gene delivery. *The FASEB Journal*, **16**, 1217-1226.
- Papisov, M. I., Bogdanov Jr, A., Schaffer, B., Nossiff, N., Shen, T., Weissleder, R. & Brady, T. J. 1993. Colloidal magnetic resonance contrast agents: effect of particle surface on biodistribution. *Journal of Magnetism and Magnetic Materials*, **122**, 383-386.
- Park, J., An, K., Hwang, Y., Park, J.-G., Noh, H.-J., Kim, J.-Y., Park, J.-H., Hwang, N.-M. & Hyeon, T. 2004. Ultra-large-scale syntheses of monodisperse nanocrystals. *Nature Materials*, **3**, 891-895.

-
- Patel, D., Moon, J. Y., Chang, Y., Kim, T. J. & Lee, G. H. 2008. Poly(d,l-lactide-co-glycolide) coated superparamagnetic iron oxide nanoparticles: Synthesis, characterization and *in vivo* study as MRI contrast agent. *Colloids and Surfaces A: Physicochemical and Engineering Aspects*, **313-314**, 91-94.
- Pecharromás, C., González-Carreño, T. & Iglesias, J. E. 1995. The infrared dielectric properties of maghemite Fe₂O₃, from reflectance measurement on pressed powders. *Physics and Chemistry of Minerals*, **22**, 21-29.
- Peltonen, L., Koistinen, P., Karjalainen, M., Hakkinen, A. & Hirvonen, J. 2002. The effect of cosolvents on the formulation of nanoparticles from low-molecular-weight poly(l)lactide. *AAPS PharmSciTech*, **3**, E32.
- Perez, J. M., Simeone, F. J., Tsourkas, A., Josephson, L. & Weissleder, R. 2003. Peroxidase Substrate Nanosensors for MR Imaging. *Nano Letters*, **4**, 119-122.
- Perkins, A. 2002. Polymer Conjugates for Imaging. *Journal of Drug Targeting*, 1-3.
- Perkins, A. C. 1998. Polymer Diagnostics: The Next Generation of Image Contrast Agents. *Journal of Drug Targeting*, **6**, 79-84.
- Perry, F. R., Charles, S. O., Alan, C. M., Terrence, G. F. & John, S. L., Jr. 1986. Ferromagnetic contrast agents: A new approach. *Magnetic Resonance in Medicine*, **3**, 217-225.
- Petri-Fink, A., Steitz, B., Finka, A., Salaklang, J. & Hofmann, H. 2008. Effect of cell media on polymer coated superparamagnetic iron oxide nanoparticles (SPIONs): Colloidal stability, cytotoxicity, and cellular uptake studies. *European Journal of Pharmaceutics and Biopharmaceutics*, **68**, 129-137.
- Pierson, H. O. 1999. *Handbook of chemical vapor deposition (CVD) principles, technology, and applications* [Online]. Norwich, NY: Knovel [Online-Anbieter]. [Accessed].
- Pinna, N., Grancharov, S., Beato, P., Bonville, P., Antonietti, M. & Niederberger, M. 2005. Magnetite Nanocrystals: Nonaqueous Synthesis, Characterization, and Solubility *Chemistry of Materials*, **17**, 3044-3049.
- Pinto Reis, C., Neufeld, R.J., Ribeiro, A. J. & Veiga, F. 2006. Nanoencapsulation I. Methods for preparation of drug-loaded polymeric nanoparticles. *Nanomedicine: Nanotechnology, Biology and Medicine*, **2**, 8-21.

-
- Piskin, E., Kaitian, X., Denkbaz, E. B. & Kucukyavuz, Z. 1995. Novel pdlla/peg copolymer micelles as drug carriers. *Journal of Biomaterials Science-Polymer Edition*, **7**, 359-373.
- Pluen, A., Boucher, Y., Ramanujan, S., Mckee, T. D., Gohongi, T., Di Tomaso, E., Brown, E. B., Izumi, Y., Campbell, R. B., Berk, D. A. & Jain, R. K. 2001. Role of tumor-host interactions in interstitial diffusion of macromolecules: Cranial vs. subcutaneous tumors. *Proceedings of the National Academy of Sciences of the United States of America*, **98**, 4628-4633.
- Prashant, C., Dipak, M., Yang, C.-T., Chuang, K.-H., Jun, D. & Feng, S.-S. 2010. Superparamagnetic iron oxide - Loaded poly (lactic acid)-d-[alpha]-tocopherol polyethylene glycol 1000 succinate copolymer nanoparticles as MRI contrast agent. *Biomaterials*, In Press, Corrected Proof.
- Pratsinis, S. E. & Vemury, S. 1996. Particle formation in gases: A review. *Powder Technology*, **88**, 267-273.
- Prene, P., Tronc, E., Jolivet, J.-P., Livage, J., Cherkaoui, R., Nogues, M., Dormann, J.-L. & Fiorani, D. 1993. Magnetic properties of isolated γ -Fe₂O₃ particles. *IEEE Transactions on Magnetics*, **29**, 2658-2660.
- Prozorov, T., Kataby, G., Prozorov, R. & Gedanken, A. 1999. Effect of surfactant concentration on the size of coated ferromagnetic nanoparticles. *Thin Solid Films*, **340**, 189-193.
- Puri, S., Kallinteri, P., Higgins, S., Hutcheon, G. A. & Garnett, M. C. 2008. Drug incorporation and release of water soluble drugs from novel functionalised poly(glycerol adipate) nanoparticles. *Journal of Controlled Release*, **125**, 59-67.
- Qu, J., Liu, G., Wang, Y. & Hong, R. 2010. Preparation of Fe₃O₄-chitosan nanoparticles used for hyperthermia. *Advanced Powder Technology*, In Press, Corrected Proof.
- Qu, S., Yang, H., Ren, D., Kan, S., Zou, G., Li, D. & Li, M. 1999. Magnetite Nanoparticles Prepared by Precipitation from Partially Reduced Ferric Chloride Aqueous Solutions. *Journal of Colloid and Interface Science*, **215**, 190-192.
- Quintanar-Guerrero, D., Allemann, E., Fessi, H. & Doelker, E. 1998. Preparation techniques and mechanisms of formation of biodegradable nanoparticle from preformed polymers. *Drug Development and Industrial Pharmacy*, **24**, 1113-28.
-

-
- Ralph, W., Hui-Cheng, C., Anna, B. & Alexei, B., Jr. 1997. Magnetically labeled cells can be detected by MR imaging. *Journal of Magnetic Resonance Imaging*, **7**, 258-263.
- Rannard, S. P. & Davis, N. J. 1999. Controlled Synthesis of Asymmetric Dialkyl and Cyclic Carbonates Using the Highly Selective Reactions of Imidazole Carboxylic Esters. *Organic Letters*, **1**, 933-936.
- Rannard, S. P. & Davis, N. J. 2000. The Selective Reaction of Primary Amines with Carbonyl Imidazole Containing Compounds: Selective Amide and Carbamate Synthesis. *Organic Letters*, **2**, 2117-2120.
- Raynal, I., Prigent, P., Peyramaure, S., Najid, A., Rebuzzi, C. C. & Corot, C. 2004. Macrophage Endocytosis of Superparamagnetic Iron Oxide Nanoparticles: Mechanisms and Comparison of Ferumoxides and Ferumoxtran-10. *Investigative Radiology*, **39**, 56-63.
- Reetz, M. T., Zonta, A., Vijayakrishnan, V. & Schimossek, K. 1998. Entrapment of lipases in hydrophobic magnetite containing sol gel materials: magnetic separation of heterogeneous biocatalysts. *Journal of Molecular Catalysis A: Chemical*, **134**, 251-258.
- Reimers, G. W. & Khalafalla, S. E. 1972. Preparing magnetic fluids by a peptizing method, [Washington], USA Department of the interior
- Rémi. H., F. C., Jacqueline.J. 1998. Carboxymethylation of dextran in aqueous alcohol as the first step of the preparation of derivatized dextrans. *Macromolecular Materials and Engineering* **254**, 61 - 65.
- Rieger, J., Stoffelbach, F., Cui, D., Imberty, A., Lameignere, E., Putaux, J.-L., Jérôme, R., Jérôme, C. & Auzély-Velty, R. 2007. Mannosylated Poly(ethylene oxide)-bPoly(ϵ -caprolactone) Diblock Copolymers: Synthesis, Characterization, and Interaction with a Bacterial Lectin *Biomacromolecules*, **8**, 2717-2725.
- Riley, T., Govender, T., Stolnik, S., Xiong, C. D., Garnett, M. C., Illum, L. & Davis, S. S. 1999. Colloidal stability and drug incorporation aspects of micellar like PLA PEG nanoparticles. *Colloids and Surfaces B: Biointerc*, **16**, 147-159.
- Robert, E., Jenny, B. D. & Napper, D. H. 1972. The preparation of aqueous entropically stabilized latices. *Journal of Polymer Science Part B: PolymrLett-ers*, **10**, 449-453.
-

-
- Rocher, V., Bee, A., Siaugue, J.-M. & Cabuil, V. 2010. Dye removal from aqueous solution by magnetic alginate beads crosslinked with epichlorohydrin. *Journal of Hazardous Materials*, **178**, 434-439.
- Rotureau, E., Raynaud, J., Choquenot, B., Marie, E., Nouvel, C., Six, J. L., Dellacherie, E. & Durand, A. 2008. Application of amphiphilic polysaccharides as stabilizers in direct and inverse free-radical miniemulsion polymerization. *Colloids and Surfaces A: Physicochemical and Engineering Aspects*, **331**, 84-90.
- Rowland, R. E. S., Taylor, P. W. & Florence, A. T. 2005. Attachment, uptake and transport of nanoparticles coated with an internalin A fragment in Caco-2 cell monolayers. *Journal of Drug Delivery Science and Technology*, **15**, 313-317.
- Saboktakin, M. R., Tabatabaie, R. M., Maharramov, A. & Ramazanov, M. A. 2010. A synthetic macromolecule as MRI detectable drug carriers: Aminodextran-coated iron oxide nanoparticles. *Carbohydrate Polymers*, **80**, 695-698.
- Saga, T., Neumann, R. D., Heya, T., Sato, J., Kinuya, S., Le, N., Paik, C. H. & Weinstein, J. N. 1995. Targeting cancer micrometastases with monoclonal-antibodies-a binding-site barrier. *Proceedings of the National Academy of Sciences of the United States of America*, **92**, 8999-9003.
- Saini, S., Stark, D. D. & Hahn, P. F. 1987. Ferrite particles: A superparamagnetic MR contrast agent for enhanced detection of liver carcinoma. *Radiology*, **162**, 217-222.
- Salazar-Alvarez, G., Muhammed, M. & Zagorodni, A. A. 2006. Novel flow injection synthesis of iron oxide nanoparticles with narrow size distribution. *Chemical Engineering Science*, **61**, 4625-4633.
- Santarelli, X., Muller, D. & Jozefonvicz, J. 1988. Dextran-coated silica packings for high-performance size-exclusion chromatography of proteins. *Journal of Chromatography A*, **443**, 55-62.
- Schneider, M., Bussat, P., Barrau, M. B., Arditi, M., Yan, F. & Hybl, E. 1992. Polymeric microballoons as ultrasound contrast agents. Physical and ultrasonic properties compared with sonicated albumin. *Investigative radiology*, **27**, 134-9.

-
- Schöpf, B., Neuberger, T., Schulze, K., Petri, A., Chastellain, M., Hofmann, M., Hofmann, H. & Von Rechenberg, B. 2005. Methodology description for detection of cellular uptake of PVA coated superparamagnetic iron oxide nanoparticles (SPION) in synovial cells of sheep. *Journal of Magnetism and Magnetic Materials*, **293**, 411-418.
- Schulze, K., Koch, A., Petri-Fink, A., Steitz, B., Kamau, S., Hottiger, M., Hilbe, M., Vaughan, L., Hofmann, M., Hofmann, H. & Von Rechenberg, B. 2006. Uptake and biocompatibility of functionalized poly(vinylalcohol) coated superparamagnetic maghemite nanoparticles by synoviocytes *in vitro*. *Journal of Nanoscience and Nanotechnology* **6**, 2829-40.
- Schutt, W., Gruttner, C., Hafeli, U., Zborowski, M., Teller, J., Putzar, H. & Schumichen, C. 1997. Applications of magnetic targeting in diagnosis and therapy--possibilities and limitations: a mini-review. *Hybridoma*, **16**, 109-17.
- Schwalbe, M., Pachmann, K., Hoffken, K. & Clement, J. H. 2006. Improvement of the separation of tumour cells from peripheral blood cells using magnetic nanoparticles. *Journal of Physics-Condensed Matter*, **18**, S2865-S2876.
- Schwertmann, U. & Cornell, R. M. 1991. Iron oxides in the laboratory preparation and characterization. *Schwertmann, U. And R. M. Cornell. Iron Oxides in the Laboratory: Preparation and Characterization. Xiv+137p. Vch Verlagsgesellschaft Mbh: Weinheim, Germany; Vch Publishers, Inc.: New York, New York, USA. Illus, XIV,137P.*
- Sébastien, B., Sophie, L., Luce Vander, E. & Robert, N. M. 2006. Specific E-selectin targeting with a superparamagnetic MRI contrast agent. *Contrast Media & Molecular Imaging*, **1**, 15-22.
- Siegel, R. W. 1993. Synthesis and properties of nanophase materials. *Materials Science and Engineering: A*, **168**, 189-197.
- Sjoegren, C. E., Briley-Saeboe, K., Hanson, M. & Johansson, C. 1994. Magnetic characterization of iron oxides for magnetic resonance imaging. *Magnetic resonance in medicine : official journal of the Society of Magnetic Resonance in Medicine / Society of Magnetic Resonance in Medicine*, **31**, 268-72.
- Sofia, S. J., Premnath, V. & Merrill, E. W. 1998. Poly(ethylene oxide) Grafted to Silicon Surfaces: Grafting Density and Protein Adsorption. *Macromolecules*, **31**, 5059-5070.
-

-
- Soppimath, K. S., Aminabhavi, T. M., Kulkarni, A. R. & Rudzinski, W. E. 2001. Biodegradable polymeric nanoparticles as drug delivery devices. *Journal of Controlled Release*, **70**, 1-20.
- Sorensen, C. M. 2002. Magnetism. In: KENNETH, J. K. (ed.) *Nanoscale Materials in Chemistry*.
- Steitz, B., Hofmann, H., Kamau, S. W., Hassa, P. O., Hottiger, M. O., Von Rechenberg, B., Hofmann-Antenbrink, M. & Petri-Fink, A. 2007. Characterization of PEI-coated superparamagnetic iron oxide nanoparticles for transfection: Size distribution, colloidal properties and DNA interaction. *Journal of Magnetism and Magnetic Materials*, **311**, 300-305.
- Stolnik, S., Illum, L. & Davis, S. S. 1995. Long circulating microparticulate drug carriers. *Advanced Drug Delivery Reviews*, **16**, 195-214.
- Storm, G., Belliot, S. O., Daemen, T. & Lasic, D. D. 1995. Surface modification of nanoparticles to oppose uptake by the mononuclear phagocyte system. *Advanced Drug Delivery Reviews*, **17**, 31-48.
- Stroh, A., Zimmer, C., Gutzeit, C., Jakstadt, M., Marschinke, F., Jung, T., Pilgrim, H. & Grune, T. 2004. Iron oxide particles for molecular magnetic resonance imaging cause transient oxidative stress in rat macrophages. *Free Radical Biology and Medicine*, **36**, 976-984.
- Sudimack, J. & Lee, R. J. 2000. Targeted drug delivery via the folate receptor. *Advanced Drug Delivery Reviews*, **41**, 147-62.
- Sugimoto, T. 2000. Fine particles : synthesis, characterization, and mechanisms of growth, *New York, Marcel Dekker*.
- Sugimoto, T. & Matijevic, E. 1980. Formation of uniform spherical magnetite particles by crystallization from ferrous hydroxide GELS. *Journal of Colloid and Interface Science*, **74**, 227-243.
- Sun, C., Lee, J. S. H. & Zhang, M. 2008. Magnetic nanoparticles in MR imaging and drug delivery. *Advanced Drug Delivery Reviews*, **60**, 1252-1265.
- Sun, J., Zhou, S., Hou, P., Yang, Y., Weng, J., Li, X. & Li, M. 2007. Synthesis and characterization of biocompatible Fe₃O₄ nanoparticles. *Journal of Biomedical Materials Research Part A*, **80**, 333-41.
- Sun, S. & Zeng, H. 2002. Size-Controlled Synthesis of Magnetite Nanoparticles. *Journal of the American Chemical Society*, **124**, 8204-8205.
-

-
- Sun, S., Zeng, H., Robinson, D. B., Raoux, S., Rice, P. M., Wang, S. X. & Li, G. 2004a. Monodisperse MFe₂O₄ (M = Fe, Co, Mn) Nanoparticles. *Journal of the American Chemical Society*, **126**, 273-279.
- Sun, W., Xie, C., Wang, H. & Hu, Y. 2004b. Specific role of polysorbate 80 coating on the targeting of nanoparticles to the brain. *Biomaterials*, **25**, 3065-3071.
- Sung, A.-M. & Piirma, I. 1994. Electrosteric Stabilization of Polymer Colloids. *Langmuir*, **10**, 1393-1398.
- Tanaka, K., Kitamura, N., Morita, M., Inubushi, T. & Chujo, Y. 2008. Assembly system of direct modified superparamagnetic iron oxide nanoparticles for target-specific MRI contrast agents. *Bioorganic & Medicinal Chemistry Letters*, **18**, 5463-5465.
- Tartaj, P., Del Puerto Morales, M., Veintemillas-Verdaguer, S., Gonzalez-Carreno, T. & Serna, C. J. 2003a. The preparation of magnetic nanoparticles for applications in biomedicine. *Journal of Physics D: Applied Physics*, **36**, R182eR197.
- Tartaj, P., Gonzalez-Carreño, T., Rebolledo, A. F., Bomatí-Miguel, O. & Serna, C. J. 2007. Direct aerosol synthesis of carboxy-functionalized iron oxide colloids displaying reversible magnetic behavior. *Journal of Colloid and Interface Science*, **309**, 68-71.
- Tartaj, P., Morales, M. D., Veintemillas-Verdaguer, S., Gonzalez-Carreno, T. & Serna, C. J. 2003b. The preparation of magnetic nanoparticles for applications in biomedicine. *Journal of Physics D-Applied Physics*, **36**, R182-R197.
- Tartaj, P., Morales, M. P., González-Carreño, T., Veintemillas-Verdaguer, S. & Serna, C. J. 2005. Advances in magnetic nanoparticles for biotechnology applications. *Journal of Magnetism and Magnetic Materials*, **290-291**, 28-34.
- Tavakoli, A., Sohrabi, M. & Kargari, A. 2007. A review of methods for synthesis of nanostructured metals with emphasis on iron compounds. *Chemical Papers*, **61**, 151-170.
- Teja, A. S. & Koh, P.-Y. 2009. Synthesis, properties, and applications of magnetic iron oxide nanoparticles. *Progress in Crystal Growth and Characterization of Materials*, **55**, 22-45.
-

-
- Thorek, D. L., Chen, A. K., Czupryna, J. & Tsourkas, A. 2006. Superparamagnetic iron oxide nanoparticle probes for molecular imaging. *Ann Biomed Eng*, **34**, 23-38.
- Thünemann, A. F., Schütt, D., Kaufner, L., Pison, U. & Möhwald, H. 2006. Maghemite Nanoparticles Protectively Coated with Poly(ethylene imine) and Poly(ethylene oxide)-block-poly(glutamic acid). *Langmuir*, **22**, 2351-2357.
- Tian, D., Dubois, P., Grandfils, C. & Jerome, R. 1997. Ring-Opening Polymerization of 1,4,8-Trioxaspiro[4.6]-9-undecanone: A New Route to Aliphatic Polyesters Bearing Functional Pendent Groups. *Macromolecules*, **30**, 406-409.
- Torchilin, V. P. 2000. Drug targeting. *European Journal of Pharmaceutical Sciences*, **11**, S81-S91.
- Tronc, E., Belleville, P., Jolivet, J. P. & Livage, J. 1992. Transformation of ferric hydroxide into spinel by Fe(II) adsorption. *Langmuir*, **8**, 313-319.
- Tsai, Z.-T., Wang, J.-F., Kuo, H.-Y., Shen, C.-R., Wang, J.-J. & Yen, T.-C. 2010. In situ preparation of high relaxivity iron oxide nanoparticles by coating with chitosan: A potential MRI contrast agent useful for cell tracking. *Journal of Magnetism and Magnetic Materials*, **322**, 208-213.
- Tsukada, Y., Hara, K., Bando, Y., Huang, C. C., Kousaka, Y., Kawashima, Y., Morishita, R. & Tsujimoto, H. 2009. Particle size control of poly(dl-lactide-co-glycolide) nanospheres for sterile applications. *International Journal of Pharmaceutics*, **370**, 196-201.
- Tueng, S., Ralph, W., Mikhail, P., Alexei, B., Jr. & Thomas, J. B. 1993. Monocrystalline iron oxide nanocompounds (MION): Physicochemical properties. *Magnetic Resonance in Medicine*, **29**, 599-604.
- Tzu-Chen, Y., Weiguo, Z., Suzanne, T. I. & Chien, H. 1993. Intracellular labeling of T-cells with superparamagnetic contrast agents. *Magnetic Resonance in Medicine*, **30**, 617-625.
- Valenzuela, R., Fuentes, M. C., Parra, C., Baeza, J., Duran, N., Sharma, S. K., Knobel, M. & Freer, J. 2009. Influence of stirring velocity on the synthesis of magnetite nanoparticles (Fe₃O₄) by the co-precipitation method. *Journal of Alloys and Compounds*, **488**, 227-231.

-
- Van Dijk-Wolthuis, W. N. E., Hoogeboom, J. A. M., Van Steenberghe, M. J., Tsang, S. K. Y. & Hennink, W. E. 1997. Degradation and Release Behavior of Dextran-Based Hydrogels. *Macromolecules*, **30**, 4639-4645.
- Van Oss, C. J. 1994. Interfacial forces in aqueous media, *New York, M. Dekker*.
- Veintemillas-Verdaguer, S., Morales, M. D., Bomati-Miguel, O., Bautista, C., Zhao, X. Q., Bonville, P., De Alejo, R. P., Ruiz-Cabello, J., Santos, M., Tendillo-Cortijo, F. J. & Ferreiros, J. 2004. Colloidal dispersions of maghemite nanoparticles produced by laser pyrolysis with application as NMR contrast agents. *Journal of Physics D-Applied Physics*, **37**, 2054-2059.
- Veintemillas-Verdaguer, S., Morales, M. P. & Serna, C. J. 1998. Continuous production of $[\gamma]\text{-Fe}_2\text{O}_3$ ultrafine powders by laser pyrolysis. *Materials Letters*, **35**, 227-231.
- Veisheh, O., Gunn, J. W. & Zhang, M. 2009. Design and fabrication of magnetic nanoparticles for targeted drug delivery and imaging. *Advanced Drug Delivery Reviews*, **62**, 284-304.
- Veld, P. J. A., Ye, W. P., Klap, R., Dijkstra, P. J. & Feijen, J. 1992. Copolymerization of epsilon-caprolactone and morpholine-2,5-dione derivatives. *Makromolekulare Chemie-Macromolecular Chemistry and Physics*, **193**, 1927-1942.
- Vennapusa, R., Hunegnaw, S. M., Cabrera, R. B. & Fernández-Lahore, M. 2008. Assessing adsorbent-biomass interactions during expanded bed adsorption onto ion exchangers utilizing surface energetics. *Journal of Chromatography A*, **1181**, 9-20.
- Vidal-Vidal, J., Rivas, J. & López-Quintela, M. A. 2006. Synthesis of monodisperse maghemite nanoparticles by the microemulsion method. *Colloids and Surfaces A: Physicochemical and Engineering Aspects*, **288**, 44-51.
- Vila, A., Sánchez, A., Tobío, M., Calvo, P. & Alonso, M. J. 2002. Design of biodegradable particles for protein delivery. *Journal of Controlled Release*, **78**, 15-24.
- Vincent, B. 1974. The effect of adsorbed polymers on dispersion stability. *Advances in Colloid and Interface Science*, **4**, 193-277.

-
- Wang, F. H., Lee, I. H., Holmstrom, N., Yoshitake, T., Kim, D. K., Muhammed, M., Frisen, J., Olson, L., Spenger, C. & Kehr, J. 2006. Magnetic resonance tracking of nanoparticle labelled neural stem cells in a rat's spinal cord. *Nanotechnology*, **17**, 1911-1915.
- Wang, L. & Muhammed, M. 1999. Synthesis of zinc oxide nanoparticles with controlled morphology. *Journal of Materials Chemistry*, **9**, 2871-2878
- Wang, L., Neoh, K.-G., Kang, E.-T., Shuter, B. & Wang, S.-C. 2010. Biodegradable magnetic-fluorescent magnetite/poly(dl-lactic acid-co-[alpha],[beta]-malic acid) composite nanoparticles for stem cell labeling. *Biomaterials*, **31**, 3502-3511.
- Wang, P., Zhu, Y., Yang, X. & Li, C. 2007. Electrochemical synthesis of magnetic nanoparticles within mesoporous silica microspheres. *Colloids and surfaces. A, Physicochemical and engineering aspects.*, **294**, 287.
- Wang, X., Zhou, L., Ma, Y., Li, X. & Gu, H. 2009. Control of aggregate size of polyethyleneimine-coated magnetic nanoparticles for magnetofection. *Nano Research*, **2**, 365-372.
- Wang, X., Zhuang, J., Peng, Q. & Li, Y. 2005. A general strategy for nanocrystal synthesis. *Nature*, **437**, 121-124.
- Wang, Y.-X., Hussain, S. & Krestin, G. 2001. Superparamagnetic iron oxide contrast agents: physicochemical characteristics and applications in MR imaging. *European Radiology*, **11**, 2319-2331.
- Weissleder, R., Bogdanov, A., Neuwelt, E. A. & Papisov, M. 1995. Long-circulating iron oxides for MR imaging. *Advanced Drug Delivery Reviews*, **16**, 321-334.
- Weissleder, R., Elizondo, G., Wittenberg, J., Rabito, C. A., Bengel, H. H. & Josephson, L. 1990. Ultrasmall superparamagnetic iron oxide: characterization of a new class of contrast agents for MR imaging. *Radiology*, **175**, 489-93.
- Weissleder, R., Moore, A., Mahmood, U., Borade, R., Benveniste, H., Chiocca, E. A. & Basilion, J. P. 2000. *In vivo* magnetic resonance imaging of transgene expression. *Nature Medicine*, **6**, 351-354.
- Weissleder, R., Stark, D. D., Engelstad, B. L., Bacon, B. R., Compton, C. C., White, D. L., Jacobs, P. & Lewis, J. 1989. Superparamagnetic iron oxide: pharmacokinetics and toxicity *American Journal of Roentgenology*, **152**, 167-73.
-

-
- Wilhelm, C., Billotey, C., Roger, J., Pons, J. N., Bacri, J. C. & Gazeau, F. 2003. Intracellular uptake of anionic superparamagnetic nanoparticles as a function of their surface coating. *Biomaterials*, **24**, 1001-1011.
- Wilhelm, C. & Gazeau, F. 2008. Universal cell labelling with anionic magnetic nanoparticles. *Biomaterials*, **29**, 3161-3174.
- Willard, M. A., Kurihara, L. K., Carpenter, E. E., Calvin, S. & Harris, V. G. 2004. Chemically Prepared Magnetic Nanoparticles. *Encyclopedia of Nanoscience and Nanotechnology*, **1**, 815-848.
- Wotschadlo, J., Liebert, T., Heinze, T., Wagner, K., Schnabelrauch, M., Dutz, S., Müller, R., Steiniger, F., Schwalbe, M., Kroll, T. C., Höffken, K., Buske, N. & Clement, J. H. 2009a. Magnetic nanoparticles coated with carboxymethylated polysaccharide shells-Interaction with human cells. *Journal of Magnetism and Magnetic Materials*, **321**, 1469-1473.
- Xia, J. H., Shen, H., Shu, B. F. & Zhang, W. 2008. Novel aqueous magnetic fluids stabilized by albumin for biological application. *Materials Research Bulletin*, **43**, 2213-2219.
- Xie, J., Huang, J., Li, X., Sun, S. & Chen, X. 2009. Iron Oxide Nanoparticle Platform for Biomedical Applications. *Current Medicinal Chemistry*, **16**, 1278-1294.
- Xie, J., Xu, C., Kohler, N., Hou, Y. & Sun, S. 2007. Controlled PEGylation of Monodisperse Fe₃O₄ Nanoparticles for Reduced Non-Specific Uptake by Macrophage Cells. *Advanced Materials*, **19**, 3163-3166.
- Xu, C. & Teja, A. S. 2008. Continuous hydrothermal synthesis of iron oxide and PVA-protected iron oxide nanoparticles. *The Journal of Supercritical Fluids*, **44**, 85-91.
- Xu, X. Q., Shen, H., Xu, J. R., Xu, J., Li, X. J. & Xiong, X. M. 2005. Core-shell structure and magnetic properties of magnetite magnetic fluids stabilized with dextran. *Applied Surface Science*, **252**, 494-500.
- Yamamoto, N., Kurisawa, M. & Yui, N. 1996. Double-stimuli-responsive degradable hydrogels: Interpenetrating polymer networks consisting of gelatin and dextran with different phase separation. *Macromolecular Rapid Communications*, **17**, 313-318.
-

-
- Yamazaki, M. & Ito, T. 1990. Deformation and instability in membrane structure of phospholipid vesicles caused by osmophobic association: Mechanical stress model for the mechanism of poly(ethylene glycol)-induced membrane fusion. *Biochemistry*, **29**, 1309-1314.
- Yang, C., Rait, A., Pirollo, K. F., Dagata, J. A., Farkas, N. & Chang, E. H. 2008. Nanoimmunoliposome delivery of superparamagnetic iron oxide markedly enhances targeting and uptake in human cancer cells *in vitro* and *in vivo*. *Nanomedicine: Nanotechnology, Biology and Medicine*, **4**, 318-329.
- Yang, F., Li, Y., Chen, Z., Zhang, Y., Wu, J. & Gu, N. 2009. Superparamagnetic iron oxide nanoparticle-embedded encapsulated microbubbles as dual contrast agents of magnetic resonance and ultrasound imaging. *Biomaterials*, **30**, 3882-3890.
- Yang, J., Park, S. B., Yoon, H.-G., Huh, Y. M. & Haam, S. 2006. Preparation of poly ϵ -caprolactone nanoparticles containing magnetite for magnetic drug carrier. *International Journal of Pharmaceutics*, **324**, 185-190.
- Yasugi, K., Nagasaki, Y., Kato, M. & Kataoka, K. 1999. Preparation and characterization of polymer micelles from poly(ethylene glycol)-poly(L-lactide) block copolymers as potential drug carrier. *Journal of Controlled Release*, **62**, 89-100.
- Yu, S. & Chow, C. M. 2004. Carboxyl group ($-\text{CO}_2\text{H}$) functionalized ferrimagnetic iron oxide nanoparticles for potential bio-applications. *Journal of Materials Chemistry*, **14**, 2781-2786.
- Zambaux, M. F., Bonneaux, F., Gref, R., Dellacherie, E. & Vigneron, C. 1999. MPEO-PLA nanoparticles: Effect of MPEO content on some of their surface properties. *Journal of Biomedical Materials Research*, **44**, 109-115.
- Zhang, G., Liao, Y. & Baker, I. 2010a. Surface engineering of core/shell iron/iron oxide nanoparticles from microemulsions for hyperthermia. *Materials Science and Engineering: C*, **30**, 92-97.
- Zhang, J., Chen, X. G., Peng, W. B. & Liu, C. S. 2008. Uptake of oleoyl-chitosan nanoparticles by A549 cells. *Nanomedicine: Nanotechnology, Biology and Medicine*, **4**, 208-214.
- Zhang, L.-Y., Zhu, X.-J., Sun, H.-W., Chi, G.-R., Xu, J.-X. & Sun, Y.-L. 2010b. Control synthesis of magnetic Fe_3O_4 -chitosan nanoparticles under UV irradiation in aqueous system. *Current Applied Physics*, **10**, 828-833.
-

-
- Zhao, H., Saatchi, K. & Häfeli, U. O. 2009. Preparation of biodegradable magnetic microspheres with poly(lactic acid)-coated magnetite. *Journal of Magnetism and Magnetic Materials*, **321**, 1356-1363.
- Zheng, W., Gao, F. & Gu, H. 2005. Magnetic polymer nanospheres with high and uniform magnetite content. *Journal of Magnetism and Magnetic Materials*, **288**, 403-410.
- Zhi, J., Wang, Y., Lu, Y., Ma, J. & Luo, G. 2006. In situ preparation of magnetic chitosan/Fe₃O₄ composite nanoparticles in tiny pools of water-in-oil microemulsion. *Reactive and Functional Polymers*, **66**, 1552-1558.
- Zhou, S., Liao, X., Li, X., Deng, X. & Li, H. 2003. Poly--lactide-co-poly(ethylene glycol) microspheres as potential vaccine delivery systems. *Journal of Controlled Release*, **86**, 195-205.
- Zhu, A., Yuan, L. & Liao, T. 2008. Suspension of Fe₃O₄ nanoparticles stabilized by chitosan and o-carboxymethylchitosan. *International Journal of Pharmaceutics*, **350**, 361-368.
- Zimmer, A. & Kreuter, J. 1995. Microspheres and nanoparticles used in ocular delivery systems. *Advanced Drug Delivery Reviews*, **16**, 61-73.
- Ziv-Polat, O., Topaz, M., Brosh, T. & Margel, S. 2010. Enhancement of incisional wound healing by thrombin conjugated iron oxide nanoparticles. *Biomaterials*, **31**, 741-747.